UNIVERSIDADE FEDERAL DO RIO GRANDE DO SUL
INSTITUTO DE GEOCIÊNCIAS
PROGRAMA DE PÓS-GRADUAÇÃO EM GEOCIÊNCIAS

O ARCO PIRATINI: IMPLICAÇÕES NA EVOLUÇÃO DO CINTURÃO DOM FELICIANO (BRASIL/URUGUAI)

DANIEL TRIBOLI VIEIRA

ORIENTADOR – Prof. Dr. Edinei Koester

COORIENTADORA – Profª. Drª. Carla Cristine Porcher

Porto Alegre – 2020

UNIVERSIDADE FEDERAL DO RIO GRANDE DO SUL
INSTITUTO DE GEOCIÊNCIAS
PROGRAMA DE PÓS-GRADUAÇÃO EM GEOCIÊNCIAS

O ARCO PIRATINI: IMPLICAÇÕES NA EVOLUÇÃO DO CINTURÃO DOM FELICIANO (BRASIL/URUGUAI)

DANIEL TRIBOLI VIEIRA

ORIENTADOR – Prof. Dr. Edinei Koester

COORIENTADORA – Profª. Drª. Carla Cristine Porcher

BANCA EXAMINADORA

     Profª. Drª. Cristine Lenz

     Prof. Dr. Lauro Valentim Stoll Nardi

     Prof. Dr. Viter Magalhães Pinto

> Tese de Doutorado apresentada como requisito parcial para a obtenção do Título de Doutor em Ciências.

Porto Alegre – 2020

Dedico esta tese à minha família, pelo incalculável apoio e estrutura.

AGRADECIMENTOS

Aos meus orientadores Edinei Koester, Carla Carla Cristine Porcher e Rodrigo Chaves Ramos, sem os quais não existiria este trabalho; ao Instituto de Geociências da UFRGS pela infraestrutura e aos seus funcionários; aos colegas de trabalho que me ajudaram de alguma forma no desenvolvimento desta tese; à FAPERGS e CNPq pelo apoio financeiro a esta pesquisa.

GRACIAS!

"Existem muitas hipóteses em ciência que estão erradas. Isso é perfeitamente aceitável, elas são a abertura para achar as que estão certas". – **Carl E. Sagan [1934-1996].**

RESUMO

O Cinturão Dom Feliciano, setor sul da Província Mantiqueira, se estende desde Punta del Este, no Uruguai, até o leste de Santa Catarina. Essa faixa móvel representa o registro da colisão entre diversos crátons, microplacas e blocos e o encerramento de pelo menos duas bacias oceânicas durante a amalgamação do paleocontinente Gondwana Ocidental no ciclo orogênico Brasiliano-Panafricano, o que reflete a sua complexa história geológica durante sua evolução geotectônica. Essa evolução está comumente relacionada a três estágios principais: Brasiliano I (clímax em torno de 900-700 Ma, correspondendo às Orogenias Passinho e São Gabriel e ao encerramento do paleo-oceano Charrua-São Gabriel); Brasiliano II (clímax em torno de 640-620 Ma, correspondendo à Orogenia Dom Feliciano nos domínios Central e Oriental, representado por intenso magmatismo continental e retrabalhamento crustal); Brasiliano III (em torno de 595-560 Ma, com geração de magmatismo granítico pré- a sintectônico, relacionado aos eventos colisionais finais do ciclo orogênico Brasiliano-Panafricano e encerramento do paleo-oceano Adamastor). O presente trabalho retoma a hipótese de uma orogenia em torno de 780 Ma registrada na porção centro-leste do Cinturão Dom Feliciano, denominada como Orogenia Piratini. Essa orogenia estaria relacionada ao encerramento do paleo-oceano Charrua e à convergência entre terrenos paleo-sulamericanos e paleo-africanos, este último representado por uma microplaca ou fragmentos do Cráton Kalahari durante a fragmentação do paleocontinente Rodínia, gerando um arco magmático continental neoproterozoico denominado de Arco Piratini. O Arco Piratini é caracterizado como um arco do tipo andino com atividade magmática entre 780-680 Ma, representado pelos ortognaisses Cerro Borri, no Uruguai, e Piratini, Várzea do Capivarita, Chácara das Pedras e Arroio Pedrado no Brasil. O presente trabalho propõe que a Orogenia Piratini culminou com a amalgamação entre o Arco Piratini e a margem leste do Cráton Rio de La Plata em torno de 660 Ma, idade do metamorfismo de alto grau registrado tanto nos ortognaisses que compõe o Arco Piratini quanto nas rochas supracrustais associadas (e.g. Suíte Metamórfica Chafalote, Uruguai). O evento colisional é seguido por um evento de descompressão em torno de 640-605 Ma, gerando a fusão parcial das rochas relacionadas à Orogenia Piratini. Esse evento estaria relacionado à nucleação de zonas de cisalhamento dúcteis em zonas de sutura (por exemplo, a Zona de Cisalhamento Transcorrente Dorsal de Canguçu, possivelmente relacionada à Sutura de Porto Alegre) e granitogênese associada, culminando no retrabalhamento das rochas relacionadas ao Arco Piratini dando origem em partes aos granitoides peraluminosos que ocorrem na porção centro-leste do Cinturão Dom Feliciano.

Palavras-chave: Orogenia; Arco Magmático; Metamorfismo de Alto Grau; Zona de Cisalhamento; Fusão Crustal

ABSTRACT

The Dom Feliciano Belt, southernmost Mantiqueira Province, extends from Southernmost Brazil (Rio Grande do Sul and Santa Catarina states) to Punta del Este, in Uruguay. This belt is interpreted as the result of the collision between cratons, minor blocks/microplates and the closure of at least two oceanic basins during the assembly of the Western Gondwana paleocontinent in the Brasiliano/Pan-African orogenic cycle, which reflects its complex geological history during its geotectonic evolution. This evolution is related to three main stages: Brasiliano I (climax at around 900-700 Ma, corresponding to the Passinho and São Gabriel Orogenies and the closure of the Charrua-São Gabriel paleo-ocean); Brasiliano II (climax at around 640-620 Ma, corresponding to the Dom Feliciano Orogeny in the Central and Eastern domains, represented by intense continental magmatism and crustal reworking); Brasiliano III (at around 595-560 Ma, with generation of pre- to syntectonic granitic magmatism, related to the final collisional events of the Brasiliano/Pan-African orogenic cycle and the closure of the Adamastor paleo-ocean). The present work revives the hypothesis of an orogenic event at around 780 Ma recorded in the central-eastern portion of the Dom Feliciano Belt, called Piratini Orogeny. This orogeny is related to the closure of the Charrua paleo-ocean and the convergence between paleo-South American and paleo-African terranes, the latter represented by a microplate or fragments of the Kalahari Craton during the fragmentation of the Rodinia paleocontinent, generating a Neoproterozoic continental magmatic arc: the Piratini Arc. The Piratini Arc is characterized as an Andean type arc with magmatic activity between 780-680 Ma, represented by the Cerro Borri orthogneisses in Uruguay, and Piratini, Várzea do Capivarita, Chácara das Pedras, and Arroio Pedrado orthogneisses in Brazil. The present work suggests that the Piratini Orogeny culminated in the amalgamation of the Piratini Arc and the eastern margin of the Rio de La Plata Craton at around 660 Ma. The latter age represents the high-grade metamorphism peak recorded both in the orthogneisses of the Piratini Arc and in associated supracrustal rocks (e.g. Chafalote Metamorphic Suite, Uruguay). The collisional event is followed by isothermal decompression stage at around 640-605 Ma, generating partial melting of the Piratini Orogeny-related rocks. This stage would be related to nucleation of ductile shear zones in suture zones (e.g. Dorsal de Canguçu Transcurrent Shear Zone, possibly related to the Porto Alegre Suture) and associated granitogenesis, culminating in the reworking of the Piratini Arc-related rocks and generation of part of the peraluminous granitoids that occur in the central-eastern portion of the Dom Feliciano Belt.

Keywords: Orogeny; Magmatic Arc; High-Grade Metamorphism; Shear Zone; Crustal Melting

LISTA DE FIGURAS

LISTA DE TABELAS

LISTA DE ABREVIATURAS

CPGq – Centro de Estudos em Petrologia e Geoquímica
CPGeo – Centro de Pesquisas Geocronológicas
IGEO – Instituto de Geociências
LA-MC-ICP-MS – Laser ablation Multi-Coletor de Espectrometria de Massas com Plasma Indutivamente Acoplado
LGI – Laboratório de Geologia Isotópica
LOI - Perda ao Fogo
ICP-OES – Espectrometria de Emissão Óptica por Plasma Acoplado Indutivamente
ICP-MS – Espectrometria de Massa com Plasma Acoplado Indutivamente
Ma – Milhões de anos
MEV – Microscópio Eletrônico de Varredura
NPA – Núcleo de Preparação de Amostras
TIMS – Espectrômetro de Massa por Ionização Termal
WDS – Espectroscopia por Comprimento de Onda Dispersivo
ZCSBC – Zona de Cisalhamento Sierra Ballena e Dorsal de Canguçu.
ZCTDC – Zona de Cisalhamento Transcorrente Dorsal de Canguçu

Abreviação de minerais segundo Whitney & Evans (2010)

Bt – biotita
Kf – K-feldspato
Pl – plagioclásio
Qtz - quartzo

SUMÁRIO

Sobre a Estrutura desta Tese:

Esta tese de Doutorado está estruturada e desenvolvida em torno de artigos publicados e submetidos em periódicos científicos. Consequentemente, sua organização compreende as seguintes partes principais:

I)   Capítulo 1 – Introdução sobre o tema, descrição do objeto da pesquisa de Doutorado e as metodologias de pesquisa desenvolvidas.

II)   Capítulo 2 – Estado da arte sobre o tema abordado: O Arco Piratini.

III)   Capítulos 3, 4, 5 e 6 – Artigos escritos pelo autor durante o desenvolvimento de seu Doutorado:

- *Sr-Nd-Hf isotopic constraints and U-Pb geochronology of the Arroio Pedrado Gneisses, Dom Feliciano Belt, Brazil: A 680 Ma shoshonitic event in the final stages of The Piratini Arc evolution*, publicado no periódico *Journal of South American Earth Sciences*, *Volume 95, 102294.*

- *Chafalote Metamorphic Suite (Uruguay): reflections on the evolution of the Punta Del Este Terrane,* publicado no periódico *Journal of South American Earth Sciences*, *Volume 98, 102420*

- *New zircon SHRIMP U-Pb ages for the synkinematic magmatism in the Dorsal de Canguçu Transcurrent Shear Zone, Dom Feliciano Belt (Brazil): tectonic implications.*

- Petrografia e química mineral do Granito São Geraldo: evidências de magmatismo peraluminoso na região de Porto Alegre, RS. Publicado no periódico Pesquisas em Geociências, Volume 3 de 2019.

IV) Capítulo 7 – Integração dos artigos na forma de discussões e modelo proposto.

V) Capítulo 8 – Conclusões sobre os temas abordados na tese de doutorado.

CAPÍTULO 1

1. INTRODUÇÃO

A presente tese é a síntese das pesquisas desenvolvidas pelo autor durante os quatro anos de doutorado em Geociências realizados na Universidade Federal do Rio Grande do Sul. Nessas pesquisas foram desenvolvidos diversos estudos como petrografia, geoquímica de rocha total e isotópica Sr-Nd-Hf, bem como análises de geocronologia U-Pb nos gnaisses denominados como Arroio Pedrado (Philipp & Machado, 2002) na região de Arroio Grande (extremo sul do estado do Rio Grande do Sul) e nas rochas supracrustais da Suíte Metamórfica Chafalote (Masquelin *et al.,* 2012) na região de Rocha, no Uruguai. Estes estudos levaram à hipótese de que tais rochas registram os estágios finais do magmatismo relacionado a um arco magmático continental durante o ciclo orogênico Piratini (ca. 780 Ma, Fragoso-Cesar, 1991; Ramos *et al.,* 2018), denominado como Arco Piratini (Fragoso-Cesar, 1991), bem como registraram na história evolutiva desta orogenia um metamorfismo de alto grau relacionado ao encerramento do paleo-oceano Charrua em 660 Ma (Ramos *et al.,* 2018).

Concomitantemente foram realizados estudos de petrografia, química mineral e geocronologia (U-Pb) em metagranitoides sincinemáticos neoproterozoicos nas regiões de Encruzilhada do Sul e Porto Alegre (porção leste e capital do estado do Rio Grande do Sul, respectivamente) correlacionando tal granitogênese com os estágios finais e/ou pós-orogênia Piratini. Partindo dessas premissas, para uma melhor compreensão sobre o tema, é apresentada no capítulo 2 uma revisão que aborda a origem, evolução e estágios finais do Arco Piratini durante a orogenia Piratini. Posteriormente, nos capítulos 3, 4, 5 e 6 são apresentados os artigos que compõem a presente tese. No capítulo 7 é apresentado o modelo proposto para geração e evolução do Arco Piratini, enquanto no capítulo 8 são apresentadas as conclusões gerais sobre o tema.

O objetivo desta tese é compreender a evolução do Arco Piratini, apresentando e integrando dados de campo, petrográficos, geoquímicos (química mineral, rocha total e isótopos de Sr-Nd-Hf) e geocronológicos (U-Pb) obtidos nas diferentes rochas de unidades geológicas estudadas. A partir dessas informações, em conjunto com os dados disponíveis na literatura, a tese propõe o significado tectônico do Arco Piratini, no contexto de evolução do Cinturão Dom Feliciano.

1.1 Metodologias

Para a obtenção dos resultados nesta pesquisa, foram utilizadas técnicas de investigação geológica compatíveis com o objetivo da tese. As metodologias e os procedimentos utilizados para a obtenção dos dados que possibilitaram o entendimento da evolução das rochas estudadas são descritas a seguir e detalhadas (p. ex. número de análises, litotipo e localização das amostras) nos artigos apresentados nos capítulos 3, 4, 5 e 6.

1.1.1 Revisão bibliográfica

Foi realizado um levantamento bibliográfico preliminar de artigos científicos, boletins, periódicos, relatórios técnicos de empresas, trabalhos de graduação, dissertações de mestrado, teses de doutorado, cartas topográficas e mapas geológicos. Foi a primeira de todas as etapas a ser iniciada e uma das últimas a ser finalizada devido à constante evolução de ideias e hipóteses referentes ao tema estudado.

1.1.2 Campo

A campanha de campo contou com a realização de perfis de carro e a pé para o mapeamento geológico (Fig. 1A), coleta de amostras, análise estrutural e dos aspectos petrográficos, construção de seções geológicas e croquis dos afloramentos representativos das diversas rochas abordadas no presente estudo. A coleta de amostras em campo priorizou aquelas sem alteração, sendo utilizadas (Fig. 1B) para análise petrográfica e análises de química mineral, rocha total, isotópica, bem como análises geocronológicas.
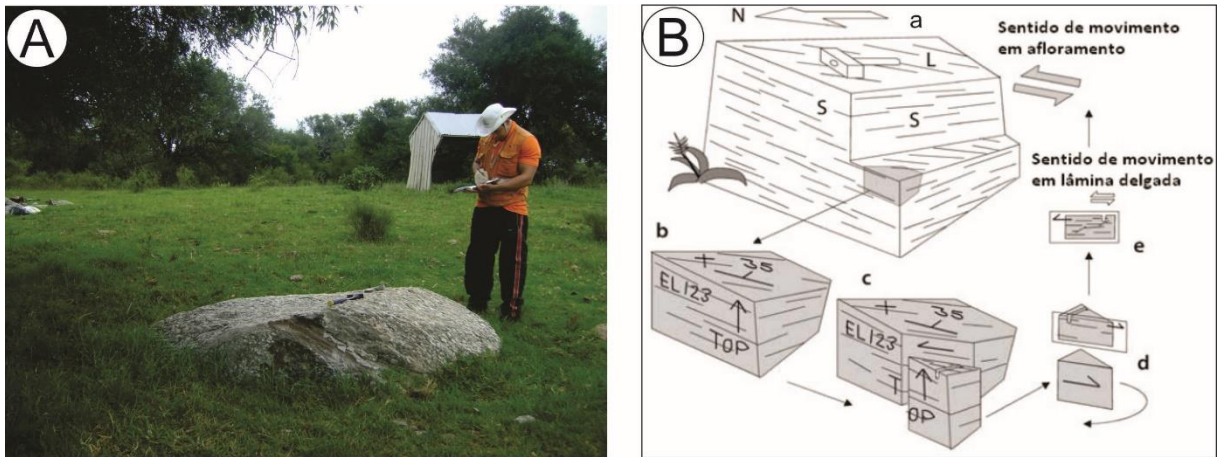
Figura 1 - Detalhe do trabalho de campo realizado. A) Realização da descrição de um dos afloramentos do Gnaisse Arroio Pedrado na região de Arroio Grande, RS; B)Modelo esquemático de como orientar uma amostra em afloramento: a) Afloramento com a foliação indicada por S e lineação por L; b) Coloca-se um plano de direção e mergulho em uma superfície para orientar a amostra no espaço; c) Marca-se o corte da amostra no plano normal a foliação e pararelo a lineação (XZ); d) Delimita-se a área onde será feita a lâmina delgada, com a marcação de orientação da amostra; e) determina-se o sentido de movimento. Modificado de Passchier & Trouw (2005).

1.1.3 Petrografia

Foram realizadas descrições petrográficas com objetivo de identificar os minerais, texturas e estruturas presentes nas rochas estudas. As análises macroscópicas (Fig. 2A) e microscópicas (Fig. 2B) das diferentes amostras foram realizadas com o uso de lupa binocular e microscópio de polarização Leica® com câmera fotográfica acoplada, ambas no Laboratório de Geologia Isotópica (LGI) do Instituto de Geociências (IGEO), Centro de Estudos em Petrologia e Geoquímica (CPGq) da Universidade Federal do Rio Grande do Sul (UFRGS). A etapa de preparação das amostras para a realização das análises petrográficas e de química mineral ocorreram junto ao Núcleo de Preparação de Amostras do CPGq. Nesta etapa foi fundamental uma seleção de amostras frescas e escolha correta do corte no plano XZ, para que informações importantes para análise microestrutural e sentido de movimento fossem analisados.
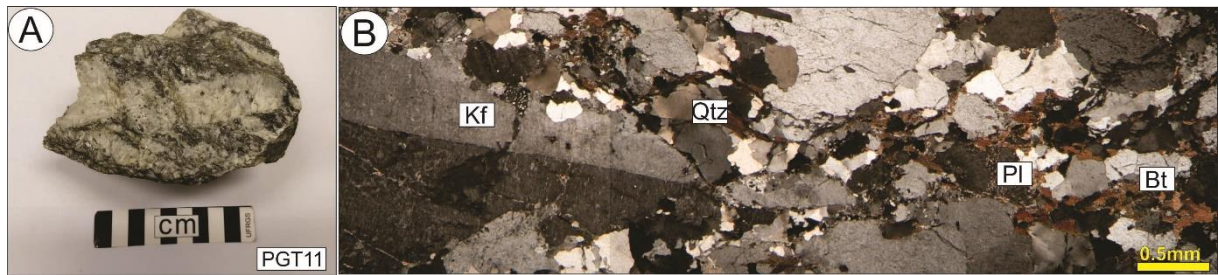
Figura 2 - Análises macroscópicas e microscópicas do Metagranito Quitéria. A) Amostra de mão evidenciando a textura porfirítica com megacristais de K-feldspato; B) Características microscópicas representativas do metagranito (nicóis cruzados, ampliação de 2,5x). Abreviações minerais: Kf = K-feldspato; Qtz = quartzo; Bt = biotita; Pl = plagioclásio.

1.1.4 Química mineral

As lâminas selecionadas para análises de química mineral foram devidamente polidas e metalizadas com carbono por evaporação. As análises foram realizadas com auxílio de uma microssonda *Cameca SXFive* (Fig. 3) equipado com cinco espectrômetros WDS (*Wavelength Dispersive Spectrometry*). Tanto a preparação quanto as análises foram realizadas no Laboratório de Microssonda Eletrônica do CPGq. Para a análise de elementos maiores nos silicatos e óxidos, as condições analíticas consistiram em voltagem de aceleração de 15 kV, corrente de 10 nA, e diâmetro do feixe eletrônico da ordem de 5 µm.

Para as análises quantitativas de microssonda eletrônica foram usados os seguintes padrões: albita para Na (8,6 % Na; 10,34 % Al; 32,03 % Si; 48,76 % O; 0,18 % K; 0,09 % Ca), wollastonita para Si e Ca (33,9337 % Ca; 23,8201 % Si; 41,17 % O; 0,0074 % Na; 0,006 % Mg; 0,006 % Ti; 0,4879 % Mn; 0,171 % Fe), diopsídio para Mg (11,23 % Mg; 18,39 % Ca; 25,88 % Si; 44,3 % O; 0,05 % Al; 0,05 % Ti; 0,04 % Mn; 0,04 % Fe), sanidina para Al e K (46,28 % O; 9,93 % Al; 30,23 % Si; 10,05 % K; 0,14 % Fe; 0,98 % Ba; 2,23 % Na), óxido de cromo para Cr (68,4195 % Cr; 31,5805 % O), rodonita para Mn (32,8499 % Mn; 22,1126 % Si; 37,7621 % O; 1,1216 % Mg; 5,0993 % Ca; 0,7905 % Fe), hematita para Fe (69,9426 % Fe; 30,0574 % O) e rutilo para Ti (59,95% Ti; 40,05 % O).

As fórmulas estruturais foram calculadas com base em 32 ânions de oxigênio para os feldspatos, 24 para biotita e 22 para muscovita, 25 para apatita e 24 para granada. As classificações e membros finais dos minerais foram determinados de acordo com as propostas de Deer *et al.* (1992) e Grew *et al.* (2013).
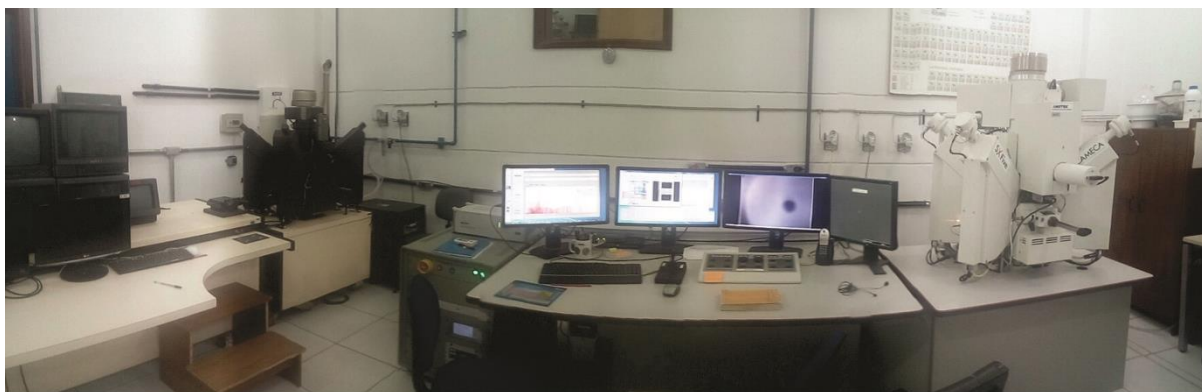
Figura 3 - Microssonda *Cameca SXFive* do Laboratório de Microssonda Eletrônica, CPGq, IGEO-UFRGS.

1.1.5 Geoquímica de rocha total

Amostras representativas foram selecionados para as análises de geoquímica de rocha total. As amostras foram preparadas no Núcleo de Preparação de Amostras (NPA) do CPGq, onde foram pulverizadas até um tamanho aproximado de 200 *mesh*. Após a moagem, uma pequena fração (cerca de 5 g) foi separada para posterior preparação para as análises de isótopos conforme descrito na seção 2.6, e o restante encaminhado para as análises de geoquímica de rocha total.

As análises geoquímicas de rocha total foram realizadas pelo laboratório *Acme Analytical Laboratories* (Vancouver, Canadá). Os elementos maiores e traços foram analisados por Espectrometria de Emissão Óptica por Plasma Acoplado Indutivamente (ICP-OES). Os elementos terras raras foram analisados por Espectrometria de Massa com Plasma Acoplado Indutivamente (ICP-MS). A perda ao fogo (LOI) foi determinada por aquecimento das amostras (pulverizadas) por 60 minutos a 1000 °C. As análises geoquímicas foram trabalhadas através do *software Geochemical Data Toolkit* (Janoušek *et al.,* 2006).

1.1.6 Geoquímica isotópica (Rb-Sr e Sm-Nd)

As amostras selecionadas para as análises isotópicas foram preparadas conforme mencionado na seção 2.5. Após a moagem foi realizada a preparação das amostras para as análises isotópicas de Rb-Sr e Sm-Nd. As amostras foram dissolvidas seguindo o procedimento analítico padrão adotado pelo Laboratório de Geologia Isotópica (LGI) do CPGq. As razões isotópicas de interesse foram então

obtidas por meio de análises em Espectrômetro de Massa por Ionização Termal (TIMS) no LGI. As amostras foram processadas no TIMS, *VG Sector 54 Thermal* (Fig. 4), em modo estático. As razões de Sr e Nd foram normalizados para ^{86}Sr / ^{88}Sr = 0,1194 e ^{146}Nd/ ^{144}Nd = 0,7219, respectivamente. As análises do padrão de Sr NIST NBS-987 foram de ^{87}Sr/^{86}Sr = 0,710260 ± 0,000014, e para o padrão de Nd, La Jolla foram obtidos valores de ^{143}Nd/^{144}Nd = 0,511859 ± 0,000010.

Figura 4 - Espectrômetro de Massa por Ionização Termal, *VG Sector 54* do LGI, CPGq-IGEO-UFRGS.

1.1.7 U-Pb e Lu-Hf em zircão por LA-MC-ICP-MS

Para a realização das análises integradas de U-Pb e Lu-Hf em zircões via *laser* multi-coletor de espectrometria de massas com plasma indutivamente acoplado (LA-MC-ICP-MS), os cristais de zircão selecionados foram separados usando líquidos densos e técnicas de separação magnéticas (Frantz) no NPA do CPGq, posteriormente catados manualmente com auxilio de lupa binocular e então montados em pastilhas (*mounts*) de resina epóxi. O imageamento dos cristais de zircão (catodoluminescência e imagens de elétrons retroespalhados), para fins de analisar suas estruturas internas (como por exemplo zonações, núcleos herdados) e assim escolher os melhores alvos, foram obtidos no LGI, usando um microscópio eletrônico de varredura (MEV) JEOL JSM-6610LV equipado com um espectrômetro de raios X dispersivo por energia, modelo Bruker XFLASH 5030. As condições analíticas foram 15 kV, tamanho do ponto de 60 µm e distância de 10 mm.

As análises de U-Pb e Lu-Hf foram realizadas no LGI, usando uma microssonda de ablação a laser (*New Wave* UP213) acoplado a um MC-ICP-MS (*Thermo Finnigan Neptune*, Fig. 5). Os dados isotópicos foram adquiridos através do modo estático *in situ* em cristais de zircão, com tamanho de ponto de 25 μm para análises de U-Pb, e de 55 μm para análises Lu-Hf, com frequência de 10 Hz e intensidade de ~ 4 J/cm^2 em 40 ciclos de 1 s. O fracionamento elementar induzido pela ablação a *laser* e a discriminação instrumental de massa foram corrigidas usando o padrão para zircão GJ-1. As incertezas foram calculadas usando propagação de erros, seguindo os procedimentos analíticos de Bertotti *et al.* (2013). As idades foram calculadas usando o *software* Isoplot (Ludwig, 2008).

Figura 5 - LA-MC-ICP-MS, *Thermo Finnigan Neptune* do LGI do CPGq-IGEO-UFRGS.

1.1.8 U-Pb SHRIMP

Para a datação radiométrica U-Pb via SHRIMP os cristais de zircão das amostras selecionadas foram separados usando as mesmas técnicas mencionadas na seção 2.7 e montados em resina epóxi juntamente com o padrão TEMORA-2 (Black *et al.,* 2004). Para identificar os alvos para as análises, foram obtidas imagens de catodoluminescência dos cristais usando um MEV, FEI Quanta 250, equipado com um detector XMAX CL, no Centro de Pesquisas Geocronológicas (CPGeo), Instituto de Geociências (IG), Universidade de São Paulo (USP), Brasil. As análises de U-Pb foram realizadas no mesmo laboratório, utilizando uma microssonda de íons SHRIMP-IIe (Fig. 6) de alta resolução, seguindo os procedimentos de Sato *et al.* (2014). Os

erros são 2σ e o chumbo comum (^{204}Pb) foi corrigido com base nas medições. A abundância de U e as relações U/Pb foram calibradas usando o padrão TEMORA-2. Os erros de ^{206}Pb/^{238}U foram em geral < 2 %. As idades foram calculadas usando o *software* Isoplot (Ludwig, 2008).

Figura 6 - Microssonda iônica SHRIMP-IIe do CPGeo, IG-USP.

CAPÍTULO 2

2. ARCO PIRATINI

2.1 Contexto Geológico

O Arco Piratini está localizado no sudeste do Cinturão Dom Feliciano, o qual representa o setor sul da Província Mantiqueira (Almeida *et al.,* 1981), conforme a Figura 7. Esse cinturão se estende desde Punta del Este, no Uruguai, até o leste de Santa Catarina, representando o registro da colisão entre diversos crátons, microplacas e blocos e o encerramento de pelo menos duas bacias oceânicas, durante a amalgamação do paleocontinente Gondwana Ocidental no ciclo orogênico Brasiliano/Panafricano (*e.g.* Gaucher *et al.,* 2009; Rapela *et al.,* 2011; Konopásek *et al.,* 2018; Hueck *et al.,* 2018; Ramos *et al.,* 2018).
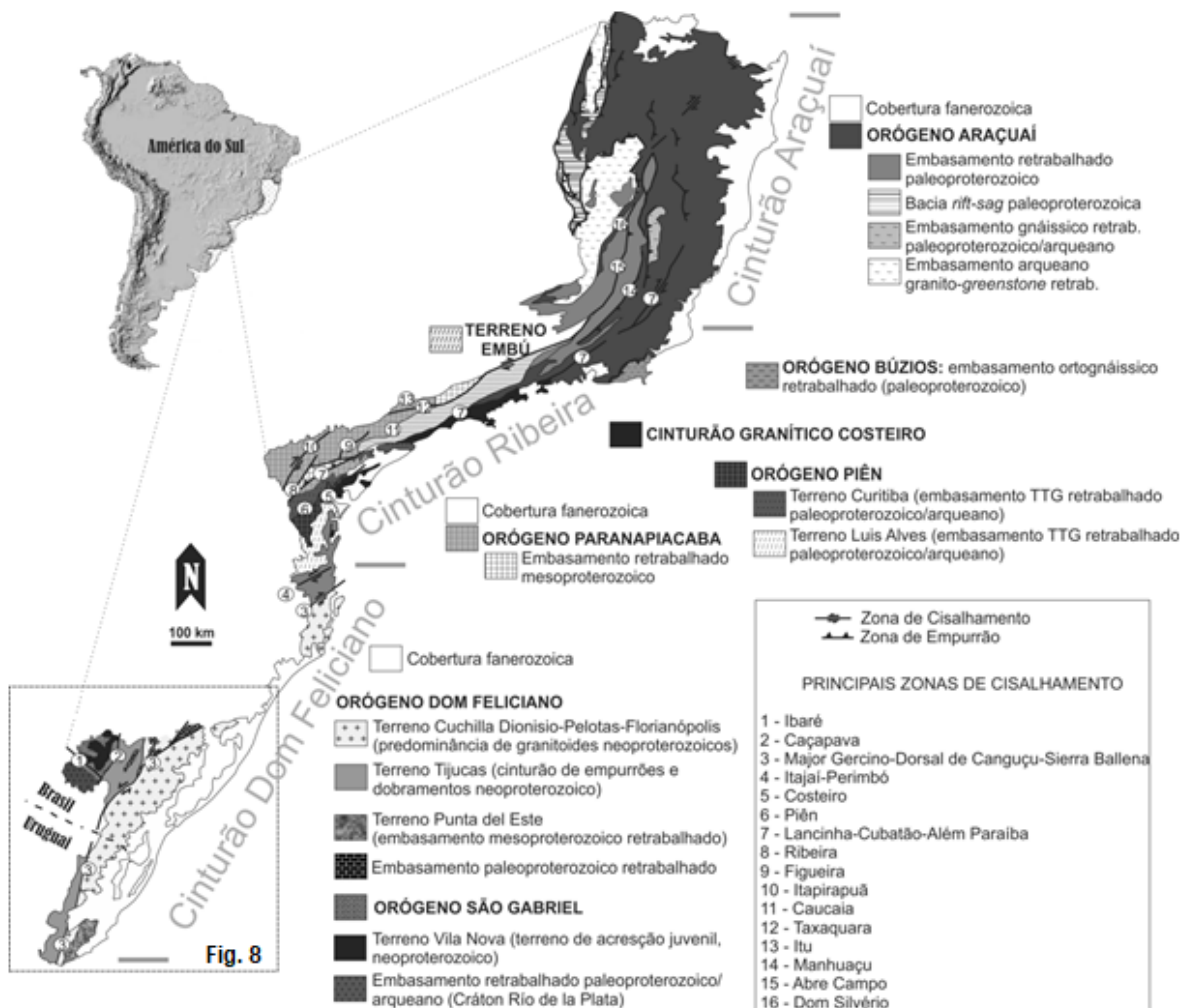
Figura 7- Mapa simplificado dos terrenos e orógenos da Província Mantiqueira (modificado de Silva *et al.*, 2005).

O Cinturão Dom Feliciano é comumente subdividido em três domínios geofísicos principais (Fernandes *et al.*, 1995a, 1995b; Costa, 1997; Lenz *et al.*, 2013; Hartmann *et al.*, 2016): domínio Ocidental (equivalente ao Terreno São Gabriel – Hartmann *et al.*, 2007; Chemale Jr. *et al.*, 2012; aflorante apenas no Escudo Sul-rio-grandense), Central (equivalente ao Terreno Tijucas e bacias Arroyo del Soldado e Camaquã – Chemale Jr. *et al.*, 1995; Hartmann *et al.*, 2007) e Oriental (equivalente ao Terreno Cuchilla Dionísio-Pelotas-Florianópolis e ao Terreno Punta del Este – Preciozi *et al.*, 1999; Bossi & Gaucher, 2004; Basei *et al.*, 2005) (Fig. 8). Esses terrenos, com distintas evoluções crustais, refletem a complexa história geológica desse cinturão durante *ca.* 450 Ma (Philipp *et al.,* 2016a), que comumente pode ser dividida em três estágios principais (Babinski *et al.*, 1997; Silva *et al.*, 2005; Saalmann *et al.*, 2011; Brito-Neves *et al.*, 2014; Philipp *et al.,* 2016a; Lusa *et al.,* 2016; Ramos *et al.,* 2017):

- Brasiliano I (clímax em torno de 900-700 Ma, relacionado às Orogenias Passinho e São Gabriel e ao encerramento do paleo-oceano Charrua-São Gabriel);

- Brasiliano II (clímax em torno de 640-620 Ma, relacionado à Orogenia Dom Feliciano nos domínios Central e Oriental, representado por intenso magmatismo continental e retrabalhamento crustal);

- Brasiliano III (em torno de 595-560 Ma, com geração de magmatismo granítico pré- a sintectônico, relacionado aos eventos colisionais finais do ciclo orogênico Brasiliano-Panafricano e encerramento do paleo-oceano Adamastor).

Os recentes trabalhos de Ramos *et al.* (2018) e Vieira *et al.* (2019) retomam a hipótese relacionada à orogenia denominada como Piratini (Fragoso-César, 1991), relacionada ao encerramento do paleo-oceano Charrua e a convergência entre terrenos paleo-sulamericanos e paleo-africanos. Este último pode representar uma microplaca ou fragmentos do Cráton Kalahari durante a fragmentação do Paleocontinente Rodinia (hipóteses semelhantes são sugeridas por Chemale, 2000; Gaucher *et al.,* 2009; Rapela *et al.,* 2011; Ramos *et al.,* 2017) gerando um arco magmático continental neoproterozoico (*ca.* 780 Ma): o Arco Piratini.
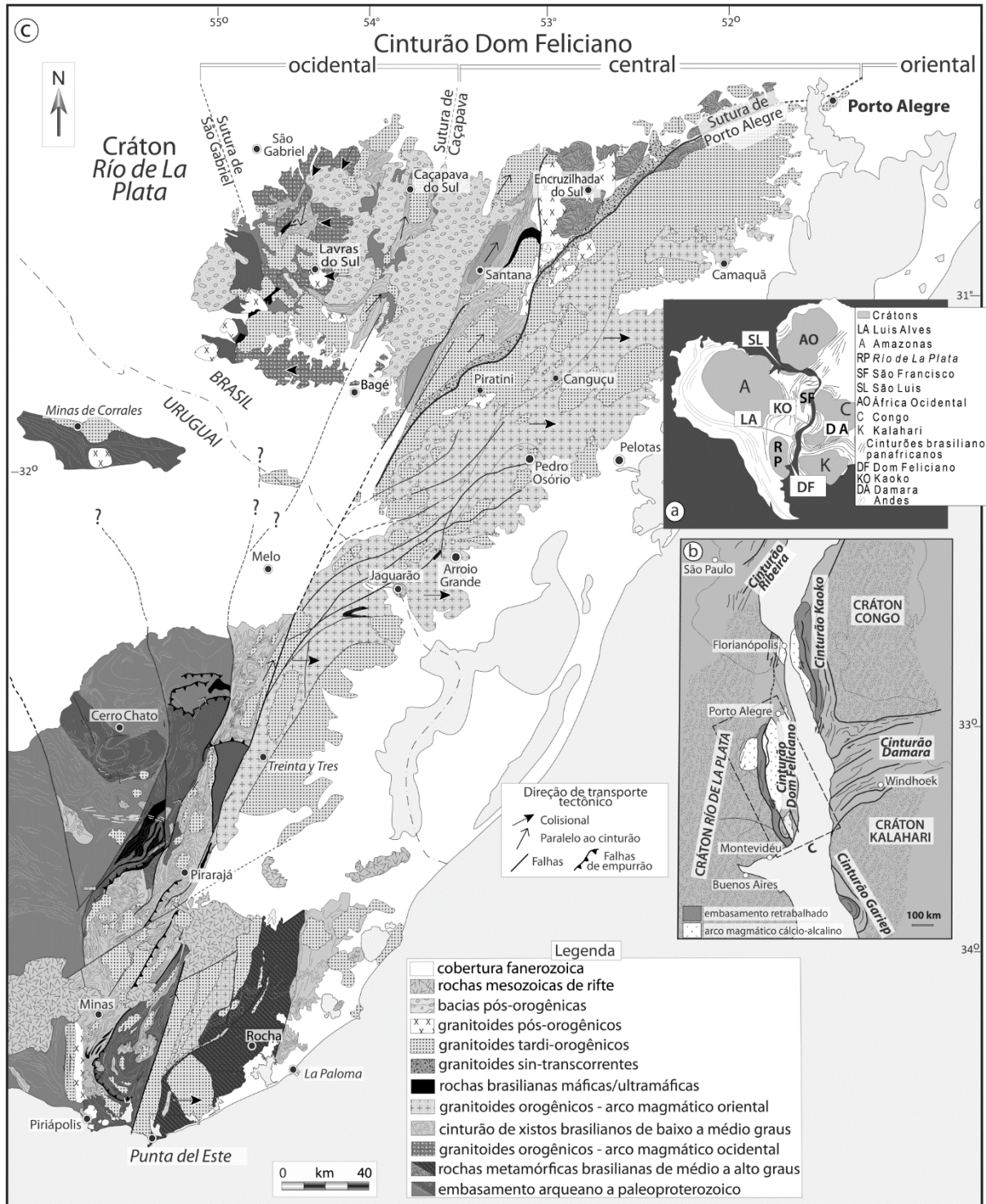
Figura 8 - Esboço geológico do Cinturão Dom Feliciano no Escudo Uruguaio-sul-rio-grandense (modificado de Masquelin *et al.*, 2012). A) Configuração do oeste do supercontinente Gondwana com as principais áreas cratônicas; B) Localização do Cinturão Dom Feliciano e cinturões africanos adjacentes na configuração do supercontinente Gondwana; C) Mapa geológico do Cinturão Dom Feliciano e Cráton Rio de La Plata no sul do Brasil e Uruguai.

2.2 Evolução do conceito e interpretações

O Arco Piratini foi originalmente definido por Fragoso-César (1991) como um arco magmático continental, composto por ortognaisses denominados como Gnaisses Piratini (Fragoso- César *et al.,* 1986), uma associação vulcano-sedimentar conhecida como Cerro da Árvore (Jost & Bitencourt, 1980) e os granitoides do Complexo Pinheiro Machado. Para Fragoso-César (1991) esse arco se desenvolveu durante a orogenia homônima em torno de 885-775 Ma e devido a semelhanças isotópicas (Soliani Jr. 1986), litológicas e estruturais, os Gnaisses Piratini foram correlacionados com os ortognaisses encontrados na região de Encruzilhada do Sul (Fig. 8), no setor central do Cinturão Dom Feliciano.

Essas associações petrotectônicas representariam um arco magmático continental do tipo andino, no qual as unidades plutônicas - ou seja, os ortognaisses em conjunto com os granitoides do Complexo Pinheiro Machado – representariam as raízes desse arco magmático, enquanto as unidades vulcano-sedimentares, por sua vez, representariam porções de uma bacia de *back-arc* (Fig. 9). Tais associações petrotectônicas seriam equivalentes em partes a Associação de Arco Magmático I propostas por Fernandes *et al.* (1995b). A ausência de relações primárias como por exemplo, contatos intrusivos entre o embasamento que constitui o Cráton Rio de La Plata e o Arco Piratini, levou Fragoso-César (1991) a sugerir que essa orogenia foi desenvolvida pela interação entre um bloco continental alóctone (possivelmente uma microplaca) e a placa oceânica Adamastor e após o encerramento do paleo-oceano, o Arco de Piratini colidiu com o Cráton Rio de La Prata. Em outras palavras, para esse autor o sistema orogênico Piratini representaria um grande terreno exótico.
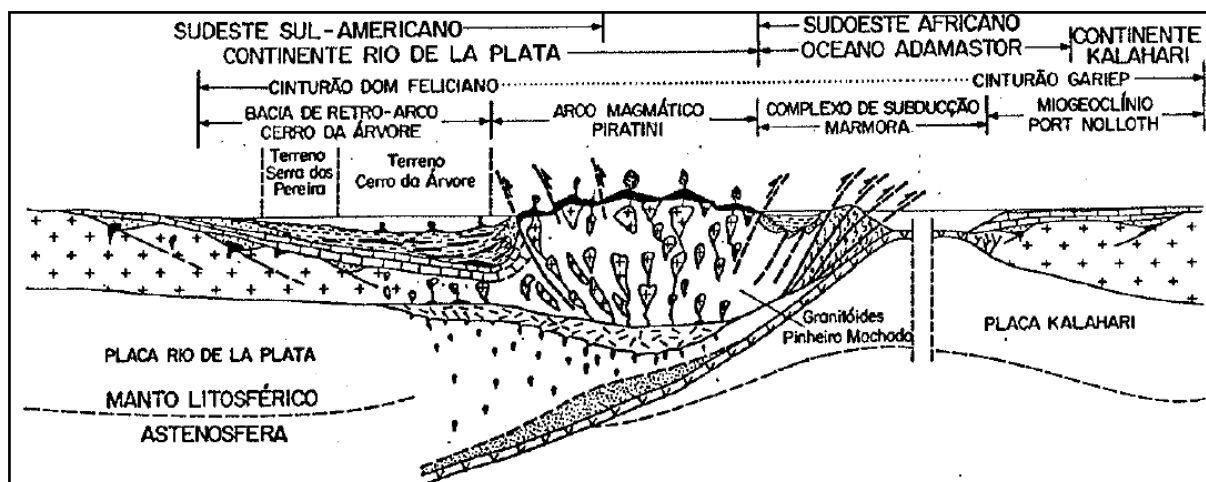
Figura 9 - Desenvolvimento da orogenia Piratini (885-775 Ma). Retirado de Fragoso-César (1991).

Em meados dos anos 90 e 2000 foram desenvolvidos diversos estudos no setor leste do Cinturão Dom Feliciano como, por exemplo Babinski *et al.* (1997), Philipp (1998), Silva *et al.* (1999), Philipp & Machado (2002) e Philipp *et al.* (2002) nos quais foram separados temporalmente os Gnaisses Piratini dos granitoides do Complexo Pinheiro Machado e individualizados em diferentes unidades e contextos geológicos. Os Gnaisses Piratini compreendem ortognaises de composições tonalíticas a granodioríticas que ocorrem como xenólitos métricos nos granitoides do Complexo Pinheiro Machado e da Suíte Intrusiva Dom Feliciano, esta última representando as unidades mais jovens do Batólito de Pelotas (Philipp *et al.,* 2016a).

Os Gnaisses Piratini apresentam assinaturas geoquímicas de arco continental e idades de cristalização de seus protólitos de *ca.* 780 Ma, já as idades de metamorfismo (fácies anfibolito) são de *ca.* 660 Ma (Silva *et al.,* 1999; Tambara *et al.,* 2019). Baseado em semelhanças petrográficas, geoquímicas e geocronológicas, Tambara *et al.* (2019) correlaciona os Gnaisses Piratini com os ortognaisses encontrados no Complexo Metamórfico Cerro Olivo (extremo sul do Cinturão Dom Feliciano, no Uruguai) denominados como Gnaisses Cerro Bori (Masquelin, 2000; Lenz *et al.,* 2011; Masquelin *et al.,* 2012).

Os Gnaisses Cerro Bori são classificados como ortognaisses tonalíticos a granodioríticos e granulitos máficos que se encontram intercalados tectonicamente com as rochas supracrustais da Suíte Metamórfica Chafalote (Masquelin *et al.,* 2012). Os Gnaisses Cerro Bori foram divididos por Lenz *et al.* (2013) em três diferentes associações: (i) Associação do Tipo I composta por gnaisses máficos com afinidade

toleítica e assinatura de magmas relacionados a um ambiente de *back-arc* transicional, (ii) Associação do Tipo II composta por gnaisses tonalíticos, com afinidade cálcio-alcalina e assinatura geoquímica relacionada a ambientes de arco continental e (iii) Associação do Tipo III composta por gnaisses máficos ricos em biotita e características geoquímicas de rochas potássicas a ultrapotássicas correlacionadas a ambientes de margens continentais ativas. Esses autores, com base nas características geoquímicas das diferentes associações e os dados geocronológicos sugeridos por Oyhantçabal *et al.* (2009) e Lenz *et al. (*2011), propuseram um modelo tectônico de evolução dos Ortognaisses Cerro Bori conforme observado na Figura 10.
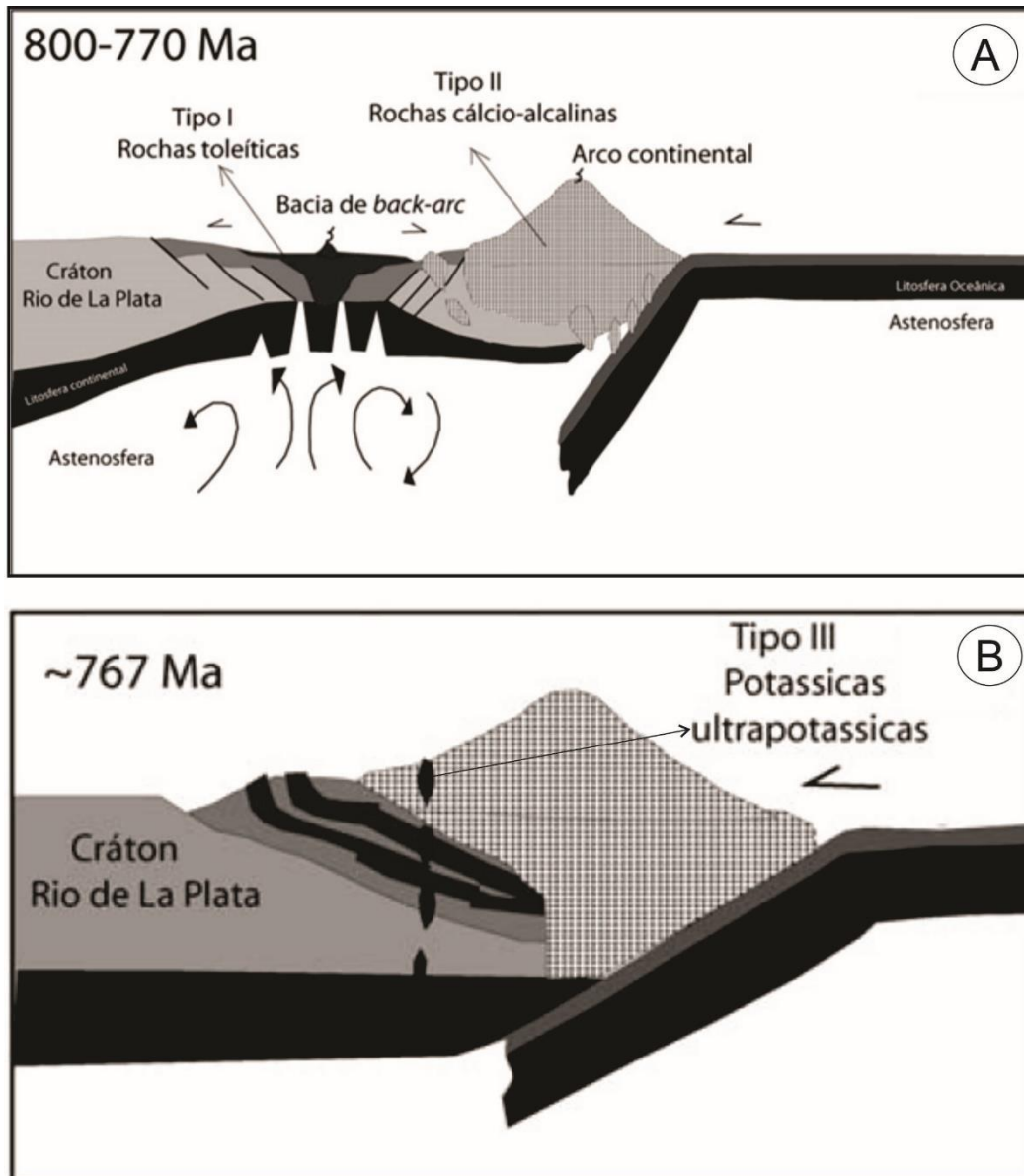
Figura 10- Modelo tectônico de evolução dos Ortognaisses Cerro Bori entre 800 e 767 Ma. A) Modelo de ambiente tectônico entre 800-770 Ma para os gnaisses do Tipo I e II; B) Modelo de ambiente tectônico em torno de 767 Ma para as rochas do Tipo III. Modificado de Lenz *et al.* (2013).

Os Gnaisses Cerro Bori mostram idade de cristalização dos protólitos em torno de 800-770 Ma (Oyhantçabal *et al.,* 2009; Lenz *et al.,* 2011; Masquelin *et al.,* 2012), similares às idades ígneas dos Gnaisses Piratini. Enquanto os Gnaisses Piratini foram submetidos a um metamorfismo de fácies anfibolito, os Gnaisses Cerro Bori foram submetidos em partes a condições metamórficas de mais alto grau (fácies anfibólito superior a fácies granulito), que afetaram o Complexo Cerro Olivo. No entanto, sua idade metamórfica é semelhante às sugeridas para os Gnaisses Piratini, em torno de 670-660 Ma (Oyhantçabal *et al.,* 2009; Lenz *et al.,* 2011; Masquelin *et al.,* 2012).

O metamorfismo de alto grau registrado no Complexo Cerro Olivo foi correlacionado por Gross *et al.* (2006; 2009) com o registrado no Complexo Várzea do Capivarita (localizado na região de Encruzilhada do Sul, setor central do Cinturão Dom Feliciano). Com base em estudos petrográficos, geoquímicos, isotópicos (Sr-Nd) e geocronológicos (U-Pb), Martil (2016) e Martil *et al.* (2017) correlacionaram os ortognaisses de ambos os complexos, demonstrando que essas rochas possuem características de orógenos acrescionários com evidências de processos de assimilação de crosta/ contaminação durante a geração do protólito ígneo (como por exemplo zircões herdados de idades paleoproterozoicas, 2,1 Ga), na qual o Complexo Arroio dos Ratos (Gregory *et al.,* 2015) foi apontado como um dos possíveis contaminantes. Os ortognaisses pertencentes ao Complexo Várzea do Capivarita segundo Martil *et al.* (2017) apresentam assinaturas geoquímicas semelhantes a de granitoides relacionados a arcos magmáticos continentais bem como idades de cristalização e metamórfica, respectivamente, de 788 ± 5 e 650 Ma, semelhantes às encontradas nos gnaisses Piratini e Cerro Bori.

Concomitante, Koester *et al.* (2016) mostram um estudo sobre a evolução dos Gnaisses Chácara das Pedras, localizado na região de Porto Alegre (Fig. 8), setor nordeste do Cinturão Dom Feliciano. Estes autores demonstraram que esses gnaisses tonalíticos possuem assinaturas isotópicas e geoquímicas características de arcos magmáticos relacionados à subducção, bem como idades de cristalização e metamórfismo de, respectivamente, 777 ± 4 e 650 Ma. Com base nesses dados, esses autores sugerem uma correlação entre os Ganisses Chácara das Pedras, Piratini e Cerro Bori. Além disso, os autores sugerem assimilação e/ ou contaminação de crosta pretérita com idades paleoproterozoicas (2,1 Ga) possivelmente as rochas do Complexo Arroio dos Ratos – assim como sugerido por Martil *et al.* (2017) para os ortognaisses do Complexo Várzea do Capivarita – durante os processos magmáticos que deram origem aos seus protólitos ígneos. Tal hipótese é corroborada pela presença de xenólitos com idades paleoproterozoicas (2,0 Ga) encontrados nos Gnaisses Chácara das Pedras (Philipp *et al.,* 2016b).

Com base nos trabalhos mencionados, Ramos *et al.* (2017, 2018) retomam e reinterpretam a hipótese original de Fragoso-César (1991), sugerindo que a cerca de 780 Ma os gnaisses,Piratini, Cerro Bori, Chácara das Pedras e Várzea do Capivarita representam os estágios iniciais da evolução do hipotético Arco Piratini ou Arco Arachania (*sensu* Ramos *et al.*, 2017), que se desenvolveu durante a abertura do

paleo-oceano Adamastor e fechamento do paleo-oceano Charrua (Fig. 11). Por sua vez, os granitoides do Complexo Pinheiro Machado que anteriormente eram parte do Arco Piratini (Fragoso-César, 1991) representariam um arco continental mais jovem, denominado como Arco Pinheiro Machado, desenvolvido durante o fechamento do paleo-oceano Adamastor entre *ca.* 640-600 Ma, como sugerido pelos xenólitos, considerado como fragmentos ofiolíticos do Complexo Arroio Grande, encontrados nos granitoides Pinheiro Machado (Ramos & Koester, 2015; Ramos *et al.,* 2017 e 2018).
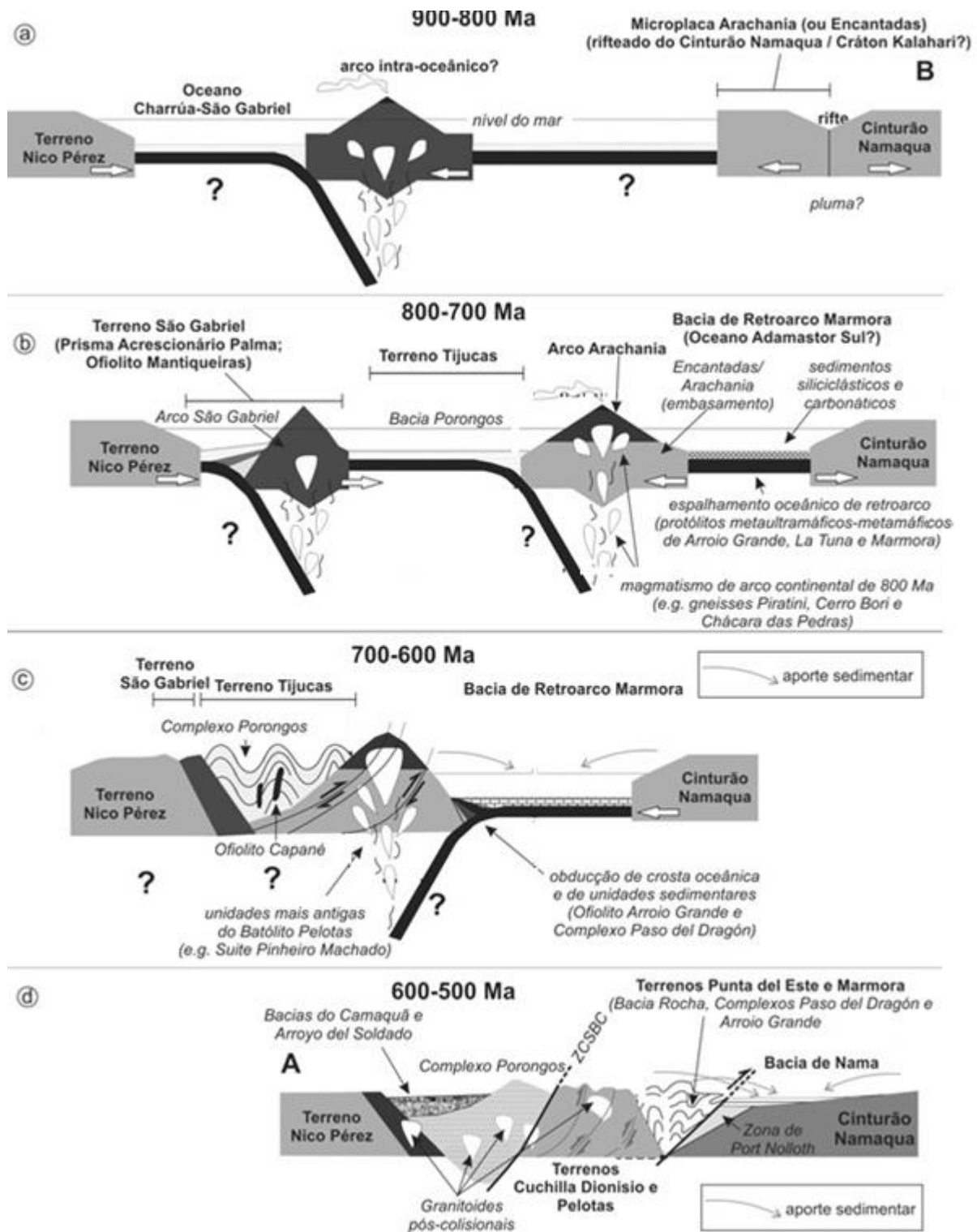
Figura 11- Evolução geodinâmica simplificada (sem escala) do Ofiolito Arroio Grande, modificado de Ramos *et al.* (2017). (a) rifteamento do Cinturão Namaqua, seguido pela (b) abertura da bacia de retroarco Marmora entre esse último e a microplaca; (c) subducção, para oeste, do assoalho oceânico da bacia Marmora sob o arco magmático Piratini/ Arachania (no qual os granitoides de arco do Batólito Pelotas-Aiguá se desenvolveram) e obducção das unidades oceânicas dos complexos Arroio Grande e Paso del Dragón; (d) situação após a colisão tangencial entre o Terreno Nico Pérez/Cinturão Dom Feliciano ocidental (*i.e.* Terrenos São Gabriel e Tijucas) e o Arco Arachania (*i.e.* Terreno Cuchilla Dionisio e Pelotas), encerramento final da bacia de retroarco (Marmora), alojamento do Terreno Marmora sobre a

Zona de Port Nolloth, geração de granitoides pós-colisionais, sedimentação sin-orogênica na Bacia de Nama. Legenda: ZCSBC: zonas de cisalhamento Sierra Ballena e Dorsal de Canguçu.

Diferentemente do Arco de São Gabriel (porção oeste do Cinturão Dom Feliciano), que se desenvolveu na margem oriental do Cráton Rio de La Plata (Lena *et al.,* 2014), cuja evolução está vinculada a um sistema de arco magmático intra-oceânico (Orogenia Passinho, *ca*. 870 Ma) e um sistema de arco continental (Orogenia São Gabriel, *ca*. 750 Ma) conforme sugerido por Saalmann *et al.* (2011) e Philipp *et al.* (2018) para a evolução do Terreno São Gabriel, o Arco Piratini teria se desenvolvido em uma Microplaca relacionada à paleo-África (Ramos *et al.,* 2017, 2018; Vieira *et al.,* 2019a). Essa microplaca é interpretada por esses autores (Koester *et al.,* 2016; Ramos *et al.,* 2017, 2018) como sendo representada pelas rochas do Complexo Encantadas (Chemale, 2000), Complexo Arroio dos Ratos (Gregory *et al.,* 2015) Arachania (Gaucher *et al.,* 2009) e a microplaca Adamastoria (Rapela *et al.,* 2011).

2.3 Suítes Magmáticas do Arco Piratini

O Arco Piratini como mencionado anteriormente é constituído por diferentes fragmentos de ortognaisses, que representariam suas suítes magmáticas, com idades tonianas em torno de 780 Ma (Tab.1) dispersos na porção centro-leste do Cinturão Dom Feliciano conforme mencionado na seção 2.2. Recentemente Vieira *et al.* (2019a) correlacionam o Gnaisse Arroio Pedrado de idade criogeniana em torno de 680 Ma com os fragmentos anteriormente mencionados, interpretando-os como suítes que juntas compõe o Arco Piratini.

Os gnaisses Arroio Pedrado (ou Unidade Cerrito, *sensu* Cruz, 2019) foram descritos por Philipp & Machado (2002) como gnaisses oftalmicos de cor cinza e foliação tectônica marcada pelo alinhamento de porfiroclastos de K-feldspato. Segundo estes autores, tais gnaisses são considerados como "septos do embasamento" expostos na região de Arroio Grande, extremo Sul do Cinturão Dom Feliciano no Brasil.

Tabela 1- Idades dos xenólitos/ *roof pendants*/ fragmentos considerados remanescentes do Arco Piratini, compilados a partir das seguintes fontes: (a) = Silva *et al.* (1999); (b) = Tambara *et al.* (2019); (c) = Koester *et al.* (2016); (d) = Martil *et al.* (2017); (e) = Vieira *et al.* (2019a); (f) = Lenz *et al.* (2011)

Localização	Unidade/ Suíte Magmatica	Litologia	Ocorrência	Afinidade Geoquímica	Idade U-Pb (Ma)	Metodologia	Interpretação
Escudo Sul-rio-grandense	Gnaisses Piratini	Tonalitos e granodioritos. Subordinadamente monzogranito e raros quartzos-dioritos	xenólitos métricos	cálcio-alcalina médio a alto-K	781 ± 5 (a)	SHRIMP	Cristalização
					784 ± 4 (b)	SHRIMP	Cristalização
					2725 ± 28 (b)	SHRIMP	Herança
					664 (b)	SHRIMP	Metamorfismo
	Gnaisses Chácara das Pedras	Granodioritos e monzogranitos. Subordinadamente tonalitos e dioritos	Xenólitos métricos e exposições contínuas	cálcio-alcalina médio a alto-K	777± 3.6 (c)	SHRIMP	Cristalização
					1752 ± 28 (c)	SHRIMP	Herança
					650 (c)	SHRIMP	Metamorfismo
	Gnaisses Várzea do Capivarita	Tonalitos e granodioritos	Lentes métricas e exposições contínuas, intercaladas tectonicamente com paragnaisses	cálcio-alcalina médio a alto-K	788 ± 5.3 (d)	SHRIMP	Cristalização
					1304 ± 20 (d)	SHRIMP	Herança
					648 ± 5 (d)	SHRIMP	Metamorfismo
					790 ± 34 (d)	LA-ICP-MS	Cristalização
					648 ± 18 (d)	LA-ICP-MS	Metamorfismo
	Gnaisses Arroio Pedrado	Monzogranitos	Matacões métricos	Shoshonitíca	680 ± 3 (e)	LA-ICP-MS	Cristalização
					660 ± 3 (e)	LA-ICP-MS	Metamorfismo
					780 (e)	LA-ICP-MS	Herança
Escudo Uruguaio	Gnaisses Cerro Bori	Tonalitos, granodioritos e menores ocorrências de granulitos máficos	Lentes métricas, intercaladas tectonicamente com paragnaisses	Toleítica a cálcio-alcalina médio a alto-K	802 - 767 (f)	SHRIMP	Cristalização
					2084 ± 28 (f)	SHRIMP	Herança
					666 to 673 (f)	SHRIMP	Metamorfismo

Vieira *et al.* (2019a) descrevem os gnaisses Arroio Pedrado como ortognaisses de composição monzogranítica, metaluminosos, com concentrações SiO_2 variando de 59,22 a 65,37% em peso, razões $Na_2O/ K_2O < 1$ e razões Ce/ Yb e Th/ Yb típicas de associações shoshoníticas. Com base em características geoquímicas como, por exemplo, anomalias negativas significativas de Ta e Nb, baixas concentrações de Yb e características isotópicas como razões intermediárias de $^{87}Sr/ ^{86}Sr$ (0,7095-0,7112) e valores negativos de $\varepsilon Nd_{(t)}$ (-3,7 a -4,2), esses autores sugerem que a origem do protolito ígneo estaria relacionada a um magmatismo relacionado à assimilação de crosta pretérita em um ambiente de subducção. Pela semelhança geoquímica e isotópica, bem como um metamorfismo de fácies anfibolito superior em torno de 660 Ma, similar ao registrado nos fragmentos de idades tonianas que compõe o Arco Piratini, levaram Vieira *et al.* (2019a) a correlacionar os Gnaisses Arroio Pedrado com as demais suítes do Arco Piratini, sugerindo uma suíte de afinidade shoshonítica relacionada aos últimos pulsos magmáticos do Arco Piratini, propondo assim uma atividade magmática mínima em torno de 100 Ma para tal evento, semelhante aos arcos contineitais (*e.g.* Paterson & Ducea, 2015).

2.4 Rochas supracrustais e metamorfismo de alto grau relacionadas ao Arco Piratini

A presença de um arco magmático continental de grande magnitude na porção SE do Cinturão Dom Feliciano como sugerido por Fragoso-César (1991), Ramos *et al.* (2017; 2018) e Vieira *et al.* (2019a), levou Vieira *et al.* (2019b) a correlacionar as rochas supracrustais que ocorrem por vezes associadas aos fragmentos do Arco Piratini (*e.g.* Suíte Metamórfica Chafalote) a um ambiente geológico similar ao destes fragmentos. A Suíte Metamórfica Chafalote é caracterizada como uma sequência metamórfica de fácies anfibolito superior a granulítica (assim como parte dos ortognaisses Cerro Bori e Várzea do Capivairita, discutidos anteriormente), composta por metapelitos migmatíticos, semipelitos, granulitos máficos, gnaisses calcissilicáticos e anfibolitos, que ocorrem como *roof-pendants* ou xenólitos no Granodiorito Piriz (Gross *et al.,* 2009; Masquelin *et al.,* 2012) e intercalada tectonicamente com os Gnaisses Cerro Bori, no contexto geológico do Complexo Cerro Olivo (Masquelin, 2000). O Complexo Cerro Olivo compreende três unidades

metamórficas e uma unidade plutônica: (i) os ortognaisses Cerro Bori; (ii) os Gnaisses Centinela, que afloram no Morro Centinela e na Península de Punta del Este, representados por *augens* gnaisses parcialmente fundidos com assinatura geoquímica de arco continental (Masquelin *et al.,* 2012); (iii) a Suíte Metamórfica Chafalote e o (iv) Granodiorito Piriz que representa a única unidade não metamórfica do complexo (Masquelin *et al.,* 2012).

As rochas que compõe esse complexo constituem em parte o embasamento do Terreno Punta del Este (Preciozzi *et al.,* 1999, Peel *et al.,* 2018; Ramos *et. al.,* 2018), a extensão mais ao sul do Cinturão Dom Feliciano. Este terreno em sua definição original (Preciozzi *et al.,* 1999), compreendia as rochas metassedimentares das formações Rocha (Sánchez-Bettucci & Mezzano, 1993) e San Carlos (Masquelin, 1990), e as rochas vulcano-sedimentares da Formação Sierra de Aguirre (Masquelin & Tabó, 1988; Campal & Schipilov, 2005), localizada entre Punta del Este (sul) e Velázquez (norte), onde o sistema de zona de cisalhamento Punta del Este-Alférez-Cordilheira marca aproximadamente o limite entre o Terreno Punta del Este e os batólitos Aiguá-Pelotas (Fragoso-César *et al.,* 1986; Basei *et al.,* 2000; Bossi & Gaucher, 2004; Basei *et al.,* 2011). Peel *et al.* (2018) sugeriram que o Terreno Punta del Este poderia ser estendido mais ao norte próximo a região de Melo (Uruguai), devido à semelhança entre o embasamento gnáissico-migmatítico encontrado na porção sul do Complexo Paso del Dragón e as rochas do Complexo Cerro Olivo. Em Ramos *et al.* (2018) foi proposto que esse terreno estende-se ao norte, até a região de Pedro Osório (sul do Brasil), devido à correlação entre as rochas do Complexo Paso del Dragón (Will *et al.,* 2014; Peel *et al.,* 2018) e as do Complexo Arroio Grande (Ramos *et al.,* 2018). Vieira *et al.* (2019a) reforça essa correlação evidenciando a presença de um embasamento metamórfico com idades metamórficas e assinaturas geoquímicas e isotópicas semelhantes às encontradas em seus pares uruguaios que constituem em partes o embasamento do Terreno Punta del Este.

As rochas metamórficas que compõem o Complexo Cerro Olivo foram afetadas por pelo menos dois eventos deformacionais, denominados como D_1 e D_2 (Masquelin, 2000; Masquelin *et al.,* 2005; Gross *et al.,* 2009). Segundo estes autores o evento D_1, mais antigo, ocorreu sob condições metamórficas de alto grau (fácies anfibolito a granulito), as principais estruturas relacionadas ao evento D_1 indicam uma direção E-W para o transporte tectônico. A deformação D_2 é correlacionada às zonas de cisalhamento transcorrentes com movimentação sinistral e com direção de

transporte NE-SW (Masquelin, 2000), sendo formadas sob condições metamórficas de mais baixo grau. Estudos petrográficos e termobarométricos realizados por Gross *et al.* (2009) na Suíte Metamórfica Chafalote indicaram quatro assembleias metamórficas distintas, onde a primeira assembleia metamórfica M_1 é somente preservada como inclusões nos porfiroblastos da assembleia M_2 que representaria o pico do metamorfismo na região seguido de um evento de descompressão quase isotérmico (M_3). A assembleia metamórfica retrógrada (M_4) é representada por texturas de reação por hidratação e substituição de minerais das assembleias M_2 e M_3. As condições de P-T calculadas por esses autores, para esses diferentes estágios foram de 7-10 kbar e 830-950 ºC (M_2), 4.8-5.5 kbar, 788-830 °C (M_3) e 3-6 kbar e 600-750 °C (M_4). A trajetória P-T calculada por Gross *et al.* (2009) para essas rochas possui sentido 'horário' e incorpora a descompressão quase isotérmica (segmento seguido de menor resfriamento) consistente com uma história de espessamento crustal seguido por colapso extensional.

O metamorfismo registrado pelas rochas desse segmento crustal são correlacionadas por Gross *et al.* (2009) e Skagseth (2016) com o metamorfismo de alto grau (*ca.* 650 Ma) no Terreno Costeiro do Cinturão Kaoko na Namíbia. Com base nos dados de geocronologia que mostram que o metamorfismo de alto grau que afetou essas rochas encontra-se em um intervalo de tempo (660-640Ma) semelhante ao sugerido para o metamorfismo que afetou as suítes do Arco Piratini e dados pré existentes na literatura (como a reinterpretação da Orogenia Piratini- Ramos *et al.,* 2018), Vieira et al. (2019b) correlacionam as rochas supracrustais da Suíte Metamórfica Chafalote ao contexto geológico do Arco Piratini. Esses autores sugerem duas hipóteses principais para a evolução da Suíte Metamórfica Chafalote e os eventos responsáveis pelo metamorfismo de alto grau:

I- O fechamento do paleo-oceano Charrua, com o desenvolvimento do Arco de Piratini entre *ca.* 780 e 660 Ma. Esta última idade representaria o tempo de colisão continental entre o Arco Piratini e a margem leste do Cráton Rio de la Plata (Ramos *et al.,* 2017; Vieira *et al.,* 2019a), gerando o estágio M_2-D_1. Nesta hipótese, o evento colisional é seguido pela descompressão isotérmica pela mudança para um regime extensional em torno de 640-600 Ma, gerando a fusão parcial dos metassedimentos (estágio M_3). Essa mudança de regime estaria relacionada à nucleação de zonas de cisalhamento dúctil (por exemplo, zonas de cisalhamento Dorsal de Canguçu no Brasil, e Sierra Ballena no Uruguai) e granitogênese relacionada e subsequente

tectonismo transcorrente (estágio M_4-D_2). Nesse modelo, os protólitos das rochas metassedimentares da Suíte Metamórfica Chafalote foram depositados em uma bacia do tipo *fore-arc*. Posteriormente, essas rochas foram metamorfizadas durante o evento colisional em *ca.* 660 Ma;

II- II- O fechamento do paleo-oceano Adamastor devido a uma subducção a oeste do Arco Piratini (Ramos *et al.,* 2018). Essa subducção geraria um novo arco magmático, o Arco Pinheiro Machado (Ramos *et al.,* 2018), representado pela suíte intrusiva homônima (*ca.* 630-610 Ma - Babinski *et al.,* 1997; Silva *et al.,* 1999; Cruz, 2019) do Terreno Cuchilla Dionisio-Pelotas (Gaucher *et al.,* 2004). Nesse modelo, os protólitos das rochas metassedimentares da Suíte Metamórfica Chafalote seriam depositados em uma bacia do tipo *back-arc*, antes da subducção, ou em uma bacia do tipo *fore-arc*, durante a subducção. Os protólitos dos granulitos máficos e anfibolitos (esses provavelmente fragmentos de crosta oceânica metamorfisados), por sua vez, representariam porções mais basais dessa bacia, enquanto as rochas metasedimentares do Complexo Arroio Grande (Ramos *et al.,* 2017) e do Complexo Paso del Dragón (Will *et al.,* 2014; Peel *et al.,* 2018) representariam as porções superficiais.

Estes autores assim como diversos outros (Fernandes *et al.,*1992; Masquelin *et al.,* 2005; Gross *et al.,* 2006 e 2009) correlacionam as rochas supracrustais e os eventos tectono-metamórficos de alto grau que ocorreram ao longo da história evolutiva do Complexo Cerro Olivo com as rochas supracrustais e a história evolutiva do Complexo Várzea do Capivarita (Gross *et al.,* 2006; Bom *et al.,* 2014; Martil *et al.,* 2017). Para Vieira *et al.* (2019b) as rochas supracrustais de ambos complexos representariam fragmentos da mesma bacia sedimentar ou, pelo menos, de bacias distintas com evolução deposicional e metamórfica semelhantes.

2.5 Retrabalhamento do Arco Piratini

O Arco Piratini como mencionado nas seções 2.2 e 2.3 é constituído por diferentes fragmentos de ortognaisses com idades entorno de 780-680 Ma dispersos na porção centro-leste do Cinturão Dom Feliciano, que ocorrem em partes como xenólitos e *roof pendants* nos granitoides do terreno Punta del Este e nos granitoides que compõe o Terreno Cuchilla Dionísio-Pelotas-Florianópolis (Bossi & Gaucher,

2004). O Terreno Cuchilla Dionísio-Pelotas-Florianópolis representa uma volumosa granitogênese neoproterozoica (ca. 633-580 Ma) relacionada aos estágios finais do ciclo orogênico Brasiliano/ Pan-Africano (ou Orogênese Dom Feliciano, *sensu* Philipp *et al.,* 2016a). Este terreno compreende um cinturão granítico descontínuo (Basei *et al.,* 2000) subdividido em três grandes batólitos principais: Batólito de Pelotas, no Escudo Sul-rio-grandense; Batólito de Florianópolis, no Escudo de Santa Catarina e o Batólito Aiguá, no Escudo Uruguaio (Fragoso-César *et al.,* 1986, Babinski *et al.,* 1997; Basei *et al.,* 2000; 2011; Oyhantçabal *et al.,* 2009; Passarelli *et al.,* 2010). Esse magmatismo está parcialmente associado ao regime tectônico transpressivo relacionado às etapas finais do Ciclo Orogênico Brasiliano/ Pan-Africano, marcado pela atividade das grandes zonas cisalhamento (Bitencourt & Nardi, 2000; Florisbal *et al.,* 2012; Philipp *et al.,* 2016a; Oriolo *et al.,* 2016).

No Escudo Sul-rio-grandense, a Zona de Cisalhamento Transcorrente Dorsal do Canguçu (ZCTDC) é a principal estrutura tectônica do Cinturão Dom Feliciano. Essa estrutura é correlacionada à Zona de Cisalhamento Transcorrente Major Gercino no escudo catarinense (por exemplo, Fernandes *et al.,* 1992; Fernandes & Koester, 1999; Bitencourt & Nardi, 2000; Florisbal *et al.,* 2012; Oriolo *et al.,* 2016) e alguns autores (Fernandes *et al.* 1992; Fernandes & Koester 1999; Oyhantçabal *et al.,* 2009, 2011b; Passarelli *et al.,* 2010, 2011; Oriolo *et al.,* 2018) sugerem que ambas estão correlacionadas com a Zona de Cisalhamento Transcorrente Sierra Ballena no Escudo Uruguaio. Essas estruturas, juntas, constituem um lineamento descontínuo com mais de 1.000 km de extensão no Cinturão Dom Feliciano (Mantovani *et al.,* 1989; Basei *et al.,* 2000, 2005, 2008; Oyhantçabal *et al.,* 2007, 2010; Passarelli *et al.,* 2011; Oriolo *et al.,* 2016).

Philipp *et al.* (2013, 2016a, 2016b) sugeriram que a colisão oblíqua entre os Crátons Río de La Plata e Kalahari, ocorrida em torno de 650 Ma, produziu grandes volumes de magmas graníticos, resultando na origem de grande parte do Terreno Cuchilla Dionísio-Pelotas-Florianópolis. Segundo esses autores tal colisão levou a formação das grandes zonas de cisalhamento e magmatismo sin-cinemático relacionado, culminando na geração dos granitoides relacionados ao Complexo Pinheiro Machado em torno de 633-609 Ma (Philipp *et al.,* 2003) e granitoides orogênicos tardios (600-580Ma), representados pelas suítes intrusivas Encruzilhada e Dom Feliciano (Philipp *et al.,* 2003).

Os novos dados apresentados por Vieira *et al.* (2019c) mostram idades de U-Pb entre 618-605 Ma para o magmatismo associado à ZCTDC. Essas idades são consistentes com os modelos propostos recentemente (Ramos et al., 2017; Vieira *et al.,* 2019a, 2019b) para a evolução do Cinturão Dom Feliciano e a granitogênese associada onde esses autores sugerem que os desenvolvimentos das grandes zonas de cisalhamento de tendência NE-SW (zonas de cisalhamento transcorrentes Dorsal de Canguçu e Major Gercino) em torno de 620 Ma ocorrem concomitante à geração do Arco Pinheiro Machado (Complexo Pinheiro Machado) este resultante da convergência entre os Crátons Kalahari, Rio de la Plata e Congo, que culminaram no fechamento das bacias orogênicas (por exemplo, bacias de Rocha-Gariep) bem como uma possível reativação das zonas de cisalhamento de tendência NE-SW e geração de magmatismo orogênico tardio em torno de 585 Ma (Ramos *et al.,* 2017; Vieira *et al.,* 2019c).

O volumoso magmatismo relacionado aos estágios finais do ciclo orogênico Brasiliano/ Pan-Africano possui grande participação crustal em sua gênese, evidenciada por diferentes autores com base em estudos geoquímicos, isotópicos e petrologia experimental (Babinski *et al.,* 1997; Silva *et al.,* 1999; 2005; Koester *et al.,* 2001a, 2001b, 2002; Philipp *et al.,* 2002; 2013; 2016c; Vieira *et al.,* 2016). A presença disseminada dos fragmentos do Arco Piratini e rochas supracrustais relacionadas, bem como de fragmentos paleproterozoicos referente ao embasamento, na forma de xenólitos e/ ou *roof pendants* nos granitoides relacionado aos estágios finais do ciclo orogênico Brasiliano/ Pan-Africano (Philipp *et al.,* 2003; Masquelin *et al.,* 2012; Philipp *et al.,* 2016b; Vieira et *al.,* 2019a; Vieira *et al.,* 2019b; Vieira *et al.,* 2019d), sugerem que parte da crosta envolvida na gênese desses granitoides esteja intrinsicamente relacionada à Orogenia Piratini.

O retrabalhamento das rochas originadas durante a Orogenia Piratini está diretamente relacionado com a gênese dos granitoides e metagranitoides peraluminosos que compõem em partes a Suíte Cordilheira (Philipp *et al.,* 2013). A Suíte Cordilheira é constituída por corpos graníticos de forma alongada, segundo a direção preferencial NE-SW, sendo composta pelos metagranitos Arroio Francisquinho e Cordilheira, na região de Encruzilhada do Sul, que possuem colocação sincinemática em relação à Zona de Cisalhamento transcorrente Dorsal de Canguçu e gênese é relacionada à fusão do embasamento metamórfico constituído pelos gnaisses do Complexo Metamórfico Várzea do Capivarita e Arroio do Ratos

(Koester *et al.,* 2001a, b; 2002; Philipp *et al.,* 2013; 2016b; Vieira *et al.,* 2019c). No extremo sudeste do Cinturão Dom Feliciano no Brasil, ocorre a presença do Granito Três Figueiras, que possui colocação sincinemática à Zona de Cisalhamento Arroio Grande, (Klein *et al.,* 2018) e gênese relacionada possivelmente à fusão do embasamento metamórfico da região constituído em partes pelo Gnaisse Arroio Pedrado (Philipp *et al.,* 2013). Já no extremo sudeste do Cinturão Dom Feliciano no Uruguai ocorre a presença do Granodiorito Piriz, que possui sua gênese relacionada à fusão das rochas relacionadas ao Complexo Cerro Olivo (Vieira *et al.,* 2019b). Recentemente na região de Porto Alegre (porção leste do Cinturão dom Feliciano), Vieira *et al.* (2019e) descrevem as primeiras evidencias de magmatismo peraluminoso possivelmente relacionado à fusão dos Gnaisses Chácara das Pedras (Koester *et al.,* 2016).

CAPÍTULO 3

Artigo *"Sr-Nd-Hf isotopic constraints and U-Pb geochronology of the Arroio Pedrado Gneisses, Dom Feliciano Belt, Brazil: A 680 Ma shoshonitic event in the final stages of The Piratini Arc evolution"*

Sr-Nd-Hf isotopic constraints and U-Pb geochronology of the Arroio Pedrado Gneisses, Dom Feliciano Belt, Brazil: A 680 Ma shoshonitic event in the final stages of The Piratini Arc evolution

Daniel Triboli Vieira[a,*], Edinei Koester[b], Rodrigo Chaves Ramos[a], Carla Cristine Porcher[b]

[a] Programa de Pós-Graduação em Geociências, Instituto de Geociências, Universidade Federal do Rio Grande do Sul, PO Box 15001, zip code 91501-970, Porto Alegre, RS, Brazil
[b] Instituto de Geociências, Universidade Federal do Rio Grande do Sul, Bento Gonçalves Avenue, 9500, zip code 91540-000, Porto Alegre, RS, Brazil

ARTICLE INFO

ABSTRACT

In this work we present whole-rock and isotopic (Sr-Nd-Hf) chemistry data and zircon U-Pb geochronology from new occurrences of the Arroio Pedrado Gneisses, located near the Brazil/Uruguay border in the southeastern sector of the Dom Feliciano Belt. These monzogranitic orthogneisses are intermediate, metaluminous, with SiO_2 concentration ranging from 59.22 to 65.37 wt%, Na_2O/K_2O ratios < 1, and Ce/Yb and Th/Yb ratios typical of shoshonitic associations. The studied samples are enriched in large ion lithophile elements (LILE) and light rare earth elements (LREE) relative to high field strength elements (HFSE), resulting in a high LILE/HFSE ratios (La_N/Lu_N ratios between 17 and 33). These features, together with significant negative Ta and Nb anomalies and low Y and Yb concentrations, fit within the characteristics of subduction-related magmatism. The whole-rock isotopic study demonstrates that the samples have intermediate $^{87}Sr/^{86}Sr_{(i)}$ ratios (0.7095–0.7112), negative $\varepsilon Nd_{(t)}$ values (−3.7 to −4.2) and Nd model ages of 1.48–1.61 Ga. The studied zircons have a wide range of $\varepsilon Hf_{(t)}$ values (−13.44 to −15.16), suggesting a crustal influence in their generation. The geochemistry and isotope characteristics indicate that these shoshonites are derived from the partial melting of a thickened lower crust, which was affected by subduction-related fluids/melts. This magma underwent significant fractional crystallization – K-feldspar, plagioclase, biotite, and amphibole, and accessory minerals such as allanite and Fe-Ti oxides – in oxidative conditions during magma ascent. The LA-ICP/MS U-Pb zircon dating reveals that the Arroio Pedrado Gneisses were emplaced during the Cryogenian, as suggested by a concordia age of 680 ± 2.9 Ma interpreted as the igneous protolith crystallization age. The metamorphic age of 660 ± 2.8 Ma (zircon rims) is interpreted as the amphibolite-facies peak which marks an early collisional event during the convergence of the Río de la Plata Craton and African-related terranes. The Arroio Pedrado Gneisses are here interpreted as representing the latest magmatic event in the construction of the allochtonous Andean-type Piratini Arc, whose evolution is constrained between ca. 780 (initial magmatism) and 650 Ma (continental collision) during the West Gondwana assembly.

1. Introduction

The West Gondwana assembly (Fig. 1A) led to the development of several orogenic belts during the Precambrian to Early Cambrian Brasiliano/Pan-African orogenic cycle (e.g. Heilbron et al., 2004; Gray et al., 2008). In South Brazil and Uruguay, the Mantiqueira Province (Almeida et al., 1981) comprises a series of mobile belts resulting from the convergence of paleo-African and paleo-South American terranes. Its southernmost sector, i.e., the Dom Feliciano Belt (e.g. Fragoso-César, 1980, 1991; Fernandes et al., 1995a, 1995b; Hueck et al., 2018),

records a complex history involving the development of multiple magmatic arcs during the convergence of, at least, three cratons (Río de la Plata, Kalahari, Congo) and minor blocks/microplates (Fig. 1B).

The magmatic arcs developed during the Dom Feliciano Belt evolution are linked to four orogenies: Passinho (Tonian – Leite et al., 1998), São Gabriel (Tonian to Cryogenian – Hartmann et al., 2011; Philipp et al., 2018), Piratini (Tonian to Cryogenian – Fragoso-César, 1991) and Dom Feliciano Orogeny (Cryogenian to Ediacaran – Chemale, 2000; Silva et al., 2005; Hartmann et al., 2007). Recently, a new hypothesis for the Piratini Orogeny was proposed (Ramos et al.,
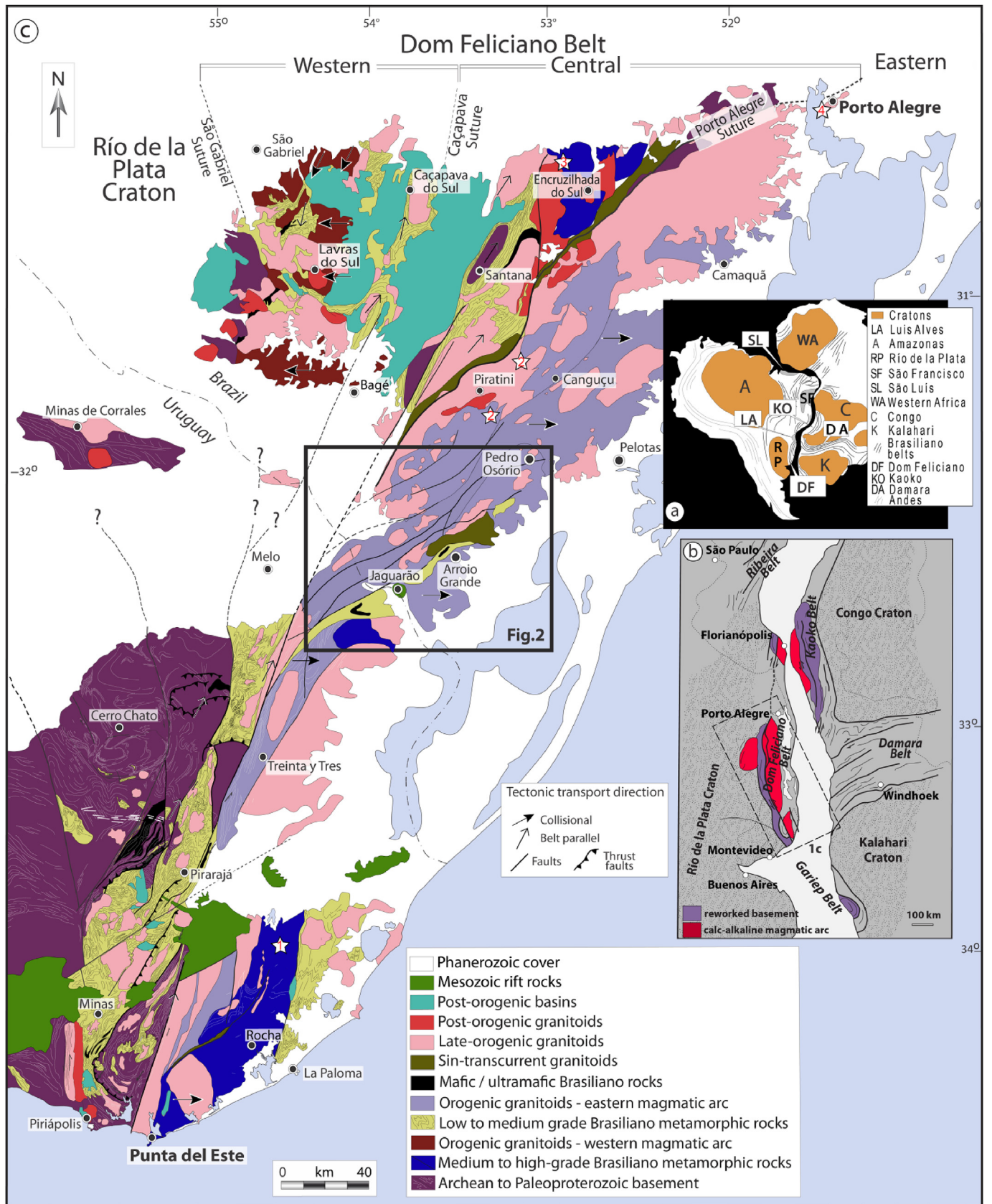
Fig. 1. Geological context of the Dom Feliciano Belt in the Uruguayan-sul-rio-grandense Shield (modified from Masquelin et al., 2012) – A) Simplified map of the West Gondwana, showing the distribution of main cratons and mobile belts; B) Location of Dom Feliciano Belt and related African belts in the West Gondwana; C) Geologic map of Dom Feliciano Belt and Río de la Plata Craton in southernmost Brazil (Rio Grande do Sul State) and easternmost Uruguay, showing the study area presented in Fig. 2 (black square). White star symbols represent the location of the ca. 780 Ma fragments/xenoliths regarded as remnants of the Piratini Arc: 1 = Cerro Bori Gneisses; 2 = Piratini Gneisses; 3 = Várzea do Capivarita Orthgneisses; 4 = Chácara das Pedras Gneisses.

2018), in which a long-lived Andean-type magmatic arc – the Piratini Arc – was developed as the result of the closure of the Charrua paleo-ocean (Fragoso-César, 1991).

The calc-alkaline continental arc magmatism of the Piratini Orogeny would have lasted from ca. 780 (first magmatic pulses) to 650 Ma (continental collision). Fragments of this arc would be represented by ca. 780 Ma orthogneisses which constitute the basement of the eastern sector of the Dom Feliciano Belt in southernmost Brazil – e.g., Piratini Gneisses (Silva et al., 1999; Tambara, 2015), Chácara das Pedras Gneisses (Philipp and Campos, 2004; Koester et al., 2016), Várzea do Capivarita Complex (Frantz et al., 1984; Martil et al., 2017) – and Uruguay – e.g., Cerro Bori Gneisses (Masquelin, 2000; Lenz et al., 2011, Masquelin et al., 2012) (Fig. 1C). Recently (Vieira et al., 2016a), new occurrences of orthogneisses were found in the southeasternmost Dom Feliciano Belt, near the Brazil/Uruguay border, named Arroio Pedrado Gneisses (Philipp and Machado, 2002). These rocks are regarded as basement, since they are found as xenoliths within supracrustal Brasiliano granitoids.

The geochemical and isotopic studies of such metamorphic xenoliths and fragments found within granitoids lead to a better understanding of the evolution of these Precambrian orogenic belts and related magmatic arcs, from their pre-collisional events to the late stages of continental collision (e.g., Ramos, 2010; Couzinié et al., 2016; Moyen et al., 2017). In pre-collisional stages, the composition of the magma is influenced by subduction-related features such as mantle enrichment by fluid/sediment input and slab melting. On the other hand, in late-to post-collisional stages, slab break-off and lithosphere delamination modify and/or generate magmas by new episodes of deep crust/mantle-derived melts, so that the same magmatic arc can show different compositions during its space-time evolution (e.g., Gill, 2010; Condie, 2015). Starting from these premises, in the present paper we present new geochemical and isotopic data that provide insights on the evolution of the Arroio Pedrado Gneisses. This work aims to investigate the relations between these rocks and other metamorphic xenoliths and fragments of the basement found in the easternmost Dom Feliciano Belt, regarded as possible remnants of the Piratini Orogeny.

2. Geological overview

In the Uruguayan-sul-rio-grandense Shield, the Dom Feliciano Belt is commonly subdivided into three main tectonic domains, based on geophysical features and petrotectonic associations: Western, Central and Eastern Domain (Fig. 1C). The Western Domain, bounded to the west by the Río de la Plata Craton, comprises the São Gabriel Terrane (Chemale, 2000; Hartmann et al., 2007), which was formed during the São Gabriel Orogeny (850-680 Ma) (e.g., arc-related gneisses and metagranitoids of the Cambaí Complex) as result of the closure of the Charrua Ocean (e.g., Palma Accretionary Complex ophiolites) (Silva et al., 2005; Hartmann et al., 2011; Saalmann et al., 2011; Philipp et al., 2016a). The Central Domain comprises the Tijucas and Encruzilhada Terranes. The Tijucas Terrane corresponds to a fold and thrust belt constituted by ca. 780 Ma metavolcanic (e.g. Porcher et al., 1999; Chemale, 2000) and metasedimentary rocks (Archean to Neoproterozoic sources) (e.g. Saalmann et al., 2006; Gruber et al., 2016; Pertille et al., 2017; Höfig et al., 2018) and shows a peak metamorphism (amphibolite facies) at around 658 ± 26 Ma (Lenz, 2006). This metamorphism is regarded as a consequence of a W-directed continental collision event (Battisti et al., 2018). The basement is constituted by the Paleoproterozoic Encantadas Gneisses (Hartmann and Chemale, 2003; Philipp et al., 2008). Oceanic mantle and crust slices, possibly related to the Charrua Ocean, are found in this terrane, represented by the Capané Ophiolite (Marques et al., 2003; Arena et al., 2018). The Encruzilhada Terrane is constituted by Paleoproterozoic basement rocks (the ca. 2.1 Ga Arroio dos Ratos Complex; e.g. Gregory et al., 2011; Gregory et al., 2015) and Neoproterozoic gneisses occurring as xenoliths in Brasiliano granitoids (e.g. Hartmann et al., 1999; Gregory et al., 2015;

Philipp et al., 2016a; Martil et al., 2017).

The Eastern Domain, in which the studied orthogneisses crop out, comprises the Cuchilla Dionisio-Pelotas (Bossi and Gaucher, 2004; Wildner et al., 2005) and Punta del Este Terranes (Preciozzi et al., 1999; Basei et al., 2005). The Cuchilla Dionisio-Pelotas Terrane is characterized by a granitic belt known as the Aiguá-Pelotas Batholith (Silva et al., 1999, 2005; Basei et al., 2000, 2011; Bossi and Gaucher, 2004; Gaucher et al., 2008; Oyhantçabal et al., 2009) and minor occurrences of metamorphic xenoliths/fragments and roof pendants regarded as basement (e.g. Philipp and Machado, 2002). The older granitoids are found in the Pinheiro Machado Complex, which show a subduction-related geochemical fingerprint and magmatic ages around 630 and 610 Ma (Philipp, 1990; Babinski et al., 1997; Loureiro et al., 2015).

The development of these continental arc-related batholiths (i.e., the granitoids found today in the Cuchilla Dionisio-Pelotas Terrane) might be attributed to a westward subduction of the South Adamastor paleo-ocean underneath paleo-South America (e.g., Porada, 1989; Fragoso-César, 1991; Germs, 1995; Frimmel et al., 1996; Chemale, 2000; Diener et al., 2017; Ramos et al., 2018). Recent hypotheses, such as those of Ramos et al. (2018), suggest that the South Adamastor oceanic plate subducted underneath an exotic terrane, constituted by a Paleo-to Mesoproterozoic basement (which might represent an African-related microplate or block, splintered from the Congo and/or Kalahari Cratons during Rodinia break-up; see similar hypotheses in, e.g., Chemale, 2000; Gaucher et al., 2009; Rapela et al., 2011) and a Neoproterozoic continental magmatic arc which was developed during the Piratini Orogeny: the Piratini Arc.

2.1. The Piratini Arc

The Piratini Arc was originally defined by Fragoso-César (1991) as a continental magmatic arc, comprising orthogneisses (the Piratini Gneisses), a volcanosedimentary association known as Cerro da Árvore, and granitoids of the Pinheiro Machado Complex (Jost and Bitencourt, 1980). For Fragoso-César (1991) this arc developed during the homonymous orogeny at around 885-775 Ma. Due to isotopic, lithological, and structural similarities, the tonalitic to granodioritic orthogneisses of the Piratini Arc were correlated to those found in the Encruzilhada do Sul region, in the central sector of the Dom Feliciano Belt (Fig. 1C). These petrotectonic associations would represent an Andean-type orogenic system, in which the plutonic units – i.e., the Piratini Gneisses and the granitoids of the Pinheiro Machado Complex – would represent the roots of the magmatic arc. The volcanosedimentary units, in turn, would represent a back-arc basin.

The absence of primary relationships between the Río de la Plata Craton and the Piratini orogenic system (e.g., intrusive contacts) led Fragoso-César (1991) to suggest that this orogeny was developed by the interaction between an allochthonous continental block (possibly a microplate) and the Adamastor oceanic plate. Following the closure of the latter paleo-ocean, the Piratini Arc collided with the Río de la Plata Craton. In other words, the Piratini orogenic system would represent a large exotic terrane.

The rocks from both Piratini Gneisses and Pinheiro Machado Complex were individualized in later works, such as those of Silva et al. (1995, 1999), Philipp (1998), Philipp and Machado (2002), Philipp et al. (2002), Loureiro (2013), Loureiro et al. (2015) and Tambara (2015). The Piratini Gneisses (Fig. 1C) comprise tonalitic to granodioritic orthogneisses, which occur as meter-sized xenoliths in granitoids of both Pinheiro Machado Complex and Dom Feliciano Intrusive Suite – the latter representing the younger units of the Aiguá-Pelotas Batholith. These gneisses show continental arc geochemical signatures, protolith crystallization ages of ca. 780 Ma and metamorphic ages of ca. 660 Ma (amphibolites facies) (Silva et al., , 1999; Tambara, 2015). Based on petrographic, geochemical and isotopic similarities, the latter author correlates the Piratini orthogneisses with those found in the high grade Cerro Olivo Complex (Masquelin, 2000; Lenz et al., 2011)

(southernmost sector of the Dom Feliciano Belt in Uruguay), known as Cerro Bori Gneisses.

The Cerro Bori Gneisses (Fig. 1C) comprise tonalitic to granodioritic orthogneisses and mafic granulites which are tectonically interleaved with metasedimentary rocks of the Chafalote Metamorphic Suite (Masquelin et al., 2012; Lenz et al., 2012). The Cerro Bori Gneisses also show a continental arc geochemical signature, similar to that of the Piratini Gneisses. The crystallization age of the protoliths are also similar, constrained at around 800-770 Ma (Oyhantçabal et al., 2009; Lenz et al., 2011, 2012; Masquelin et al., 2012). Whilst the Piratini Gneisses underwent amphibolite facies metamorphism, those of the Cerro Bori underwent a higher grade condition (upper amphibolite-to granulite facies), which affected the Cerro Olivo Complex as a whole. However, its metamorphic age is similar to that of the Piratini Gneisses, constrained at around 670-660 Ma, together with a partial melting event recorded at around 650-640 Ma (Lenz et al., 2011).

The high P-T metamorphism of the Cerro Olivo Complex was correlated to that found in the Várzea do Capivarita Complex (Fig. 1C), located in the Encruzilhada Terrane, central sector of the Dom Feliciano Belt (Gross et al., 2006, 2009). Based on petrological, geochemical, isotopic (Sr-Nd), and geochronological (U-Pb) similarities, Martil (2016) and Martil et al. (2017) correlated the migmatites, ortho- and paragneisses from both complexes, demonstrating that these rocks show characteristics of accretionary orogens, yielding Paleo-to Mesoproterozoic T_{DM} and strong evidence of processes such as crustal assimilation/contamination during the protolith generation, in which the Paleoproterozoic Arroio dos Ratos Complex could be a possible contaminant. These rocks were interpreted as the expression of the same magmatic event or, alternatively, as fragments of the roots of very similar continental magmatic arcs (Martil et al., 2017). It is noteworthy that the Várzea do Capivarita orthogneisses yield crystallization and metamorphic ages of, respectively, 788 ± 5 and 650 Ma (Martil, 2016), which are very similar to those found in the above mentioned Piratini and Cerro Bori Gneisses.

Concomitantly, Koester et al. (2016) show a new study regarding the evolution of the Chácara das Pedras Gneisses (Fig. 1C), located in the northeasternmost sector of the Dom Feliciano Belt in the Uruguayan-sul-rio-grandense Shield. The latter authors demonstrated that these tonalitic orthogneisses show subduction-related magmatic arc signatures and yield crystallization and metamorphic ages of, respectively, 777 ± 4 and 650 Ma. Based on these similarities, these authors suggest a correlation between the Chácara das Pedras, Piratini and Cerro Bori Gneisses. Furthermore, the authors suggest crustal assimilation of Paleoproterozoic contaminants during the magmatic processes – possibly, rocks from the Arroio dos Ratos Complex, as also suggested for the Várzea do Capivarita orthogneisses –, a hypothesis that was strengthened by the ca. 2.1 Ga xenoliths found within the Chácara das Pedras Gneisses (Philipp et al., 2016b).

Based on the latter works, Ramos et al. (2017, 2018) revive and reinterpret the original hypothesis of Fragoso-César (1991), suggesting that the ca. 780 Ma orthogneisses mentioned above – i.e., Piratini, Cerro Bori, Chácara das Pedras and Várzea do Capivarita Orthogneisses – might represent the initial stages of the evolution of the hypothetical Piratini Arc (Table 1), which would have developed during the closure of the Charrua paleo-ocean. In turn, the granitoids of the Pinheiro Machado Complex would represent a younger continental arc, named Pinheiro Machado Arc, developed during the closure of the Adamastor paleo-ocean between ca. 640-600 Ma, as suggested by xenoliths, regarded as ophiolitic fragments of the Arroio Grande Complex (Fig. 2), found in Pinheiro Machado granitoids (Ramos and Koester, 2015; Ramos et al., 2017, 2018).

Differently from the São Gabriel Arc (westernmost Dom Feliciano Belt), developed on the eastern margin of the Río de la Plata Craton (e.g., Lena et al., 2014) and whose evolution is linked to an intra-oceanic arc system (Passinho Orogeny, ca. 870 Ma) and a continental arc system (São Gabriel Orogeny, ca. 750 Ma) – see hypotheses for the

evolution of the São Gabriel Terrane in, e.g., Saalmann et al. (2011) and Philipp et al. (2018) –, the Piratini Arc would have developed on an African-related microplate (Ramos et al., 2017, 2018). The latter would be represented by the Encantadas (Chemale, 2000), Arachania (Gaucher et al., 2009) and/or Adamastoria microplates (Rapela et al., 2011), regarded as African-related blocks/microplates accreted in the Dom Feliciano Belt during the Brasiliano/Pan-African events (see the Adamastoria hypothesis in Rapela et al., 2011). In other words, the Piratini Arc would be developed on the basement of both Cuchilla Dionisio-Pelotas and Punta del Este Terranes.

In this model, the development of the Piratini Arc is synchronous to the opening of a back-arc system which led to the development of the South Adamastor Ocean. Since the Piratini Arc fragments are located mostly west of the South Adamastor remnants (e.g., Arroio Grande-Paso del Dragón Complex in Dom Feliciano Belt; Marmora Terrane in Gariep Belt), the subduction is supposed to be eastward, related to the closure of the older Charrua Ocean underneath paleo-African terranes. Ramos et al. (2018) also suggest that the Piratini Arc remnants (from now on, referred as "suites" of the Piratini Arc, assuming the hypothesis of a comagmatic origin for these orthogneisses) differ from the granitoids of the Damara Orogen (Namibia) which, despite the similar magmatic ages (around 800-750 Ma), were formed in an extensional environment (crustal thinning, intracontinental rifting), possibly during the evolution of the Pan-African rifts (e.g. Jung et al., 2007; Konopásek et al., 2008; Frimmel, 2018).

2.2. Local geology

The studied Arroio Pedrado Gneisses are regarded as fragments of the basement of the Arroio Grande Complex region, recently considered as the Brazilian extension of the allochtonous Punta del Este Terrane (see Peel et al., 2018; Ramos et al., 2018), comprising the area east of the Ayrosa Galvão Shear Zone (Fig. 2) (NE-SW, high-angle, ductile; Machado et al., 1995). This region, also known as the Southeastern Domain (Ramos et al., 2014), comprises a gneiss-migmatitic basement – also considered as the Metagranitoid Domain of the Pinheiro Machado Complex (Trainini, 1987; Wildner et al., 2005) or as the Erval Intrusive Suite (Philipp, 1998) –, the ca. 800-650 Ma oceanic rocks of the Arroio Grande Complex (Ramos et al., 2018) – correlatable to the Paso del Dragón Complex in Uruguay –, and post-collisional Brasiliano granitoids with magmatic ages of ca. 580 Ma.

The most representative granitoids in the region comprise the Capão do Leão, Três Figueiras and Chasqueiro granites. The Três Figueiras (Philipp et al., 2013; Klein et al., 2018) is a peraluminous leucogranite emplaced along the Arroio Grande Shear Zone – an E-W bifurcation of the Ayrosa Galvão Shear Zone –, with magmatic ages of ca. 585 Ma. The Capão do Leão monzogranite (ca. 583 Ma) has metaluminous affinity and presence of garnet as main mineral phase and centimeter-sized miarolitic cavities (Philipp et al., 2002). The ca. 574 Ma Chasqueiro granite (Vieira et al., 2016b) is a high-K calc-alkaline porphyritic monzo-to syenogranite. The Arroio Pedrado Gneisses are found as meter-sized xenoliths in the latter Três Figueiras and Chasqueiro granites (Fig. 2).

The Arroio Pedrado Gneisses were described by Philipp and Machado (2002) as light gray augen gneisses, with metamorphic foliation marked by K-feldspar porphyroclasts. Since they are regarded as the basement of the Arroio Grande region, Vieira et al. (2016a) suggested that these rocks could be correlatable to other basement fragments found in the eastern sector of the Dom Feliciano Belt, which, as previously mentioned, would be related to the Piratini Arc.

Vieira et al. (2016a) obtained a crystallization age of ca. 680 Ma for the Arroio Pedrado Gneisses, which is within the timeframe of the subduction-related magmatism of the Piratini Arc so that, in the present paper, we aim to answer two main questions: what is the relation between the Arroio Pedrado Gneisses and the older (ca. 780 Ma) Piratini Arc suites? Could these rocks be regarded as the final magmatic events

Table 1
Ages of the xenoliths/fragments regarded as remnants of the hypothetical Piratini Arc, compiled from the following sources: (a) = Silva et al. (1999); (b) = Tambara (2015); (c) = Koester et al. (2016); (d) = Martil et al. (2017); (e) = Lenz et al. (2011). See location in Fig. 1C (white star symbols).

Location	Unit	Rock type	Occurrence	U-Pb zircon age (Ma)	Method	Interpretation
Sul-rio-grandense Shield (Brazil)	Piratini Gneisses	Tonalites and granodiorites. Subordinated monzogranites and rare quartz-diorites	Meter- to decameter-sized xenoliths	781 ± 5 (a)	SHRIMP	Crystallization
				784 ± 4 (b)	SHRIMP	Crystallization
				2725 ± 28 (b)	SHRIMP	Inherited
				664 (b)	SHRIMP	Metamorphism
	Chácara das Pedras Gneisses	Granodiorites and monzogranites. Subordinated tonalites and diorites	Meter-sized xenoliths and kilometer-sized continuous exposures	777 ± 3.6 (c)	SHRIMP	Crystallization
				1752 ± 28 (c)	SHRIMP	Inherited
				650 (c)	SHRIMP	Metamorphism
	Várzea do Capivarita Gneisses	Tonalites and diversified granitoids	Meter-sized lenses, tectonically interleaved with paragneisses	788 ± 5.3 (d)	SHRIMP	Crystallization
				1304 ± 20 (d)	SHRIMP	Inherited
				648 ± 5 (d)	SHRIMP	Metamorphism
				790 ± 34 (d)	LA-ICP-MS	Crystallization
				648 ± 18 (d)	LA-ICP-MS	Metamorphism
Uruguayan Shield	Cerro Bori Gneisses	Tonalitic, granodioritic and sienitic gneisses. Minor occurrences of mafic granulites and mafic gneisses	Meter-sized lenses, tectonically interleaved with paragneisses	802 to 767 (e)	SHRIMP	Crystallization
				2084 ± 28 (e)	SHRIMP	Inherited
				666 to 673 (e)	SHRIMP	Metamorphism
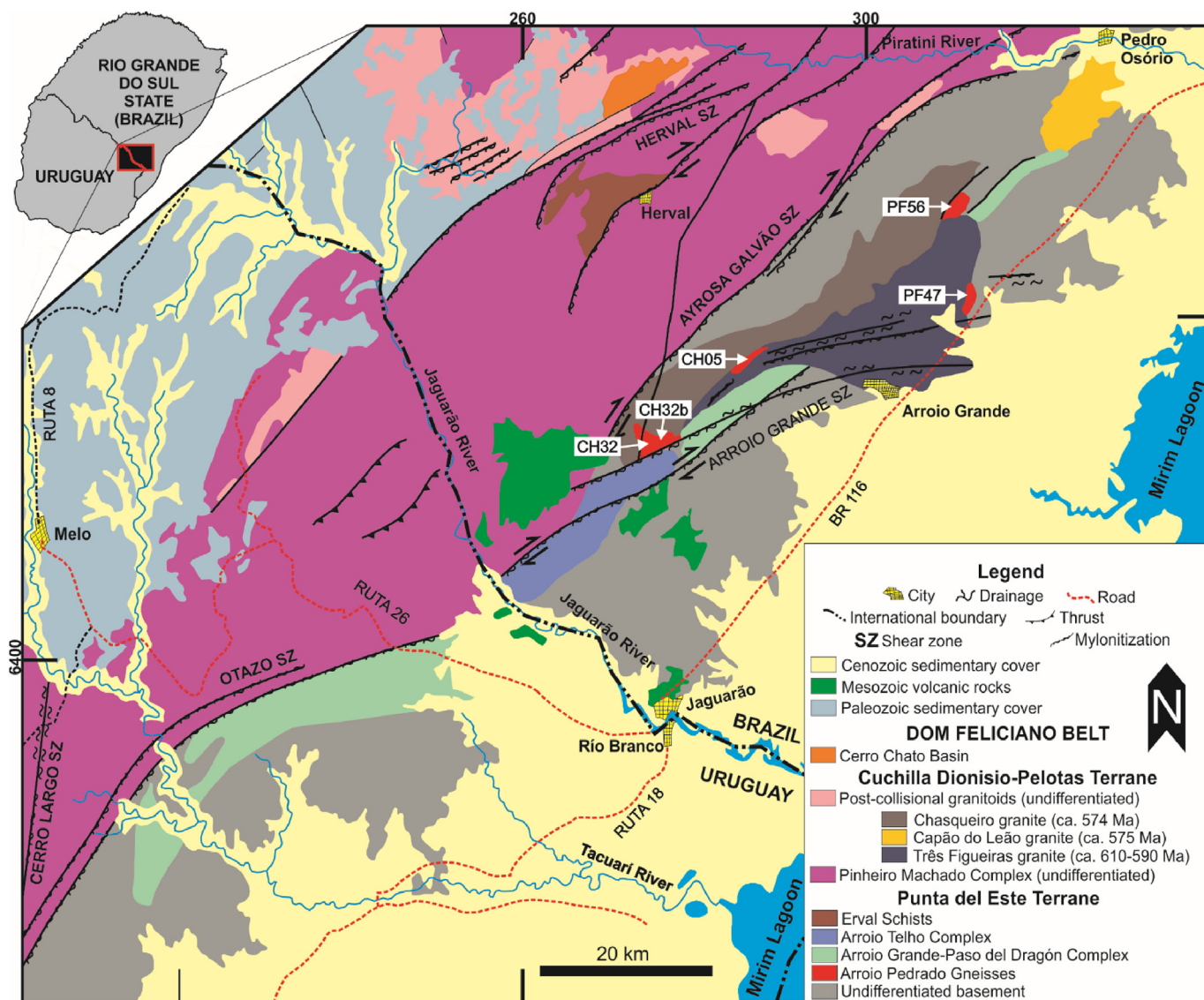
Fig. 2. Geological map of the Cuchilla Dionisio-Pelotas and Punta del Este terranes near Brazil/Uruguay border (modified from Ramos et al., 2018). White arrows indicate the location of the studied samples.
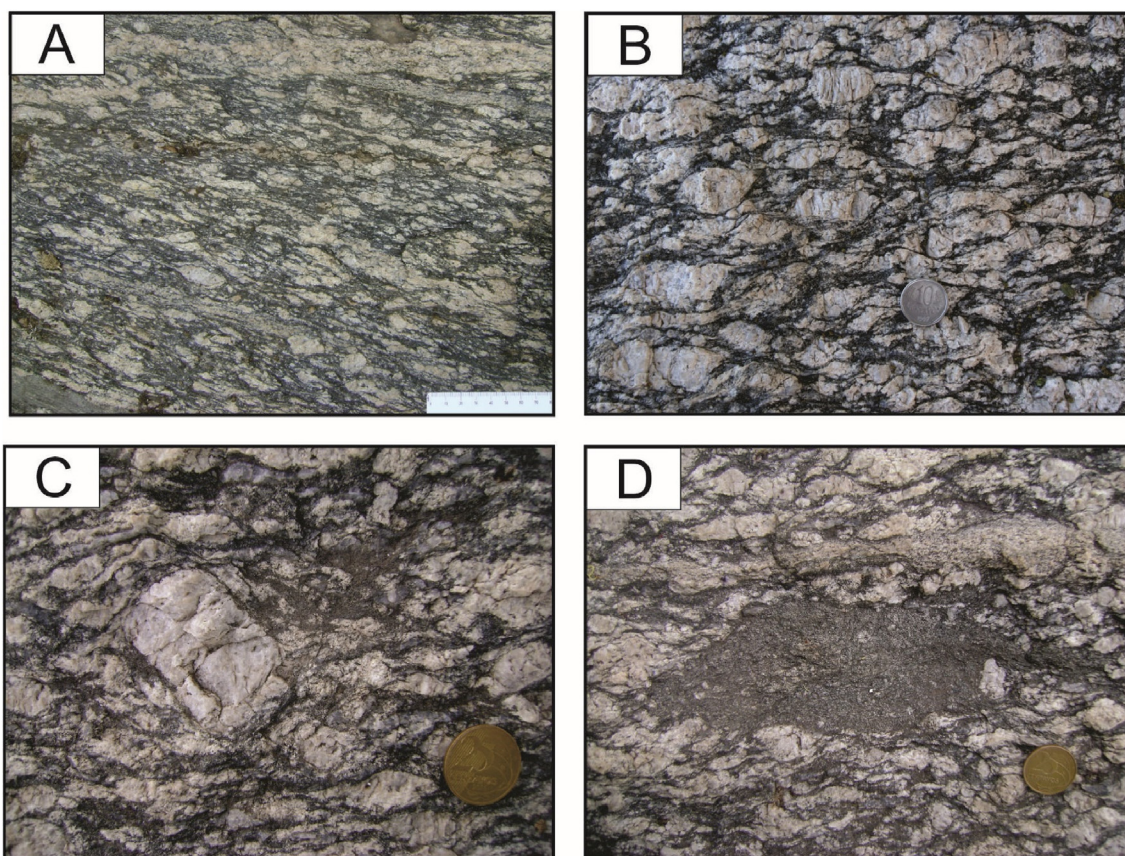
Fig. 3. Macroscopic features of the Arroio Pedrado Gneisses – (A) Discontinuous and incipient mm-thick banding, and parallel subvertical tectonic foliation; (B) Tectonic foliation marked by elongated K-feldspar porphyroclasts and biotite; (C) Detail of relic igneous K-feldspar phenocryst; (D) Centimeter-sized microgranular mafic enclaves showing assimilation of K-feldspar porphyroclasts.

of the Piratini Arc orogeny?

3. Materials and methods

For this work, five representative and less altered samples of the Arroio Pedrado Gneisses were selected for the geochemistry analyses (see location of the samples in Fig. 2). The rocks were powdered to < 200 mesh size in the Núcleo de Preparação de Amostras (NPA), Centro de Estudos em Petrologia e Geoquímica (CPGq), Instituto de Geociências (IGeo) of the Universidade Federal do Rio Grande do Sul (UFRGS). Later, they were analyzed in Acme Analytical Laboratories Ltd. (Canada) for whole rock geochemical data. The major and trace elements were analyzed by Inductively Coupled Plasma Optical Emission Spectrometry (ICP-OES), and the rare earth elements (REE) by Inductively Couple Plasma Mass Spectrometry (ICP-MS). The loss on ignition (LOI) was determined by heating the powdered samples for 60 min at 1000 °C.

Prior to the Rb-Sr and Sm-Nd isotopic systems analyses, the powdered samples (N = 3) were properly spiked (with mixed ^{87}Rb/^{84}Sr and ^{149}Sm/^{150}Nd tracers) and processed using standard dissolution procedures with HF, HNO$_3$, and HCl in Teflon vial, and warmed on a hot plate until complete material dissolution. Column procedures used cationic AG50W-X8 resin (200–400 mesh) in order to separate Rb, Sr, and REE, followed by Sm and Nd separation using anionic LN-B50-A resin (100–150 μm). The samples were run in a VG Sector 54 Thermal Ionization Mass Spectrometer (TIMS) at the Laboratório de Geologia Isotópica (LGI), CPGq-IGEO-UFRGS, in static mode. Nd and Sr ratios were normalized to ^{86}Sr/^{88}Sr = 0.1194 and ^{146}Nd/^{144}Nd = 0.7219, respectively. Measurements for the Sr NIST standard NBS-987 gave ^{87}Sr/^{86}Sr = 0.710260 ± 0.000014, and for the Nd La Jolla, standard

values of ^{143}Nd/^{144}Nd = 0.511859 ± 0.000010 were obtained.

For the U-Pb and Lu-Hf analyses by Laser Ablation Multi-collector Inductively Coupled Plasma Mass Spectrometry (LA-MC-ICP-MS), zircon crystals from sample CH-05 were separated using heavy liquid and magnetic techniques at the NPA-CPGq-IGeo-UFRGS and mounted in epoxy resin. Cathodoluminescence and secondary electron images of the selected zircon grains were taken at the LGI-CPGq-IGeo-UFRGS, using a JEOL JSM-6610LV scanning electron microscope equipped with a Bruker XFLASH 5030 energy dispersive X-ray spectrometer. Analytical conditions were 15 kV, spot size of 60 μm, and working distance of 10 mm. The U-Pb and Lu-Hf analyses were performed at the same laboratory, using a laser ablation microprobe (New Wave UP213) coupled to a MC-ICP-MS (Thermo Finnigan Neptune). Isotope data were acquired using static mode with spot size of 25 μm for U-Pb analyses, and of 55 μm for Lu-Hf analyses, with frequency of 10 Hz and intensity of ~4 J/cm^2. The analyses were made in 40 cycles of 1 s. Laser-induced elemental fractionation and instrumental mass discrimination were corrected using the GJ-1 standard zircon. Uncertainties were calculated using error propagation, following the analytical procedures of Bertotti et al. (2013). The ages were calculated using Isoplot software (Ludwig, 2008).

4. Results

4.1. Petrography

The Arroio Pedrado Gneisses crop out as meter-sized boulders with monzogranitic composition. These rocks are medium-to coarse-grained, showing a discontinuous and incipient mm-thick banding (Fig. 3A), and a parallel, subvertical tectonic foliation (average 83°, SE-dip) marked
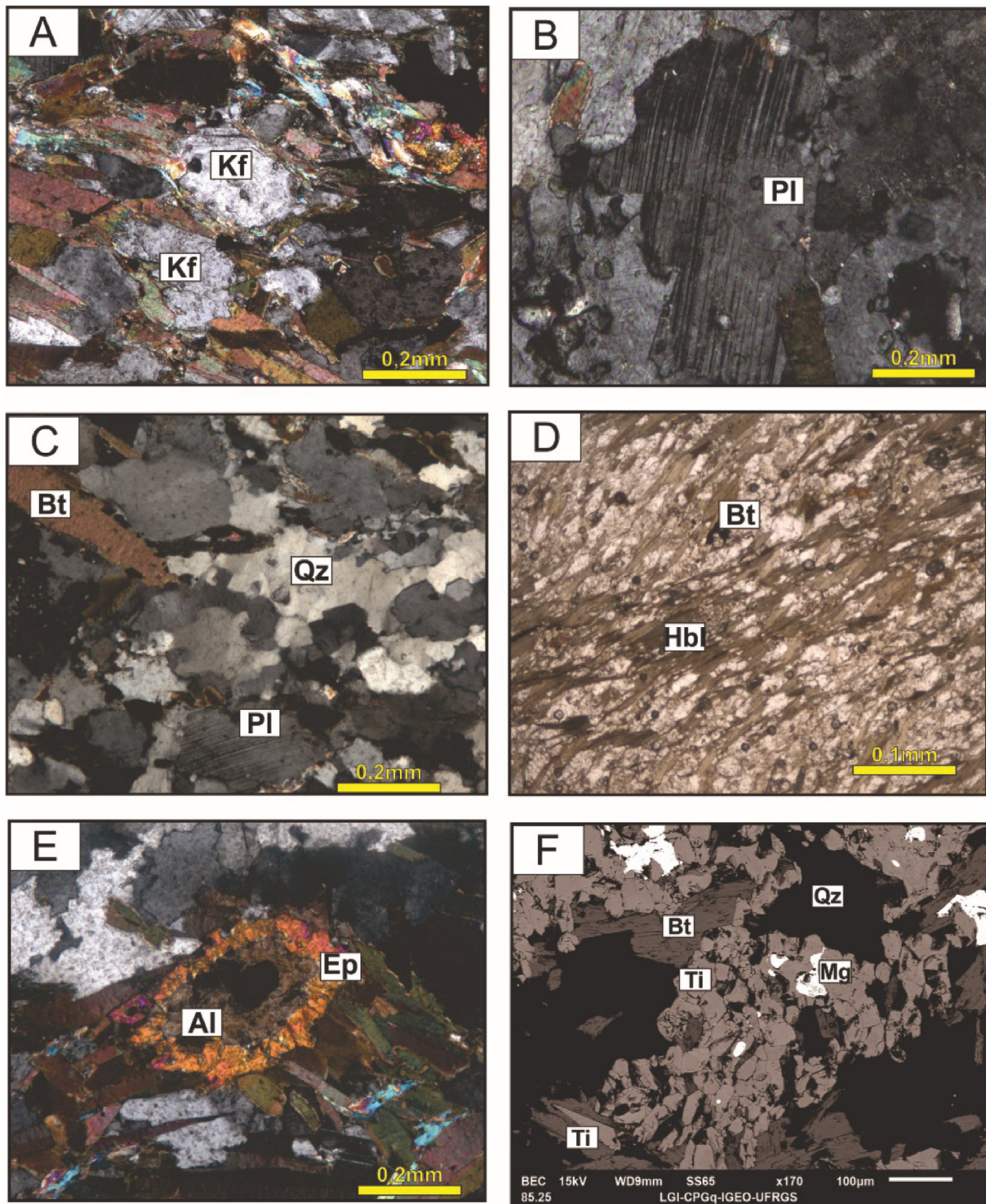
Fig. 4. Photomicrographs of the Arroio Pedrado Gneisses – (A) Detail of the K-feldspar porphyroclasts with asymmetric recrystallization tails; (B) Detail of a deformed plagioclase crystal; (C) Subgrain formation and beginning of quartz recrystallization; (D) Lepidoblastic aggregates formed by biotite and minor hornblende; (E) Coronitic texture of allanite + epidote; (F) Backscattered electron image showing the Qz-Mg-Ti-Bt paragenesis, indicative of oxidative conditions. Abbreviations: Kf = K-Feldspar; Qz = quartz; Bt = biotite; Hbl = hornblende; Al = allanite; Ep = Epidote; Pl = plagioclase; Ti = titanite; Mg = magnetite.

by K-feldspar porphyroclasts and elongated biotite crystals (Fig. 3B). Elongated crystals (quartz, biotite, feldspars) also mark the sub-horizontal stretching lineation (average 10°, ENE-dip). Relics of igneous K-feldspar porphyroclasts are common (Fig. 3C). Centimeter-sized microgranular mafic enclaves with different shapes can be found, suggesting the coexistence and partial mixing of mafic and felsic magmatism (Fig. 3D).

The microscopy results indicate that the studied gneisses are composed of K-feldspar (25–45%), quartz (15–20%), plagioclase (25–40%), biotite (6–10%), and rare hornblende (< 1%). Common accessory minerals include apatite, zircon, allanite, titanite, and epidote (< 1%). Muscovite and sericite occur as secondary minerals. Opaque minerals are characterized as magnetite and hematite.

K-feldspar porphyroclasts are embedded in a matrix of fine-to

Table 2

Major, trace, and rare earth elements of the Arroio Pedrado Gneisses. *Total iron as Fe_2O_3. LOI = Loss on Ignition.

Sample	CH05	PF56	CH32	CH32B	PF47
SiO_2	61.72	65.37	62.47	59.22	62.85
Al_2O_3	16.68	15.24	16.90	15.68	16.09
Fe_2O_3*	5.52	5.40	10.79	10.44	6.86
MnO	0.07	0.08	0.16	0.16	0.14
MgO	1.49	2.07	2.95	2.71	1.62
CaO	3.50	3.03	5.79	4.57	3.18
Na_2O	2.91	3.40	2.96	2.70	4.05
K_2O	5.30	3.45	3.07	3.81	2.65
TiO_2	1.01	0.78	2.00	1.73	1.15
P_2O_5	0.30	0.29	0.61	0.52	0.37
LOI	1.0	0.5	1.9	1.1	0.7
Ba	2308	1397	1097	1267	1100
Co	11.6	11.1	20.1	21.1	11.9
Cr	< 20	80	30	30	30
Ga	20.2	22.9	24.7	21.8	29.5
Hf	9.3	8.0	17.8	16.4	10.1
Ho	0.66	0.71	1.65	1.30	1.33
Nb	9.3	12.7	21.2	19.4	37.6
Ni	< 20	40	31	< 20	< 20
Pb	4.4	4.8	4.1	4.1	2.6
Rb	98.5	262.4	128.1	130.1	262.4
Sr	508.9	354.6	406.8	554.1	354.6
Ta	0.5	0.7	0.8	1.1	6.3
Th	2.7	21.1	7.1	8.1	3.2
Y	19.8	19.0	43.0	33.2	34.8
Zr	425.3	323.8	766.2	673.6	414.6
La	57.1	69.1	94.1	74.6	51.9
Ce	107.6	143.4	203.7	170.6	98.8
Pr	12.45	17.27	26.83	20.38	14.6
Nd	49.2	58.6	103.8	78.0	58.6
Sm	8.16	11.72	17.56	12.79	11.72
Eu	2.20	1.57	2.78	2.48	2.18
Gd	6.43	6.88	13.30	10.15	10.41
Tb	0.74	0.82	1.71	1.36	1.42
Dy	4.30	3.94	8.75	7.04	7.01
Ho	0.66	0.71	1.65	1.30	1.33
Er	1.77	1.73	4.29	3.45	3.30
Tm	0.25	0.26	0.63	0.45	0.45
Yb	1.35	1.52	3.72	3.08	2.69
Lu	0.21	0.21	0.53	0.44	0.39

Table 3

Selected oxides (recalculated to molar) used for the calculation of the Chemical Index of Alteration (CIA). CIA (molar) = $Al_2O_3/(Al_2O_3 + CaO + Na_2O + K_2O)$ * 100.

Sample	Na_2O	CaO	K_2O	Al_2O_3	CIA
CH05	0.046	0.062	0.056	0.163	49.690
PF56	0.054	0.054	0.036	0.149	50.670
CH32	0.047	0.103	0.032	0.165	47.445
Ch32b	0.043	0.0814	0.040	0.153	48.164
PF47	0.065	0.056	0.028	0.157	51.237

Fig. 5. MFW ternary diagram, modified from Ohta and Arai (2007).

mafic minerals are represented mainly by biotite and subordinate hornblende, both occurring as lepidoblastic aggregates. The latter are generally found in contact with K-feldspar porphyroclasts (Fig. 4D) or separated by mm-sized felsic bands.

Allanite occurs as large crystals, with a typical grain size ranging from 0.1 to 0.8 mm. It is commonly replaced or rimmed by epidote, featuring a coronitic texture (Fig. 4E). The other accessory minerals include fine-to medium-grained epidote, titanite, apatite, and zircon.

Two titanite textures are observed. The primary (magmatic) titanite is light brown-colored, mm-sized (0.4–4.0 mm), idiomorphic, elliptic to elongated, and shows straight contacts with adjacent phases. The secondary titanite is xenomorphic, found as fine-grained irregular crystals in contact with opaque minerals (Fig. 4G).

The apatite occurs as < 0.5 mm crystals, usually prismatic, found as inclusions in K-feldspar and biotite crystals. The zircon occurs as zoned euhedral < 0.3 mm prismatic crystals usually included in biotite. Pleochroic haloes around the latter inclusions are common. The opaque minerals, mostly magnetite, occur as < 1.5 mm crystals and were interpreted as primary (magmatic), occurring as inclusions in allanite, biotite, quartz, plagioclase, K-feldspar, and titanite.

4.2. Whole-rock geochemistry

The whole-rock geochemistry results are summarized in Table 2. In order to verify possible chemical changes caused by weathering, we used the approach by Bersan et al. (2018), combining the Chemical Index of Alteration (CIA) (Nesbitt and Young, 1982) with the MFW diagram (Ohta and Arai, 2007). As shown in Table 3, the studied samples show CIA values (molar $Al_2O_3/[Al_2O_3 + CaO + Na_2O + K_2O]$ * 100) between 47.44 and 51.23, which fall within the range of unaltered granitoids (Nesbitt and Young, 1982). The MFW diagram (Fig. 5) demonstrates that the samples experienced only minor alteration, plotting near the fresh granitoid (intermediate) trend.

In order to verify possible chemical changes during metamorphism, we compare the concentrations shown in Table 2 with the average composition of granitoids presented in Goswami and Bhattacharyya (2014). The comparison demonstrates that, despite localized differences – e.g., higher concentrations of TiO_2, P_2O_5, and Fe_2O_3, which we attribute to, respectively, the high content of titanite, apatite, and magnetite –, the major and trace element concentrations are similar to the average shoshonitic granitoids (Figs. 6 and 7) and, possibly, were

coarse-grained quartz, plagioclase and K-feldspar, and medium-to coarse-grained aggregates of biotite, with rare fine-grained hornblende. K-feldspar megacrysts are up to 45 mm in length and occasionally have an idiomorphic shape and simple twinning. Most of the deformed porphyroclasts show undulose extinction and typical core and mantle structure (Fig. 4A). Small inclusions of quartz, plagioclase, and minor biotite are common, occurring predominantly at the rims, featuring a poikilitic texture. Plagioclase occurs in its characteristic tabular prismatic form (0.5–1.6 mm) and generally shows deformation features such as undulose extinction, subgrain formation, curved and displaced polysynthetic twinning, and occurrence of kink bands (Fig. 4B).

The quartz shows strong undulose extinction and tends to form aggregates, often recrystallized by bulging and subgrain rotation (Fig. 4C), with formation of subgrains and growth of new grains. The

Fig. 6. SiO$_2$ vs. major oxides variation diagrams. Average granitoid compositions compiled from Goswami and Bhattacharyya (2014).

not modified by metamorphism.

Together, these results suggest that the Arroio Pedrado Gneisses did not undergo significant post-emplacement chemical changes. Thus, in the following discussions these orthogneisses will be treated from the geochemistry of their protoliths.

4.3. U-Pb geochronology

Cathodoluminescence images of 13 zircon crystals from sample CH05 were taken to identify potential xenocrystic cores and internal morphologies such as growth related textures, recrystallization zones, and overgrowth rims. The analyzed zircon crystals are characterized by subhedral prismatic shapes (150–200 μm), with rounded to subrounded borders. The internal structures (Fig. 8) are interpreted as primary – oscillatory zoning formed during igneous crystallization – and

secondary – convolute zoning and overgrowths formed during regional metamorphism and/or by hydrothermal crystallization (Corfu et al., 2003).

The obtained U-Pb LA-MC-ICP-MS data are given in Table 4 and plotted on two concordia diagrams. The diagram presented in Fig. 9A shows a concordia age of 680 ± 2.9 Ma, which is interpreted as the igneous crystallization age of the protolith. The concordia age of 660 ± 2.8 Ma (Fig. 9B) is interpreted as the age of peak metamorphism. The zircon crystals with ages between 780 and 750 Ma (Table 4) are interpreted as inherited.

4.4. Lu-Hf isotope results

The in situ Lu-Hf analyses were carried out on 10 zircon crystals (sample CH05), and the results are presented in Table 5. The εHf$_{(t)}$
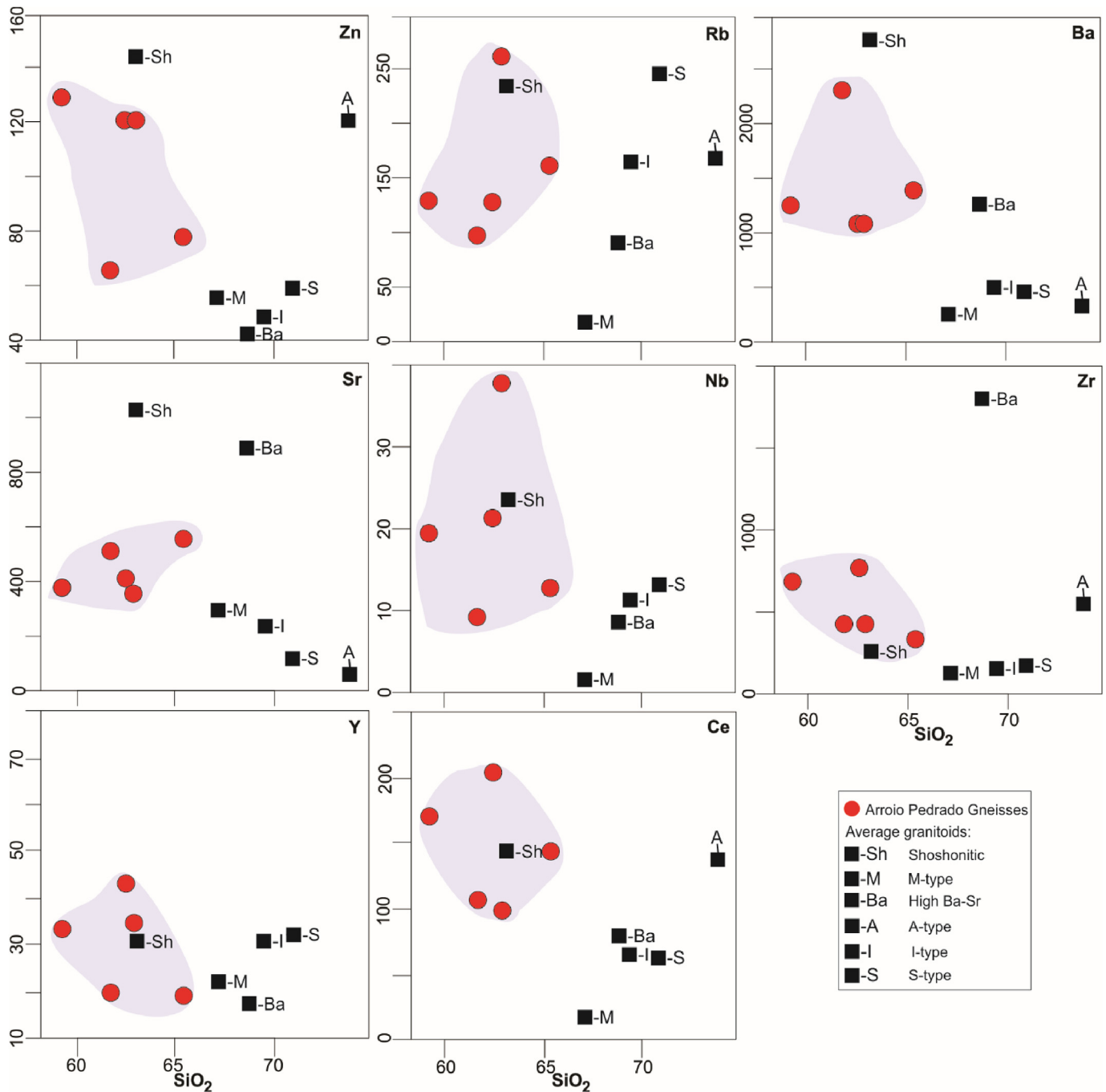
Fig. 7. SiO₂ vs. trace elements variation diagrams. Average granitoid compositions compiled from Goswami and Bhattacharyya (2014).

values and the $^{176}Hf/^{177}Hf$ ratios were calculated using the crystallization age (680 Ma, as shown in section 4.3) of the Arroio Pedrado Gneisses.

4.5. Whole-rock Sr-Nd isotope geochemistry

Whole-rock Rb-Sr and Sm-Nd isotope data were obtained from 3 samples of the Arroio Pedrado Gneisses. The isotopic compositions are shown, respectively, in Tables 6 and 7. The initial isotopic ratios were calculated using the crystallization age (680 Ma, as shown in section 4.3) of the studied gneisses.

The analyzed samples have variable $^{87}Sr/^{86}Sr_{(680)}$ ratios, ranging from 0.708328 to 0.711289 (Table 6). The isotopic compositions show relatively uniform $^{143}Nd/^{144}Nd_{(680)}$ ratios which range from 0.511761

to 0.511581, corresponding to $\varepsilon Nd_{(680)}$ values between -3.70 and -4.30. The depleted-mantle model ages (T_{DM}) range from 1.61 to 1.48 Ga (Table 7).

5. Discussions

5.1. Petrographic and geochemical classification

The Arroio Pedrado Gneisses are characterized by monzogranitic compositions. Relic coarse-grained, hypidiomorphic, porphyritic textures are preserved in less deformed domains of these gneisses, suggesting a plutonic protolith. The partial equilibrium of the plagioclase + alkali feldspar + biotite + hornblende paragenesis is consistent with amphibolite facies metamorphism. The crystallization
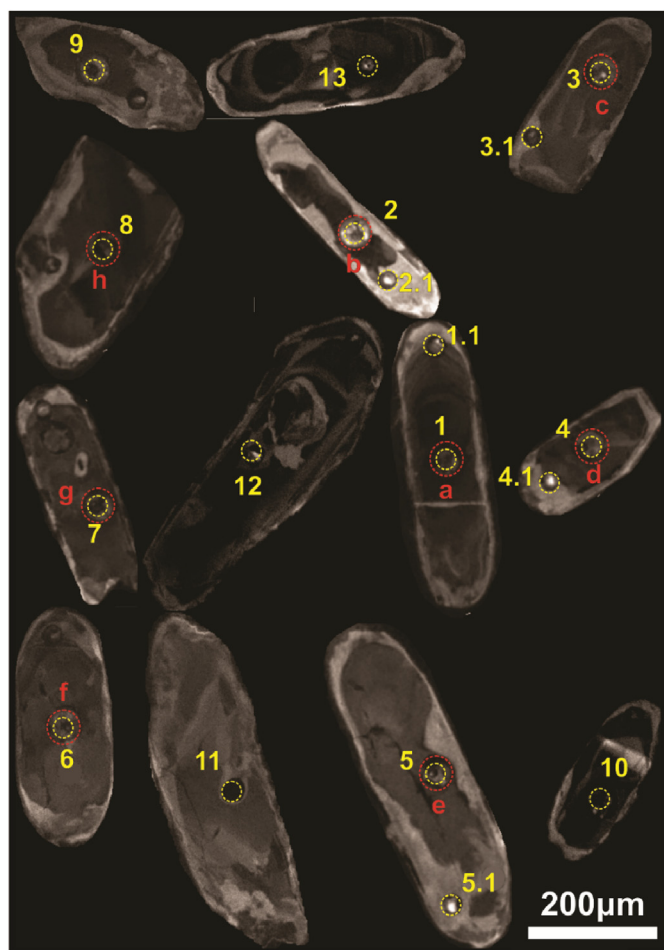
Fig. 8. Cathodoluminescence images of zircon crystals from sample CH05, showing the location of the analyzed spots. Yellow circles = U-Pb LA-MC-ICP-MS analyses (25 μm). Red circles = Lu-Hf analyses (55 μm, see section 4.4). (For interpretation of the references to color in this figure legend, the reader is referred to the Web version of this article.)
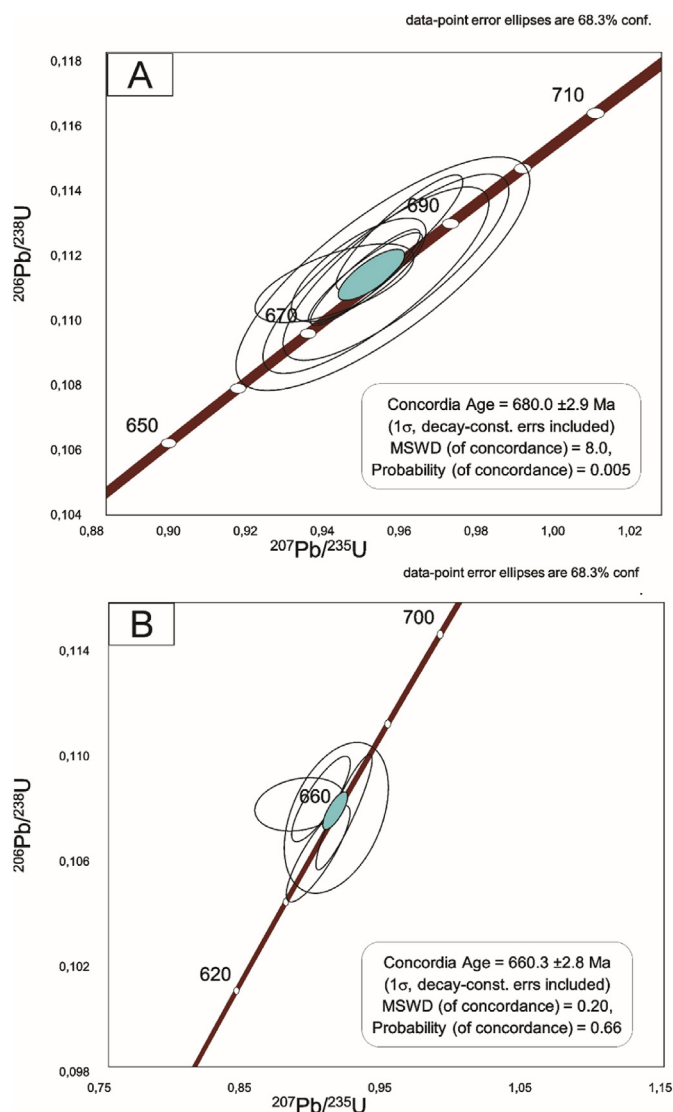
Fig. 9. Concordia diagrams for sample CH05 – (A) Zircon cores (N = 9); (B) Recrystallized zircon rims (N = 5).

Table 4

LA-MC-ICP-MS U-Pb data (sample CH05). The analyses marked in bold were used for the calculation of the concordia ages.

							Apparent ages							
Spot (c) = core (r) = rim	Th/U	^{207}Pb/^{206}Pb	2σ	^{206}Pb/^{238}U	2σ	^{207}Pb/^{235}U	2σ	^{207}Pb/^{206}Pb	2σ	^{206}Pb/^{238}U	2σ	^{207}Pb/^{235}U	2σ	Rho	Conc. (%)
1 (c)	**0.17**	**.06227**	**1.2**	**.11161**	**1.7**	**.9582**	**2.1**	**683.4**	**25.6**	**682.1**	**11.2**	**682.4**	**10.4**	**.82**	**99.81**
2 (c)	**0.25**	**.06070**	**1.0**	**.11215**	**1.8**	**.9386**	**2.0**	**628.7**	**22.0**	**685.2**	**11.5**	**672.2**	**10.0**	**.86**	**108.99**
3 (c)	**0.24**	**.06215**	**1.7**	**.11140**	**2.2**	**.9547**	**2.7**	**679.4**	**36.0**	**680.9**	**14.0**	**680.5**	**13.6**	**.79**	**100.23**
4 (c)	**0.17**	**.06141**	**0.5**	**.11290**	**1.1**	**.9559**	**1.2**	**653.6**	**11.3**	**689.6**	**6.9**	**681.2**	**5.9**	**.89**	**105.50**
5 (c)	**0.16**	**.06145**	**0.8**	**.11165**	**1.0**	**.9459**	**1.3**	**654.9**	**17.8**	**682.3**	**6.2**	**676.0**	**6.3**	**.74**	**104.19**
6 (c)	**0.20**	**.06103**	**0.6**	**.11067**	**1.2**	**.9312**	**1.4**	**640.2**	**13.9**	**676.6**	**7.7**	**668.3**	**6.7**	**.87**	**105.68**
7 (c)	**0.18**	**.06229**	**1.3**	**.11165**	**1.9**	**.9282**	**2.0**	**684.4**	**24.6**	**683.1**	**10.2**	**683.4**	**11.4**	**.82**	**99.88**
8 (c)	**0.22**	**.06217**	**1.7**	**.11140**	**2.2**	**.9547**	**2.7**	**679.4**	**36.0**	**680.9**	**14.0**	**680.5**	**13.6**	**.79**	**100.23**
9 (c)	0.17	.06319	0.9	.12710	1.5	1.1074	1.7	714.7	18.3	771.3	11.0	756.9	9.3	.86	107.92
10 (c)	0.15	.06501	1.4	.12847	2.4	1.1516	2.8	774.7	29.5	779.1	18.0	778.0	15.3	.87	100.57
11 (c)	0.08	.06168	2.9	.12833	3.4	1.0914	4.5	663.1	63.1	778.3	24.7	749.2	23.7	.75	117.38
12 (c)	0.20	.05959	2.4	.10815	0.6	.8886	2.5	588.8	52.0	662.0	4.0	645.6	11.8	.22	112.43
13 (c)	0.16	.06196	0.6	.10784	1.4	.9213	1.5	672.7	12.9	660.2	8.5	663.0	7.2	.91	98.15
1.1 (r)	**0.16**	**.06158**	**1.3**	**.10624**	**1.2**	**.9021**	**1.7**	**659.7**	**27.5**	**650.9**	**7.2**	**652.8**	**8.3**	**.85**	**98.67**
2.1 (r)	**0.38**	**.06458**	**6.3**	**.10670**	**2.8**	**.9500**	**6.9**	**760.5**	**132.3**	**653.5**	**17.1**	**678.1**	**33.9**	**.40**	**85.93**
3.1 (r)	**0.21**	**.05959**	**2.4**	**.10815**	**0.6**	**.8886**	**2.5**	**588.8**	**52.0**	**662.0**	**4.0**	**645.6**	**11.8**	**.22**	**112.43**
4.1 (r)	**0.17**	**.06158**	**1.3**	**.10624**	**1.2**	**.9021**	**1.7**	**659.7**	**27.5**	**650.9**	**7.2**	**652.8**	**8.3**	**.85**	**98.67**
5.1 (r)	**0.22**	**.06184**	**0.7**	**.13336**	**2.8**	**1.1372**	**2.8**	**700.2**	**29.4**	**678.1**	**33.9**	**653.5**	**17.1**	**.60**	**92.04**

Table 5

Lu-Hf analyses from sample CH05.

Spot	$^{176}Lu/^{177}Hf$	$^{176}Hf/^{177}Hf$	Erro (1 SD)	$\varepsilon Hf(0)$	$^{176}Hf/^{177}Hf$ (t)	εHf (t)	$^{176}Hf/^{177}Hf$ (t chur)	$^{176}Hf/^{177}Hf$ (DM)	U-Pb Age (Ma)	T_{DM} (Ga)	f (Lu/Hf)	Int.^{178}Hf (V)
a	0.001126	0.281949	0.00018	- 9.11	0.281934	- 14.66	0.282348	0.282733	680	1.84	- 0.97	1.32
b	0.000784	0.281930	0.00016	− 29.77	0.281920	- 15.16	0.282348	0.282733	680	1.84	- 0.98	1.54
c	0.001078	0.281949	0.00024	- 29.12	0.281935	- 14.64	0.282348	0.282733	680	1.83	- 0.97	1.24
d	0.000963	0.281937	0.00021	- 29.51	0.281925	- 14.99	0.282348	0.282733	680	1.84	- 0.97	1.30
e	0.000924	0.281937	0.00020	- 29.54	0.281925	- 14.99	0.282348	0.282733	680	1.84	- 0.97	1.48
f	0.001502	0.281958	0.00028	- 28.77	0.281939	- 14.49	0.282348	0.282733	680	1.84	- 0.95	0.99
g	0.000606	0.281957	0.00020	- 28.84	0.281949	- 14.15	0.282348	0.282733	680	1.80	- 0.98	1.30
h	0.001502	0.281968	0.00020	- 28.44	0.281949	- 14.16	0.282348	0.282733	680	1.83	- 0.95	1.16

Table 6

Whole rock Rb-Sr isotope data for the Arroio Pedrado Gneisses.

Sample	Rb (ppm)	Sr (ppm)	$^{87}Rb/^{86}Sr$	Error (SD abs)	$^{87}Sr/^{86}Sr$	SE (%)	$^{87}Sr/^{86}Sr(t)$	t (Ma)
CH05	98.5	508.9	0.54	0.054670	0.716594	0.0010	0.711289	680
CH32	128.1	406.8	0.88	0.088943	0.718167	0.0006	0.709536	680
PF56	262.4	354.6	2.09	0.209013	0.728609	0.0017	0.708328	680

Table 7

Whole rock Sm-Nd isotope data for the Arroio Pedrado Gneisses.

Sample	Sm (ppm)	Nd (ppm)	$^{147}Sm/^{144}Nd$	$^{143}Nd/^{144}Nd$ (t = 0)	SE (%)	ε Nd (0)	ε Nd (t)	T_{DM} (Ga)	$^{143}Nd/^{144}Nd$ (t)
CH05	8.16	49.2	0.093869	0.511993	0.0025	- 12.58	- 4.2	1.48	0.511574
CH32	17.56	103.8	0.093283	0.511997	0.0010	- 12.49	- 4.3	1.50	0.511581
PF56	11.72	58.6	0.077137	0.512111	0.0009	- 10.28	- 3.7	1.61	0.511761

of hydrated mineral phases such as hornblende and biotite, even in the early stages of magmatic differentiation, suggests a water-satured magma. The titanite + magnetite + quartz paragenesis, together with the presence of allanite-epidote coronas, are indicative of oxidative conditions (Wones, 1989).

The alkali content of the samples ($Na_2O + K_2O$) range from 6.65 to 8.75 wt% and the Na_2O/K_2O ratios are < 1, except for sample PF47 which shows a higher value (1.52). The samples show a subalkaline character defined by the relatively low alkali contents, which is consistent with the mineralogical composition observed in the rock.

The studied samples are metaluminous (CH samples) to weakly peraluminous (PF samples) (Fig. 10A) and show major oxide concentrations which are consistent with both high-K calc-alkaline and shoshonitic granitoids (Figs. 6 and 10B). The trace element concentrations are consistent with a shoshonitic composition (e.g. Morrison, 1980; Tauson, 1983; Nardi, 1986), as shown in the diagrams of Figs. 7, 10C and 10D.

The Arroio Pedrado Gneisses are enriched in large ion lithophile elements (LILE) relative to the high field strength elements (HFSE) (Fig. 10E). The high concentrations of LILE such as Sr and Ba are indicative of late fractionation of feldspar and/or crustal contamination of the parent magma. The Nb and Ta negative anomalies strengthen the latter hypothesis, except for sample PF47, which shows higher Ta and Nb concentration reflecting the abundance of titanite.

The samples are strongly enriched in REE (Σ REE = 252.42 to 483.35). Chondrite-normalized patterns (Fig. 10F) demonstrate enrichment of light REE relative to heavy REE (La_N/Lu_N 17 to 33), and negative Eu anomalies (Eu/Eu* 0.60 to 0.93). The REE patterns are similar to those of both intermediate and potassic gneisses (Mogk et al., 2004), with light REE enrichment between 100 and 300 times chondritic values, and heavy REE around 10–20 chondritic values.

5.2. Source of magmatism

The sources proposed for shoshonitic magmatism are discussed by several authors (Bloomer et al., 1989; Rogers, 1992; Wyman and Kerrich, 1993; Müller and Groves, 1995; Wang et al., 2007; Chen et al., 2010) and include subcontinental lithospheric mantle, metasomatized subarc mantle, fractional crystallization with crustal assimilation, and delaminated or thickened lower crust (e.g., Meen, 1987; Feeley and Cosca, 2003). Several trace element characteristics of the Arroio Pedrado Gneisses are consistent with the latter scenario.

The trace element concentrations suggest an active continental arc setting for the origin of the Arroio Pedrado Gneisses (Fig. 11). The subduction-related signature can be observed in the diagrams shown in Fig. 11A, where the studied samples plot near the La apex (sediment and/or fluid input), and in Fig. 11C, where the samples plot along the subduction trend. Negative Nb, Ta, Sr, P, and Ti anomalies, together with the LILE enrichment observed in Fig. 10E spidergram, strengthen this hypothesis (e.g., Pearce, 1982; Pearce et al., 1990; Hawkesworth et al., 1993). The exception is for sample PF47, which shows high Nb and Ta concentrations relative to the other studied samples (as shown in the previous section), consequently tending toward the Nb and Ta apex of the diagrams shown, respectively, in Fig. 11A and B, suggesting higher interaction with crustal material or even assimilation of different crustal sources.

The trace element characteristics suggest that the Arroio Pedrado Gneisses might have been generated by partial melting of thickened lower crust. High Sm/Yb (4.15–6.29) and La/Yb ratios (19.3–45.5) suggest a thickened-crust setting, since high values of both ratios require sequestration of HREE by garnet at high pressures in lower crust or mantle wedge (e.g., Kay et al., 2013). However, the lower concentrations of Cr (< 20–80 ppm), Ni (< 20–40 ppm), Co (11.1–21.1 ppm), together with low Mg# values (31.8–43.1), indicate insignificant mantle-derived magma input and preclude interaction of the melt with the lithospheric mantle (e.g., Wang et al., 2006; Wu, 2015). A thickened lower crust setting is further strengthened by the Zr saturation temperature of the studied samples, inferred from the concentrations presented in Table 2, which constrain the upper temperature limit for zircon crystallization. These temperatures, which range between 831 and 873 (equations of Watson and Harrison, 1983) and 785–815 °C (equations of Boehnke et al., 2013), suggest that the gneiss
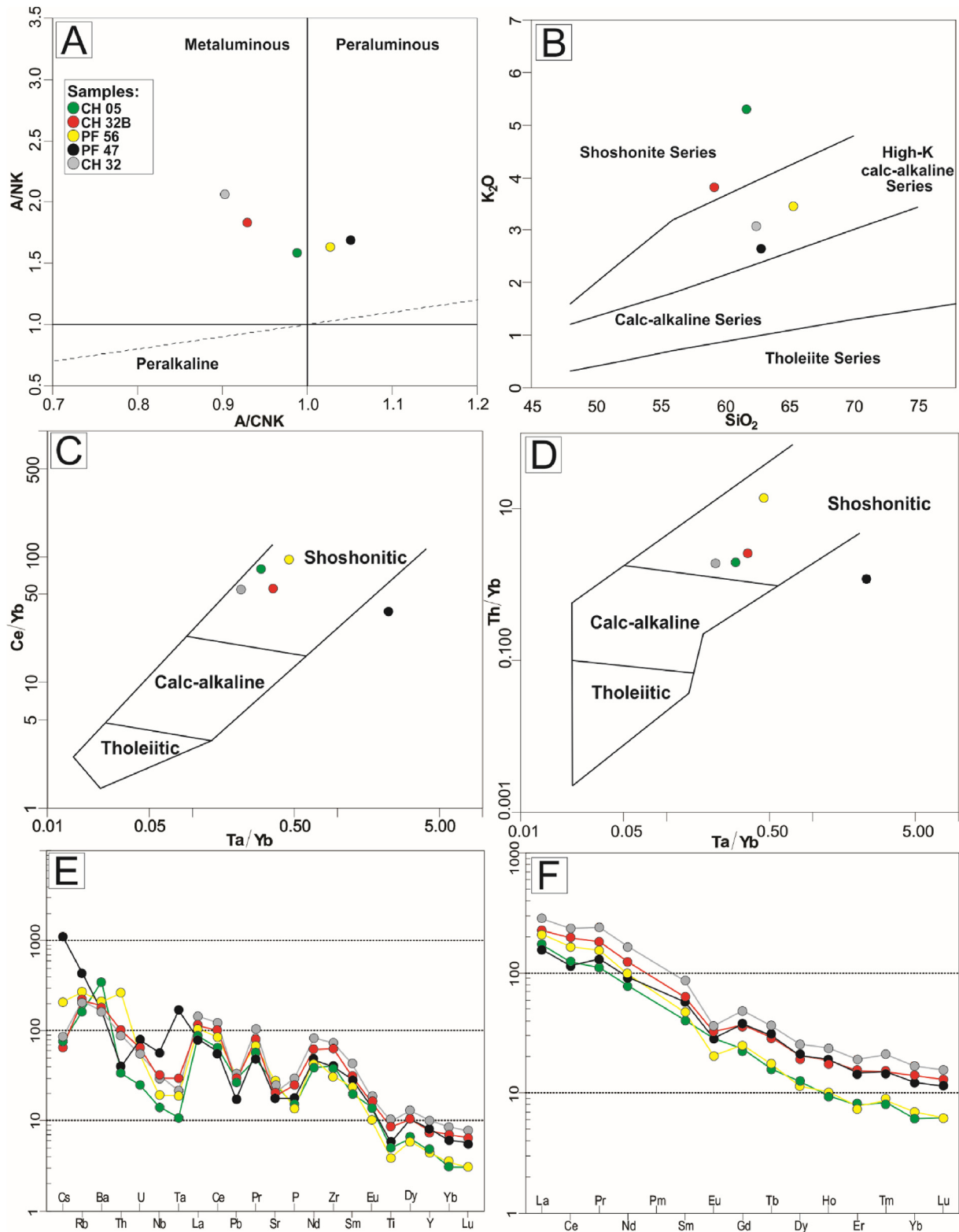
Fig. 10. Classification diagrams for the Arroio Pedrado Gneisses – (A) A/CNK vs. A/NK diagram, modified from Shand (1943); (B) K$_2$O vs. SiO$_2$, modified from Peccerillo and Taylor (1976); (C) Ta/Yb vs. Ce/Yb and (D) vs. Th/Yb, modified from Ivanov et al. (2019) after Pearce (1982); (E) Chondrite-normalized multi-element diagram (Nakamura, 1974); (F) Primitive mantle-normalized (McDonough and Sun, 1995) REE spider diagram.

protoliths were derived from melts generated at upper amphibolite-granulite facies temperatures.

The Sr-Nd isotopic features of the Arroio Pedrado Gneisses (Tables 6 and 7) show that these rocks have intermediate, uniform ^{87}Sr/^{86}Sr$_{(i)}$ ratios (0.708–0.711) and low ϵNd$_{(t)}$ values (- 3.7 to – 4.3). These

features fit with those of the granitic gneisses derived from melting of thickened lower crust (e.g. Lai et al., 2007; Zhang et al., 2015). Although the low ^{87}Sr/^{86}Sr(i) and near zero ϵNd values could represent mixing between crustal- and mantle-derived components (partial melting of mantle and crustal sources, or mixed crustal and mantle
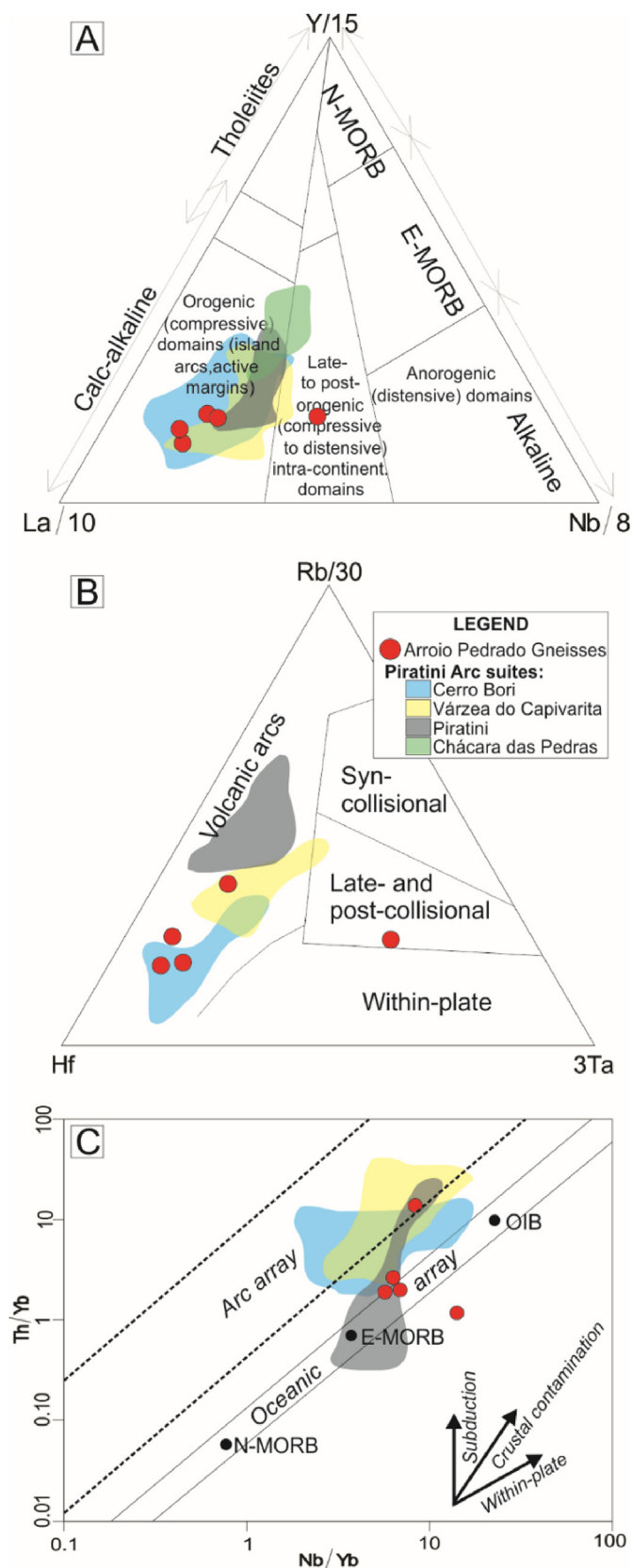
Fig. 11. Tectonic discrimination diagrams – (A) La–Nb–Y ternary diagram modified from Cabanis and Lecolle (1989); (B) Hf–Ta–Rb ternary diagram modified from Harris et al. (1986); (C) Nb/Yb versus Th/Yb diagram modified from Pearce (2008).

magmas), the geochemistry of the protoliths suggests that mantle-derived input possibly plays a minor role in the genesis of the magma, so that partial melting of thickened lower crust is the preferred hypothesis. In this scenario, the mantle might have played a role as a possible heating source.

5.3. Comparison with the Piratini Arc suites

In this section we compare the geochemical and isotopic features of the Arroio Pedrado Gneisses with those of the Piratini Arc suites. The trace and REE geochemical data of the Piratini Arc suites were compiled from the dataset of Philipp and Campos. (2004), Lenz et al. (2012), Tambara (2015) and Martil et al. (2017), respectively, for the Chácara das Pedras, Cerro Bori, Piratini and Várzea do Capivarita suites.

The Arroio Pedrado Gneisses show similar trace and REE patterns when compared to those of the ca. 780 Ma Piratini Arc suites (Figs. 12 and 13), suggesting similar sources and evolution processes. The orthogneisses from the latter suites show negative Nb, Ta, Sr, P, and Ti anomalies, suggesting a subduction-related origin (e.g., Thompson et al., 1984; Hawkesworth et al., 1993; Pearce and Peate, 1995; Gill, 2010). The diagrams also suggest a continental arc setting for all these orthogneisses, since the observed patterns are similar to those of the continental arc rocks from, e.g., the Southern Volcanic Zone of the Andes (e.g. Varekamp et al., 2010) and subduction-related continental granitoids (Winter 2011). The continental arc origin is further strengthened by trace element concentrations such as Th, Nb, Ta, and Hf, illustrated by the geotectonic diagrams shown in Fig. 11, which suggest that these rocks were generated in an active margin/continental arc environment.

Similar to the Arroio Pedrado Gneisses, the older Piratini Arc suites show low concentrations of Mg, Cr, Ni, Co, suggesting minor mantle-derived input. However, differently from the deep crustal depths suggested for the evolution of the Arroio Pedrado Gneisses (section 5.2), the Piratini Arc suites show trace element characteristics which suggest an evolution at relative shallower crustal levels. Compared to the Arroio Pedrado Gneisses, the Piratini Arc suites show lower Sm/Yb and La/Yb ratios of, respectively, 2.59 and 15.9 for the Piratini, 3.03 and 21.6 for the Cerro Bori, 2.9 and 14.3 for the Chácara das Pedras, and 2.5 to 17.9 for the Várzea do Capivarita orthogneisses. These characteristics are similar to those of the Andean Mountains, which show progressive and substantial crustal thickening over time – i.e., from the older 780 Ma Piratini Arc suites to the 680 Ma Arroio Pedrado Gneisses.

Interestingly, the Zr saturation temperatures of the Piratini Arc suites are lower than those of the Arroio Pedrado Gneisses (section 5.2), respectively constrained between 801 and 754 (Piratini), 817–774 (Cerro Bori), 799–753 (Chácara das Pedras) and 805–759 °C (Várzea do Capivarita) (values referring, respectively to the equations of Watson and Harrison, 1983 and Boehnke et al., 2013). These temperatures suggest an emplacement at relatively shallower crustal levels, or even that the Piratini Arc crust was thinner around 780 Ma.

Compared to the Piratini Arc suites, both the lower $^{87}Sr/^{86}Sr_{(i)}$ and slightly higher $^{143}Nd/^{144}Nd_{(i)}$ ratios of the Arroio Pedrado Gneisses (Fig. 14A) suggest a lower influence of subduction-related melts, and higher influence of incoming deep-crust melt flows (e.g. Rollinson, 1993).

The $\varepsilon Nd_{(680)}$ vs. $^{87}Sr/^{86}Sr_{(680)}$ diagram shown in Fig. 14A suggests that the samples from the Arroio Pedrado Gneisses might represent thickened lower crust-derived melts (e.g. Wen et al., 2008; Xiong et al., 2014), reinforcing the interpretations discussed in section 5.2. Possible crustal sources are represented by rocks regarded as basement of the Piratini Arc suites and the arc itself (Fig. 14B), thus explaining the presence of inherited Paleo-to Mesoproterozoic zircons found in the orthogneisses of the Piratini Arc. Rocks that might be regarded as basement of the Piratini Arc suites are represented, respectively by (i) the Paleoproterozoic units of both the Arroio dos Ratos (Silva et al., 2005; Gregory et al., 2015) and Encantadas Complex (May, 1990;
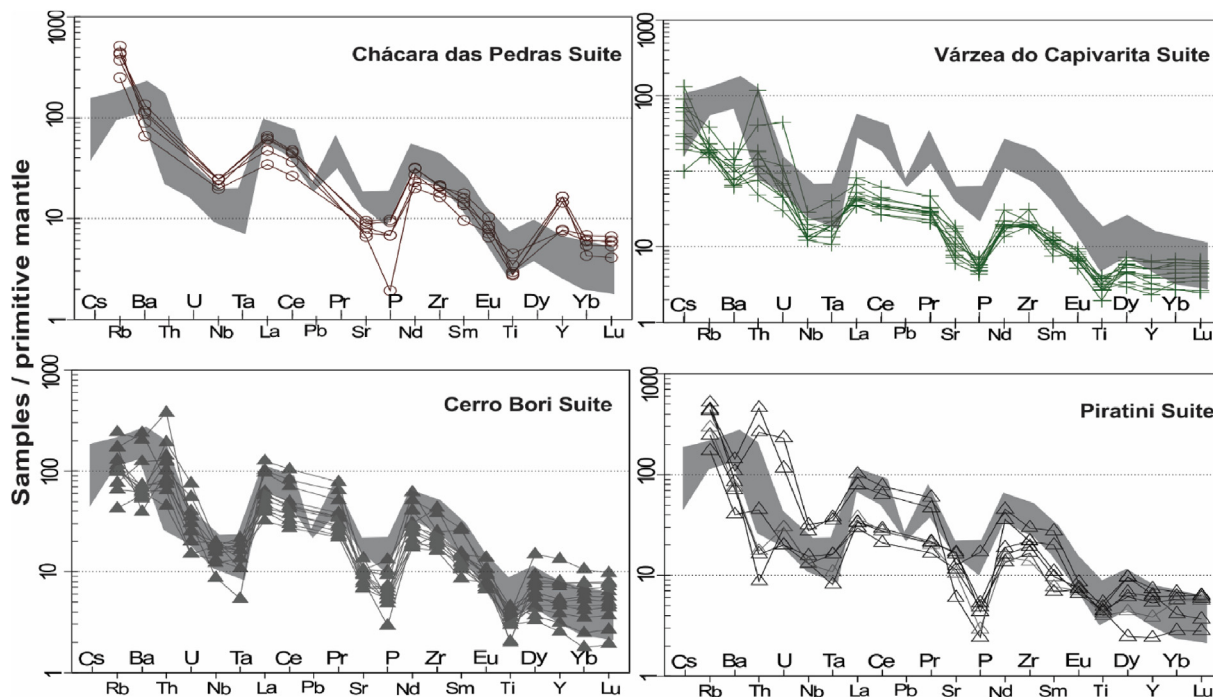
Fig. 12. Primitive mantle-normalized (McDonough and Sun, 1995) multi-element spider diagrams. Gray fields represent the patterns of the Arroio Pedrado Gneisses shown in Fig. 10E.
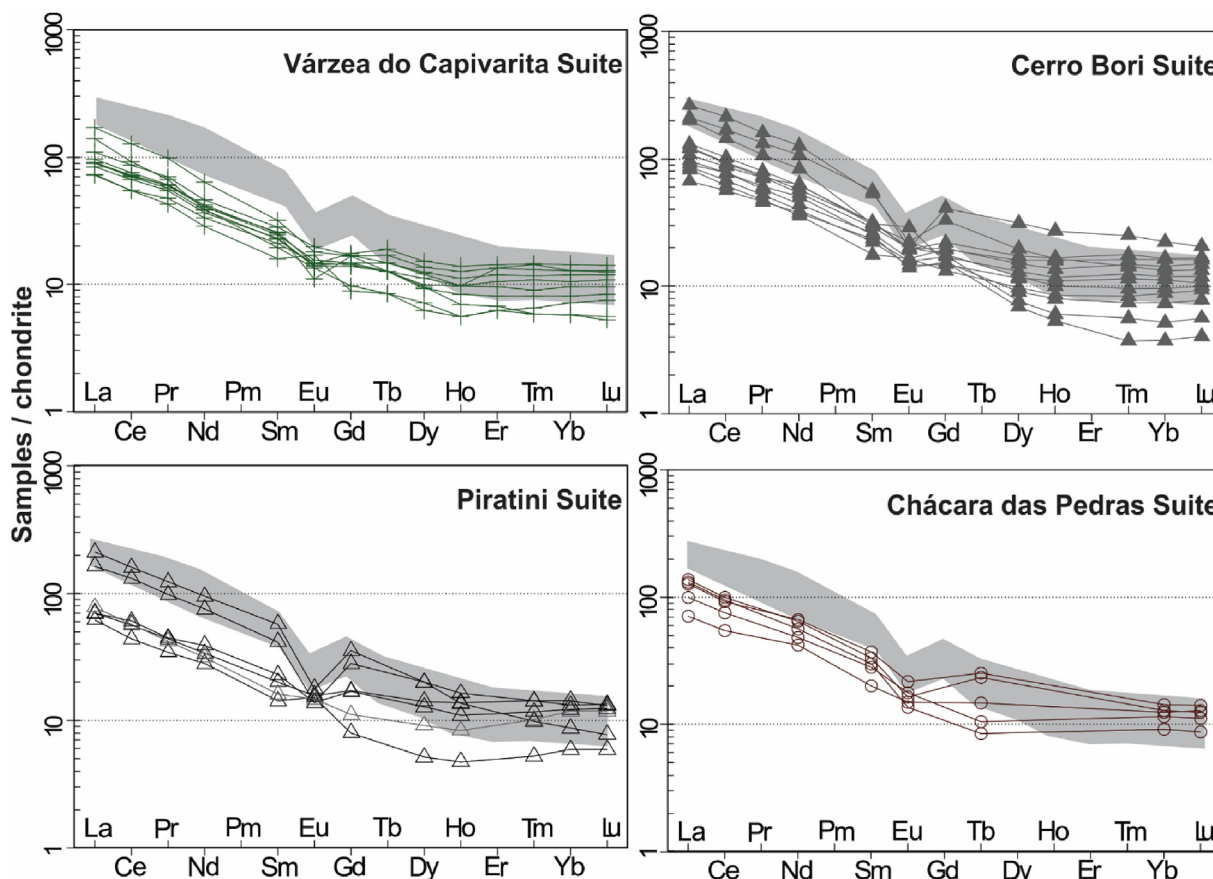
Fig. 13. Chondrite-normalized REE diagram (Nakamura, 1974). Gray fields represent the patterns of the Arroio Pedrado Gneisses shown in Fig. 10F.
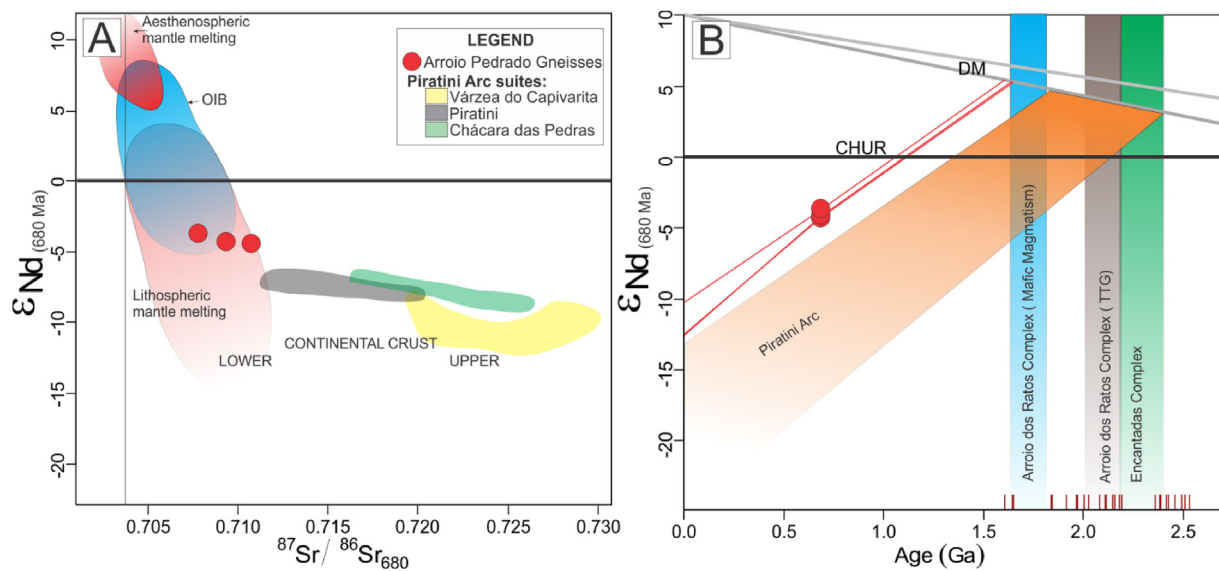
Fig. 14. (A) $^{87}Sr/^{86}Sr_{(680)}$ vs. $\epsilon Nd_{(680)}$ diagram (modified from DePaolo and Wasserburg, 1979); (B) Diagram of $\epsilon Nd_{(680)}$ vs. time relative to the depleted mantle (DM) and chondritic uniform reservoir (CHUR) (modified from DePaolo, 1981). Sources: Chácara das Pedras Gneisses data from Koester et al. (2016); Várzea do Capivarita Orthogneisses data from Martil et al. (2017); Piratini Gneisses data from Tambara, 2016; Arroio dos Ratos Complex ages = Gregory et al. (2015); Encantadas Complex ages = Philipp et al. (2008, Philipp et al., 2016a,b).
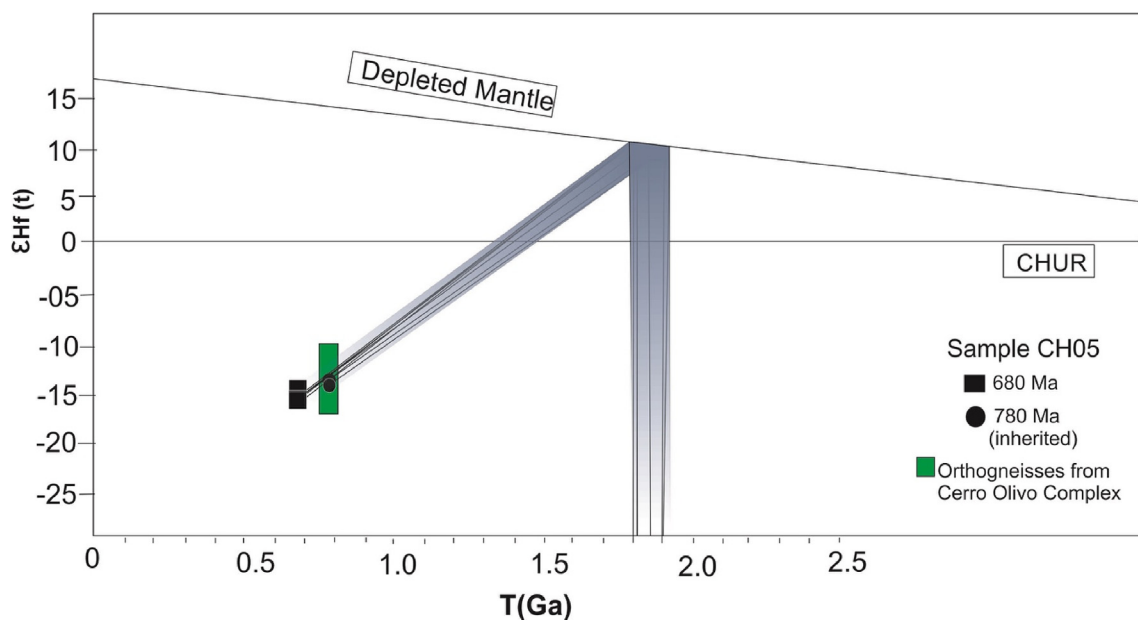
Fig. 15. $\epsilon Hf_{(t)}$ vs. t (U-Pb ages) diagram for sample CH05. The evolution trends were calculated from a $^{176}Lu/^{177}Hf$ ratio of 0.0113. CHUR = chondritic uniform reservoir. Cerro Olivo Complex data extracted from Will et al. (2019).

Philipp et al., 2008 and Philipp et al., 2016a); (ii) Paleoproterozoic xenoliths recently found in Piratini and Pelotas region (Vieira et al., 2019); (iii) Paleoproterozoic xenoliths found in the Chácara das Pedras gneisses (Philipp et al., 2016b); and (iv) Mesoproterozoic units of the basement of the Punta del Este Terrane (Basei et al., 2011).

In turn, the 780-770 Ma ages found in the Arroio Pedrado Gneisses (Table 4) probably are inherited zircons which represent the assimilation and recycling of the Tonian suites of the Piratini Arc (Table 1), further strengthening the hypothesis that the Arroio Pedrado Gneisses might represent the late magmatic pulses of the Piratini Arc, as proposed in the present work. This hypothesis also explains the highly negative ϵHf values which are similar to those found in the orthogneisses of the Cerro Olivo Complex (Will et al., 2019), correlatable to the Tonian units of the Piratini Arc. Together with the Nd and Hf T_{DM}

ages of the Piratini Arc rocks (Tables 5 and 7; Figs. 14B and 15), it implies that Tonian to Paleoproterozoic continental crust was reworked during the evolution of the Piratini Arc as a whole (from the Tonian units to the Arroio Pedrado Gneisses). This assumption is strengthened by both the negative ϵNd and ϵHf values (-3 to -15) and T_{DM} which suggest the presence of a continental crust whose ages are similar to those found in both the Arroio dos Ratos and Encantadas Complex, which, as mentioned above, are regarded as basement of some suites of the Piratini Arc.

Thus, the Arroio Pedrado Gneisses possibly represent granitic gneisses derived from melting of thickened lower crust, with a possible minor mantle component. The geochemical similarities between the Arroio Pedrado Gneisses and the Piratini Arc suites suggest that the latter suites probably were assimilated by the melts that generated the

800-780 Ma

Tijucas Terrane

Piratini arc

Porongos-Lavalleja basin

Charrua Ocean

Paleoproterozoic Crust
(2.0-2.2 Ga)

sediment supply

mantle lithosphere

oceanic crust

780 Ma arc magmatism (Piratini, Cerro Bori, Chácara das Pedras, Várzea do Capivarita orthogneisses)

A

780-680 Ma

fragments of Paleoproterozoic crust

680 Ma shoshonitic magmatism (Arroio Pedrado Gneiss)

B

680-650 Ma

São Gabriel Terrane   **Tijucas Terrane**   **Piratini Arc**

Río de la Plata Craton

Ophiolites

C

Fig. 16. Simplified geodynamic evolution of the Piratini Arc, modified from Ramos et al. (2017). A) Eastward subduction underneath an African-related microplate and beginning of the Piratini Arc magmatism; B) Thickening of the Piratini Arc and partial melting of the lower crust; C) Slab break-off after continent-continent collision and beginning of the orogenic collapse.

Arroio Pedrado Gneisses, acting as contaminants to the source. The Zr saturation temperatures, together with the geochemical and isotopic data (section 5.2) suggest that the Arroio Pedrado Gneisses were derived from melts generated at upper amphibolite-granulite facies temperatures, in a subduction-related setting.

Based on the data presented in this paper, it is reasonable to suggest that the obtained age of 680 Ma, interpreted as the crystallization age of the Arroio Pedrado Gneisses (Fig. 9A), potentially represents a deep-crustal magmatism triggered by subduction-related heat sources (Fig. 16A an 16B) prior to continental collision (in our model, the collision between the Río de la Plata Craton and the Piratini Arc) (Fig. 16C). As suggested by metamorphic peak ages, a collisional event in the Dom Feliciano Belt is constrained at around 660 Ma (e.g. Gross et al., 2006, 2009). Thus, the peak metamorphic age of 660 Ma obtained for the Arroio Pedrado Gneisses (Fig. 9B) is in good agreement with those reported for the Piratini Arc suites by, e.g., Lenz et al. (2011), Tambara (2015), Martil et al. (2017), and Koester et al. (2016).

6. Conclusions

From the study presented in this paper, we draw the following conclusions.

- The Arroio Pedrado Gneisses yield Cryogenian magmatic crystallization age of 680 ± 2.9 Ma. These rocks crystallized from a water-satured magma under oxidative conditions;
- The parental magma of the Arroio Pedrado Gneisses shows a metaluminous to weakly peraluminous character and shoshonitic signature;
- The partial equilibrium of the plagioclase + alkali feldspar + biotite + hornblende paragenesis is consistent with amphibolite facies metamorphism. Peak metamorphism is dated at 660 ± 2.8 Ma;
- The geochemical data supports a continental magmatic arc setting for these gneisses, linked to the evolution of the Piratini Arc;
- Negative εNd and εHf values, together with $^{87}Sr/^{86}Sr_{(i)}$ values suggest that the Arroio Pedrado Gneisses were generated by partial melting of thickened mafic lower crust, with a possible minor mantle component;
- From the ages of inherited zircons (ca. 780 Ma), εHf values (−13 to −15), and Nd model ages (1.4–1.6 Ga), the probable crustal components are rocks from the Paleoproterozoic basement (e.g., Arroio dos Ratos Complex) and the Piratini Arc itself;
- The magmatic activity of the Piratini Arc is constrained between 780 and 680 Ma. At around 660-650 Ma the arc underwent amphibolite-facies metamorphism;
- All these features together suggest that the evolution of the Piratini Arc is possibly similar to that of the Andean Mountains, not only regarding the subduction-related crustal thickening, but also the long time span of magmatic arc activity (at least 100 Ma) in the proposed scenario.

Acknowledgements

References

Almeida, F.F.M., Hasui, Y., Brito-Neves, B.B., Fuck, R.A., 1981. Brazilian structural provinces: an introduction. Earth Sci. Rev. 17, 1–29.

Arena, K.R., Hartmann, L.A., Lana, C.C., 2018. U–Pb–Hf isotopes and trace elements of metasomatic zircon delimit the evolution of Neoproterozoic Capané ophiolite in the southern Brasiliano Orogen. Int. Geol. Rev. 60 (7), 911–928.

Babinski, M., Chemale Jr., F., Van Schmus, W.R., Hartmann, L.A., Silva, L.C., 1997. U-Pb and Sm-Nd geochronology of the Neoproterozoic granitic-gneissic Dom Feliciano belt, southern Brazil. J. South Am. Earth Sci. 10 (3/4), 263–274.

Basei, M.A.S., Siga, J.R.O., Masquelin, H., Harara, O.M., Reis Neto, J.M., Preciozzi, F., 2000. The Dom Feliciano belt of Brazil and Uruguay and its foreland domain the rio de la Plata craton: framework, tectonic evolution and correlation with similar provinces of southwestern Africa. In: Cordani, U.G., Milani, E.J., Thomaz Filho, A., Campos, D.A. (Eds.), Rio de Janeiro, SBG, Tectonic Evolution of South American Platform, pp. 311–334.

Basei, M.A.S., Frimmel, H.E., Nutman, A.P., Preciozzi, F., Jacob, J., 2005. A connection between the Neoproterozoic Dom Feliciano (Brazil/Uruguay) and Gariep (Namibia/ South Africa) orogenic belts – evidence from a reconnaissance provenance study. Precambrian Res. 139, 195–221.

Basei, M.A.S., Campos Neto, M.C., Castro, N.A., Nutman, A.P., Wemmer, M.T., Yamamoto, M.T., Hueck, M., Osako, L., Siga Jr., O., Passarelli, C.R., 2011. Tectonic evolution of the Brusque group, Dom Feliciano belt, Santa Catarina. J. South Am. Earth Sci. 32, 324–350.

Battisti, M.A., Bitencourt, M.F., De Toni, G.B., Nardi, L.V.S., Konopásek, J., 2018. Metavolcanic rocks and orthogneisses from Porongos and Várzea do Capivarita complexes: a case for identification of tectonic interleaving at different crustal levels from structural and geochemical data in southernmost Brazil. J. South Am. Earth Sci. 88, 253–274.

Bersan, S.M., Danderfer, A., Abreu, F.R., Lana, C., 2018. Petrography, geochemistry and geochronology of the potassic granitoids of the rio Itacambiruçu Supersuite: implications for the Meso- to Neoarchean evolution of the Itacambira-Monte Azul block. Braz. J. Geol. 48 (1), 1–24.

Bertotti, A.L., Chemale Jr., F., Kawashita, K., 2013. Lu-Hf em Zircão por LA-ICP-MS: Aplicação em Gabro do Ofiolito de Aburrá, Colômbia. Pesqui. em Geociencias 40 (2), 117–127.

Bloomer, S.H., Stern, R.J., Fisk, E., Geschwind, C.H., 1989. Shoshonitic volcanism in the Northern Mariana arc: Mineralogic and major and trace element characteristics. J. Geophys. Res. 94, 4469–4496.

Boehnke, P., Watson, E.B., Trail, D., Harrison, T.M., Scmitt, A.K., 2013. Zircon saturation re-revisited. Chem. Geol. 351, 324–334.

Bossi, J., Gaucher, C., 2004. The Cuchilla Dionisio terrane, Uruguay: an allochthonous block accreted in the Cambrian to SW-Gondwana. Gondwana Res. 7 (3), 661–674.

Cabanis, B., Lecolle, M., 1989. Le diagramme La/10-Y/15-Nb/8: unountil pour la discrimination de las series volcaniques et la mise en evidence des processos de mélange et/ou dês contamination crustal. Comptes rendus de l'Académie des Sciences, Paris 309, 2023–2029.

Chemale Jr., F., 2000. Evolução geológica do Escudo sul-rio-grandense. In: Holz, M., De Ros, L.F. (Eds.), Geologia Do Rio Grande Do Sul. Porto Alegre, Edição CIGO/UFRGS, pp. 13–52.

Chen, J.L., Xu, J.F., Wang, B.D., Kang, Z.Q., Jie, L., 2010. Origin of Cenozoic alkaline potassic volcanic rocks at Konglong Xing, Lhasa terrane, Tibetan plateau: products of partial melting of a mafic lower-crustal source? Chem. Geol. 273, 286–299.

Condie, K.C., 2015. Earth as an Evolving Planetary System, third ed. Elsevier, Amsterdam, pp. 350.

Corfu, F., Hanchar, J.M., Hoskin, P.O.W., Kinny, P., 2003. Atlas of zircon textures. In: In: Hanchar, J.M., Hoskin, P.O.W. (Eds.), Mineralogical Society of America and Geochemical Society, Reviews in Mineralogy & Geochemistry, vol. 53. pp. 469–500.

Couzinié, S., Laurent, O., Moyen, J.-F., Zeh, A., Bouilhol, P., Villaros, A., 2016. Postcollisional magmatism: crustal growth not identified by zircon Hf–O isotopes. Earth Planet. Sci. Lett. 456, 182–195.

DePaolo, D.J., 1981. Neodymium isotopes in the Colorado Front Range and crust–mantle evolution in the Proterozoic. Nature 29 (1), 193–196.

DePaolo, D.J., Wasserburg, G.J., 1979. Petrogenetic mixing models and Nd-Sr isotopic patterns. Geochim. Cosmochim. Acta 43 (4), 615–627.

Diener, J.F.A., Thomas, R.J., Macey, P.H., 2017. Pan-african accretionary metamorphism in the Sperrgebiet domain, Gariep belt, SW Namibia. Precambrian Res. 292, 152–162.

Feeley, T.C., Cosca, M.A., 2003. Time vs. composition trends of magmatism at Sunlight volcano, Absaroka volcanic province, Wyoming. Geol. Soc. Am. Bull. 115, 714–728.

Fernandes, L.A.D., Menegat, R., Costa, A.F.U., Koester, E., Porcher, C.C., Tommasi, A., Kraemer, G., Ramgrab, G.R., Camozzato, E., 1995a. Evolução tectônica do Cinturão Dom Feliciano no Escudo Sul-riograndense: Parte I – Uma contribuição a partir do registro geológico. Rev. Bras. Geociencias 25 (4), 351–374.

Fernandes, L.A.D., Menegat, R., Costa, A.F.U., Koester, E., Porcher, C.C., Tommasi, A., Kraemer, G., Ramgrab, G.R., Camozzato, E., 1995b. Evolução tectônica do Cinturão Dom Feliciano no Escudo Sul-riograndense: Parte II – Uma contribuição a partir das assinaturas geofísicas. Rev. Bras. Geociencias 25 (4), 375–384.

Fragoso-César, A.R.S., 1980. O Cráton Rio de Ia Plata e o Cinturão Dom Feliciano no Escudo Uruguaio-Sul-Riograndense. In: 31th Congresso Brasileiro de Geologia. Curitiba. Proceedings, vol. 5. pp. 2879–2892.

Fragoso-César, A.R.S., 1991. Tectônica de placas no Ciclo Brasiliano: as orogenias dos cinturões Dom Feliciano e Ribeira no Rio Grande do Sul. PhD Thesis. São Paulo, Universidade de São Paulo, pp. 367.

Frantz, J.C., Lima, E.F., Machado, R.P., Naumann, M.P., 1984. Contribuição à geologia da região de Encruzilhada do Sul - RS. In: 33th Congresso Brasileiro de Geologia. Rio de Janeiro, Proceedings, vol. 5. pp. 2407–2416.

Frimmel, H.E., 2018. The Gariep belt. In: Siegesmund, S., Basei, M., Oyhantçabal, P., Oriolo, S. (Eds.), Geology of Southwest Gondwana. Springer, Regional Geology Reviews, pp. 353–386.

Frimmel, H.E., Hartnady, C.J.H., Koller, F., 1996. Geochemistry and tectonic setting of magmatic units in the Pan-African Gariep Belt, Namibia. Chem. Geol. 130 (1–2), 101–121.

Gaucher, C., Finney, S., Poiré, D.G., Valencia, V.A., Grove, M., Blanco, G., Pamoukaghlián, K., Gómez Peral, L., 2008. Detrital zircon ages of Neoproterozoic sedimentary successions in Uruguay and Argentina: insights into the geological evolution of the Río de la Plata Craton. Precambrian Res. 167, 150–170.

Gaucher, C., Frimmel, H.E., Germs, G.J.B., 2009. Tectonic events and palaeogeographic evolution of southern Gondwana in the Neoproterozoic and Cambrian. In: In: Gaucher, C., Sial, A.N., Halverson, G.P., Frimmel, H.E. (Eds.), Neoproterozoic-Cambrian Tectonics, Global Change and Evolution: a Focus on Southwestern Gondwana, vol. 16. Elsevier, pp. 295–316 Developments in Precambrian Geology.

Germs, G.J.B., 1995. The Neoproterozoic of southwestern Africa, with emphasis on platform stratigraphy and paleontology. Precambrian Res. 73, 137–151.

Gill, R., 2010. Igneous Rocks and Processes: a Practical Guide. Wiley-Blackwell, Chichester, pp. 428.

Goswami, B., Bhattacharyya, C., 2014. Petrogenesis of shoshonitic granitoids, eastern India: implications for the late Grenvillian post-collisional magmatism. Geosci. Front. 5 (6), 821–843.

Gray, D.R., Foster, D.A., Meert, J.G., Goscombe, B.D., Armstrong, R., Trouw, R.A.J., Passchier, C.W., 2008. A Damara orogen perspective on the assembly of southwestern Gondwana. In: In: Pankhurst, R.J., Trouw, R.A.J., Brito-Neves, B.B., De Wit, M.J. (Eds.), West Gondwana: Pre-cenozoic Correlations across the South Atlantic Region, vol. 294. Geological Society of London, Special Publication, pp. 257–278.

Gregory, T.R., Bitencourt, M.F., Nardi, L.V.S., 2011. Structural and petrological characterization of the Arroio dos Ratos complex metatonalites and metadiorites at its type-section, region of Quitéria. RS. Pesquisas em Geociências 38 (1), 85–108.

Gregory, T.R., Bitencourt, M.F., Nardi, L.V., Florisbal, L.M., Chemale Jr., F., 2015. Geochronological data from TTG-type rock associations of the Arroio dos Ratos Complex and implications for crustal evolution of southernmost Brazil in Paleoproterozoic times. J. South Am. Earth Sci. 57, 49–60.

Gross, A.O.M.S., Porcher, C.C., Fernandes, L.A.D., Koester, E., 2006. Neoproterozoic low-pressure/high-temperature collisional metamorphic evolution in the Várzea do Capivarita Metamorphic Suite, SE Brazil: thermobarometric and Sm/Nd evidence. Precambrian Res. 147 (1–2), 41–64.

Gross, A.O.M.S., Droop, G.T.R., Porcher, C.C., Fernandes, L.A.D., 2009. Petrology and thermobarometry of mafic granulites and migmatites from the Chafalote metamorphic suite: new insights into the Neoproterozoic P–T evolution of the Uruguayan–sul- rio-grandense Shield. Precambrian Res. 170, 157–174.

Gruber, L., Porcher, C.C., Koester, E., Bertotti, A.L., Lenz, C., Fernandes, L.A.D., Remus, M.V.D., 2016. Isotope geochemistry and geochronology of syn-depositional volcanism in Porongos Metamorphic Complex, Santana da Boa Vista Antiform, Dom Feliciano Belt, Brazil: onset of an 800 Ma continental arc. J. Sediment. Environ. 1 (2), 202–221.

Harris, N.B.W., Pearce, J.A., Tindle, A.G., 1986. Geochemical characteristics of collision zone magmatism. In: In: Coward, M.P., Ries, A.C. (Eds.), Collision Tectonics, vol. 19. Geological Society of London, Special Paper, pp. 115–158.

Hartmann, L.A., Chemale Jr., F., 2003. Mid amphibolite facies metamorphism of harzburgites in the Neoproterozoic Cerro Mantiqueiras Ophiolite, southernmost Brazil. Ann. Braz. Acad. Sci. 75 (1), 109–128.

Hartmann, L.A., Leite, J.A.D., Mc Naughton, N.J., Santos, J.O.S., 1999. Deepest exposed crust of Brazil–SHRIMP establishes three events. Geology 27, 947–950.

Hartmann, L.A., Chemale Jr., F., Philipp, R.P., 2007. Evolução geotectônica do rio grande do sul no Pré-Cambriano. In: Ianuzzi, R., Frantz, J.C. (Eds.), 50 Anos de Geologia: Instituto de Geociências. Contribuições. Porto Alegre, Comunicação e Identidade, pp. 97–123.

Hartmann, L.A., Philipp, R.P., Santos, J.O.S., McNaughton, N.J., 2011. Time frame of 753-680 Ma juvenile accretion during the São Gabriel orogeny, southern Brazilian Shield. Gondwana Res. 19, 84–99.

Hawkesworth, C.J., Gallagher, K., Hergt, J.M., McDermott, F., 1993. Trace element fractionation processes in the generation of island arc basalts. Philos. Trans. R. Soc. Lond. 342 (1663), 179–191.

Heilbron, M., Pedrosa-Soares, A.C., Campos Neto, M., Silva, L.C., Trouw, R.A.J., 2004. A Província Mantiqueira. In: Mantesso Neto, A., Bartorelli, A., Carneiro, C.D.R., Brito Neves, B.B. (Eds.), O desvendar de um continente: a moderna geologia da América do Sul e o legado da obra de Fernando Flávio Marques de Almeida. São Paulo, Beca, pp. 203–234.

Höfig, D.F., Marques, J.C., Basei, M.A.S., Giusti, R.O., Kohlrausch, C., Frantz, J.C., 2018. Detrital zircon geochronology (U-Pb LA-ICP-MS) of syn-orogenic basins in SW Gondwana: new insights into the Cryogenian-Ediacaran of porongos complex, Dom Feliciano belt, southern Brazil. Precambrian Res. 306, 189–208.

Hueck, M., Oyhantçabal, P., Philipp, R.P., Basei, M.A.S., Siegesmund, S., 2018. The Dom Feliciano belt in southern Brazil and Uruguay. In: Siegesmund, S., Basei, M., Oyhantçabal, P., Oriolo, S. (Eds.), Geology of Southwest Gondwana. Springer, Regional Geology Reviews, pp. 267–302.

Ivanov, A.V., Levitskii, I.V., Levitskii, V.I., Corfu, F., Demonterova, E.I., Reznitskii, L.Z., Pavlova, L.A., Kamenetsky, V.S., Savatenkov, V.M., Powerman, V.I., 2019. Shoshonitic magmatism in the Paleoproterozoic of the south-western Siberian Craton: an analogue of the modern post-collision setting. Lithos 328–329, 88–100.

Jost, H., Bitencourt, M.F., 1980. Estratigrafia e tectônica de uma fração da faixa de dobramentosde Tijucas no Rio Grande do Sul. Acta Geol. Leopoldensia 7 (6), 27–60.

Jung, S., Hoffer, E., Hoernes, S., 2007. Neo-Proterozoic rift-related syenites (Northern

Damara Belt, Namibia): geochemical and Nd–Sr–Pb–O isotope constraints for mantle sources and petrogenesis. Lithos 96, 415–435.

Kay, S.M., Mpodozis, C., Gardeweg, M., 2013. Magma sources and tectonic setting of Central Andean andesites (25.5-28°S) related to crustal thickening, forearc subduction erosion and delamination. In: In: Gómez-Tuena, A., Straub, S.M., Zellmer, G.F. (Eds.), Orogenic Andesites and Crustal Growth, vol. 385. Geological Society of London, Special Publications, pp. 303–334 1.

Klein, F.G., Koester, E., Vieira, D.T., Porcher, C.C., Ramos, R.C., Philipp, R.P., 2018. Geologia do Granito Três Figueiras: magmatismo peraluminoso de 585 Ma no sudeste do Cinturão Dom Feliciano. Pesqui. em Geociencias 45 (2), e0665.

Koester, E., Porcher, C.C., Pimentel, M.M., Fernandes, L.A.D., Vignol-Lelarge, M.L., Oliveira, L.D., Ramos, R.C., 2016. Further evidence of 777 Ma subduction-related continental arc magmatism in Eastern Dom Feliciano Belt, southern Brazil: the Chácara das Pedras Orthogneiss. J. South Am. Earth Sci. 68, 155–166.

Konopásek, J., Košler, J., Tajčmanová, L., Ulrich, S., Kitt, S.L., 2008. Neoproterozoic igneous complex emplaced along major tectonic boundary in the Kaoko Belt (NW Namibia): ion probe and LA-ICP-MS dating of magmatic and metamorphic zircons. J. Geol. Soc. 165 (1), 153–165.

Lai, S.C., Qin, J.F., Li, Y.F., 2007. Partial melting of thickened Tibetan crust: geochemical evidence from Cenozoic adakitic volcanic rocks. Int. Geol. Rev. 49, 357–373.

Leite, J.A.D., Hartmann, L.A., McNaughton, N.J., Chemale Jr., F., 1998. SHRIMP U/Pb zircon geochronology of Neoproterozoic juvenile and crustal-reworked terranes in southernmost Brazil. Int. Geol. Rev. 40, 688–705.

Lena, L.O.F., Pimentel, M.M., Philipp, R.P., Armstrong, R., Sato, K., 2014. The evolution of the Neoproterozoic São Gabriel juvenile terrane, southern Brazil based on high spatial resolution U-Pb ages and 18O data from detrital zircons. Precambrian Res. 247, 126–138.

Lenz, C., 2006. Evolução metamórfica dos metapelitos da Antiforme Serra dos Pedrosas: condições e idades do metamorfismo. Master Degree Dissertation, Porto Alegre. Universidade Federal do Rio Grande do Sul, pp. 111p.

Lenz, C., Fernandes, L.A.D., McNaughton, N.J., Porcher, C.C., Masquelin, H., 2011. U-Pb SHRIMP ages for the Cerro Bori orthogneisses, Dom Feliciano belt in Uruguay: evidences of a ~800 Ma magmatic and ~650 Ma metamorphic event. Precambrian Res. 185, 149–163.

Lenz, C., Porcher, C.C., Fernandes, L.A.D., Masquelin, H., Koester, E., Conceição, R.V., 2012. Geochemistry of the Neoproterozoic (800 - 767 Ma) Cerro Bori orthogneisses, Dom Feliciano belt in Uruguay: tectonic evolution of an ancient continental arc. Mineral. Petrol. 1, 10.

Loureiro, P.O., 2013. Evolução magmática do Complexo Pinheiro Machado na região de Monte Bonito, Pelotas, RS. - Porto Alegre. Instituto de Geociências, Universidade Federal do Rio Grande do Sul. Graduation Monography, pp. 75.

Loureiro, P.O., Koester, E., Weinberg, R., Porcher, C.C., Pimentel, M.M., Knijnik, D.B., 2015. Magmatic evolution of Pinheiro Machado complex in Monte Bonito region, southern Brazil. In: VIII Hutton Symposium on Granites and Related Rocks, Florianópolis. Book of Abstracts, pp. 125.

Ludwig, K.R., 2008. Isoplot 3.70, a Geochronological Toolkit for Microsoft Excel, vol. 4. Geochronology Center, Special Publication, Berkeley, pp. 76p.

Marques, J.C., Roisenberg, G.A., Jost, H., Frantz, J.C., Teixeira, R.S., 2003. Geologia e geoquímica das rochas metaultramáficas da antiforme Capané, Suíte Metamórfica Porongos, RS. Rev. Bras. Geociencias 33 (1), 83–94.

Martil, M.M., 2016. O magmatismo de Arco Continental pré-colisional (790 Ma) e a reconstituição espaço-temporal do regime transpressivo (650 Ma) no Complexo Várzea do Capivarita, Sul da Província Mantiqueira. Instituto de Geociências, Universidade Federal do Rio Grande do Sul, pp. 167 PhD Thesis.

Martil, M.M., Bitencourt, M.F., Nardi, L.V.S., Koester, E., Pimentel, M.M., 2017. Precollisional, Tonian (ca. 790 Ma) continental arc magmatism in southern Mantiqueira Province, Brazil: geochemical and isotopic constraints from the Várzea do Capivarita Complex. Lithos 274–275, 39–52.

Masquelin, H., 2000. Evolução Estrutural e Metamórfica do Complexo Cerro Olivo, Sudeste do Uruguay. Unpublished Ph.D. thesis. Instituto de Geociências, Universidade Federal do Rio Grande do Sul, Porto Alegre v.1: 1–227, v.2: 1–117,1 map.

Masquelin, H., Fernandes, L.A.D., Lenz, C., McNaughton, N.J., Porcher, C.C., 2012. The Cerro Olivo complex: a pre-collisional Neoproterozoic magmatic arc in eastern Uruguay. Int. Geol. Rev. 54 (10), 1161–1183.

May, G.E., 1990. Pan-African Magmatism and Regional Tectonics of South Brazil. Ph.D. Thesis. Open University, Milton Keynes, pp. 343.

Machado, R., Philipp, R.P., Mello, F., 1995. Reconhecimento de zonas de cisalhamento dúcteis de alto ângulo com cinemática superposta na extremidade sul do Batólito Pelotas, RS. In: V Simpósio Nacional de Estudos Tectônicos, Gramado, Boletim de Resumos Expandidos, pp. 52–53.

McDonough, W.F., Sun, S.S., 1995. The composition of the Earth. Chem. Geol. 120, 223–253.

Meen, J.K., 1987. Formation of shoshonites from calcalkaline basalt magmas: geochemical and experimental constraints from the type locality. Contrib. Mineral. Petrol. 97, 333–351.

Mogk, D.W., Burger, H.R., Mueller, P.A., D'Arcy, K., Heatherington, A.L., Wooden, J.L., Abeyta, R.L., Martin, J., Jacob, L.J., 2004. Geochemistry of quartzofeldspathic gneisses and metamorphic mafic rocks of the Indian Creek and Pony–Middle mountain metamorphic suites, Tobacco root Mountains, Montana. In: In: Brady, J.B., Burger, H.R., Cheney, J.T., Harms, T.A. (Eds.), Precambrian Geology of the Tobacco Root Mountains, Montana, vol. 377. Geological Society of America, Special Paper, Boulder, pp. 15–46.

Morrison, G.W., 1980. Characteristics and tectonic setting of the shoshonite rocks association. Lithos 13, 97–108.

Moyen, J.F., Paquette, J.L., Ionov, D.A., Gannoun, A., Korsakov, A.V., Golovin, A.V.,

Moine, B.N., 2017. Paleoproterozoic rejuvenation and replacement of Archaean lithosphere: evidence from zircon U–Pb dating and Hf isotopes in crustal xenoliths at Udachnaya, Siberian craton. Earth Planet. Sci. Lett. 457, 149–159.

Müller, D., Groves, D.I., 1995. Potassic Igneous Rocks and Associated Gold–Copper Mineralization. Springer-Verlag, Berlin.

Nakamura, N., 1974. Determination of REE, Ba, Fe, Mg, Na and K in carbonaceous and ordinary chondrites. Geochim. Cosmochim. Acta 38, 757–775.

Nardi, L.V.S., 1986. As rochas granitóides da série shoshonítica. Rev. Bras. Geociencias 16 (1), 3–10.

Nesbitt, H.W., Young, G.M., 1982. Early Proterozoic climates and plate motions inferred from major element chemistry of lutites. Nature 299, 715–717.

Ohta, T., Arai, H., 2007. Statistical empirical index of weathering in igneous rocks: a new tool for evaluating the degree of weathering. Chem. Geol. 240, 280–297.

Oyhantçabal, P., Siegesmund, S., Wemmer, K., Frei, R., Layer, P., 2009. Geochronological constraints on the evolution of the southern Dom Feliciano belt (Uruguay). J. Geol. Soc. Lond. 166, 1–11.

Pearce, J.A., 1982. Trace element characteristics of lavas from de-structive plate boundaries. In: Thorpe, R.S. (Ed.), Andesites. John Wiley & Sons, New York, pp. 525–548.

Pearce, J.A., 2008. Geochemical fingerprinting of oceanic basalts with applications to ophiolite classification and the search for Archean oceanic crust. Lithos 100, 14–48.

Pearce, J.A., Peate, D.W., 1995. Tectonic implications of the composition of volcanic arc magmas. Annu. Rev. Earth Planet Sci. 23, 251–285.

Pearce, J.A., Bender, J.F., De Long, S.E., Kidd, W.S.F., Low, P.J., Güner, Y., Şaroğlu, F., Yılmaz, Y., Moorbath, S., Mitchell, J.G., 1990. Genesis of collision volcanism in eastern Anatolia, Turkey. J. Volcanol. Geotherm. Res. 44, 189–229.

Peccerillo, A., Taylor, S.R., 1976. Geochemistry of Eocene calc-alkaline volcanic rocks from the Kastamonu area, northern Turkey. Contrib. Mineral. Petrol. 58, 63–81.

Peel, E., Sánchez-Bettucci, L., Basei, M.A.S., 2018. Geology and geochronology of Paso del Dragón Complex (northeastern Uruguay): implications on the evolution of the Dom Feliciano Belt (Western Gondwana). J. South Am. Earth Sci. 85, 250–262.

Pertille, J., Hartmann, L.A., Santos, J.O.S., McNaughton, N.J., Armstrong, R., 2017. Reconstructing the Cryogenian–Ediacaran evolution of the porongos fold and thrust belt, southern brasiliano orogen, based on zircon U–Pb–Hf–O isotopes. Int. Geol. Rev. 59, 1532–1560.

Philipp, R.P., 1990. Geologia e Petroquímica dos granitóides da região de Monte Bonito, Pelotas. RS. Porto Alegre. Instituto de Geociências, Universidade Federal do Rio Grande do Sul. Master Degree Dissertation, pp. 231.

Philipp, R.P., 1998. A evolução geológica e tectônica do BatólitoPelotas no Rio Grande do Sul. Instituto de Geociências,Universidade de São Paulo, São Paulo, Tese de Doutorado, pp. 255p.

Philipp, R.P., Campos, R.S., 2004. Geologia, petrográfica e litogeoquímica dos Gnaisses Porto Alegre, RS, Brasil: implicações geotectônicas. Pesqui. em Geociencias 31 (2), 79–94.

Philipp, R.P., Machado, R., 2002. Ocorrência e significado dos Septos do Embasamento encontrados nas suítes graníticas do Batólito Pelotas, RS, Brasil. Pesqui. em Geociencias 29 (1), 43–57.

Philipp, R.P., Machado, R., Nardi, L.V.S., Lafon, J.M., 2002. O magmatismo granítico Neoproterozóico do Batólito Pelotas no sul do Brasil: novos dados e revisão de geocronologia regional. Rev. Bras. Geociencias 32 (2), 277–290.

Philipp, R.P., Lusa, M., Nardi, L.V.S., 2008. Petrology of dioritic, tonalitic and trondhjemitic gneisses from Encantadas Complex, Santana da Boa Vista, southernmost Brazil: paleoproterozoic continental-arc magmatism. An Acad. Bras Ciências 80 (4), 735–748.

Philipp, R.P., Massone, H.J., Campos, R.S., 2013. Peraluminous leucogranites of Cordilheira suite, record of Neoproterozoic collision and generation of Pelotas batholith, Dom Feliciano belt, southern Brazil. J. South Am. Earth Sci. 43, 8–24.

Philipp, R.P., Pimentel, M.M., Chemale Jr., F., 2016a. Tectonic evolution of the Dom Feliciano belt in southern Brazil: geological relationships and U-Pb geochronology. Braz. J. Geol. 46 (1), 83–104.

Philipp, R.P., Jelinek, A.R., Chemale Jr., F., 2016b. Post-collisional Neoproterozoic magmatism of the Pelotas batholith, Dom Feliciano belt, RS, southernmost Brazil. Int. Geol. Rev (submitted).

Philipp, R.P., Pimentel, M.M., Basei, M.A.S., 2018. The tectonic evolution of the São Gabriel terrane, Dom Feliciano belt, southern Brazil: the closure of the Charrua ocean. In: Siegesmund, S., Basei, M., Oyhantçabal, P., Oriolo, S. (Eds.), Geology of Southwest Gondwana. Springer, Regional Geology Reviews, pp. 243–265.

Porada, H., 1989. Pan-African rifting and orogenesis in southern to Equatorial Africa and eastern Brazil. Precambrian Res. 44, 103–136.

Porcher, C.C., McNaughton, N.J., Leite, J.A.D., Hartmann, L.A., Fernandes, L.A.D., 1999. Idade SHRIMP em zircão: vulcanismo ácido do Complexo Metamórfico Porongos. In: I Simpósio Sobre Vulcanismo e Ambientes Associados, Gramado. Abstracts, pp. 110.

Preciozzi, F., Masquelin, H., Basei, M.A.S., 1999. The Namaqua/Grenville terrane of eastern Uruguay. In: II Simpósio Sul Americano de Geologia Isotópica. Córdoba, Abstracts, pp. 338–340.

Ramos, V.A., 2010. The tectonic regime along the Andes: present settings as a key for the Mesozoic regimes. Geol. J. 45, 2e25.

Ramos, R.C., Koester, E., 2015. Lithogeochemistry of the meta-igneous units from Arroio grande ophiolitic complex, southernmost Brazil. Braz. J. Geol. 45 (1), 65–78.

Ramos, R.C., Toniolo, J.A., Pinto, G.R., Koester, E., 2014. Zona de cisalhamento (sutura) de Arroio Grande e o novo Domínio Geofísico Sudeste (Escudo Sul-rio-grandense): discussões baseadas em dados geofísicos e de campo. In: VI Simpósio Brasileiro de Geofísica, Porto Alegre. Book of Abstracts.

Ramos, R.C., Koester, E., Porcher, C.C., 2017. Chemistry of chromites from Arroio grande ophiolite (Dom Feliciano belt, Brazil) and their possible connection with the Nama group (Namibia). J. South. Am. Earth Sci. 80, 192–206.

Ramos, R.C., Koester, E., Vieira, D.T., Porcher, C.C., Gezatt, J.N., Silveira, R.L., 2018. Insights on the evolution of the Arroio grande ophiolite (Dom Feliciano belt, Brazil) from Rb-Sr and SHRIMP U-Pb isotopic geochemistry. J. South Am. Earth Sci. 86, 38–53.

Rapela, C.W., Fanning, C.M., Casquet, C., Pankhurst, R.j., Spalletti, L., Poiré, D., Baldo, E.G., 2011. The Rio de La Plata craton and the adjoining Pan-African/brasiliano terranes: their origins and incorporation into south-west Gondwana. Gondwana Res. 20, 673–690.

Rogers, N.W., 1992. Potassic magmatism as a key to trace-element enrichment processes in the upper mantle. J. Volcanol. Geotherm. Res. 50, 85–99.

Rollinson, H.R., 1993. Using Geochemical Data: Evaluation, Presentation, Interpretation. Longman, London, pp. 352p.

Saalmann, K., Remus, M.V.D., Hartmann, L.A., 2006. Structural evolution and tectonic setting of the porongos belt, southern Brazil. Geol. Mag. 143 (1), 59–88.

Saalmann, K., Gerdes, A., Lahaye, Y., Hartmann, L.A., Remus, M.V.D., Läufer, A., 2011. Multiple accretion at the eastern margin of the Rio de la Plata craton: the prolonged Brasiliano orogeny in southernmost Brazil. Int. J. Earth Sci. 100, 355–378.

Shand, S.J., 1943. Eruptive Rocks. Their Genesis, Composition, Classiﬁcation, and Their Relation to Ore-Deposits with a Chapter on Meteorite. Nova Iorque, John Wiley & Sons, pp. 444.

Silva, L.C., Hartmann, L.A., McNaughton, N.J., Fletcher, I.R., 1999. SHRIMP U/Pb zircon dating of Neoproterozoic granitic magmatism and collision in the Pelotas Batholith, Southernmost Brazil. Int. Geol. Rev. 41, 531–551.

Silva, L.C., McNaughton, N.J., Armstrong, R., Hartmann, L.A., Fletcher, I.R., 2005. The Neoproterozoic Mantiqueira Province and its African connections: a zircon-based U-Pb geochronologic subdivision for the Brasiliano/Pan-African systems of orogens. Precambrian Res. 136, 203–240.

Tambara, G.B., 2015. Gnaisses Piratini: magmatismo de 784 Ma no sudeste do Cinturão Dom Feliciano, RS. Master Degree Dissertation. Universidade Federal do Rio Grande do Sul, Porto Alegre, pp. 51.

Tauson, L.V., 1983. Geochemistry and metallogeny of the latitic series. Int. Geol. Rev. 25, 125–135.

Thompson, R.N., Morrison, M.A., Henry, G.L., Parry, S.J., 1984. An assessment of the relative roles of crust and mantle in magma genesis: an elemental approach. Philos. Trans. R. Soc. Lond. 310, 549–590.

Trainini, D.R., 1987. Projeto Mapas Metalogenéticos e de Previsão de Recursos Minerais, Folhas SI-22 Jaguarão-Rio Grande. Porto Alegre, Convênio DNPM/CPRM. 8 mapas. Escala 1:250.000.

Varekamp, J.C., Hesse, A., Mandeville, C.W., 2010. back-arc basalts from the Loncopue grabem (province of Neuquen, Argentina). J. Volcanol. Geotherm. Res. 197, 313–328.

Vieira, D.T., Koester, E., Porcher, C.C., 2016a. Magmatismo Neoproterozoico (680 Ma) no sudeste do Escudo Sul-RioGrandense: U-Pb e Lu-Hf LA-MC-ICP-MS em zircão. In: 48th Congresso Brasileiro de Geologia, Porto Alegre. Proceedings, ID 8889.

Vieira, D.T., Koester, E., Bertotti, A.L., 2016b. Petrologia do granito Chasqueiro, região de Arroio grande, sudeste do Escudo sul-rio-grandense. Braz. J. Geol. 46, 79–108.

Vieira, D.T., Koester, E., Ramos, R.C., Porcher, C.C., Barbosa, L.D.M., Bastos, V., Rodrigues, F., Horn, A.C., 2019. Idade U-Pb paleoproterozoica (2,1 Ga) em meta-gabro no Domínio Leste do Cinturão Dom Feliciano, RS. In: XVII Simpósio Nacional de Estudos Tectônicos, XI International Symposium on Tectonics, and XI Simpósio Sul-Brasileiro de Geologia, Bento Gonçalves. Book of Abstracts, pp. 417.

Wang, X.C., Liu, Y.S., Liu, X.M., 2006. Mesozoic adakites in the Ligqiu Basin of the central NOrth China Craton: partial melting of underplated basaltic lower crust. Geochem. J. 40, 447–461.

Wang, J., Hattori, K., Kilian, R., Stern, C.R., 2007. Metasomatism of sub-arc mantle peridotites below southernmost South America: reduction of fO2 by slab-melt. Contrib. Mineral. Petrol. 153, 607–624.

Watson, E.B., Harrison, T.M., 1983. Zircon saturation revisited temperature and composition effects in a variety of crustal magma types. Earth Planet. Sci. Lett. 64, 295–304.

Wen, D.-R., Chung, S.-L., Song, B., Iizuka, Y., Yang, H.-J., Ji, J., Liu, D., Gallet, S., 2008. Late Cretaceous Gangdese intrusions of adakitic geochemical characteristics, SE Tibet: petrogenesis and tectonic implications. Lithos 105, 1–11.

Wildner, W., Ramgrab, G.E., Lopes, R.C., Iglesias, C.M.F., 2005. Mapa Geológico Do Estado Do Rio Grande Do Sul. Porto Alegre. CPRM – Serviço Geológico do Brasil escala 1:750.000.

Will, T.M., Gaucher, C., Ling, X.-X., Li, X.-H., Li, Q.-L., Frimmel, H.E., 2019. Neoproterozoic magmatic and metamorphic events in the Cuchilla Dionisio terrane, Uruguay, and possible correlations across the south Atlantic. Precambrian Res. 320, 303–322.

Winter, J.D., 2011. Principles of Igneous and Metamorphic Petrology. John Wiley, pp. 467.

Wones, D.R., 1989. Significance of the assemblage titanite + magnetite + quartz in granitic rocks. Am. Mineral. 74, 744–749.

Wu, M., 2015. Ages, Geochemistry and Metamorphism of the Neoarchean Basement in Shandong Province: Implications for Evolution of the North China Craton. Springer, Berlin, pp. 221p.

Wyman, D.A., Kerrich, R., 1993. Archean shoshonitic lamprophyres of the Abitibi Subprovince, Canada: petrogenesis, age, and tectonic setting. J. Petrol. 34, 1067–1109.

Xiong, F., Ma, C., Zhang, J., Liu, B., Jiang, H., 2014. Reworking of old continental lithosphere: an important crustal evolution mechanism in orogenic belts, as evidenced by Triassic I-type granitoids in the East Kunlun orogen, Northern Tibetan Plateau. J. Geol. Soc. 171 (6), 847–863.

Zhang, Y., Sun, M., Yuan, C., Xu, Y., Long, X., Tomurhuu, D., He, B., 2015. Magma mixing origin for high Ba–Sr granitic pluton in the Bayankhongor area, central Mongolia: response to slab roll-back. J. Asian Earth Sci. 113, 353–368.

CAPÍTULO 4

Artigo *"Chafalote Metamorphic Suite (Uruguay): reflections on the evolution of the Punta Del Este Terrane"*

Chafalote Metamorphic Suite (Uruguay): Reflections on the evolution of the Punta del Este Terrane

Daniel Triboli Vieira[a,*], Carla Cristine Porcher[b], Edinei Koester[b], Rodrigo Chaves Ramos[a], Andreia Oliveira Monteiro da Silva Gross[c], Henri Masquelin[d], Luis Alberto D'Ávila Fernandes[b]

[a] Programa de Pós-Graduação em Geociências, Instituto de Geociências, Universidade Federal do Rio Grande do Sul. PO Box 15001, Zip code 91501-970, Porto Alegre, RS, Brazil
[b] Departamento de Geologia, Universidade Federal do Rio Grande do Sul. Bento Gonçalves Avenue, 9500, Zip code 91540-000, Porto Alegre, RS, Brazil
[c] Serviço Geológico do Brasil (CPRM), PO Box 105, Zip code 90840-030, Porto Alegre, RS, Brazil
[d] Instituto de Ciencias Geológicas, Facultad de Ciencias, Universidad de la República. Iguá 4225, Zip code 11400, Montevideo, Uruguay

ABSTRACT

The Chafalote Metamorphic Suite, located in the Uruguayan sector of the Punta del Este Terrane, south-easternmost Dom Feliciano Belt, comprises semipelitic, migmatitic metapelites, mafic granulites, and calc-silicate/amphibolitic gneisses. These supracrustal rocks occur as roof pendants in a granodiorite belonging to the Cerro Olivo Complex. The main structure of the Chafalote Metamorphic Suite is a composite S_0/S_1 banding, related to the main deformation event (D_1) developed under upper-amphibolite/granulite facies conditions. This work presents an integrated study on the latter rocks, involving different geochronological methods (monazite U-Pb LA-ICP-MS and zircon U-Pb SHRIMP) and whole rock Sm-Nd isotope data in order to better understand the metamorphic evolution of the Chafalote Metamorphic Suite during the amalgamation of the SW Gondwana paleocontinent in the Neoproterozoic. The studied rocks record a peak metamorphic event (M_2) occurred at around 660 Ma (monazite U-Pb ages), which was followed by decompression and partial melting (M_3 event) at around 640 Ma (zircon U-Pb ages), probably during the late stages of the D_1 event. The retrograde metamorphic event (M_4) is related to the transition between the D_1 and the development of NE-SW striking, low-grade sinistral shear zones (D_2 event) and intrusion of syn-to post-orogenic Brasiliano granitoids of the Aiguá Batholith at around 600 Ma. The metamorphic conditions, together with geochronological and isotopic similarities, allow the correlation between the studied high-grade metasedimentary rocks and those from the Paso del Dragón Complex in Uruguay, and from the Várzea do Capivarita, Arroio Grande, and Telho Complex in Brazil. The latter rocks possibly share similar source areas and represent different portions of the Neoproterozoic fore-arc and/or back-arc basins developed in the Dom Feliciano Belt during the Brasiliano/Pan-African orogenic cycle.

1. Introduction

The study of Neoproterozoic metamorphic associations which constitute the Punta del Este Terrane, southeasternmost sector of the Dom Feliciano Belt (Preciozzi et al., 1999; Basei et al., 2011), is hampered by an incomplete geologic record. Some of these occurrences, which represent exposed old orogenic roots (e.g. Cerro Olivo Complex – Masquelin et al., 2012) reworked during the amalgamation of the Southwest Gondwana paleocontinent (Fig. 1A and B), record high-grade peak metamorphism associated with migmatization, obliterating

previous metamorphic events and sometimes the nature of protoliths.

The understanding of the whole tectonic scenario remains unclear, even with the significant progress made on the reconstruction of P-T-t paths of the Neoproterozoic high-grade metamorphism recorded in the Dom Feliciano Belt (Masquelin et al., 2005; Gross et al., 2006, 2009; Philipp et al., 2013; Bom et al., 2014; Skagseth, 2016; Martil et al., 2017; Ramos et al., 2019). In addition to constraining the P-T conditions, the dating of such events, together with considerations regarding the provenance of the protoliths, is essential for the understanding of the regional metamorphic evolution and the crustal behavior during the

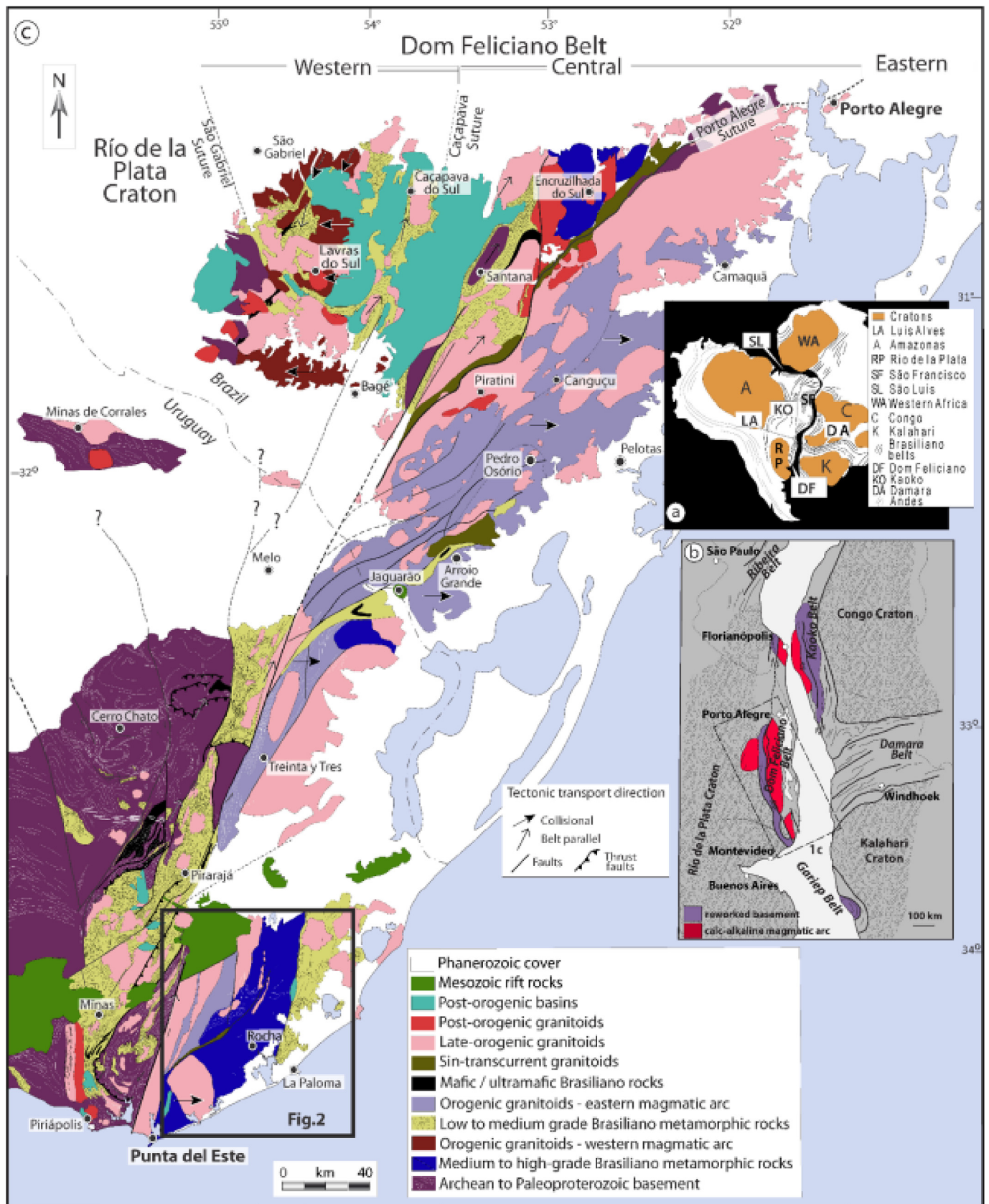**Fig. 1.** Geological map of the Uruguayan-Sul-Rio-Grandense Shield (modified from Masquelin et al., 2012). A) Configuration of the West Gondwana paleocontinent; B) Location of the Dom Feliciano Belt and Damara Orogen in the context of the West Gondwana paleocontinent; C) Simplified geological map of the Dom Feliciano Belt and Río de La Plata Craton in Rio Grande do Sul state (Brazil) and Uruguay.

orogenic event.

In high-grade metamorphic terranes, the determination of the duration of the events is based on chemical and isotopic features of minerals which are stable under high P-T conditions, such as zircon and monazite (Harley et al., 2007). Zircon can provide reliable and robust ages regarding its recrystallization and growth/overgrowth during the different stages of metamorphism, thus constraining the timing of the events which affected the host rock (Rubatto and Hermann, 2003; Zheng et al., 2009; Liu and Liou, 2011). Monazite, in turn, is less susceptible to Pb loss and isotopic inheritance (Rubatto et al., 2001; Foster et al., 2002; Hermann and Rubatto, 2003), growing and recrystallizing only during high-grade metamorphism (Ayers et al., 2002, 2006; Wan et al., 2005; Williams et al., 2007; Buick et al., 2010). On the other hand, due to its relative robust behavior, the Sm-Nd isotopic system is of particular interest in provenance studies of metasedimentary rocks. The fact that Sm and Nd are both rare earth elements (REE) and show similar chemical behavior is an advantage in relation to isotopic pairs such as K-Ar, Rb-Sr and U-Pb, since they are normally not fractionated during the most common geological processes (e.g. Dickin, 2018). Thus, Sm-Nd isotopic systematics constitute an important additional tool for the investigation of basins with complex geologic histories (Boghossian et al., 2000; Stevenson et al., 2000).

Starting from these premises, this contribution presents integrated studies on petrography (optical microscopy), geochronology (U-Pb SHRIMP in zircon, and U-Pb LA-ICP-MS in monazite), and Sm-Nd isotope data of metasedimentary rocks from the Chafalote Metamorphic Suite (Masquelin et al., 2001), a metamorphic association belonging to the previously mentioned Cerro Olivo Complex, located in the southeastern sector of the Punta del Este Terrane in Uruguay. The goal of this work is to characterize the absolute ages of the high-grade events which affected these rocks and thus allowing a comparison with other high-grade events related to the evolution of the Dom Feliciano Belt during the Brasiliano/Pan-African orogenic cycle.

2. Geological context

The Chafalote Metamorphic Suite is located in the Dom Feliciano Belt, southernmost Mantiqueira Province (Almeida et al., 1981). This Neoproterozoic to Early Cambrian orogenic belt extends from southernmost Brazil (Rio Grande do Sul and Santa Catarina states) to Punta del Este, in Uruguay (Fig. 1C), and is interpreted as the result of the collision between Río de La Plata, Congo, and Kalahari Cratons, and other minor blocks/microplates during the Brasiliano/Pan-African orogenic cycle (e.g. Fernandes et al., 1995a, 1995b; Basei et al., 2000; Heilbron et al., 2004; Gaucher et al., 2009; Oyhantçabal et al., 2009, 2011; Konopásek et al., 2016; Santos et al., 2017; Hueck et al., 2018). Its African counterpart is the Damara Orogen, comprising the Kaoko, Damara and Gariep Belts (Fig. 1B) in Namibia and South Africa (e.g. Gray et al., 2008; Frimmel et al., 2011; Oyhantçabal et al., 2011; Konopásek et al., 2018).

The Chafalote Metamorphic Suite is one of the metamorphic associations which constitute the basement of the Punta del Este Terrane, southeasternmost sector of the Dom Feliciano Belt. This terrane, in its original definition (Preciozzi et al., 1999), comprised the metasedimentary rocks of the Rocha (Sánchez-Bettucci and Mezzano, 1993) and San Carlos Formations (Masquelin, 1990), and the volcano-sedimentary rocks of the Sierra de Aguirre Formation (Masquelin and Tabó, 1988; Campal and Schipilov, 2005), located between Punta del Este (south) and Velázquez (north). The Punta del Este-Alférez-Cordillera shear zone system roughly marks the limit (Basei et al., 2011) between the Punta del Este Terrane and the Brasiliano batholiths (i.e., the Aiguá-Pelotas Batholith, Central Granitic Terrane or Cuchilla Dionisio Terrane – Fragoso-César et al., 1986; Basei et al., 2000; Bossi and Gaucher, 2004) located further west/northwest.

In Peel et al. (2018) it was suggested that the Punta del Este Terrane could be extended further north to Melo region, due to the similarity

between the gneissic-migmatitic basement found near the Paso del Dragón Complex and that of the Cerro Olivo Complex (the basement of the original definition of this terrane). Recently, in Ramos et al. (2018) it was suggested that this terrane could be extended further north to Arroio Grande and Pedro Osório region (Brazil) (Fig. 1C), due to the correlation between the oceanic rocks of the Paso del Dragón (Will et al., 2014; Peel et al., 2018) and Arroio Grande Complex (Ramos et al., 2018) and the presence of a gneissic basement (Arroio Pedrado Gneisses – Vieira et al., 2019) with metamorphic ages and geochemical signatures similar to those found in its Uruguayan counterparts.

In the southernmost sector of the Punta del Este Terrane the basement is composed of migmatites and high-grade metamorphic rocks of the Cerro Olivo Complex (Masquelin et al., 2001). This complex comprises: (i) the Cerro Bori Gneisses (crystallization and metamorphic ages of, respectively, ca. 780-750 Ma and ca. 670-640 Ma), comprising tonalitic to granodioritic orthogneisses with a continental arc geochemical signature (Oyhantçabal et al., 2009; Lenz et al., 2011, 2013; Masquelin et al., 2012); (ii) the Centinela Gneisses, represented by partially melted augen gneisses, with a continental arc geochemical signature (Masquelin et al., 2012) similar to that of the Cerro Bori Gneisses; (iii) the Chafalote Metamorphic Suite, focus of the present work, which crops out in the central and eastern portions of the Cerro Olivo Complex (Fig. 2); (iv) the Manantiales mylonitic and migmatites gneisses and (v) the Piriz Granodiorite, a cordierite-bearing peraluminous granitoid (Masquelin et al., 2012).

The Cerro Olivo Complex was intruded by syn-to post-orogenic Brasiliano granitoids (~620-550 Ma) of the Aiguá Batholith, and by rhyolitic dikes of the Sierra de los Ríos Formation (Masquelin et al., 2005, 2012). The older granitoids of the latter batholith, as well as the rocks of the Cerro Olivo Complex, show a mylonitic foliation related to transcurrent shear zones found in the region (e.g. Sierra Ballena, Otazo, Cerro Amaro, and Alférez-Cordillera shear zones – Masquelin and Gómez-Rifas, 1998; Oyhantçabal et al., 2009, Sánchez Betucci et al., 2010; Oriolo et al., 2016).

The Chafalote Metamorphic Suite, focus of this study is a sequence of upper amphibolite to granulite facies, comprises semipelitic, migmatitic metapelites, mafic granulites, and calc-silicate/amphibolitic gneisses. These rocks occur as roof-pendants and also as xenoliths in the Piriz granodiorite (Fig. 2) (Masquelin, 2000; Masquelin et al., 2005, 2012; Gross et al., 2009). This suite was affected by two main deformation events, named D_1 and D_2 (Masquelin, 2000; Masquelin et al., 2005; Gross et al., 2009). The D_1 occurred under high-grade metamorphic conditions, resulting in E-W striking planar structures and granoblastic texture. The D_2 is characterized by the development of NE-SW striking, low-grade sinistral shear zones (Masquelin, 2000). The main planar structure found in this suite is a composite banding (S_0/S_1) represented by millimeter-to meter-thick pre-D_1 (S_0) bedding. This composite banding was affected by at least two isoclinal folding episodes during the D_1 (Fig. 3A). The D_1 structures were disjointed and truncated by D_2 mylonitic zones (Fig. 3B).

Previous petrographic and thermobarometric studies (Gross et al., 2009), carried out on semi-pelitic migmatites associated with garnet-rich leucosomes (Fig. 3C and D) and mafic granulite lenses intercalated with metapelites (Fig. 3E), recognized four distinct metamorphic assemblages, named M_1, M_2 (7–10 kbar and 830-950 °C), M_3 (4.8–5.5 kbar and 788–830 °C), and M_4 (3–6 kbar and 600–750 °C). The M_1 assemblage, only preserved as inclusion phases in porphyroblasts of the M_2, which would represent the regional peak metamorphism (recorded in the mafic granulites), is followed by almost-isothermal post-peak decompression (M_3). The retrograde M_4 assemblage is represented by hydration reaction textures replacing minerals of both M_2 and M_3.

The clockwise P-T path proposed for the abovementioned rocks (Gross et al., 2009) is consistent with crustal thickening followed by extensional collapse. Some authors (e.g. Gross et al., 2009; Skagseth, 2016) suggested that the high-grade event recorded in the Cerro Olivo Complex is correlatable to that of the Coastal Terrane (Kaoko Belt,
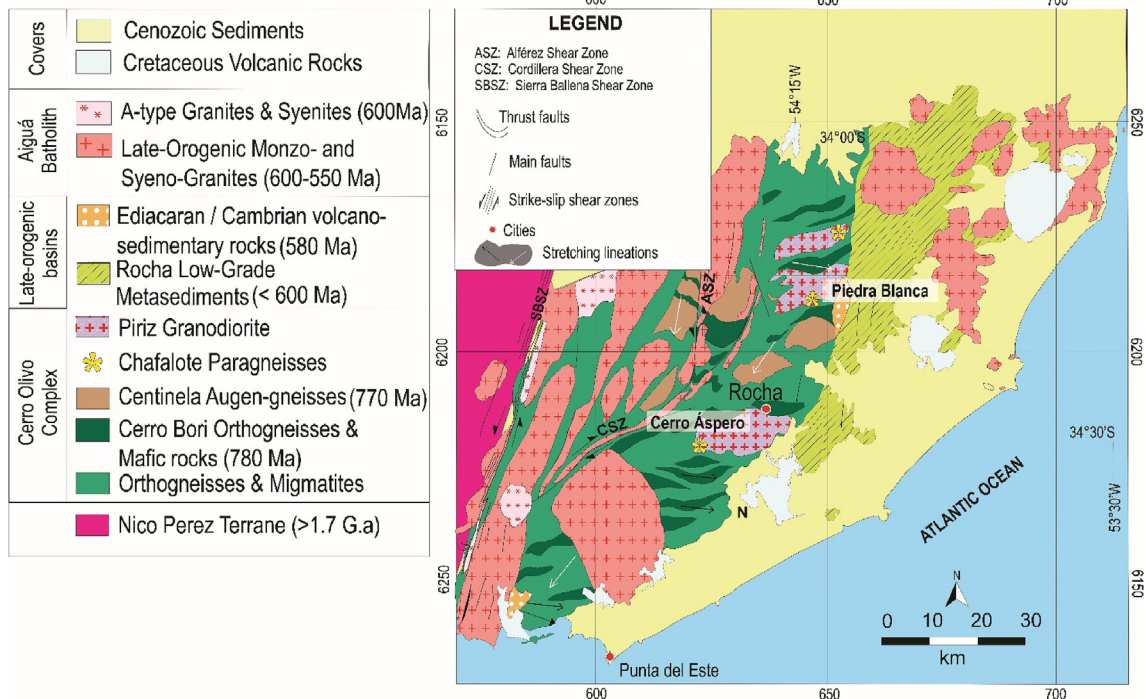
Fig. 2. Location of the study area (modified from Masquelin et al., 2012). Simplified geological map of the Dom Feliciano Belt in southeasternmost Uruguay showing the main occurrences of the Chafalote Metamorphic Suite. Ages: Masquelin et al. (2017).

westernmost Namibia) and Várzea do Capivarita Complex (central sector of the Dom Feliciano Belt in Brazil), which reached peak metamorphism at around 650 Ma. In order to better constrain the time frame of the latter events and further investigate the tectonic significance of the Chafalote Metamorphic Suite, this study focuses on the same

occurrences studied by Gross et al. (2009), which crop out in the Cerro Áspero and Piedra Blanca roof pendants.
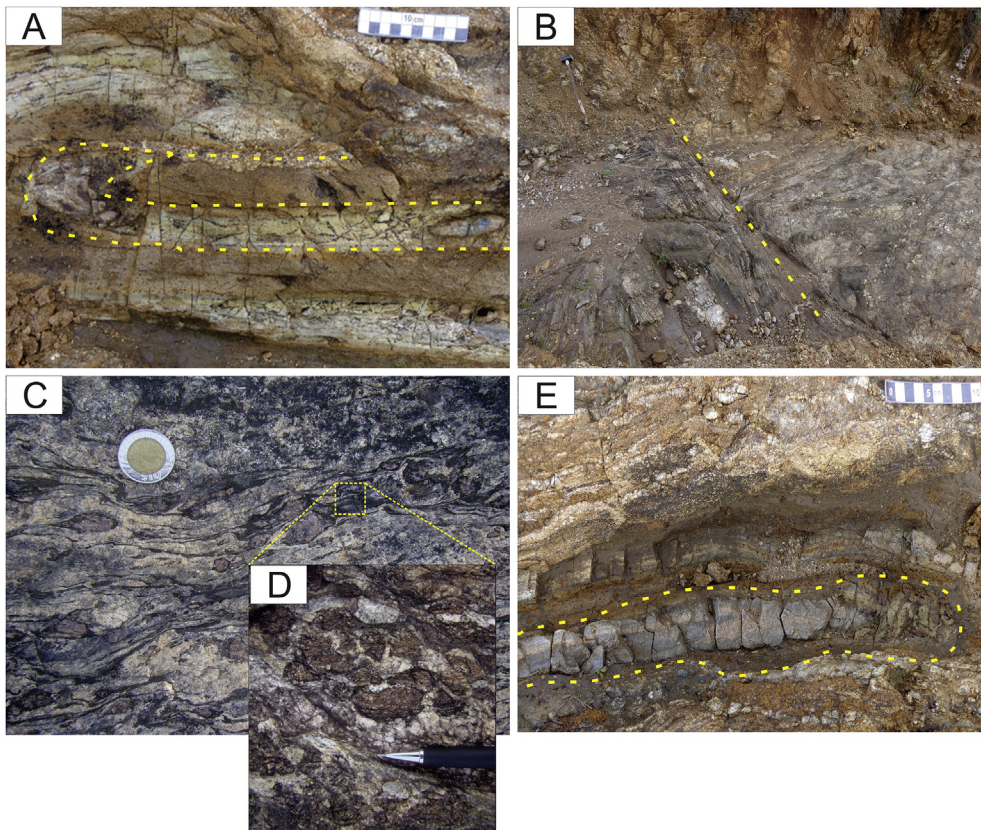
Fig. 3. Macroscopic features of metasedimentary rocks from the Chafalote Metamorphic Suite – A) Composite banding (S_0/S_1) of the metapelite, affected by the D_1 event (xz plane); B) D_1 structures truncated by D_2 mylonitic zones (xy plane); C) Coarse-grained garnet-bearing leucosome lenses found in the Cerro Áspero roof pendant (xy plane); D) Detail of deformed coarse-grained garnet crystals found in the leucosomes; E) Mafic granulite lenses within metapelites of the Piedra Blanca roof pendant (xz plane).
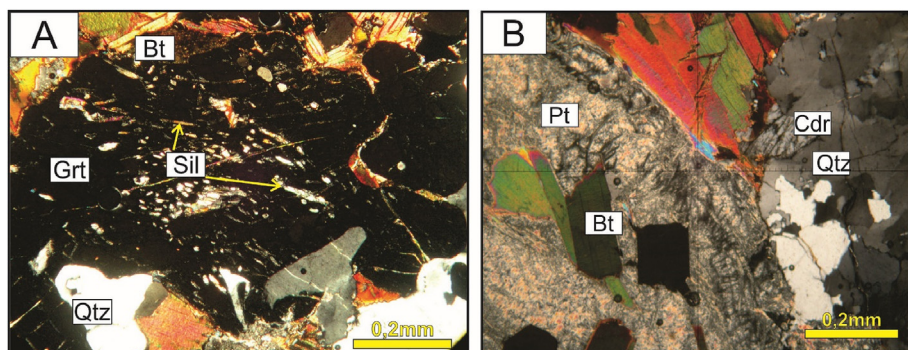
Fig. 4. Photomicrographs of samples from the Cerro Áspero roof pendant – A) Garnet porphyroblasts with inclusion of sillimanite (crossed polars, 10× magnification); B) Pinite alteration in cordierite (crossed polars, 5× magnification). Mineral abbreviations: Bt = biotite; Crd = cordierite; Grt = garnet; Qtz = quartz; Sil = sillimanite; Pt = pinite.

3. Materials and methods

Representative samples from the Cerro Áspero and Piedra Blanca roof pendants (Fig. 2B) were selected for this work. The preparation of polished thin sections for petrography was performed at the Núcleo de Preparação de Amostras, Centro de Estudos em Petrologia e Geoquímica (CPGq), Instituto de Geociências (IGEO), Universidade Federal do Rio Grande do Sul (UFRGS), Brazil. The optical microscopy study was carried out at Laboratório de Geologia Isotópica (CPGq-IGEO-UFRGS), using a Leica DMLP polarizing microscope equipped with a Leica DC 300F digital camera.

For the U-Pb SHRIMP radiometric dating, 18 zircon crystals from sample FR-16 (leucosome within a metapelite from the Cerro Áspero roof pendant) were selected, after heavy liquid and magnetic separation, and mounted in epoxy resin together with the TEMORA-2 standard (Black et al., 2004). In order to identify the best targets for the analyses, cathodoluminescence images of crystals in the mount were obtained using a FEI Quanta 250 scanning electron microscope, equipped with a XMAX CL detector, at the Centro de Pesquisas Geocronológicas, Instituto de Geociências, Universidade de São Paulo, Brazil. The U-Pb analyses were carried out at the same laboratory using a SHRIMP-IIe high resolution ion microprobe, following the procedures of Sato et al. (2014). Errors are 2σ. Common Pb was corrected on the basis of the measured ^{204}Pb. U abundance and U/Pb ratios were calibrated against the TEMORA-2 standard. The ^{206}Pb/^{238}U errors are < 2%. The ages were calculated using Isoplot software (Ludwig, 2008).

For the U-Pb LA-ICP-MS radiometric dating, monazite crystals from sample 02-09 (mafic granulites from the Piedra Blanca roof pendant) were selected, after heavy liquid and magnetic separation, and mounted in epoxy resin. In order to determine internal structures prior to the U-Pb analyses, backscattering electron images of the latter crystals were obtained using a JEOL JSM-6610LV scanning electron microscope, at the Laboratório de Geologia Isotópica (CPGq-IGEO-UFRGS). The U-Pb analyses were carried out at the same laboratory using a ThermoFinnigan Neptune mass spectrometer coupled to a laser ablation system (UP 213, Nd:YAG). The U abundance and U/Pb ratios were calibrated against the 44069 standard (Aleinikoff et al., 2006) and the ages were calculated using Isoplot software (Ludwig, 2008).

Three metapelite samples (05, 02-20, and 44A) from Cerro Áspero and Piedra Blanca roof pendants were selected for Sm-Nd (whole-rock) isotope analysis. The samples were pulverized to 200 mesh, washed in 2.5 N HCl, spiked with ^{149}Sm/^{150}Nd tracers, and completely dissolved in HF, HNO$_3$, and HCl. Anionic LN-B50-A resin (100–150 µm) was used for Sm and Nd separation. Each element was collected and the samples were posteriorly dried and loaded with 0.25 N H$_3$PO$_4$ on a single Ta (for Sm) and on a triple Ta-Re-Ta (for Nd) filament. The samples were run in a VG Sector 54 multi-collector thermal ionization mass spectrometer (TIMS) at the Laboratório de Geologia Isotópica (CPGq-IGEO-UFRGS), in static mode. Nd ratios were normalized to ^{146}Nd/^{144}Nd = 0.7219. Standard values of ^{143}Nd/^{144}Nd (Nd$_2$O$_3$ LaJolla Nd standard; Lugmair and Carlson, 1978) are 0.511859 ± 0.000010. Standard errors for

^{147}Sm/^{144}Nd were ± 1% or smaller, based on interactive sample analysis and spike recalibration, and < 0.0057% for ^{143}Nd/^{144}Nd ratios. The calculations (initial ^{143}Nd/^{144}Nd, εNd, model ages) were made using GCDKit software (Janoušek et al., 2006).

4. Results

4.1. Petrographic aspects of the studied samples

4.1.1. Cerro Áspero roof pendant

The Cerro Áspero roof pendant comprises a sequence of upper amphibolite to granulite-facies migmatitic metapelites. These rocks show a composite banding (S$_0$/S$_1$), marked by the alternation of Si-poor layers constituted by garnet-biotite-cordierite-spinel, and Si-rich layers with garnet + biotite + cordierite + plagioclase + quartz + K-feldspar and leucocratic segregations. The latter segregations, interpreted as leucosomes, occur as elongated lenses parallel to/or cutting the banding, suggesting in situ partial melting.

The M$_1$ assemblage of the migmatitic metapelites is preserved only as inclusions of sillimanite, quartz, and biotite in garnet porphyroblasts (Fig. 4A) of the M$_2$ assemblages (Table 1). The M$_3$ stage in the migmatitic metapelites is marked by the presence of leucosomes constituted mainly by quartz, K-feldspar, garnet, and cordierite. The M$_4$ stage in the migmatitic metapelites is represented by the presence of hydrated retrograde minerals such as chlorite replacing biotite, and pinite replacing cordierite (Fig. 4B).

4.1.2. Piedra Blanca roof pendant

The Piedra Blanca roof pendant comprises a tectonic intercalation of metapelites and mafic granulites. The metapelites can be broadly divided into two main types, represented by garnet-sillimanite-rich metapelites and semipelites. These rocks show a S$_0$/S$_1$ composite banding, marked by parallel, continuous garnet- and sillimanite-rich layers (1–3 m thick) intercalated with (parallel, continuous) semipelite layers (10–50 cm thick) and with meter-sized mafic granulite lenses. The metapelites show a well-developed tectonic foliation marked by elongated biotite and sillimanite crystals, and a recrystallized matrix showing interlobate to granoblastic polygonal texture which suggests high-temperature recovery process (Passchier and Trouw, 2005).

The M$_1$ assemblage in the semipelites is represented by inclusions of biotite and quartz in garnet porphyroblasts and orthopyroxenes (Fig. 5A) of the M$_2$ assemblages (Table 2). The M$_4$ minerals are represented by cummingtonite replacing orthopyroxene, and by chlorite replacing biotite.

The mafic granulites occur as lenticular boudins with 0.5–1.5 m in length. These rocks are medium-grained and show a granoblastic poligonal texture. Two types of mafic granulites are identified: garnet-orthopyroxene-clinopyroxene mafic granulite and orthopyroxene-clinopyroxene mafic granulite. The M$_1$ assemblage is constituted by inclusions of hornblende and quartz in pyroxene and garnet porphyroblasts (Fig. 5C) of the M$_2$ assemblages (Table 2). The M$_3$ stage is marked

Table 1
Mineral assemblages of the migmatitic metapelites from the Cerro Áspero roof pendant. Mineral abbreviations: Bt = biotite; Crd = cordierite; Grt = garnet; Ilm = ilmenite; Kfs = K-feldspar; Pl = plagioclase; Qtz = quartz; Sil = sillimanite; Spl = spinel; Pt = pinite.

SAMPLE	ROCK TYPE	M_1	M_2	M_3	M_4
251	Migmatitic metapelite	Sil-Qtz-Bt inclusions in Grt (M_2)	Grt + Crd + Bt + Sil + Spl + Pl + Kfs ± Ilm	Abundant anatectic melt	Chl and Pt replacing Bt and Crd
FR-16	Leucosome			Grt + Crd + Bt + Sil + Qtz + Pl + Ilm + Spl	Retrograde Bt and Sil around Grt
05	Migmatitic metapelite	Sil-Qtz-Bt inclusions in Grt (M_2)	Grt + Crd + Bt + Sil + Qtz + Pl + Ilm + Spl	Abundant anatectic melt	Chl and Pt replacing Bt and Crd

by orthopyroxene and plagioclase in intergrowths and coronae texture. The M_4 assemblages are represented by cummingtonite replacing orthopyroxene.

4.2. Zircon U-Pb SHRIMP analyses

In order to estimate the age of segregation and crystallization of the leucosome associated with the migmatitic metapelites from the Cerro Áspero roof pendant, U-Pb (SHRIMP) analyses were performed in zircon crystals from sample FR-16. The analyzed zircon grains are subhedral to anhedral. Their length and width proportion varies between 2:1 and 1:1 (predominance of 1:1), and grain size between 100 and 200 mm (Fig. 6). Some zircon grains show recrystallized rims and internal zoning, suggesting overgrowth during high-grade metamorphism.

The results of the U-Pb analyses are shown in Table 3. The radiometric $^{206}Pb/^{238}U$ ages obtained in zircon cores range between 1600 and 644 Ma. The radiometric ages obtained in the rims range between 780 and 670 Ma. The results are graphically represented in a frequency histogram (Fig. 7).

4.3. Monazite U-Pb LA-ICP-MS analyses

In order to better constrain the age of peak metamorphism, U-Pb (LA-ICP-MS) analyses were performed in monazite crystals from sample 02-9 (mafic granulite from Piedra Blanca roof pendant), since these rocks record, so far, the highest P-T conditions in the region (Gross et al., 2009). The analyzed crystals (N = 5) are subangular to rounded, showing different zoning patterns: (i) concentric, (ii) intergrowth (sector zoning), and (iii) mixed between these two patterns (Fig. 8). The morphology, together with the zoning patterns, suggest that these monazite crystals were formed during high-grade metamorphism (Spear and Pyle, 2002).

Within error, the $^{207}Pb/^{206}Pb$ radiometric ages obtained in the three zoning patterns are similar (Table 4). The concentric zoning yield ages of 672 ± 12 and 673 ± 14 Ma. The sector zoning yield younger ages of 660 ± 12 and 663 ± 13 Ma. The mixed zoning yield an age of 669 ± 10 Ma. Fig. 9 shows a discordant age of 667 ± 27 Ma, which is very similar to the latter $^{207}Pb/^{206}Pb$ ages.

4.4. Whole-rock Sm-Nd analyses

Whole-rock Sm-Nd analyses were performed in metapelites from Cerro Áspero and Piedra Blanca roof pendants, in order to determine the model ages and possible correlation with other units of the Chafalote Metamorphic Suite and also with other high-grade metasedimentary rocks from the southern sector of the Dom Feliciano Belt. The results are shown in Table 5.

The $^{143}Nd/^{144}Nd$ ratios of the analyzed rocks range between 0.511706 and 0.512066. The $^{147}Sm/^{144}Nd$ ratios range between 0.108789 and 0.129330. Using the age of 660 Ma – mean age of monazite grains shown in previous section – as reference for the re-calculation, the whole-rock data yield Nd model ages (DePaolo, 1981) between 1.99 and 1.79 Ga, and negative $\varepsilon Nd_{(660Ma)}$ between − 4.6 and − 11.50.

5. Discussions

5.1. Geochronologic constraints of the high-grade metamorphic event

Previous studies demonstrated that the Piedra Blanca mafic granulites underwent high P-T conditions (800–850 °C and 7.5–10 kbar, Gross et al., 2009; ca. 830–840 °C and 7.5–10.5 kbar, Skagseth, 2016), interpreted as the peak regional metamorphism. Using (here and in the following discussions) the conversion factor of 1 kbar = 3.7 km (Tulloch and Challis, 2000), it is possible to estimate the maximum
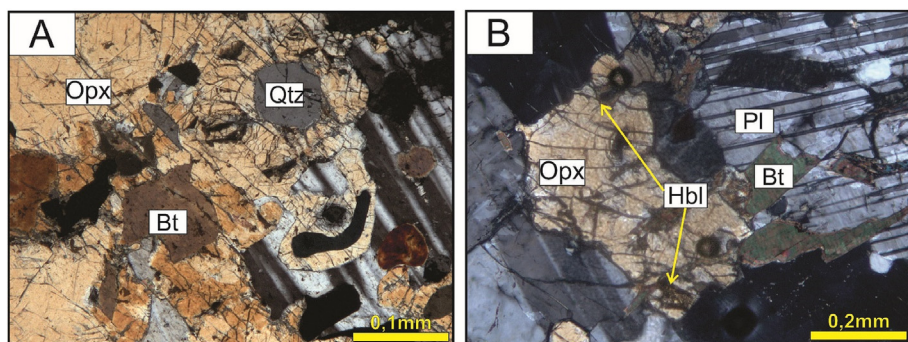
Fig. 5. Photomicrographs of samples from Piedra Blanca roof pendant; A) Orthopyroxene porphyroblasts with inclusions of biotite and quartz (crossed polars, 10× magnification); B) Orthopyroxene porphyroblasts with inclusions of hornblende (crossed polars, 5× magnification). Mineral abbreviations: Bt = biotite; Hbl = hornblende; Opx = orthopyroxene; Pl = plagioclase; Qtz = quartz.

burial depths at ca. 27–37 km for these rocks.

Since the closure temperature of monazite in U-Pb system is higher than 700 °C and this mineral is generally not preserved as detrital grains in high grade metasedimentary rocks (e.g. Spear and Pyle, 2002), the obtained monazite ages for sample 02-9 (between ca. 660 ± 12 and 673 ± 14 Ma; see section 4.3) are interpreted here as peak metamorphic ages, related to the M_2 event. This interpretation is strengthened by the textures observed in the analyzed monazites (Fig. 8), which are compatible with high-T metamorphism (e.g. Zhu and Onions, 1999; Spear and Pyle, 2002).

For the Cerro Áspero migmatitic metapelites it is not possible to estimate the M_2 conditions (Gross et al., 2009). During exhumation (M_3 event), these rocks were re-equilibrated at 4.0–5.5 kbar (Gross et al., 2009; Skagseth, 2016), corresponding to depths of ca. 14.8 and 20.4 km. In relation to the mafic granulites, the pelitic migmatites show a decrease of pressure (Gross et al., 2009; Skagseth, 2016). According to Gross et al. (2009), it may represent: (i) rheological contrast, since the pelites are less competent than mafic granulites. Therefore, their plastic deformation would reduce the grain size, decreasing the intergranular diffusion length, thus increasing the diffusion rate; (ii) the presence of localized fluids promoting intergranular diffusion and leading to catalyzation of metamorphic reactions. These fluids could be related to dehydration of minerals such as biotite and muscovite. Thus, the introduction of fluids could promote re-equilibration of metamorphic assemblages; (iii) the presence of localized, partially molten material, providing an effective diffusion pathway.

Therefore it is plausible to suggest that the M_3 stage occurred during the decompression event, which is related to the re-equilibration and partial melting of the metapelites. This partial melting represents a prograde reaction as evidenced by inclusions (sillimanite, quartz, biotite; see Table 2) in cordierite and garnet porphyroblasts which, together with the presence of mineral segregations constituted mainly by quartz, K-feldspar, garnet, and cordierite (leucosomes), suggest a possible dehydration melting reaction (e.g. Patiño Douce and Harris, 1998; Weinberg and Hasalova, 2015).

It seems plausible that the leucocratic segregations formed during the M_3 stage are related to the crystallization of the Piriz Granodiorite, in which the roof pendants studied in this paper are located. This

cordierite-bearing peraluminous granitoid (CPG) shows a composition (plagioclase, quartz, K-feldspar, biotite, muscovite, cordierite, garnet) similar to those of the leucosomes mentioned above. According to Barbarin (1999), the CPGs are associated with the climax of orogenesis, being related to underplating or localized injections of mantle-derived material. These rocks tend to be dispersed through the mountain belt, forming laccoliths and plutons locally rooted in the high-grade metamorphic rocks. Thus, it seems possible that the melts generated during the M_3 event formed pools and veins that cut the metapelite layers, subsequently formed large bodies such as the Piriz Granodiorite. As shown above, the age of peak metamorphism (M_2) is constrained at around 667 Ma. Thus, the younger ages of ca. 640 Ma obtained in zircon cores from the leucosome (sample FR-16) might represent the age of its extraction and crystallization, and might be interpreted as the age of the decompression event followed by partial melting of the metapelites (M_3).

The retrograde metamorphic assemblages (M_4) observed in the studied rocks are possible related to the transition between the D_1 and D_2 events and intrusion of syn-to post-orogenic Brasiliano granitoids (~620-550 Ma) of the Aiguá Batholith (Masquelin et al., 2005, 2012), involving the formation of hydrated minerals that indicate static retrograde metamorphism as a result of fluid influx.

5.2. Correlations

The U-Pb ages of the leucosomes associated with migmatitic metapelites presented in this study can be divided into three groups: (i) Tonian to Cryogenian ages of ca. 800-680 Ma; (ii) Mesoproterozoic ages of ca. 1300-1000 Ma; (iii) and Paleoproterozoic ages of ca. 1600 Ma. These ages are very similar to those found in the migmatitic metapelites regarded as basement of the Paso del Dragón Complex (Peel et al., 2018), located further north near the Brazil/Uruguay border, considered the northern extension of the Cerro Olivo Complex. Furthermore, the migmatites from both Paso del Dragón and Cerro Olivo Complex show a similar peak metamorphic age of ca. 660 Ma (Oyhantçabal et al., 2009; Lenz et al., 2011; Peel et al., 2018).

In the Brazilian extension of the Punta del Este Terrane (sensu Ramos et al., 2018), the correlatable Arroio Telho Complex (Cruz et al.,

Table 2

Mineral assemblages of representative samples from the Piedra Blanca roof pendant. Abbreviations: Bt = biotite; Cpx = clinopyroxene; Chl = chlorite; Cum = cummingtonite; Grt = garnet; Hbl = hornblende; Ilm = ilmenite; Kfs = K-feldspar; Opx = orthopyroxene; Pl = plagioclase; Qtz = quartz; Rt = rutile; Sil = sillimanite; Spl = spinel.

SAMPLE	ROCK TYPE	M_1	M_2	M_3	M_4
44A	Semipelites	Bt-Qz inclusions in Grt and Opx (M_2)	Grt + Bt + Pl + Opx + Qtz + Ilm + Rt		Cum replacing Opx, and Chl replacing Bt
02–20	Sil-rich metapelite		Grt + Sil + Bt + Qtz + Kfs + Ilm + Rt		Chl replacing Bt
02–9	Opx-Cpx mafic granulite	Brown Hbl-Qz inclusions in Grt and Opx	Opx + Cpx + Hbl + Bt + Qtz + Pl	Opx + Pl in intergrowths and coronae	Cum replacing Opx
45C	Grt-Opx mafic granulite	Brown Hbl-Qz inclusions in Grt and Opx	Grt + Opx + Cpx + Bt + Qtz + Pl	Opx + Pl in intergrowths and coronae	Cum replacing Opx
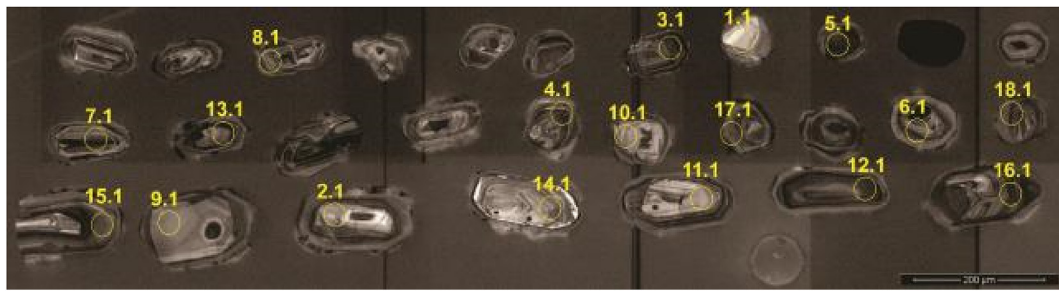
Fig. 6. Cathodoluminescense images of zircon crystals from sample FR-16 (leucosome from Cerro Áspero roof pendant). Yellow circles represent the spots of U-Pb analysis. (For interpretation of the references to colour in this figure legend, the reader is referred to the Web version of this article.)

Table 3
U-Pb SHRIMP data for sample FR-16 (leucosome from Cerro Áspero roof pendant). Pb_c = common lead (corrected using measured[204]Pb). Pb^* = radiogenic lead.

Spot	U	Th	$^{232}Th/^{238}U$	± %	$^{206}Pb_c$	$^{206}Pb^*$	$^{208}Pb^*$	$^{206}Pb^*/^{238}U$	± %	$^{207}Pb^*/^{235}U$	± %
	ppm	ppm			(%)	ppm	ppm				
10.1	243	246	1.05	0.52	0.23	22	7.0	9.51	1.5	0.93	3.3
4.1	861	912	1.09	0.15	0.02	77	26.1	9.52	1.0	0.91	2.0
3.1	315	423	1.39	0.19	0.11	28	12.1	9.49	1.1	0.93	5.4
1.1	581	5	0.01	1.02	0.13	55	0.2	9.06	0.8	0.94	1.0
17.1	402	19	0.05	0.54	0.19	41	0.7	8.45	0.9	1.02	1.1
14.1	323	63	0.20	0.32	4.52	32	1.4	8.55	2.3	1.14	3.8
15.1	311	133	0.44	0.26	0.18	35	4.8	7.59	0.9	1.20	1.2
12.1	482	69	0.15	1.34	0.64	53	2.6	7.84	0.9	1.12	1.1
16.1	491	91	0.19	0.89	0.59	60	3.8	7.01	0.9	1.30	1.1
11.1	431	80	0.19	0.29	0.91	65	3.9	5.73	1.1	1.76	1.5
18.1	343	31	0.09	0.46	0.60	52	0.8	5.65	0.9	1.93	3.3
9.1	462	77	0.17	0.30	0.09	74	3.8	5.32	1.1	1.99	1.4
13.1	126	59	0.48	0.37	0.66	21	2.9	5.23	2.1	2.11	2.2
2.1	163	44	0.28	0.39	0.37	28	2.3	4.99	1.0	2.22	2.4
7.1	275	39	0.15	0.41	3.03	47	0.7	4.88	1.8	2.87	2.6
6.1	315	115	0.38	0.26	0.14	58	6.8	4.71	0.9	2.35	1.0
8.1	553	249	0.46	0.21	0.11	107	14.9	4.42	1.1	2.65	1.4
5.1	154	54	0.36	0.36	0.09	37	4.0	3.55	1.4	3.83	2.2

Spot	$^{207}Pb^*/^{206}Pb^*$	± %	$^{206}Pb/^{238}U$ Age	1σ error	$^{207}Pb/^{206}Pb$ Age	1σ error	$^{208}Pb/^{232}Th$ Age	1σ error	% Discordant	Err. corr.
10.1	0.0641	2.9	644	± 9	633	± 31	628	± 11	−2	0.032
4.1	0.0628	1.7	644	± 6	621	± 12	632	± 6	−3	0.032
3.1	0.0643	5.0	646	± 7	625	± 25	632	± 8	−3	0.032
1.1	0.0620	0.6	675	± 5	685	± 14	888	± 141	+2	0.035
17.1	0.0626	0.7	721	± 6	741	± 17	884	± 45	+3	0.041
14.1	0.0704	3.3	713	± 16	1001	± 148	774	± 143	+30	0.025
15.1	0.0660	1.0	798	± 7	763	± 26	777	± 15	−5	0.040
12.1	0.0639	0.8	774	± 6	919	± 14	1025	± 24	+16	0.042
16.1	0.0661	0.8	860	± 7	968	± 15	1054	± 22	+11	0.047
11.1	0.0731	1.1	1037	± 11	1118	± 25	1204	± 34	+7	0.054
18.1	0.0791	3.1	1051	± 9	1140	± 64	924	± 57	+9	0.029
9.1	0.0769	0.9	1110	± 12	1131	± 16	1133	± 20	+2	0.055
13.1	0.0799	2.0	1127	± 22	1201	± 25	1133	± 50	+7	0.055
2.1	0.0806	2.2	1177	± 11	1224	± 45	1195	± 28	+4	0.057
7.1	0.1017	1.9	1202	± 19	1691	± 35	1340	± 37	+32	−0.019
6.1	0.0805	0.7	1241	± 10	1201	± 11	1233	± 17	−4	0.065
8.1	0.0850	1.0	1314	± 14	1288	± 19	1286	± 17	−2	0.067
5.1	0.0985	1.8	1600	± 20	1549	± 36	1508	± 32	−3	0.083

2016), located between the above mentioned Paso del Dragón Complex (Uruguay) and Arroio Grande Complex (Brazil), is found. This metasiliciclastic association is constituted by metapelites (garnet-, tourmaline-, and sillimanite-rich) and associated medium-to high-grade feldspathic gneisses. These rocks underwent partial melting, generating leucosomes with granitic composition.

Similar petrographic and geochronological features suggest that the metasedimentary rocks from the Paso del Dragón, Arroio Telho, and Arroio Grande Complex are correlatable (Ramos et al., 2018). The U-Pb provenance ages of detrital zircon from metapelites of the Arroio Grande-Arroio Telho Complex (ca. > 1800 to < 640 Ma; Beloni et al.,

2016; Iglesias et al., 2018) are similar to those of the Paso del Dragón Complex (Peel et al., 2018). In turn, these ages match those presented in this work for the Chafalote Metamorphic Suite. Thus, it is plausible to suggest that the protolith of all these metasedimentary units could represent contemporaneous sedimentation in different portions of the same basin. This correlation is strengthened by the peak metamorphic age of ca. 660 Ma found in the basement of both the Paso del Dragón (Peel et al., 2018) and Arroio Grande Complex (Vieira et al., 2019). Furthermore, the basement of the latter records a partial melting event dated at ca. 640 Ma (Ramos et al., 2018), which is the same age attributed in this work for the partial melting event that produced the M_3
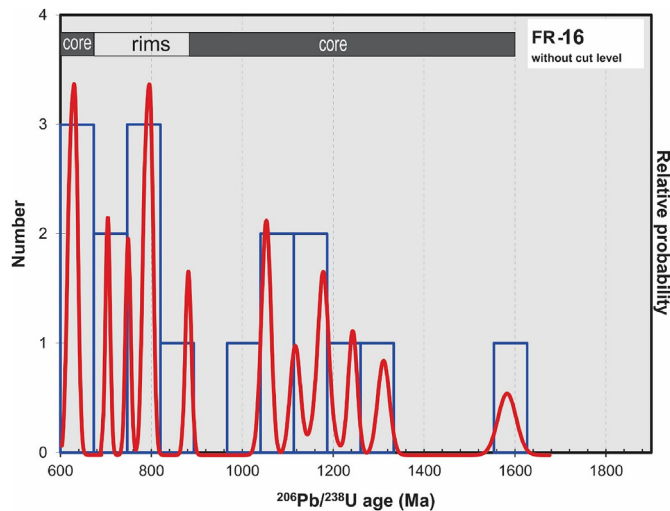
Fig. 7. Frequency histogram and relative probability plot of seventeen U-Pb ages from sample FR-16 (leucosome from Cerro Áspero roof pendant).

leucosome discussed in the previous section.

The correlation between these lithologies corroborates the hypothesis suggested by Peel et al. (2018), in which the high-grade rocks found south of Paso del Dragón Complex constitute, together with Cerro Olivo Complex, the basement of the Punta del Este Terrane. Furthermore, it is plausible to assume that these rocks served as the main source of detrital material for the late metasiliciclastic rocks from both Paso del Dragón (Uruguay) and Telho-Arroio Grande Complex (Brazil).

Based on similar high-grade conditions, previous works (e.g. Fernandes et al., 1992; Gross et al., 2006, 2009; Martil et al., 2017) suggested the correlation between the metasedimentary rocks of the Chafalote Metamorphic Suite and those found in the Várzea do Capivarita Complex, located in the central sector of the Dom Feliciano Belt in the Sul-rio-grandense Shield (Fig. 1C). This hypothesis is strengthened when the T_{DM} and the negative $\varepsilon Nd_{(660Ma)}$ values presented in this study (Table 5) are compared to those shown in Gross et al. (2006) for the metasedimentary rocks of the Várzea do Capivarita Complex (T_{DM} values 1.2–1.9 Ga and negative $\varepsilon Nd_{(660Ma)}$ values between - 5 and −12), suggesting a long history of crustal residence prior to the metamorphism of both sedimentary basins.

The latter hypothesis is strengthened also by the similar U-Pb ages

of the leucosomes associated with migmatitic metapelites presented in this study (see section 4.2) and the detrital ages (ca. 2.2–0.63 Ga) suggested by Gruber et al. (2016) from metasedimentary rocks of the Várzea do Capivarita Complex, as well as the same age of the high-grade metamorphism (ca. 650 Ma, Martil et al., 2017) recorded in these metasedimentary rocks. Regarding the ages of potential source areas for both basins, they are interpreted as mixed, comprising older, Paleo-to Mesoproterozoic (1.2–2.2 Ga) sources, and younger, Neoproterozoic sources (ca. 800–640 Ma). Therefore it is possible to suggest that the supracrustal rocks of the Várzea do Capivarita Complex and those of the Punta del Este Terrane can be represent fragments from the same sedimentary basin or, at least, from distinct basins with similar depositional and metamorphic evolution.

5.3. Tectonic implications

Several numerical and analytical models improved the understanding of the deep-crust behavior and tectonic configurations which favor high-T conditions (e.g. Beaumont et al., 2001, 2006; Jamieson et al., 2002, 2007; Culshaw et al., 2006; Goscombe and Gary, 2007; Faccenda et al., 2008). For rocks that reached high temperatures such as those reported in this paper, a cautious interpretation regarding possible tectonic settings for the protoliths is required.

According to Gross et al. (2009), the high P-T conditions recorded for the peak metamorphism of the Chafalote Metamorphic Suite are indicative of crustal thickening in convergent orogens. The steep P-T-t path would represent decompression due to deformation-controlled, rather than erosion-controlled, exhumation, resulting from the transition to an extensional regime. Recent works have suggested that the Cerro Olivo Complex is characterized by a multiphase evolution, related to the closure of a paleo-oceanic basin and the development of a continental magmatic arc (e.g. Ramos et al., 2018; Vieira et al., 2019), thus compatible with a crustal thickening setting.

As previously mentioned in section 2, calc-alkaline continental magmatic arc rocks are found in the Cerro Olivo Complex, represented by the Cerro Bori Gneisses, with magmatic ages ranging between 802 ± 12 and 767 ± 9 Ma (Lenz et al., 2011; Masquelin et al., 2012). According to Lenz et al. (2011) these gneisses underwent the same high-grade metamorphism as the supracrustal rocks of the Chafalote Metamorphic Suite, dated at 676 ± 10 and 666 ± 11 Ma (the similar interval presented in the present paper for the mafic granulite; see section 4.3), and underwent partial melting at around 654–630 Ma (see

Fig. 8. Backscattered electron images of monazite crystals from sample 02-9 (mafic granulite from Piedra Blanca roof pendant), showing the zoning patterns (A and B = concentric; C and D = intergrowth; E = mixed) and obtained radiometric ages. Yellow circles represent the spots of U-Pb analyses. (For interpretation of the references to colour in this figure legend, the reader is referred to the Web version of this article.)

Table 4

U-Pb LA-ICP-MS data for sample 02-9 (mafic granulite from Piedra Blanca roof pendant).

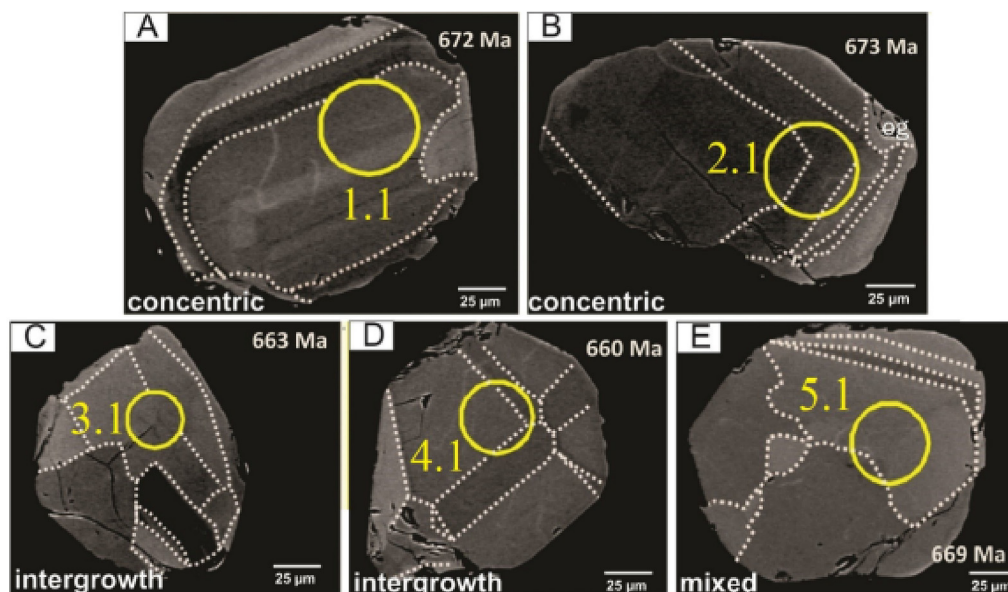| Spot	$^{207}Pb/$ ^{235}U	Concordia %	$^{206}Pb/$ ^{238}U	%	Rho 1	$^{206}Pb/$ ^{238}U	error	$^{207}Pb/$ ^{235}U	error	$^{207}Pb/$ ^{206}Pb	error	Discor. (%)	f206
3.1	1.11934	2.02	0.13161	0.49	0.24	797	4	763	15	663	13	− 20	0.0003
4.1	1.07952	1.97	0.12714	0.79	0.40	772	6	743	15	660	12	− 17	0.0000
1.1	1.03875	1.85	0.12164	0.58	0.31	740	4	723	13	672	12	− 10	0.0000
2.1	1.04275	2.19	0.12206	0.84	0.39	742	6	725	16	673	14	− 10	0.0000
5.1	1.08487	1.67	0.12720	0.60	0.36	772	5	746	12	669	10	− 15	0.0000
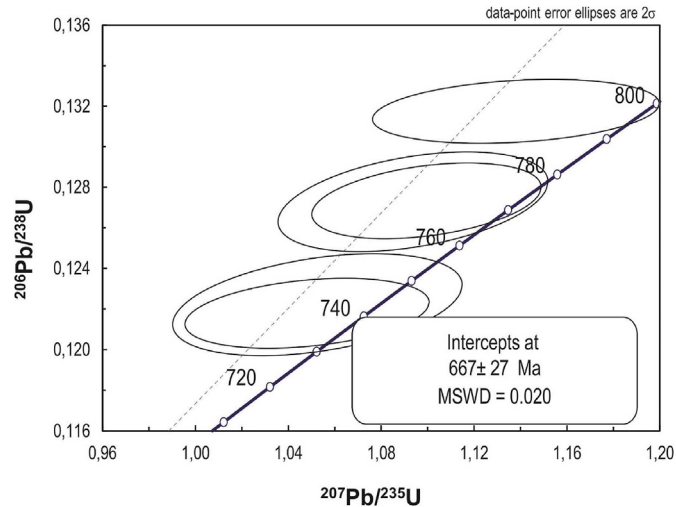
Fig. 9. Concordia diagram for monazite ages of sample 02-9 (mafic granulite from Piedra Blanca roof pendant).

also, e.g., Oyhantçabal et al., 2009 and Lenz et al., 2011). The latter ages match those presented in the present paper for the migmatitic metapelites.

Due to geochemical and isotopic similarities, the orthogneisses of the Cerro Bori were compared and correlated (Vieira et al., 2019) to those found in the Brazilian sector of the Dom Feliciano Belt (e.g. Piratini Gneisses, Tambara et al., 2019; Chácara das Pedras Gneisses, Koester et al., 2016; Várzea do Capivarita Gneisses, Martil et al., 2017). These rocks were interpreted as metamorphic remnants of an Andean-type magmatic arc named Piratini Arc (Vieira et al., 2019), whose evolution is constrained between ca. 780 (initial magmatism) and 660 Ma (continental collision) during the assembly of the West Gondwana paleocontinent. Thus, taking into consideration the geographic proximity between the Cerro Bori Gneisses and the Chafalote Metamorphic Suite, it is plausible to assume that the rocks from the latter reached peak metamorphism at the base of a thickened continental crust (i.e., the Piratini Arc).

Based on the discussions presented in this paper it is possible to suggest two main hypotheses for the evolution of the Chafalote Metamorphic Suite and the events responsible for the high-grade metamorphism of the Punta del Este Terrane as a whole:

I- The closure of the Charrua paleo-ocean due to an eastward subduction, with the development of the Piratini Arc between ca. 780 and 660 Ma. The latter age would represent the time of continental collision between the Piratini Arc and the eastern margin of the Río de la Plata Craton (Ramos et al., 2017; Vieira et al., 2019), generating the M_2-D_1 structures. In this hypothesis, the collisional event is followed by isothermal decompression by the change to an extensional regime at around 640-600 Ma, generating partial melting (M_3). This deformation would be related to the nucleation of ductile shear zones (e.g. Dorsal de Canguçu Shear Zone in Brazil, and Sierra Ballena Shear Zone in Uruguay) and related granitogenesis, and subsequent transcurrent tectonism (M_4-D_2 structures). In this model, the protoliths of the metasedimentary rocks of the Chafalote Metamorphic Suite were deposited in a fore-arc basin. Afterwards, these rocks were metamorphosed during the collisional event at ca. 660 Ma;

II- The closure of the South Adamastor paleo-ocean due to a westward subduction underneath the Piratini Arc (Ramos et al., 2018). This subduction generated a new continental arc – the Pinheiro Machado Arc (Ramos et al., 2018) –, represented by the oldest intrusive suite (ca. 630-610 Ma – Babinski et al., 1997; Silva et al., 1999; Hueck et al., 2018) of the Cuchilla Dionisio-Pelotas Terrane. In this hypothesis, the Pinheiro Machado Arc might be older than 630 Ma, so that the ca. 640 Ma granitoids generated in the partial melting event recorded in the Arroio Grande Complex in Brazil (see section 6) would represent the initial magmatic events of the latter arc. In this model the protoliths of the metasedimenary rocks of Chafalote Metamorphic Suite were deposited in a back-arc basin, prior to the subduction, or in a fore-arc basin, during the subduction. The protoliths of the mafic granulites and amphibolites, in turn, would represent slices of oceanic crust, with a back-arc signature (Lenz et al., 2014) similar to that of the metamafites from Arroio Grande Complex in Brazil (Ramos et al., 2017) and from Paso del Dragón Complex in Uruguay (Will et al., 2014).

6. Concluding remarks

From the study presented in this paper, we draw the following conclusions:

I. The metamorphic peak (M_2 stage) reached high temperatures at around 660 ± 12 and 673 ± 14 Ma, as a response to a major thermal perturbation associated to crustal thickening, followed by voluminous partial melting caused by tectonic exhumation at ca. 640 Ma during the M_3 stage. The M_4 stage is related to the transition between the D_1 and D_2 events and intrusion of syn-to post-orogenic Brasiliano granitoids,

Table 5

Whole-rock Sm-Nd data of metapelites from the Chafalote Metamorfhic Suite.

Sample	Occurrence	Sm (ppm)	Nd (ppm)	$^{147}Sm/^{144}Nd$	$^{143}Nd/^{144}Nd$	εNd (i)	εNd ($t_{660\,Ma}$)	TDM (Ga)
05	Cerro Áspero	9.75	53.18	0.110827	0.511741	− 17.1	− 9.99	1.98
251	Cerro Áspero	7.36	40.92	0.108789	0.511706	− 18.8	− 11.49	1.99
44A	Piedra Blanca	7.98	37.97	0.126979	0.512066	− 10.4	− 4.6	1.79
02–20	Piedra Blanca	7.36	34.42	0.129330	0.512065	− 11.17	− 5.58	1.84

involving the formation of hydrated retrograde minerals indicating static retrograde metamorphism as a result of fluid influx at ca. 600 Ma;

II. The metasedimentary rocks of the Chafalote Metamorphic Suite are correlatable to those found in the northern extension of the Punta del Este Terrane, i.e., Paso del Dragón Complex (Uruguay) and Arroio Grande-Telho Complex (Brazil). These metasedimentary rocks share similar detrital sources and metamorphic evolution, and possibly represent different portions of the same fore-arc and/or back-arc basin related to the Tonian and Cryogenian events of the Brasiliano/Pan-African orogenic cycle. It is noteworthy that, as shown in previous works, the metasedimentary rocks found in the Várzea do Capivarita (central sector of the Dom Feliciano Belt in the Sul-rio-grandense Shield, Brazil) and those from the Chafalote Metamorphic Suite share similar detrital zircon profiles and metamorphic histories, and thus would represent fragments of the same basin, or of different basins with similar evolution.

Declaration of competing interest

We have no conflict of interest to declare.

Acknowledgements

References

Aleinikoff, J.N., Schenk, W.S., Plank, M.O., Srogi, L.A., Fanning, C.M., Kamo, S.L., Bosbyshell, H., 2006. Deciphering igneous and metamorphic events in high-grade rocks of the Wilmington complex, Delaware: morphology, cathodoluminescence and backscattered electron zoning, and SHRIMP U–Pb geochronology of zircon and monazite. Geol. Soc. Am. Bull. 118, 39–64.

Almeida, F.F.M., Hasui, Y., Brito-Neves, B.B., Fuck, R.A., 1981. Brazilian structural provinces: an introduction. Earth Sci. Rev. 17, 1–29.

Ayers, J.C., Dunkle, S., Gao, S., Miller, C.F., 2002. Constraints on timing of peak and retrograde metamorphism in the Dabie Shan Ultrahigh-Pressure Metamorphic Belt, east-central China, using U–Th–Pb dating of zircon and monazite. Chem. Geol. 186, 315–331.

Ayers, J.C., Loflin, M., Miller, C.F., Barton, M.D., Coath, C.D., 2006. In situ oxygen isotope analysis of monazite as a monitor of fluid infiltration during contact metamorphism: birch Creek Pluton aureole, White Mountains, Eastern California. Geology 34, 653–656.

Babinski, M., Chemale Jr., F., Van Schmus, W.R., Hartmann, L.A., Silva, L.C., 1997. U-Pb and Sm-Nd geochronology of the neoproterozoic granitic-gneissic Dom Feliciano belt, southern Brazil. J. South Am. Earth 10 (3/4), 263–274.

Barbarin, B., 1999. A review of the relationships between granitoid types, their origins and their geodynamic environments. Lithos 46, 605–626.

Basei, M.A.S., Siga J.R., O., Masquelin, H., Harara, O.M., Reis Neto, J.M., Preciozzi, F., 2000. The Dom Feliciano belt of Brazil and Uruguay and its foreland domain the rio de la Plata craton: framework, tectonic evolution and correlation with similar provinces of southwestern Africa. In: Cordani, U.G., Milani, E.J., Thomaz Filho, A., Campos, D.A. (Eds.), Rio de Janeiro, SBG, Tectonic Evolution of South American Platform, pp. 311–334.

Basei, M.A.S., Peel, E., Sánchez-Bettucci, L., Preciozzi, F., Nutman, A.P., 2011. The basement of the Punta del Este Terrane (Uruguay): an African Mesoproterozoic fragment at the eastern border of the South American Río de La Plata craton. Int. J. Earth Sci. 100 (2–3), 289–304.

Beaumont, C., Jamieson, R.A., Nguyen, M.H., Lee, B., 2001. Himalayan tectonics explained by extrusion of a low-viscosity crustal channel coupled to focused surface denudation. Nature 414, 738–742.

Beaumont, C., Nguyen, M., Jamieson, R.A., Ellis, S., 2006. Crustal flow modes in large hot orogens. In: In: Law, R.D., Searle, M., Godin, L. (Eds.), Channel Flow, Ductile Extrusion and Exhumation of Lower-Mid Crust in Continental Collision Zones, vol. 268. Geological Society, London, Special Publications, pp. 91–145.

Beloni, M.S., Porcher, C.C., Koester, E., Ramos, R.C., Lana, C., Wegner, A.C., 2016. Caracterização U/Pb de zircão detrítico e geoquímica isotópica (Sm/Nd) em rocha-total dos xistos e quartzitos de Arroio Grande – RS. In: 48th Congresso Brasileiro de Geologia. Annals, Porto Alegre.

Black, L.P., Kamo, S.L., Allen, C.M., Davis, D.W., Aleinikoff, J.N., Valley, J.W., Mundil, R., Campbell, I.H., Korsch, R.J., Williams, I.S., Foudoulis, C., 2004. Improved 206Pb/238U microprobe geochronology by the monitoring of a trace-element-related matrix

effect; SHRIMP, ID-TIMS, ELA-ICP-MS and oxygen isotope documentation for a series of zircon standards. Chem. Geol. 205, 115–140.

Boghossian, N.D., Patchett, P.J., Ross, G.M., Gehrels, J.E., 2000. Nd isotopes and the source of sediments in the miogeocline of the Canadian cordillera. J. Geol. 104 (3), 259–277.

Bom, F.M., Philipp, R.P., Zvirtes, G., 2014. Origem e evolução do Complexo Várzea do.

Bossi, J., Gaucher, C., 2004. The Cuchilla Dionisio terrane, Uruguay: an allochthonous block accreted in the cambrian to SW-Gondwana. Gondwana Res. 7 (3), 661–674.

Buick, I.S., Clark, C., Rubatto, D., Hermann, J., Pandit, M., Hand, M., 2010. Constraints on the Proterozoic evolution of the Aravalli–Delhi Orogenic belt (NWIndia) from monazite geochronology and mineral trace element geochemistry. Lithos 120, 511–528.

Campal, N., Schipilov, A., 2005. La Formación Cerros de Aguirre: evidencias de magmatismo Vendiano en el Uruguay. Lat. Am. J. Sedimentol. Basin Anal. 12, 161–174.

Capivarita, Encruzilhada do Sul, RS. Pesquisas em Geociências, 41(2), 131-153.

Cruz, R.F., Iglesias, C.M.F., Camozzato, E., 2016. Mapeamento geológico do sudeste do Rio Grande do Sul, descrição de novas unidades geológicas em novo domínio geotectônico no extremo sul do estado. Abstracts In: XLVIII Congresso Brasileiro de Geologia, (Porto Alegre).

Culshaw, N.G., Beaumont, C., Jamieson, R.A., 2006. The orogenic superstructure-infrastructure concept: revisited, quantified, and revived. Geology 34, 733–736.

DePaolo, D.J., 1981. Neodymium isotopes in the Colorado Front Range and crust–mantle evolution in the Proterozoic. Nature 29 (1), 193–196.

Dickin, A.P., 2018. Radiogenic Isotope Geology, 3th edition. Cambridge University Press, pp. 550p.

Faccenda, M., Gerya, T.V., Chakraborty, S., 2008. Styles of post-subduction collisional orogeny: influence of convergence velocity, crustal rheology and radiogenic heat production. Lithos 103, 257–287.

Fernandes, L.A.D., Tommasi, A., Porcher, C.C., 1992. Deformation patterns in the southern Brazilian branch of the Pan-African Dom Feliciano belt. J. South Am. Earth Sci. 5, 77–96.

Fernandes, L.A.D., Menegat, R., Costa, A.F.U., Koester, E., Porcher, C.C., Tommasi, A., Kraemer, G., Ramgrab, G.R., Camozzato, E., 1995a. Evolução tectônica do Cinturão Dom Feliciano no Escudo Sul-riograndense: parte I – Uma contribuição a partir do registro geológico. Rev. Bras. Geociencias 25 (4), 351–374.

Fernandes, L.A.D., Menegat, R., Costa, A.F.U., Koester, E., Porcher, C.C., Tommasi, A., Kraemer, G., Ramgrab, G.R., Camozzato, E., 1995b. Evolução tectônica do Cinturão Dom Feliciano no Escudo Sul-riograndense: parte II – Uma contribuição a partir das assinaturas geofísicas. Rev. Bras. Geociencias 25 (4), 375–384.

Foster, G., Gibson, H.D., Parrish, R.R., Horstwood, M., Fraser, J., Tindle, A., 2002. Textural, chemical and isotopic insight into the nature and behaviour of metamorphic monazite. Chem. Geol. 191, 183–207.

Fragoso-César, A.R.S., Figueiredo, M.C.H., Soliani Jr., E., Faccini, U.F., 1986. Obatólito pelotas (Proterozóico Superior/Eo-Paleozóico) no Escudo do rio Grande do sul. In: XXXIV Congresso Brasileiro de Geologia, Goiânia, Annals, vol. 3. pp. 1322–1343.

Frimmel, H.E., Basei, M.A.S., Gaucher, C., 2011. Neoproterozoic geodynamic evolution of SW-Gondwana: a southern African perspective. Int. J. Earth Sci. 100, 323–354.

Gaucher, C., Frimmel, H.E., Germs, G.J.B., 2009. Tectonic events and palaeogeographic evolution of southern Gondwana in the neoproterozoic and cambrian. In: In: Gaucher, C., Sial, A.N., Halverson, G.P., Frimmel, H.E. (Eds.), Neoproterozoic-Cambrian Tectonics, Global Change and Evolution: a Focus on Southwestern Gondwana. Elsevier, Developments in Precambrian Geology, vol. 16. pp. 295–316.

Goscombe, B., Gray, D.R., 2007. The coastal terrane of the Kaoko Belt, Namibia: outboard arc-terrane and tectonic significance. Precambrian Res. 155, 139–158.

Gray, D.R., Foster, D.A., Meert, J.G., Goscombe, B.D., Armstrong, R., Trouw, R.A.J., Passchier, C.W., 2008. A Damara orogen perspective on the assembly of southwestern Gondwana. In: Pankhurst, R.J., Trouw, R.A.J., Brito-Neves, B.B., De Wit, M.J. (Eds.), West Gondwana: Pre-cenozoic Correlations across the South Atlantic Region. Geological Society of London, Special Publication, 294, pp. 257–278.

Gross, A.O.M.S., Porcher, C.C., Fernandes, L.A.D., Koester, E., 2006. Neoproterozoic low-pressure/high-temperature collisional metamorphic evolution in the Várzea do Capivarita Metamorphic Suite, SE Brazil: thermobarometric and Sm/Nd evidence. Precambrian Res. 147 (1–2), 41–64.

Gross, A.O.M.S., Droop, G.T.R., Porcher, C.C., Fernandes, L.A.D., 2009. Petrology and thermobarometry of mafic granulites and migmatites from the Chafalote metamorphic suite: new insights into the neoproterozoic P–T evolution of the Uruguayan–sul- rio-grandense Shield. Precambrian Res. 170, 157–174.

Harley, S.L., Kelly, N.M., Möller, A., 2007. In: Zircon Behavior and the Thermal Histories of Mountain Chains: Elements. vol. 3. pp. 25–30. https://doi.org/10.2113/gselements.3.1.25.

Heilbron, M., Pedrosa-Soares, A.C., Campos Neto, M., Silva, L.C., Trouw, R.A.J., 2004. A província Mantiqueira. In: Mantesso Neto, A., Bartorelli, A., Carneiro, C.D.R., Brito Neves, B.B. (Eds.), O desvendar de um continente: a moderna geologia da América do Sul e o legado da obra de Fernando Flávio Marques de Almeida. São Paulo, Beca, pp. 203–234.

Hermann, J., Rubatto, D., 2003. Relating zircon and monazite domains to garnet growth zones: age and duration of granulite facies metamorphism in the Val Malenco lower crust. J. Metamorph. Geol. 21, 833–852.

Hueck, M., Oyhantçabal, P., Philipp, R.P., Basei, M.A.S., Siegesmund, S., 2018. The Dom Feliciano belt in southern Brazil and Uruguay. In: Siegesmund, S., Basei, M., Oyhantçabal, P., Oriolo, S. (Eds.), Geology of Southwest Gondwana. Springer, Regional Geology Reviews, pp. 267–302.

Iglesias, C.M.F., Camozzato, E., Klein, C., 2018. Geologia e recursos minerais da folha Curral de Pedras, SI.22V-A-I. CPRM. Mapa, color. Escala, Porto Alegre 1:100.000. 2018.

Jamieson, R.A., Beaumont, C., Nguyen, M.H., Lee, B., 2002. Interaction of metamorphism, deformation and exhumation in large convergent orogens. J. Metamorph.

Geol. 20 1525-1314.

Jamieson, R.A., Beaumont, C., Nguyen, M.H., Culshaw, N.G., 2007. Synconvergent ductile flow in variable-strength continental crust: numerical models with application to the western Grenville orogen. Tectonics 26, TC5005.

Janoušek, V., Gerdes, A., Vrána, S., Finger, F., Erban, V., Friedl, G., Braithwaite, C.J.R., 2006. Low-pressure granulites of the Lišov Massif, southern Bohemia: viséan metamorphism of late Devonian plutonic arc rocks. J. Petrol. 47, 705–744.

Koester, E., Porcher, C.C., Pimentel, M.M., Fernandes, L.A.D., Vignol-Lelarge, M.L., Oliveira, L.D., Ramos, R.C., 2016. Further evidence of 777 Ma subduction-related continental arc magmatism in Eastern Dom Feliciano Belt, southern Brazil: the Chácara das Pedras Orthogneiss. J. South Am. Earth Sci. 68, 155–166.

Konopásek, J., Sláma, J., Košler, J., 2016. Linking the basement geology along the AfricaSouth America coasts in the south atlantic. Precambrian Res. 280, 221–230.

Konopásek, J., Janoušek, V., Oyhantçabal, P., Sláma, J., Ulrich, S., 2018. Did the circum-Rodinia subduction trigger the Neoproterozoic rifting along the Congo–Kalahari Craton margin? Int. J. Earth Sci. 107 (5), 1859–1894.

Lenz, C., Porcher, C.C., Fernandes, L.A.D., Masquelin, H., Koester, E., Conceição, R.V., 2011. U-Pb SHRIMP ages for the Cerro Bori orthogneisses, Dom Feliciano belt in Uruguay: evidences of a ~800 Ma magmatic and ~650 Ma metamorphic event. Precambrian Res. 185 (3–4), 149–163.

Lenz, C., Porcher, C.C., Fernandes, L.A.D., Masquelin, H., Koester, E., Conceição, R.V., 2013. Geochemistry of the neoproterozoic (800-767 Ma) Cerro Bori orthogneisses, Dom Feliciano belt in Uruguay: tectonic evolution of an ancient continental arc. Mineral. Petrol. 107 (5), 785–806.

Lenz, C., Fernandes, L.A.D., Koester, E., Porcher, C.C., 2014. Geoquímica e idades U-Pb SHRIMP do magmatismo máfico sin a pós colisional registrado nos ortognaisses do Complexo Cerro Olivo, Uruguai. Cad. Geocienc. 11 (1–2), 49–60.

Liu, F.L., Liou, J.G., 2011. Zircon as the best mineral for P-Ttime history of UHP metamorphism: a review on mineral inclusions and U-Pb SHRIMP ages of zircons from the DabieSulu UHP rocks. J. Asian Earth Sci. 40, 1–39.

Ludwig, K.R., 2008. Isoplot 3.70, a geochronological toolkit for microsoft excel. Berkeley, Geochronol. Center, Spec. Publ. 4, 76p.

Lugmair, G.W., Carlson, R.W., 1978. The Sm–Nd history of KREEP. In Proceedings 9th. Lunar Planet Sci. Conf. 689–704.

Martil, M.M., Bitencourt, M.F., Nardi, L.V.S., Koester, E., Pimentel, M.M., 2017. Precollisional, Tonian (ca. 790 Ma) continental arc magmatism in southern Mantiqueira Province, Brazil: geochemical and isotopic constraints from the Várzea do Capivarita Complex. Lithos 274–275, 39–52.

Masquelin, H., 1990. Analisis estructural de las zonas de cizalla en las migmatitas de Punta del Este,Uruguay. Actas Geologica Leopoldense 12, 139–158.

Masquelin, H., 2000. Evolução Estrutural e Metamórfica do Complexo Cerro Olivo, Sudeste do Uruguay. Unpub. [Ph.D. thesis]. UFRGS, Porto Alegre v.1: 1–227, v.2: 1–117, 1 map.

Masquelin, H., Gómez- Rifas, C., 1998. Neoproterozoic to early paleozoic belt in Uruguay and rio Grande do sul a contribution. 1998. Zbl. Geol. Palaont. Teil I 681–699.

Masquelin, H., Tabó, F., 1989. Memoria Explicativa de la Carta Geológica del Uruguay, Hoja Chafalote, Escala 1:100.000. DINAMIGE-Fac. de Agron.-Fac. de H. y Ciencias, pp. 20.

Masquelin, H., Silva, A.O.M., Porcher, C.C., Fernandes, L.A.D., Morales, E., 2001. Geología y geotermobarometría de la Suite Metamórfica Chafalote, basamento pre-brasiliano, sureste del Uruguay. In: 11th Congresso Latino Americano de Geologia, Montevideo,Actas.

Masquelin, H., Nessi, A., Paris, A., 2005. Rocas metapelíticas de la Suite Metamórfica Chafalote (SE del Escudo Uruguayo. Rev. Soc. Urug. Geol. 12, 57–72.

Masquelin, H., Fernandes, L.A.D., Lenz, C., Porcher, C.C., McNaughton, N.J., 2012. The Cerro Olivo complex: a pre-collisional neoproterozoic magmatic arc in eastern Uruguay. Int. Geol. Rev. 54, 1161–1183.

Masquelin, H., Silva Lara, H., Sánchez Bettucci, L., Núñez Demarco, P., Pascual, S., Muzio, R., Peel, E., Scaglia, F., 2017. Lithologies, structure and basement-cover relationships in the schist belt of the Dom Feliciano Belt in Uruguay. Braz. J. Genet. 47 (1), 21–42.

Oriolo, S., Oyhantçabal, P., Wemmer, K., Heidelbach, F., Pfänder, J., Basei, M.A.S., Hueck, M., Hannich, F., Sperner, B., Siegesmund, S., 2016. Shear zone evolution and timing of deformation in the Neoproterozoic transpressional Dom Feliciano Belt, Uruguay. J. Struct. Geol. 92, 59–78.

Oyhantçabal, P., Siegesmund, S., Wemmer, K., Frei, R., Layer, P., 2009. Geochronological constraints on the evolution of the southern Dom Feliciano belt (Uruguay). J. Geol. Soc. Lond. 166, 1–11.

Oyhantçabal, P., Siegesmund, S., Wemmer, K., Passchier, C.W., 2011. The transpressional connection between Dom Feliciano and Kaoko belts at 580–550 Ma. Int. J. Earth Sci. 100, 379–390.

Passchier, C.W., Trouw, R.A.J., 2005. Microtectonics. Springer, Berlin, pp. 366p.

Patiño Douce, A.E., Harris, N., 1998. Experimental constraints on Himalayan anatexis. J. Petrol. 39 (4), 689–710.

Peel, E., Sánchez-Bettucci, L., Basei, M.A.S., 2018. Geology and geochronology of Paso del Dragón Complex (northeastern Uruguay): implications on the evolution of the Dom Feliciano Belt (Western Gondwana). J. South Am. Earth Sci. 85, 250–262.

Philipp, R.P., Massone, H.J., Campos, R.S., 2013. Peraluminous leucogranites of the \

cordilheira suite: a record of neoproterozoic collision and the generation of the pelotas batholith, Dom Feliciano belt, southern Brazil. J. South Am. Earth Sci. 43 (08–24).

Preciozzi, F., Masquelin, H., Basei, M.A.S., 1999. The namaqua/grenville terrane of eastern Uruguay. In: 2nd Simpósio Sul-Americano de Geologia Isotópica. Córdoba.Actas, pp. 338–340.

Ramos, R.C., Koester, E., Porcher, C.C., 2017. Chemistry of chromites from Arroio Grande ophiolite (Dom Feliciano belt, Brazil) and their possible connection with the nama group (Namibia). J. South Am. Earth Sci. 80, 192–206.

Ramos, R.C., Koester, E., Vieira, D.T., Porcher, C.C., Gezatt, J.N., Silveira, R.L., 2018. Insights on the evolution of the Arroio Grande ophiolite (Dom Feliciano belt, Brazil) from Rb-Sr and SHRIMP U-Pb isotopic geochemistry. J. South Am. Earth Sci. 86, 38–53.

Ramos, R.C., Koester, E., Vieira, D.T., 2019. Plagioclase-hornblende geothermobarometry of metamafites from the Arroio Grande ophiolite, Dom Feliciano belt, southernmost Brazil. J. South Am. Earth Sci. 95, 102262.

Rubatto, D., Hermann, J., 2003. Zircon formation during fluid circulation in eclogites (Monviso, Western Alps): implications for Zr and Hf budget in subduction zones. Geochem. Cosmochim. Acta 67, 2173–2187. https://doi.org/10.1016/S0016-7037(02)01321-2.

Rubatto, D., Williams, I.S., Buick, I.S., 2001. Zircon and monazite response to prograde metamorphism in the Reynolds Range, central Australia. Contrib. Mineral. Petrol. 140, 458–468.

Sánchez Bettucci, L., Mezzano, A., 1993. Análisis sedimentológico y faciológico de la Formación rocha (Ex-Grupo rocha). Revista Brasilera de Geociencias 23, 323–329.

Sánchez Bettucci, L., Peel, E., Masquelin, H., 2010. Neoproterozoic tectonic synthesis of Uruguay. Int. Geol. Rev. 52, 51–78.

Santos, J.O.S., Chernicoff, C.J., Zappettini, E.O., McNaughton, N.J., Hartmann, L.A., 2017. Large geographic and temporal extensions of the Río de la Plata Craton, South America, and its metacratonic eastern margin. Int. Geol. Rev. 61, 56–85 2019.

Sato, K., Tassinari, C.C.G., Basei, M.A.S., Siga Jr., O., Onoe, A.T., de Souza, M.D., 2014. Microssonda Iônica de Alta Resolução e de Alta Sensibilidade (SHRIMP IIe/MC) do Instituto de Geociências da Universidade de São Paulo, Brasil: método analítico e primeiros resultados. Revista do Instituto de Geociências – USP 14 (3), 3–18.

Silva, L.C., Hartmann, L.A., McNaughton, N.J., Fletcher, I.R., 1999. SHRIMP U/Pb zircon dating of Neoproterozoic granitic magmatism and collision in the Pelotas Batholith, Southernmost Brazil. Int. Geol. Rev. 41, 531–551.

Skagseth, I.G., 2016. Metamorphic conditions in the Coastal-Punta del Este Terrane of the Kaoko-Dom Feliciano Belt in Namibia and Uruguay. Master Degree Dissertation. UiT Norges Arktiske Universitet.

Spear, F.S., Pyle, J.M., 2002. Apatite, monazite, and xenotime in metamorphic rocks. In: Reviews in Mineralogy & Geochemistry . Phosphates: Geochemical, Geobiological, and Materials Importance, vol. 48. pp. 293–336.

Stevenson, R.K., Whittaker, S., Mountjoy, E.W., 2000. Geochemical and Nd isotopic evidence for sedimentary-source changes in the Devonian miogeocline of the southern Canadian Cordillera. GSA Bull. 112 (4), 531–539.

Tambara, G.B., Koester, E., Ramos, R.C., Porcher, C.C., Vieira, D.T., Lenz, C., Fernandes, L.A.D., 2019. Geoquímica e geocronologia dos Gnaisses Piratini: magmatismo cálcio-alcalino médio a alto-K de 784 Ma (U-Pb SHRIMP) no SE do Cinturão Dom Feliciano (RS, Brazil). n. Pesqui. em Geociencias 46 (2), e0769.

Tulloch, A.J., Challis, G.A., 2000. Emplacement depths of Paleozoic-Mesozoic plutons from western New Zealand estimated by hornblende-Al geobarometry. N. Z. J. Geol. Geophys. 43, 555–567.

Vieira, D.T., Koester, E., Ramos, R.C., Porcher, C.C., 2019. Sr-Nd-Hf isotopic constraints and U-Pb geochronology of the Arroio Pedrado gneisses, Dom Feliciano belt, Brazil: a 680 Ma shoshonitic event in the final stages of the Piratini Arc evolution. J. South Am. Earth Sci. 95, 102294.

Wan, Y., Li, R., Wilde, S.A., Liu, D., Chen, Z., Yan, L., Song, T., Yin, X., 2005. UHP metamorphism and exhumation of the Dabie Orogen, China: evidence from SHRIMP dating of zircon and monazite from a UHP granitic gneiss cobble from the Hefei Basin. Geochem. Cosmochim. Acta 69, 4333–4348.

Weinberg, R.F., Hasalova, P., 2015. Water-fluxed melting of the continental crust: a review. Lithos 212, 158–188.

Will, T.M., Frimmel, H.E., Gaucher, C., Bossi, J., 2014. Geochemical and isotopic composition of pan-African metabasalts from southwestern Gondwana: evidence of cretaceous south atlantic opening along a neoproterozoic back-arc. Lithos 202–203, 363–381.

Williams, M.L., Jercinovic, M.J., Hetherington, C.J., 2007. Microprobe monazite geochronology: understanding geologic processes by integrating composition and chronology. Annu. Rev. Earth Planet Sci. 35, 137–175.

Zheng, Y.-F., Chen, R.-X., Zhao, Z.-F., 2009. Chemical geodynamics of continental subduction-zone metamorphism: insights from studies of the Chinese Continental Scientific Drilling (CCSD) core samples. Tectonophysics 475, 327–358.

Zhu, X.K., Onions, R.K., 1999. Zonation of monazite in metamorphic rocks and its implications for high temperature thermocronology: a case study from the Lewisian terrain. Earth Planet. Sci. Lett. 171, 209–220.

CAPÍTULO 5

Artigo *"New zircon SHRIMP U-Pb ages for the synkinematic magmatism in the Dorsal de Canguçu Transcurrent Shear Zone, Dom Feliciano Belt (Brazil): tectonic implications"*

Journal of South American Earth Sciences <Evise
Support@elsevier.com>
Sex, 04/10/2019 19:07
Você ⌄

This message was sent automatically.

Reference: SAMES_2019_450
Title: New zircon SHRIMP U-Pb ages for the synkinematic magmatism in the Dorsal de
Canguçu Transcurrent Shear Zone, Dom Feliciano Belt (Brazil): tectonic implications
Journal: Journal of South American Earth Sciences

Dear Mr. Vieira,

I am currently identifying and contacting reviewers who are acknowledged experts in the
field. Since peer review is a voluntary service it can take time to find reviewers who are
both qualified and available. While reviewers are being contacted, the status of your
manuscript will appear in EVISE® as 'Reviewer Invited'.

Once a reviewer agrees to review your manuscript, the status will change to 'Under
Review'. When I have received the required number of expert reviews, the status will
change to 'Ready for Decision' while I evaluate the reviews before making a decision on
your manuscript.

To track the status of your manuscript, please log into EVISE® and go to 'My Submissions'
via: http://www.evise.com/evise/faces/pages/navigation/NavController.jspx?
JRNL_ACR=SAMES

Kind regards,

Journal of South American Earth Sciences

Have questions or need assistance?
For further assistance, please visit our Customer Support site. Here you can search for
solutions on a range of topics, find answers to frequently asked questions, and learn more
about EVISE® via interactive tutorials. You can also talk 24/5 to our customer support
team by phone and 24/7 by live chat and email.

Copyright © 2018 Elsevier B.V. | Privacy Policy

Elsevier B.V., Radarweg 29, 1043 NX Amsterdam, The Netherlands, Reg. No. 33156677.

New zircon SHRIMP U-Pb ages for the synkinematic magmatism in the Dorsal de Canguçu Transcurrent Shear Zone, Dom Feliciano Belt (Brazil): tectonic implications

Daniel Triboli VIEIRA [1], Edinei KOESTER [2], Rodrigo Chaves RAMOS [1], Carla Cristine PORCHER[2] and Luis Alberto D'Ávila FERNANDES [2]

1. Programa de Pós-Graduação em Geociências, Instituto de Geociências, Universidade Federal do Rio Grande do Sul. Caixa Postal 15.001, CEP 91501-970, Porto Alegre, RS, Brazil. E-mail: danieltriboli@hotmail.com, rodrigo.chaves@ufrgs.br.

2. Departamento de Geologia, Instituto de Geociências, Universidade Federal do Rio Grande do Sul. Av. Bento Gonçalves, 9500, CEP 91540-000, Porto Alegre, RS, Brazil. E-mail: koester@ufrgs.br, carla.porcher@ufrgs.br, ladfernandes@gmail.com

Abstract.

The Dorsal de Canguçu Transcurrent Shear Zone (DCTSZ) is the main Neoproterozoic structure of the Dom Feliciano Belt in the Rio Grande do Sul sector (Brazil), developed during the late stages of the Brasilano/Pan-African orogenic cycle. This structure, together with its northern – Major Gercino Transcurrent Shear Zone (Santa Catarina sector, Brazil) – and southern extension – Sierra Ballena Transcurrent Shear Zone (Uruguay), constitute a 1,000 km long discontinuous lineament. Synkinematic granitoids are widespread along the DCTSZ. The main units are represented by the mantle-derived Quitéria metagranite, and the peraluminous Arroio Francisquinho and Cordilheira metagranites (Cordilheira Suite). In order to better constrain the time frame of the synkinematic magmatism associated with the DCTSZ, we present in this paper new zircon SHRIMP (Sensitive High Resolution Ion Micro Probe) U-Pb ages for this magmatism. The Quitéria metagranite yielded a concordia U-Pb age of 618 Ma, interpreted as the magmatic crystallization age. The Arroio Francisquinho and Cordilheira metagranites yielded concordia U-Pb ages of, respectively, 615 and 608 Ma, interpreted as the magmatic crystallization ages. The latter ages constrain the main phase of synkinematic magmatism in the DCTSZ. Zircon rims of the studied samples yielded U-Pb ages between ca. 580-540 Ma, interpreted as the age of possible reactivations of the DCTSZ, thus constraining the timing of late-tectonic activity. Zircon crystals interpreted as inherited yielded U-Pb ages ranging from 1800 to 650 Ma for the three studied rocks. These inherited ages are similar to those found in detrital zircon from the regional gneissic basement. The new ages for the earliest synkinematic magmatism in the DCTSZ match those of the Major Gercino Shear Zone, strengthen previous correlation between both shear zones. On the other hand, the earliest shear-related magmatism related to the Sierra Ballena Shear Zone, classically interpreted as the Uruguayan counterpart of the latter two shear zones, is younger (ca. 580 Ma), so that the origin of the Sierra Ballena Shear Zone is possibly related to a younger tectonic event. From the new data present in this work it is suggested that the origin of the DCTSZ is possibly related to the convergence between the Río de la Plata Craton and the recently proposed Piratini Arc at ca. 660 Ma. Possible reactivations of the shear zone might be

related to the convergence of the Kalahari and Río de la Plata cratons at ca. 580 Ma. Younger reactivations (ca. 540 Ma) could be related to late-orogenic relaxation.

Keywords. Geochronology; Neoproterozoic; Reactivation; Quitéria metagranite; Cordilheira Suite; Sul-rio-grandense Shield

1 Introduction

In the Dom Feliciano Belt (southernmost Brazil and Uruguay), southern sector of the Mantiqueira Province (Almeida et al., 1981), the Cuchilla Dionisio-Pelotas-Florianópolis Terrane (Bossi and Gaucher, 2004) represents remnants of a voluminous Neoproterozoic granitogenesis related to the late stages of the Brasiliano/Pan-African orogenic cycle. This terrane comprises a discontinuous granitic belt (Basei et al., 2000) subdivided into three main batholiths: Pelotas Batholith, in the Sul-rio-grandense Shield; Florianópolis Batholith, in the Santa Catarina Shield; and Aiguá Batholith, in the Uruguayan Shield (e.g. Fragoso-César et al., 1986, Babinski et al., 1997; Basei et al., 2000; 2011; Oyhantçabal et al., 2009; Passarelli et al., 2010). This magmatism is partially associated with the transpressive tectonic regime related to the final stages of the Brasiliano/Pan-African Orogenic Cycle, marked by the activity of mega-shear zones (e.g. Bitencourt and Nardi, 2000; Philipp et al., 2016a; Oriolo et al., 2016).

In the Sul-rio-grandense Shield the Dorsal do Canguçu Transcurrent Shear Zone (DCTSZ) is the main tectonic feature of the Dom Feliciano Belt. In the central sector of the latter belt (Encruzilhada do Sul region), a large synkinematic magmatism is associated with this shear zone (Tommasi et al., 1994; Koester et al., 1997; Bitencourt and Nardi, 2000). Its possible sources and processes are discussed by several authors (e.g. Fernandes et al., 1995a,b; Koester, 1995; Nardi and Frantz, 1995; Philipp, 1998; Koester et al., 2001a, 2001b, 2002; Frantz et al., 2003; Philipp et al., 2013; Knijnik, 2018). The main granitic plutons associated with the DCTSZ are the Quitéria, Arroio Francisquinho and Cordilheira metagranites. These rocks are interpreted as an important mantle-derived magmatism followed by intense crustal reworking occurred at between 650 and 625 Ma (Frantz et al., 2003; Philipp et al., 2013). However, the time interval for the synkinematic magmatic activity of the DCTSZ is poorly constrained by available geochronological data.

Shear zones such as the DCTSZ represent structures that allow the study of the period between partial melting processes, magmatic transport and crustal exhumation of the related

synkinematic granitoids (e.g. Oriolo et al., 2016). These studies, however, are hampered by the overlap of tectonic events such as reactivation of the shear zone, in which the rocks reach high temperatures, thus resetting the radiometric clocks of the minerals commonly used for the various dating systems (e.g., Cherniak and Watson, 2000; Oriolo et al., 2016).

In order to better constrain the time frame of the synkinematic magmatism associated with the DCTSZ, we present in this paper new zircon SHRIMP (Sensitive High Resolution Ion Micro Probe) U-Pb ages for this magmatism, together with a reappraisal of the geochronological data available for the main synkinematic metagranites emplaced along this shear zone. The main goal of this study is to suggest the duration of the main tectono-magmatic activity and possible reactivations of the DCTSZ, further contributing to the discussions on the evolution of the Dom Feliciano Belt during the Cryogenian.

2 Geological Overview

The study area is located in the Dom Feliciano Belt, southernmost Mantiqueira Province (Almeida et al., 1981). This Neoproterozoic to Early Cambrian orogenic belt extends from Southernmost Brazil (Rio Grande do Sul and Santa Catarina states) to Punta del Este, in Uruguay (Fig. 1), and is interpreted as the result of the collision between Río de La Plata, Congo, and Kalahari Cratons, and other minor blocks/ microplates during the Brasiliano/ Pan-African orogenic cycle (e.g. Fernandes et al., 1995a and 1995b; Basei et al., 2000; Heilbron et al., 2004; Gaucher et al., 2009; Oyhantçabal et al., 2009 and 2011; Konopásek et al., 2016; Santos et al., 2017; Hueck et al., 2018; Ramos et al.,2018 and Vieira et al., 2019).

The Dom Feliciano Belt is subdivided into distinct terranes (Wildner et al., 2007; Phillipp et al., 2016a) and/ or domains (Fernandes et al., 1995a and 1995b; Costa, 1997; Basei et al., 2000) by crustal-scale transcurrent shear zones (Fig. 1). The latter shear zones are considered to play an important role in the generation and rise of magmas which, associated with the transcurrent activity and high regional thermal gradient, induced an extensive crustal reworking event, responsible for the formation of the bulk of the Cuchilla Dioniso-Pelotas-Florianópolis Terrane (Fig. 1) in the eastern domain of the Dom Feliciano Belt (e.g. Fragoso-César et al., 1986; Philipp, 1998; Basei et al., 2000; Bitencourt and Nardi, 2000; Philipp et al., 2016).

Bitencourt and Nardi (2000) suggest that the magmatism related to these batholiths was controlled, in successive steps between 650 and 580 Ma, by a shear zone system known as the Southern Brazilian Shear Belt, comprising several kilometer-thick, anastomosed ductile shear zones (Fig. 1). Most of these shear zones are subvertical, with predominant N-S and N60E direction, with clockwise to counterclockwise displacement. In southern Brazil the main structure of the Southern Brazilian Shear Belt is the DCTSZ in the Rio Grande do Sul sector (Fig.1). This structure is correlated to the Major Gercino Transcurrent Shear Zone in the Santa Catarina sector (e.g. Fernandes et al. 1992; Fernandes and Koester 1999; Bitencourt and Nardi 2000; Florisbal et al 2012; Oriolo et al., 2016) and some authors(e.g. Fernandes et al. 1992; Fernandes and Koester 1999; Oyhantçabal et al., 2009, 2011b; Passarelli et al., 2010, 2011; Oriolo et al., 2018) suggest that both shear zones are correlated to the Sierra Ballena Transcurrent Shear Zone in eastern Uruguay. These structures, together, constitute a discontinuous lineament over 1,000 km long through the whole Dom Feliciano Belt (Mantovani et al., 1989; Basei et al., 2000, 2005, 2008; Oyhantçabal et al., 2007, 2010; Passarelli et al., 2011; Oriolo et al., 2016).

The latter lineament has been interpreted as the main Brasiliano suture, juxtaposing the cratonic cores of South America and Africa (Basei et al., 2000, 2005, 2008; Bossi and Gaucher, 2004; Gaucher et al., 2009; Passarelli et al., 2010, 2011a; Frimmel et al., 2011, 2013). On the other hand, several authors (e.g., Fernandes et al., 1992, 1995a, b; Fernandes and Koester, 1999; Bitencourt and Kruhl, 2000; Koester et al., 2001b; Philipp and Machado, 2005; Oyhantçabal et al., 2007, 2009; Saalmann et al., 2011; Chemale et al., 2012; Florisbal et al., 2012 ; Philipp et al., 2013, 2016a; Lara et al., 2017) consider the strike-slip shearing along the system and its associated granitogenesis as the result of post-collisional processes during the evolution of the Dom Feliciano Belt. Similarities in the crystallization ages and geochemical, isotopic, and geophysical signatures of granitoids on both sides of these shear zones are commonly seen as evidence of a post-collisional setting after ca. 650-630 Ma, i.e., the age of the earliest shear-related intrusions.

Some authors (e.g., Fernandes et al., 1995a, b; Costa, 1997; Fernandes and Koester, 1999; Koester et al., 2001c, 2016; Masquelin et al., 2012) argued that, if the shear system once acted as a suture zone, this event pre-dated the shearing event responsible for its present configuration. In this sense, Fernandes et al. (1995a, b) on basis in large-scale geophysical

discontinuities proposed the existence of the Porto Alegre Suture in the Sul-rio-grandense Shield, approximately parallel to the Dorsal do Canguçu Shear Zone (Fig.1), which would correspond to the suture zone of an older collision during the Cryogenian (Koester et al., 2016).
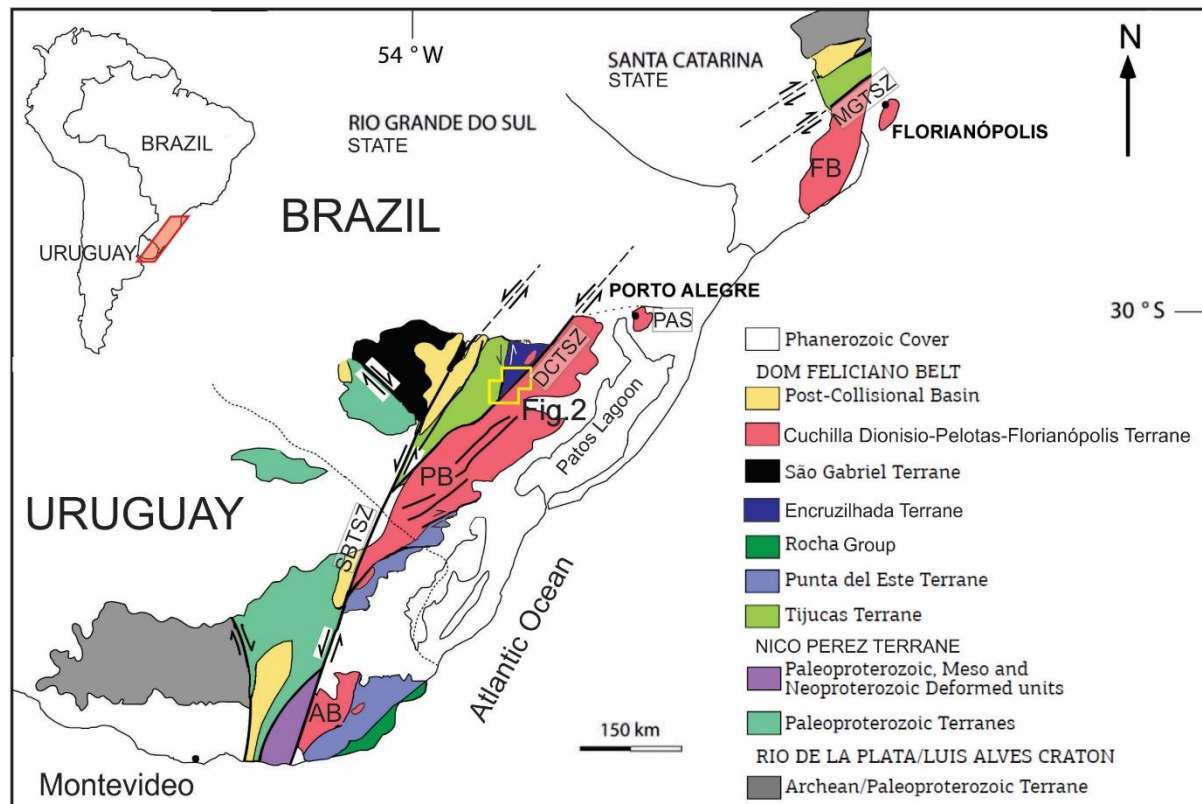
Figure 1. Simplified geological map of the southern Brazilian and Uruguayan shields (modified from Oyhantçabal et al., 2011, Rapela et al., 2011 and Philipp et al., 2016a) showing the study area presented in Fig. 2 (yellow square). Legend: Batholiths: AB= Aiguá Batholith, PB= Pelotas Batholith and FB= Florianópolis Batholith. Transcurrent Shear Zones: MGTSZ= Major Gercino; DCTSZ= Dorsal de Canguçu, SBTSZ= Sierra Ballena. PAS= Porto Alegre Suture.

2.2 Dorsal de Canguçu Transcurrent Shear Zone

The DCTSZ extends for ca. 200 km in a NE-SW direction, constituting the main tectonic feature of the Dom Feliciano Belt in the Rio Grande do Sul sector (Fig. 2) (e.g. Tommasi et al., 1994; Fernandes et al., 1995; Nardi and Bitencourt, 2000; Koester et al., 2001a; Oriolo et al., 2018). This structure is transected in its central portion by the N-S oriented, essentially brittle, Passo do Marinheiro Shear Zone (Basei et al., 2000, 2005, 2008; Passarelli et al., 2011). The DCTSZ records different stages of transcurrent activity at between 658 and 531 Ma (Philipp et

al., 2013). The early stage is represented by the synkinematic granitoids emplaced along this shear zone (Tommasi et al., 1994). This magmatism is characterized by the porphyritic, mantle-derived, high-K Quitéria metagranite, and by the fine- to medium-grained, equigranular Arroio Francisquinho and Cordilheira peraluminous metagranites which, together, constitute the Cordilheira Suite (Fig. 2) (Fragoso-César et al., 1986; Mesquita, 1991; Nardi and Frantz, 1995; Koester et al., 1997; Philipp, 1998; Fernandes and Koester, 1999; Koester et al., 2001a, b; Koester et al., 2002; Philipp and Machado, 2005; Philipp et al., 2013). The study of the features originated during the transcurrent stage, e.g., distribution, geometry, macro and microstructures, is hampered by: (a) the progressive high- temperature deformation from magmatic to solid state and low temperature events (e.g. milonites e phyllonite generation) (Tomassi et al., 1994; Fernandes et al., 1995a); (b) massive intrusion of younger (ca. 580 Ma) granitoids (Philipp et al., 2016a).

The Quitéria metagranite synkinematic fabric is subvertical with subordinate NE-SW steep dips. Its foliation and stretching lineations are mostly subhorizontal, with NE-SW trends, defined by the orientation of K-feldspar megacrysts (Fernandes et al., 1995a). In the peraluminous Cordilheira Suite, the early displacement of the DCTSZ is recorded in the NE-SW mylonitic texture marked by preferentially oriented feldspar porphyroclasts and by recrystallized quartz ribbons.
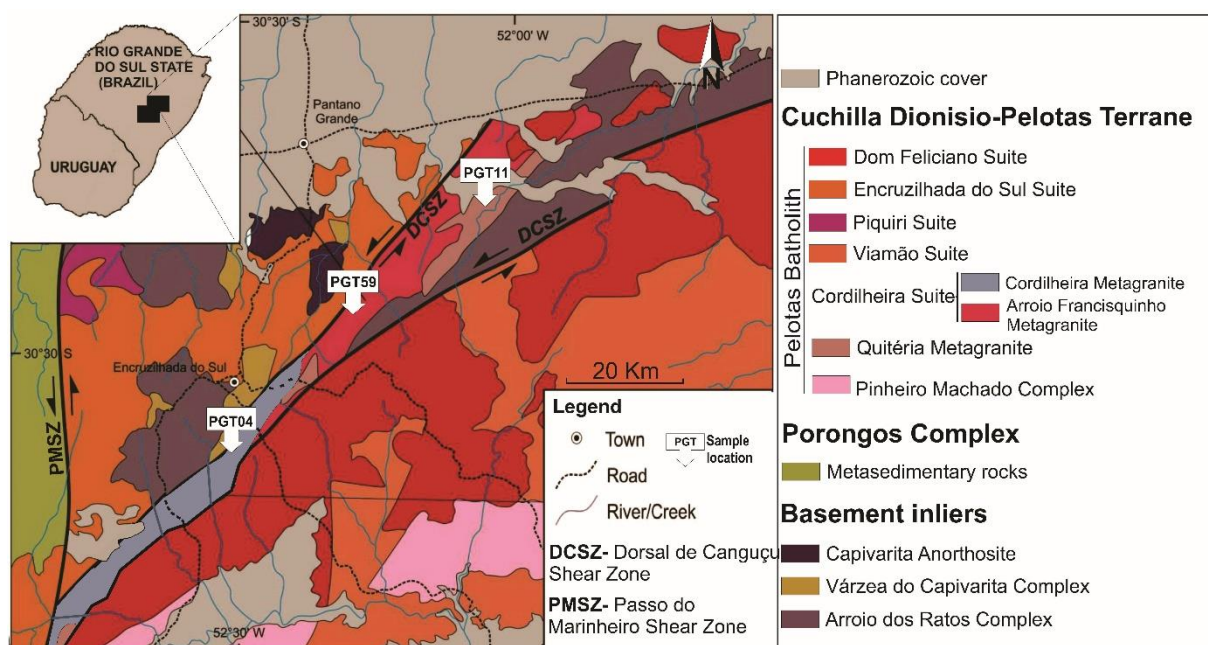
Figure 2. Simplified geological map of the Encruzilhada do Sul region with location of the analyzed samples. Modified from Wildner et al. (2006); Philipp et al. (2016a) and Hueck et al. (2018).

The temporal relationship between these granitoids is marked by meter-sized xenoliths and roof pendants of the Quitéria metagranite in the peraluminous leucogranites (UFRGS, 1988, 1992, 1993; Koester et al., 2001b). These granites show intrusive relationships, crosscut by pegmatites and greisens. The older Arroio Francisquinho is the most penetratively deformed, cut by the Cordilheira metagranite, which is also deformed. However, the deformation in the latter is mainly concentrated along the boundaries of the granitic body (Tessari and Picada 1966; Fernandes et al., 1995a).

Geochronological constraints (Tab. 1) suggest that the Quitéria metagranite could be the oldest granite in the Pelotas Batholith, with a zircon SHRIMP U-Pb age of 658±4 Ma (Frantz et al., 2003). The peraluminous granites of the Cordilheira Suite yield zircon SHRIMP U-Pb ages between ca. 634 and 625 ± 6 Ma (Arroio Francisquinho and Cordilheira metagranites; Frantz et al., 2003). Recently, Knijnik (2018) showed a new SHRIMP U-Pb age of 634 Ma for the Quitéria metagranite, which is similar to that presented in Koester et al. (2008) (631±6 Ma; zircon TIMS U-Pb). Knijnik (2018) also presented new zircon and monazite SHRIMP U-Pb age for the Arroio Francisquinho metagranite in the Encruzilhada do Sul region (609 Ma).
Based on Rb-Sr analyses, Koester et al. (1997) suggested an age of ca. 672 Ma for the Quitéria metagranite, and of ca. 629-617 Ma for the Cordilheira Suite (respectively, Arroio Francisquinho and Cordilheira metagranites). Based on K-Ar analyses in biotite, these authors suggested ages between 600 and 575 Ma for the Quitéria metagranite. The same authors suggested, based on K-Ar in muscovite, ages of 624 ± 41 and 586 ± 11 Ma for, respectively, the Arroio Francisquinho and Cordilheira metagranites. Additionally, Philipp et al. (2003) presented biotite Ar-Ar ages from mylonites associated with the DCTSZ between ca. 537 and 531 Ma, suggesting late tectonic activity.

Table 1. Geochronological data of the main rocks associated with the Dorsal de Canguçu Transcurrent Shear zone.

Unit	SHRIMP/ U-Pb (Ma)	LA-ICP-MS/ U-Pb (Ma)	TIMS/ U-Pb (Ma)	Ar-Ar (Ma)	K-Ar (Ma)	Rb-Sr (Ma)	Reference
Quitéria metagranite	658±4						Frantz et al. (2003)
	631±6						Knijnik (2018)

Rock					Reference
		631±6			Koester et al. (2008)
			597±11	672±21	Koester et al. (1997)
	625 ± 6				Frantz et al. (2003)
Arroio Francisquinho metagranite	609.3 ± 7.0				Knijnik (2018)
			586±11	629±23	Koester et al. (1997)
	634 ± 6				Frantz et al. (2003)
Cordilheira metagranite			624± 41 and 578± 32	617± 48	Koester et al. (1997)
Mylonites		**537-531**			Philipp et al. (2003)

3 Materials and methods

Representative samples from the Quitéria (PGT11), Arroio Francisquinho (PGT59) and Cordilheira (PGT04) metagranites were collected in the study area (Fig. 2). The preparation of polished thin sections for petrography was performed at the Laboratório de Separação de Minerais, Centro de Estudos em Petrologia e Geoquímica (CPGq), Instituto de Geociências (IGEO), Universidade Federal do Rio Grande do Sul (UFRGS), Brazil. The optical microscopy study was carried out at Laboratório de Geologia Isotópica (CPGq-IGEO-UFRGS), using a Leica DMLP polarizing microscope equipped with a Leica DC 300F digital camera.

For the U-Pb SHRIMP radiometric dating, the zircon crystals from the three samples were selected, after heavy liquid and magnetic separation, and mounted in epoxy resin together with the TEMORA-2 standard (Black et al., 2004). In order to identify the best targets for the analyses, cathodoluminescence images of crystals in the mount were obtained using a FEI Quanta 250 scanning electron microscope (SEM), equipped with a XMAX CL detector, at the Centro de Pesquisas Geocronológicas, Instituto de Geociências, Universidade de São Paulo (USP), Brazil. The U-Pb analyses were carried out at the same laboratory using a SHRIMP-IIe high resolution ion microprobe, following the procedures of Sato et al. (2014). Errors are 2σ. Common lead was corrected on the basis of the

measured ^{204}Pb. U abundance and U/Pb ratios were calibrated against the TEMORA-2 standard. The ^{206}Pb/^{238}U errors are < 2%. The ages were calculated using Isoplot software (Ludwig, 2008).

4 Results

4.1 Quitéria Metagranite

The analyzed zircon crystals of the PGT11 sample in the SEM (Fig. 3) are euhedral to subhedral (150-200 µm) and subrounded. Some crystals are fragments of larger grains. The internal oscillatory zoning are interpreted as primary, formed during igneous crystallization (Corfu et al., 2003). Some zircons show rims with low luminescence (Fig. 3), probably representing areas with high U concentration (e.g. spots 1.1, 3.1, and 16.1). Concentrations of U and Th range, respectively, from 134 to 1215 ppm and 43 to 791 ppm, yielding Th/U ratios between 0.10 and 1.02 (Table 2).

All 17 analyzed spots were plotted in a concordia diagram (Fig. 4A), in which 7 spots yielded a concordia age of 618.9 ±4.4 Ma (MSWD = 7.7) interpreted as the magmatic crystallization age (Fig. 4B). A group of 6 spots show ^{206}Pb/^{238}U ages between 580-520 Ma, which suggest generation of new rims and/or Pb loss, possibly related to the transcurrent activity (Kirkland et al., 2009). Four spots yielded older ^{206}Pb/^{238}U ages between 784 and 640 Ma, which are interpreted as inherited.
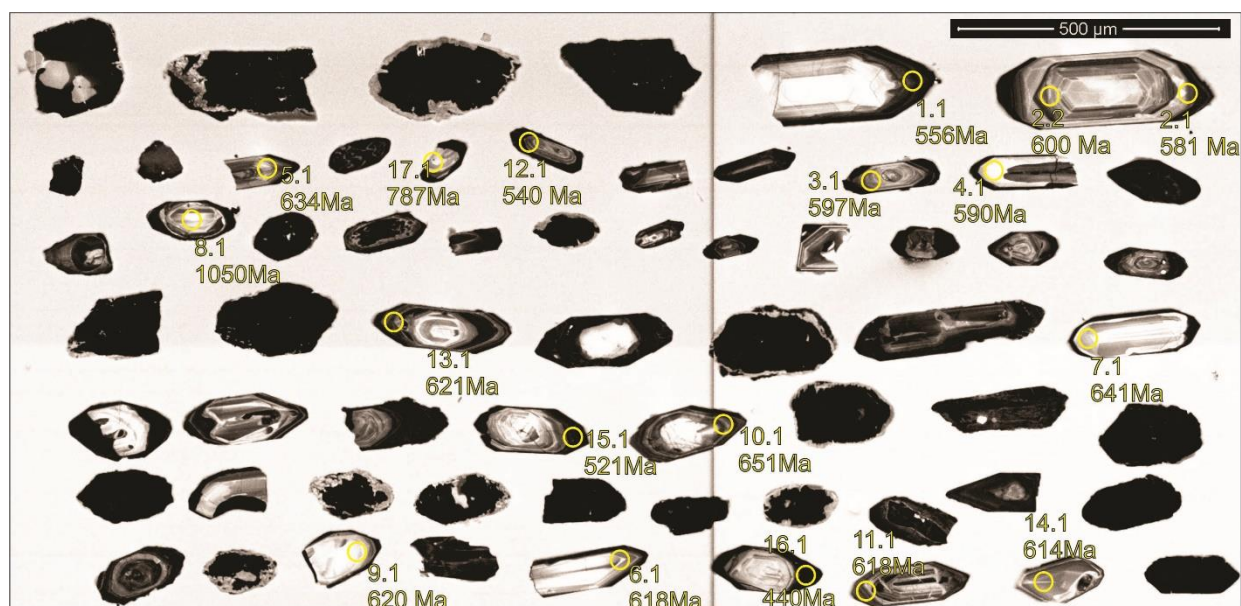
Figure 3. Cathodoluminescence images of zircon crystals from sample PGT11 (Quitéria Metagranite). Yellow circles represent the spots of U-Pb analysis.

Table 2. SHRIMP U-Pb data for sample PGT11 (Quitéria Metagranite). Pb_c = common lead (corrected using measured ^{204}Pb). Pb^* = radiogenic lead. The analyses marked in bold were used for the calculation of the concordia ages.

Spot	U ppm	Th ppm	$^{232}Th/^{238}U$	$^{206}Pb_c$ (%)	$^{206}Pb^*$ ppm	$^{206}Pb^*/^{238}U$	± %	$^{208}Pb^*/^{232}Th$	± %
1.1	711	463	0.67	1.26	56	0.09	2.1	0.03	2.2
2.1	1108	175	0.16	4.44	94	0.10	2.1	0.09	2.4
2.2	**260**	**79**	**0.31**	**3.12**	**22**	**0.10**	**2.1**	**0.06**	**3.4**
3.1	**145**	**89**	**0.63**	**6.36**	**13**	**0.10**	**2.2**	**0.05**	**3.0**
4.1	543	126	0.24	3.40	46	0.10	2.1	0.10	3.4
5.1	**292**	**174**	**0.61**	**0.28**	**26**	**0.10**	**2.1**	**0.03**	**2.5**
6.1	**268**	**200**	**0.77**	**1.41**	**23**	**0.10**	**2.1**	**0.03**	**2.4**
7.1	799	791	1.02	0.08	72	0.10	2.1	0.03	2.2
8.1	144	60	0.43	3.19	23	0.18	2.1	0.08	2.8
9.1	**339**	**261**	**0.79**	**0.11**	**29**	**0.10**	**2.1**	**0.03**	**2.4**
10.1	908	87	0.10	0.03	83	0.11	2.1	0.03	2.8
11.1	187	36	0.20	3.43	22	0.13	2.1	0.10	3.4
12.1	173	87	0.52	3.28	13	0.09	2.2	0.04	4.2
13.1	**1215**	**170**	**0.14**	**0.07**	**106**	**0.10**	**2.1**	**0.03**	**2.5**
14.1	**284**	**53**	**0.19**	**0.41**	**24**	**0.10**	**2.1**	**0.03**	**3.3**
15.1	1785	256	0.15	16.29	156	0.10	2.1	0.29	2.3
16.1	134	43	0.33	7.49	9	0.08	2.7	0.09	23.5

Spot	$^{207}Pb^*/^{206}Pb^*$	$^{206}Pb/^{238}U$ Age	1σ error	$^{207}Pb/^{206}Pb$ Age	1σ error	$^{208}Pb/^{232}Th$ Age	1σ error	% Discordant	Err. corr.
1.1	0.874	565	±12	624.57	±69	473	±15	12	0.024
2.1	0.876	583	±13	642.84	±195	538	±123	11	0.029
2.2	**0.877**	**595**	**±13**	**710.89**	**±116**	**670**	**±66**	**19**	**0.034**
3.1	**0.877**	**598**	**±15**	**629.49**	**±34**	**602**	**±65**	**5**	**0.031**
4.1	0.876	566	±14	674.13	±16	1268	±84	14	0.066
5.1	**0.880**	**634**	**±14**	**615.35**	**±37**	**635**	**±17**	**-3**	**0.032**
6.1	**0.878**	**619**	**±14**	**567.41**	**±16**	**610**	**±25**	**-8**	**0.031**
7.1	0.880	643	±15	623.40	±15	633	±14	-3	0.032
8.1	0.913	1058	±23	1223.47	±124	943	±90	17	0.049
9.1	**0.879**	**618**	**±14**	**693.22**	**±31**	**636**	**±16**	**12**	**0.032**
10.1	0.881	650	±13	660.61	±13	673	±19	2	0.034
11.1	0.891	784	±17	832.97	±162	896	±147	6	0.047
12.1	0.871	524	±13	682.72	±201	518	±46	31	0.026
13.1	**0.879**	**620**	**±12**	**653.85**	**±15**	**647**	**±19**	**5**	**0.033**
14.1	**0.878**	**617**	**±13**	**599.62**	**±43**	**540**	**±33**	**-2**	**0.027**
15.1	0.871	511	±17	959.17	±645	1052	±469	84	0.059
16.1	0.866	423	±25	1780.3	±730	954	±249	297	0.049

New zircon SHRIMP U-Pb ages for the synkinematic magmatism in the Dorsal de Canguçu Transcurrent Shear Zone, Dom Feliciano Belt (Brazil): tectonic implications

| 89
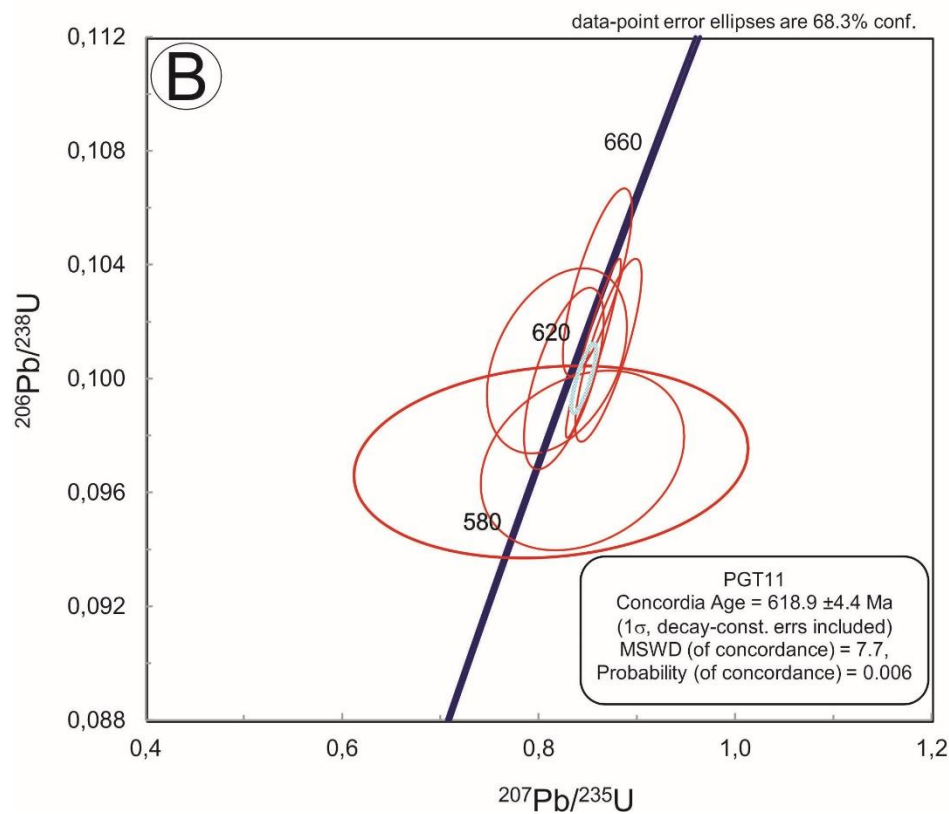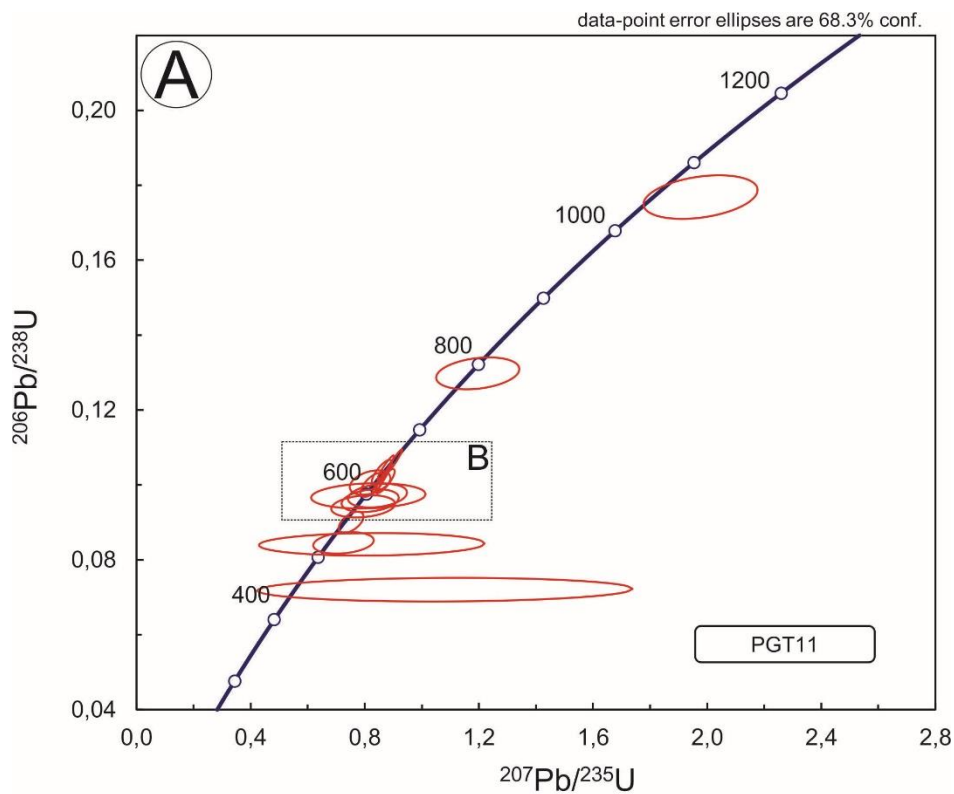
Figure 4. Zircon SHRIMP U-Pb ages from sample PGT11 (Quitéria Metagranite) – A) Concordia diagram showing all 17 analyzed spots; C) Detail of "A" showing the 618.9 ± 4 Ma concordia age interpreted as the crystallization age of the sample**.**

4.2 Arroio Francisquinho Metagranite

Two populations are observed in the analyzed zircon crystals from sample PGT59 (Fig. 5). The first population (spots 1.1, 1.2, 2.1, 3.1, 3.2, 4.1, 6.1, 10.1, 11.1, 14.1, 15.1, 16.1) is characterized by subrounded, euhedral to subhedral crystals (50-150 µm). The second population is characterized by rounded, anhedral grains (spots 5.1, 7.1, 9.1, 12.1, 13.1, 17.1). The internal oscillatory zoning in the crystals are interpreted as primary, formed during igneous crystallization. Zircon crystals from the second population are unzoned, showing internal homogeneity, suggesting crystallization during high-grade metamorphism (Corfu et al., 2003). The U and Th concentrations of the analyzed crystals (Tab. 3) range, respectively, from 195 to 3383 ppm and from 21 to 911 ppm, yielding Th/U ratios between 0.10 and 0.81.

All 19 analyzed spots were plotted in a concordia diagram (Fig. 6A). Six spots yielded a concordia age of 615.2 ± 13 Ma (MSWD = 0.87), interpreted as the magmatic crystallization age of the sample (Fig. 6B). Similar to what is observed for sample PGT11 (Quitéria metagranite, see section 4.1), a group of 5 spots shows $^{206}Pb/^{238}U$ ages between 570 and 520 Ma, which suggest generation of new rims and/or Pb loss, possibly related to transcurrent activity. Nine spots yielded older $^{206}Pb/^{238}U$ ages between 784 and 680 Ma, which are interpreted as inherited.
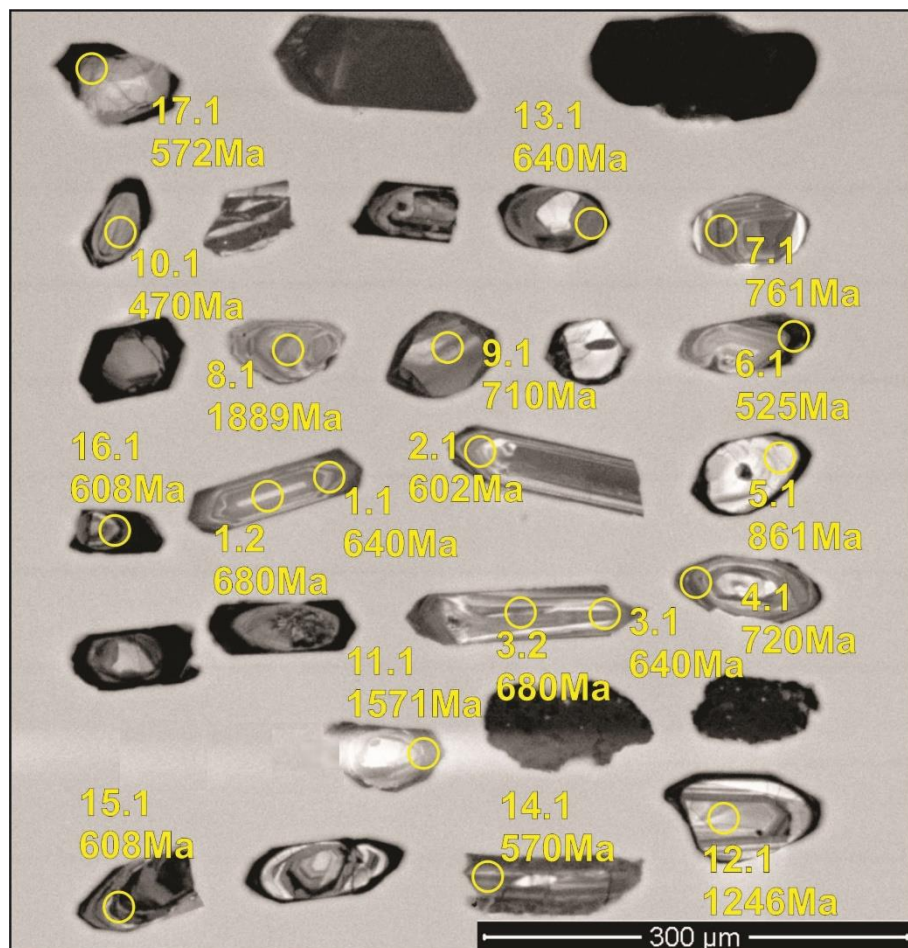
Figure 5. Cathodoluminescence images of zircon crystals from sample PGT59 (Arroio Francisquinho metagranite). Yellow circles represent the spots of U-Pb analysis.

Table 3. Zircon SHRIMP U-Pb data for sample PGT59 (Arroio Francisquinho metagranite). Pb_c = common lead (corrected using measured ^{204}Pb). Pb^* = radiogenic lead. The analyses marked in bold were used for the calculation of the concordia ages.

Spot	U ppm	Th ppm	^{232}Th / ^{238}U	$^{206}Pb_c$ (%)	$^{206}Pb^*$ ppm	$^{206}Pb^*$/ ^{238}U	± %	$^{208}Pb^*$/ ^{232}Th	± %
1.1	397	191	0.50	0.51	36	0.105	1.44	0.035	2.0
17.1	408	184	0.47	3.17	34	0.096	1.44	0.041	1.8
2.1	919	710	0.80	0.58	78	0.099	1.41	0.032	1.7
15.1	494	55	0.14	0.47	43	0.099	1.42	0.046	2.2
16.1	414	21	0.06	1.49	38	0.100	1.42	0.102	2.6
3.1	532	207	0.40	1.20	47	0.103	1.42	0.037	1.8
3.2	467	194	0.43	1.58	45	0.113	1.42	0.046	4.0
1.2	549	202	0.38	0.63	53	0.112	1.41	0.040	2.2
13.1	1237	543	0.45	12.23	127	0.119	1.39	0.103	3.3
14.1	1508	711	0.49	13.22	138	0.107	1.54	0.093	5.2
4.1	1165	47	0.04	1.83	121	0.121	1.43	0.169	3.5
5.1	340	145	0.44	7.87	46	0.156	1.59	0.121	4.2

6.1	340	145	0.44	8.12	27	0.093	1.43	0.072	4.1
7.1	686	444	0.67	0.20	74	0.126	1.40	0.040	1.6
8.1	195	93	0.49	1.33	58	0.346	1.45	0.109	1.7
9.1	807	320	0.41	6.51	87	0.125	1.79	0.087	2.2
10.1	3383	683	0.21	15.94	124	0.043	1.40	0.075	2.4
11.1	580	52	0.09	0.26	138	0.277	1.40	0.108	1.9
12.1	590	182	0.32	1.73	110	0.218	1.48	0.121	1.7

Spot	$^{207}Pb^*/$ $^{206}Pb^*$	$^{206}Pb/$ ^{238}U Age	1σ error	$^{207}Pb/$ ^{206}Pb Age	1σ error	$^{208}Pb/$ ^{232}Th Age	1σ error	% Discordant	Err. corr.
1.1	**0.880**	**639**	**±9**	**616.9**	**±47**	**647**	**±17**	**-4**	**.0015**
17.1	0.875	572	±8	547.5	±164	540	±37	-4	.0014
2.1	**0.877**	**602**	**±8**	**655.9**	**±39**	**600**	**±11**	**5**	**.0014**
15.1	**0.878**	**607**	**±8**	**663.3**	**±40**	**693**	**±48**	**6**	**.0014**
16.1	**0.878**	**609**	**±8**	**683.8**	**±78**	**794**	**±192**	**7**	**.0014**
3.1	**0.879**	**627**	**±9**	**616.7**	**±65**	**602**	**±22**	**-2**	**.0015**
3.2	0.883	677	±9	678.2	±109	735	±40	0	.0017
1.2	0.883	679	±9	654.2	±40	704	±21	-4	.0016
13.1	**0.880**	**637**	**±10**	**865.7**	**±51**	**651**	**±140**	**36**	**.0025**
14.1	0.875	567	±11	895.0	±648	605	±151	58	.0026
4.1	0.886	720	±10	**1057.5**	±67	1056	±274	47	.0018
5.1	0.897	861	±16	**1856.9**	±238	1154	±202	116	.0036
6.1	0.872	525	±10	**1856.9**	±238	693	±121	254	.0022
7.1	0.889	761	±10	**763.7**	±18	772	±13	0	.0018
8.1	1	1889	±23	2099.78	±28	1661.1	±64	11.141	.0057
9.1	1	710	±13	1092.34	±218	861.9	±90	53.884	.0024
10.1	1	226	±24	886.46	±648			291.482	.0011
11.1	0.960	1571	±19	**1871.5**	±8	1730	±62	19	.0042
12.1	0.930	1246	±17	**1944.32**	±44	1805	±79	56	.0036
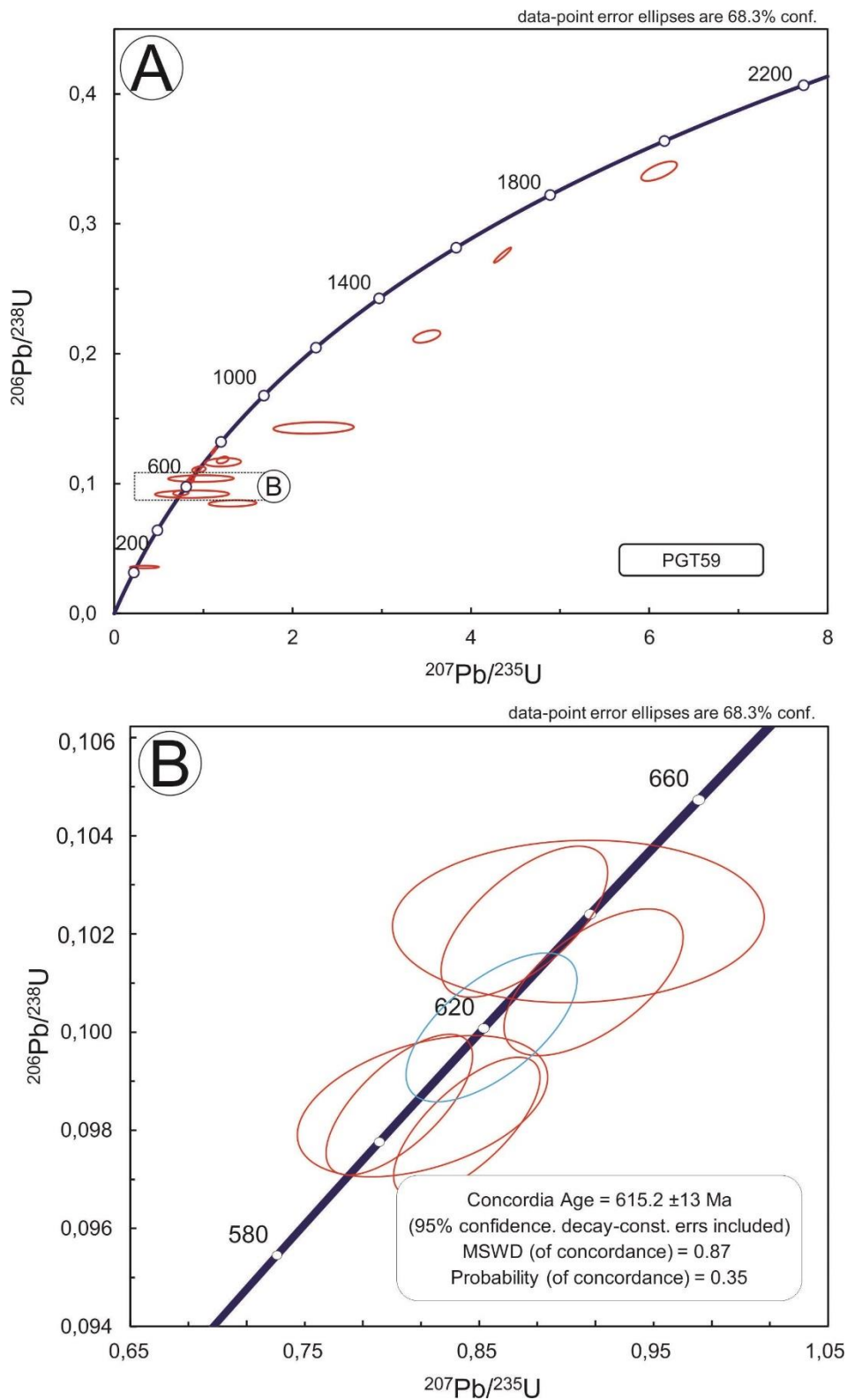
Figure 6. Zircon SHRIMP U-Pb ages from sample PGT59 (Arroio Francisquinho metagranite). A) Concordia diagram showing all 19 analyzed spots; C) Detail of "A" showing the 615.2 ± 13 Ma Concordia age interpreted as the crystallization age of the sample

4.3 Cordilheira Metagranite

The analyzed zircon crystals from sample PGT04 (Fig. 7) are subrounded, euhedral to subhedral (100-250 μm). The internal oscillatory zoning is interpreted as primary, formed during igneous crystallization. Some rims show low luminescence (Fig. 7), probably due to high U concentrations (Corfu et al., 2003). The U and Th concentrations (Table 4) range, respectively, from 47 to 1032 ppm and from 21 to 627 ppm, yielding Th/U ratios between 0.05 and 0.93.

All 20 analyzed spots were plotted in a concordia diagram (Fig. 8A). Six spots yielded a concordia age of 607.3 ±12 Ma (MSWD = 1.8) interpreted as the magmatic crystallization age of the sample (Fig. 8B). Other group of 6 spots shows $^{206}Pb/^{238}U$ ages between 580 and 470 Ma which suggest generation of new rims and/or Pb loss, probably related to transcurrent activity, similar to what is observed in the Quitéria and Arroio Francisquinho samples. Eight spots yielded older $^{206}Pb/^{238}U$ ages between 1500 and 750 Ma, which are interpreted as inherited.

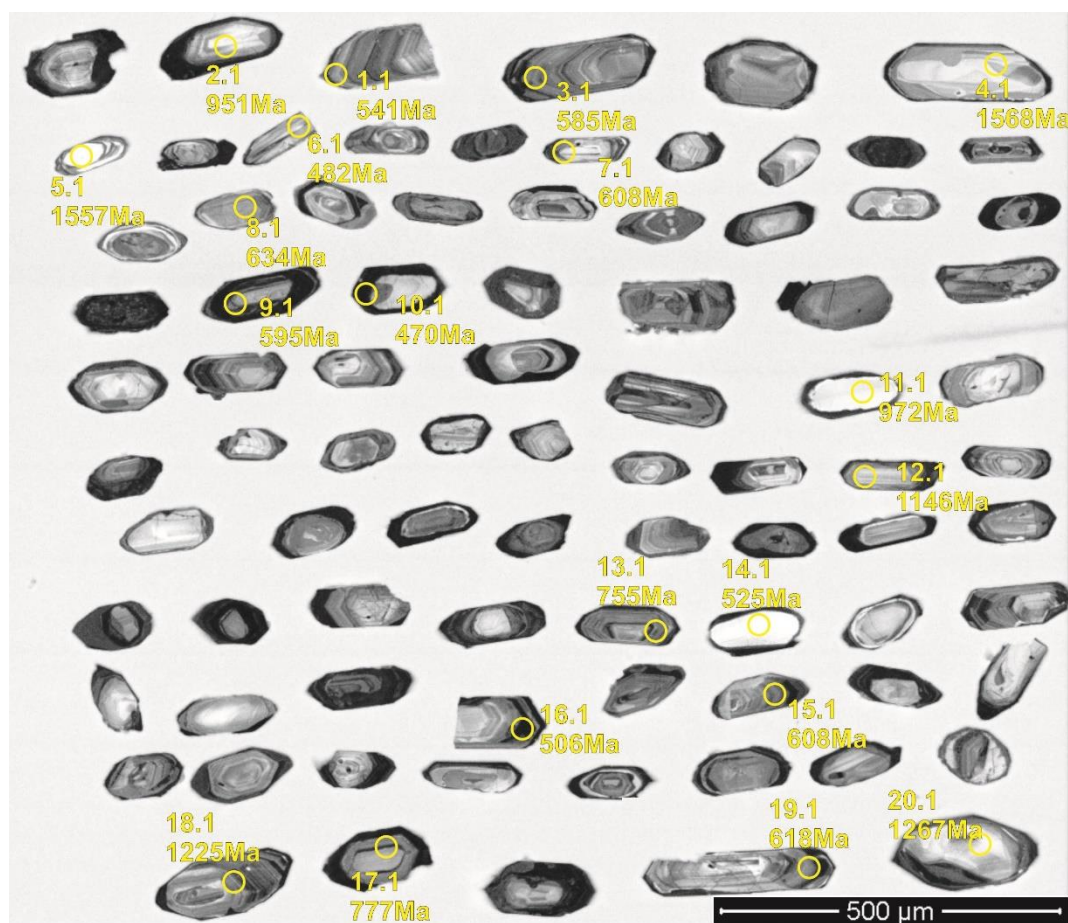**Figure 7.** Cathodoluminescence images of zircon crystals from sample PGT04 (Cordilheira metagranite). Yellow circles represent the spots of U-Pb analysis.

Table 4. Zircon SHRIMP U-Pb data for sample PGT04 (Cordilheira metagranite). Pb_c = common lead (corrected using measured ^{204}Pb). Pb* = radiogenic lead. The analyses marked in bold were used for the calculation of the concordia ages.

Spot	U ppm	Th ppm	^{232}Th / ^{238}U	$^{206}Pb_c$ (%)	$^{206}Pb*$ ppm	$^{206}Pb*$/ ^{238}U	± %	$^{208}Pb*$/ ^{232}Th	± %
1.1	611	118	0.20	0.55	46	0.09	1.4	0.01	4.6
2.1	231	174	0.78	2.31	32	0.16	1.4	0.06	1.7
3.1	**604**	**28**	**0.05**	**0.43**	**49**	**0.10**	**1.4**	**0.05**	**3.8**
4.1	103	37	0.37	0.06	24	0.28	1.5	0.08	2.6
5.1	93	43	0.49	0.65	22	0.28	1.6	0.10	2.2
6.1	656	60	0.09	2.77	45	0.08	1.5	0.06	3.5
7.1	**493**	**55**	**0.12**	**0.48**	**42**	**0.10**	**1.4**	**0.04**	**2.3**
8.1	**296**	**19**	**0.07**	**0.15**	**26**	**0.10**	**1.5**	**0.03**	**5.2**
9.1	**255**	**23**	**0.09**	**0.76**	**21**	**0.10**	**1.5**	**0.05**	**4.4**
10.1	506	51	0.10	1.99	34	0.08	1.4	0.05	4.9
11.1	71	37	0.53	0.52	10	0.16	1.6	0.06	2.8
12.1	218	106	0.50	0.21	37	0.19	1.5	0.06	3.0
13.1	1032	627	0.63	0.98	111	0.13	1.4	0.03	1.5
14.1	49	44	0.93	5.44	4	0.09	1.7	0.04	2.7
15.1	**412**	**21**	**0.05**	**1.47**	**36**	**0.10**	**1.4**	**0.10**	**2.7**
16.1	244	64	0.27	2.64	18	0.08	1.5	0.04	3.6
17.1	405	89	0.23	1.10	45	0.13	1.4	0.06	1.9
18.1	320	201	0.65	0.11	58	0.21	1.4	0.06	1.7
19.1	**345**	**32**	**0.10**	**0.59**	**30**	**0.10**	**1.4**	**0.04**	**2.8**
20.1	192	71	0.38	1.38	36	0.22	1.5	0.11	2.2

Spot	$^{207}Pb*$/ $^{206}Pb*$	^{206}Pb/ ^{238}U Age	1σ error	^{207}Pb / ^{206}Pb Age	1σ error	^{208}Pb / ^{232}Th Age	1σ error	% Discordant	Err. corr.
1.1	0.9	539	±7	612.23	±36	99	±19	13	18.6
2.1	0.9	931	±14	1425.16	±69	942	±32	50	3.2
3.1	**0.9**	**585**	**±8**	**566.85**	**±34**	**536**	**±82**	**-3**	**14.5**
4.1	1.0	1573	±23	1517.87	±15	1539	±40	-3	2.6
5.1	1.0	1519	±24	1940.69	±29	1786	±62	25	3.3
6.1	0.9	483	±7	492.87	±153	244	±139	2	50.4
7.1	**0.9**	**607**	**±8**	**662.34**	**±39**	**693**	**±46**	**9**	**6.4**
8.1	**0.9**	**634**	**±9**	**659.24**	**±33**	**565**	**±70**	**4**	**12.0**
9.1	**0.9**	**594**	**±9**	**671.79**	**±65**	**670**	**±85**	**13**	**12.2**
10.1	0.9	469	±7	513.10	±119	287	±86	9	27.8
11.1	0.9	969	±15	1057.41	±62	1048	±40	9	3.7
12.1	0.9	1147	±16	1128.03	±17	1119	±28	-2	2.5

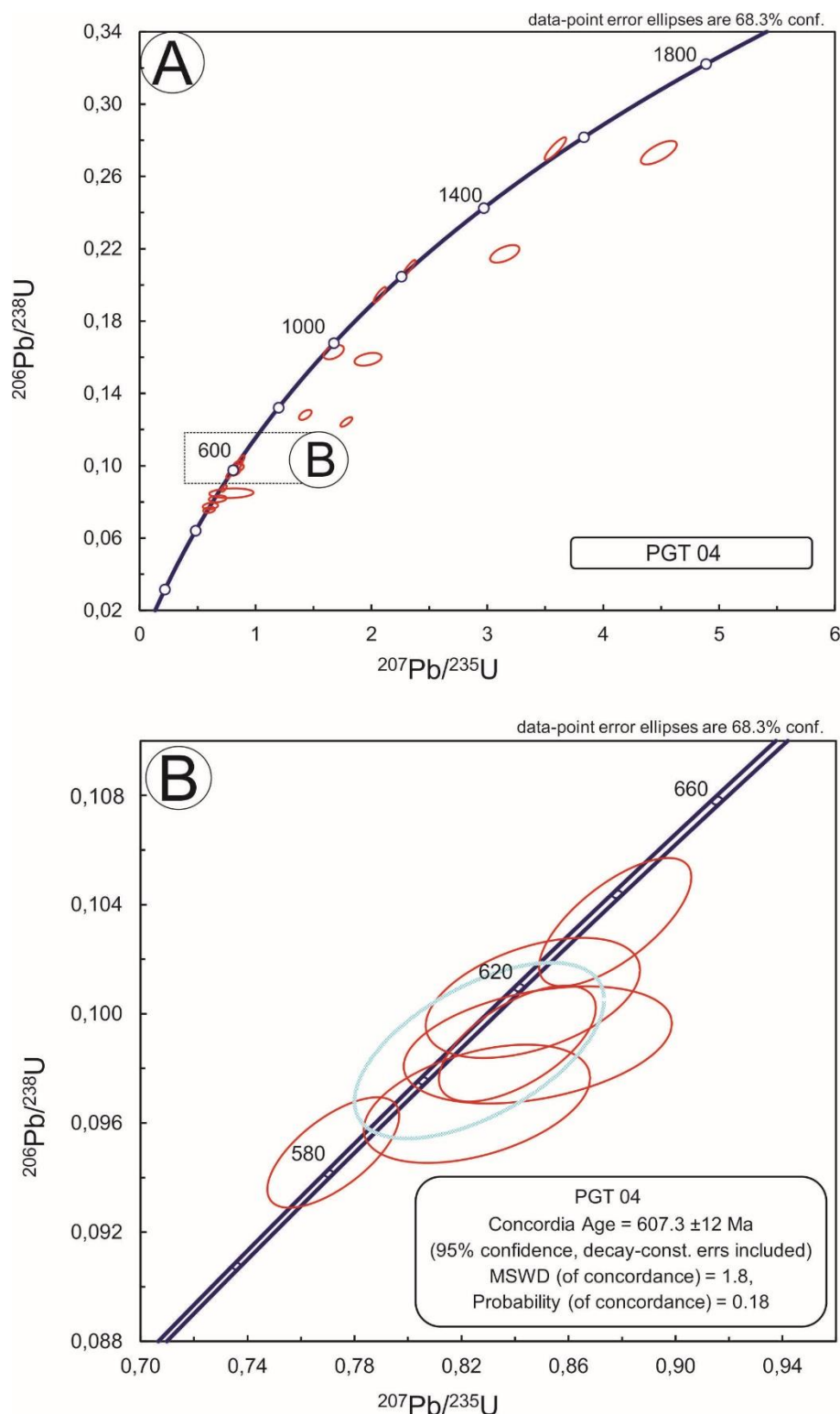|									
13.1	0.9	720	±11	1699.34	±23	577	±13	125	2.3
14.1	0.9	520	±10	860.31	±328	499	±47	64	9.2
15.1	**0.9**	**607**	**±8**	**682.75**	**±77**	**794**	**±182**	**12**	**21.1**
16.1	0.9	505	±8	596.75	±158	394	±55	18	13.2
17.1	0.9	763	±11	1219.37	±41	968	±43	57	4.3
18.1	0.9	1226	±17	1210.36	±14	1229	±21	-1	1.7
19.1	**0.9**	**618**	**±9**	**641.06**	**±40**	**583**	**±86**	**4**	**14.1**
20.1	0.9	1237	±18	1718.48	±40	1835	±62	36	3.2

Figure 8. zircon SHRIMP U-Pb ages from sample PGT04 (Cordilheira metagranite). A) Concordia diagram showing all 20 analyzed spots; B) Detail of "A" showing the 607.3 ± 12 Ma Concordia age, interpreted as the magmatic crystallization age of the sample.

5 Discussions

5.1 New U-Pb ages for the synkinematic magmatism in the DCTSZ

The new geochronological data obtained in this study show ^{206}Pb/^{238}U ages between 618 and 608 Ma for the synkinematic magmatism associated with the DCTSZ. These ages are consistent with the model suggested by Koester et al. (2001b); Koester et al. (2002) and Philipp et al. (2013), in which large volumes of granitic magma were generated when the DCTSZ was still active. The first magma pulses generated the Quitéria metagranite and associated (subordinated) mafic rocks. The rise of mantle-derived magmas, together with the transcurrent activity that possibly acted as a channel for magma and fluid migration, played an essential role in (i) partial melting of the gneisses from the Várzea do Capivarita Complex (regional basement), and (ii) the generation, extraction, and emplacement of the peraluminous melts which generated the Arroio Francisquinho and Cordilheira metagranites. This model is strengthened by the ages of inherited zircon found in the studied metagranites (1800 to 650 Ma), which are similar to those found in detrital zircon of gneisses from the Várzea do Capivarita Complex (Gruber et al., 2016; Philipp et al., 2016b).

Rims of the studied zircon crystals record possible reactivations of the DCTSZ, as suggested by the U-Pb ages between 585-540 Ma. These rims might represent the influence of post-magmatic fluids and deformation caused by the transcurrent activity of the shear zone (Kirkland et al., 2009). Interestingly, these ages are similar to the K-Ar ages (585 Ma) in biotite and muscovite from the Quitéria, Francisquinho and Cordilheira metagranites (Koester et al., 1997), interpreted as the magmatic cooling age. However, these ages might represent the crystallization age of newly formed minerals resulting from the reactivation and/or resetting of the K-Ar isotopic system, since the reactivation of the DCTSZ possible reached temperatures higher than 440 °C (Tommasi et al., 1994). The latter reactivation could be linked to the initiation of the ca. 580 Ma magmatism in the Encruzilhada do Sul region (Philipp et al., 2003; Oliveira et al., 2015). Additionally, it is possible to suggest a younger reactivation at around 540 Ma based on the new U-Pb ages presented in this work, which are similar to the Ar-Ar ages of biotite from mylonites associated with the DCTSZ presented by Philipp et al. (2003), interpreted as an indication of late tectonic activity.

Previous works (Frantz et al., 2003; Koester et al., 2008; Knijnik, 2018) presented U-Pb ages between 658 and 631 Ma for the Quitéria metagranite, between 635 and 609 Ma for the Francisquinho metagranite and of 624 ± 6 Ma for the Cordilheira metagranite (Frantz et al., 2003). However, these ages are not consistent with the model proposed by Koester et al. (2001b); Koester et al. (2002) and Philipp et al. (2013), which suggested that the rocks from the Várzea do Capivarita Complex are the main crustal source of the synkinematic magmatism and underwent high-grade metamorphism, followed by a partial melting event at around 650-620 Ma (Gross et al., 2006; Gruber et al., 2016; Philipp et al., 2016b; Martil et al., 2017).

The DCTSZ metagranitoids do not record the mentioned high-grade metamorphic event, so that only the solid state deformation related to the transcurrent activity of the shear zone is observed (Tommasi et al., 1994). Thus, it is plausible to suggest that the crystallization age of these metagranites are younger than the mentioned high-grade event, as suggested by the new radiometric ages presented in this paper.

5.2 Correlation with Major Gercino (Santa Catarina sector) and Sierra Ballena (Uruguayan sector) Shear Zones

The new data presented in this study strengthen previous correlation between the DCTSZ and the Major Gercino Shear Zone, located in the Santa Catarina sector (Fig. 1). According to Florisbal et al. (2012), the earliest intrusions associated with the latter shear zone are represented by the high-K, porphyritic Quatro Ilhas granitoids (ca. 620 Ma). As in the DCTSZ, the earliest magmatism is followed by a younger peraluminous magmatism, represented by the Mariscal granite (Ca. 610 Ma). Furthermore, the reactivation ages are similar, constrained between 580-540 Ma (K-Ar in muscovite and biotite from mylonites associated with this shear zone; Passarelli et al., 2010). According to Passarelli et al. (2010), the latter reactivation ages represent late tectonic activity that occurred after the ca. 620-610 Ma main transcurrent stage. The reactivation event could be related to the intrusion of the Zimbros Suite at around 589-586 Ma (Chemale et al., 2012).

In the Uruguayan sector, the Sierra Ballena Shear Zone is classically interpreted as the southern extension of the DCTSZ, with associated synkinematic magmatism constrained at around 580 Ma (Basei et al., 2000, Sánchez-Bettucci et al., 2003; Oyhantçabal et al 2010;

Oriolo et al., 2018). The latter age fits those of its Brazilian counterparts, which are interpreted as the age of the reactivation event mentioned above. As in its Brazilian counterparts, a younger reactivation is dated at around 540 Ma (Basei et al., 2000), based on Ar-Ar ages of biotite from mylonites associated with the Sierra Ballena Shear Zone.

5.3 Tectonics implications of the new data

Philipp et al. (2013, 2016a, 2016b) suggested that the oblique collision between the Río de La Plata and Kalahari Cratons, that occurred at around 650 Ma, produced large volumes of granitic magma, resulting in the bulk of the Pelotas Terrane. According to these authors, the latter collision produced the DCTSZ, which when still active, contributed to the synkinematic magmatism and deformation of the Quitéria, Arroio Francisquinho and Cordilheira metagranites. The latter event culminated in the generation of granitoids related to the Pinheiro Machado Complex at around 633-609 Ma (Philipp et al., 2003). At around 600-550 Ma the DCTSZ was reactivated, resulting in late-orogenic granitoids, represented by the intrusive suites of the Pelotas Terrane (Philipp et al., 2003).

The new data presented in this work show younger U-Pb ages for the synkinematic magmatism associated with the DCTSZ. These new ages are consistent with recently proposed models (Ramos et al., 2017; Vieira et al., 2019a, b) for the evolution of the Dom Feliciano Belt and associated granitogenesis. The latter models suggested the presence of an Andean-type magmatic arc – the Piratini Arc – active at around 780-680 Ma, whose fragments are dispersed throughout the Dom Feliciano Belt. Thus, the main deformation stage that occurred at around 660 Ma would be related to the collision between the Río de la Plata Craton and the mentioned Piratini Arc.

According to Vieira et al (2019b), this deformation stage was followed by decompression and partial melting at around 640 Ma, probably during the late stages of the collision event, culminating in the development of NE-SW-trending shear zone at the expense of pre-existing sutures (e.g., the Porto Alegre Suture) and voluminous magmatism at around 620 Ma. The development of the NE-SW-trending shear zones could be concomitant to the generation of the Pinheiro Machado Arc (Pinheiro Machado Complex), resulting from the convergence between Kalahari, Río de La Plata and Congo Cratons, which lead to the closure

of orogenic basins (e.g., Rocha-Gariep basins), reactivation of shear zones, and generation of late-orogenic magmatism at around 580 Ma (Ramos et al., 2017).

The younger reactivations that occurred at around 540 Ma can be explained by the large-scale decrease of regional compression, followed by localized strike-slip deformation along the main shear zones. This post-orogenic stage is recorded in the low-grade metasedimentary rocks of the Tijucas Terrane (Chemale et al., 2000; Zvirtes et al., 2015; Oriolo et al., 2016).

6 Conclusions

From the study presented in this paper, we draw the following conclusions:

I- The main synkinematic magmatism along to DCTSZ is represented by the Quitéria metagranite which shows a crystallization age of 618.9 ± 4 Ma, followed by the peraluminous magmatism represented by the Arroio Francisquinho and Cordilheira metagranites (Cordilheira Suite) showing crystallization ages of, respectively, 615 and 607 Ma. These ages define the main period of tectonic and magmatic activity related to DCTSZ. The reactivation ages 580-540 Ma define the late tectonic activity that occurred after the main period of tectonic and magmatic activity related to DCTSZ. The ages of inherited zircon found in the studied metagranites (1800 to 650 Ma), which are similar to those found in detrital zircon of gneisses from the Várzea do Capivarita Complex.

II- The new ages for the earliest shear-related magmatism in the DCTSZ presented in this study fit those of the earliest shear-related magmatism in the Major Gercino Shear Zone (Santa Catarina sector). Additionally, the ages of late reactivations are similar in both shear zones, suggesting a possible correlation between these tectonic structures. On the other hand, the earliest shear-related magmatism related to the Sierra Ballena Shear Zone (Uruguayan sector) – classically interpreted as the Uruguayan counterpart of the latter shear zones – is younger (ca. 580 Ma), so that the origin of the latter is possibly related to a younger tectonic event;

III- The origin of the DCTSZ is possibly related to the convergence between the Río de la Plata Craton and the Piratini Arc at around 660 Ma. Such collisional event lead to the formation of the Porto Alegre Suture, which later became de DCTSZ. Possible reactivations of the shear zone might be related to the convergence of the Kalahari and Río de la Plata cratons at around 580 Ma. Younger reactivations, at around 540 Ma, could be related to late-orogenic relaxation.

References

Almeida, F.F.M., Hasui, Y., Brito-Neves, B.B., Fuck, R.A., 1981. Brazilian structural provinces: an introduction. Earth Sci. Rev. 17, 1–29.

Babinski, M., Chemale Jr., F., Van Schmus, W.R., Hartmann, L.A., Silva, L.C., 1997. U-Pb and Sm-Nd geochronology of the Neoproterozoic Granitic-Gneissic Dom Feliciano Belt, Southern Brazil. Journal of South American Earth Sciences, 10(3/4), 263-274

Basei, M.A.S., Campos Neto, M.C., Castro, N.A., Nutman, A.P., Wemmer, M.T., Yamamoto, M.T., Hueck, M., Osako, L., Siga Jr., O., Passarelli, C.R., 2011. Tectonic evolution of the Brusque Group, Dom Feliciano belt, Santa Catarina, Journal of South American Earth Sciences, 32, 324-350.

Basei, M.A.S., Frimmel, H.E., Nutman, A.P., Preciozzi, F., Jacob, J., 2005. A connection between the Neoproterozoic Dom Feliciano (Brazil/Uruguay) and Gariep (Namibia/South Africa) orogenic belts – evidence from a reconnaissance provenance study. Precambrian Research, 139, 195-221.

Basei M.A.S., Frimmel H.E., Nutman A.P., Preciozzi F. 2008. West Gondwana amalgamation based on detrital zircon ages from Neoproterozoic Ribeira and Dom Feliciano belts of SouthAmerica and comparison with coeval sequences from SW Africa. In: Pankhurst R.J., Trouw R.A.J., Brito Neves B.B., de Wit M.J. (eds). West Gondwana, Pre-Cenozoic correlations across the South Atlantic region. Geological Society, London, Special Publication, 294:239-256.

Basei, M.A.S., Siga JR., O., Masquelin, H., Harara, O.M., Reis Neto, J.M., Preciozzi, F., 2000. The Dom Feliciano Belt of Brazil and Uruguay and its Foreland Domain the Rio de la Plata Craton: framework, tectonic evolution and correlation with similar provinces of Southwestern Africa. In: Cordani, U. G., Milani, E. J., Thomaz Filho, A., Campos, D. A. (Eds.). Rio de Janeiro, SBG, Tectonic Evolution of South American Platform, p. 311-334.

Bitencourt, M.F., Kruhl, J.H., 2000. Crustal-scale shearing, magmatism and the development of deformation structures: an example from Santa Catarina (Southern Brazil). Zeitschrift für Angewandte Geologie 229–236 (SH1/2000).

Bitencourt, M.F., Nardi, L.V.S., 2000. Tectonic setting and sources of magmatism related to the Southern Brazilian Shear Belt. Revista Brasileira de Geociências 30, 186–189

Black, L.P., Kamo, S.L., Allen, C.M., Davis, D.W., Aleinikoff, J.N., Valley, J.W., Mundil, R., Campbell, I.H., Korsch, R.J., Williams, I.S., Foudoulis, C., 2004. Improved 206Pb/238U microprobe geochronology by the monitoring of a trace-element-related matrix effect; SHRIMP, ID-TIMS, ELA-ICP-MS and oxygen isotope documentation for a series of zircon standards. Chem. Geol. 205, 115–140.

Bossi, J., Gaucher, C., 2004. The Cuchilla Dionisio Terrane, Uruguay: An allochthonous block accreted in the Cambrian to SW-Gondwana. Gondwana Research, 7(3), 661-674.

Chemale Jr. F. 2000. Evolução Geológica do Escudo Sul-Rio-Grandense. *In*: Holz M., De Ros L.F. (eds.) *Geologia do Rio Grande do Sul*. Editora UFRGS, Porto Alegre, p. 13-52.

Chemale, Jr. F., Mallmann, G., Bitencourt, M.F., Kawashita, K., 2012. Time constraints on magmatism along the Major Gercino Shear Zone, southern Brazil: implications for West Gondwana reconstruction. Gondwana Research 22 (1), 184–199.

Cherniak, D.J., Watson, E.B., 2000. Pb diffusion in zircon. Chemical Geology 172, 5-24.

Corfu, F., Hanchar, J.M., Hoskin, P.O.W., Kinny, P., 2003. Atlas of zircon textures. In: Hanchar, J.M, Hoskin, P.O.W. (Eds.). Mineralogical Society of America and Geochemical Society, Reviews in Mineralogy & Geochemistry, 53, 469-500.

Costa A.F.U. 1997. Teste e modelagem geofísica da estruturação das associações litotectônicas pré-cambrianas no Escudo Sul-rio-grandense. PhD Thesis, Instituto de Geociências, Universidade Federal do Rio Grande do Sul, Porto Alegre. 291p.

Fernandes, L.A.D., Koester, E., 1999. The Neoproterozoic Dorsal de Canguçu strike-slip shear zone: its nature and role in the tectonic evolution of southern Brazil. Journal of African Earth Sciences 29, 3-24.

Fernandes, L.A.D., Menegat, R., Costa, A.F.U., Koester, E., Porcher, C.C., Tommasi, A., Kraemer, G., Ramgrab, G.R., Camozzato, E., 1995a. Evolução tectônica do Cinturão Dom Feliciano no Escudo Sul-riograndense: Parte I – Uma contribuição a partir do registro geológico. Revista Brasileira de Geociências, 25(4), 351-374.

Fernandes, L.A.D., Menegat, R., Costa, A.F.U., Koester, E., Porcher, C.C., Tommasi, A., Kraemer, G., Ramgrab, G.R., Camozzato, E., 1995b. Evolução tectônica do Cinturão Dom Feliciano no Escudo Sul-riograndense: Parte II – Uma contribuição a partir das assinaturas geofísicas. Revista Brasileira de Geociências, 25(4), 375-384.

Fernandes, L.A.D.; Tommasi, A.; Porcher, C.C., 1992. Deformation patterns in the southern Brazilian branch of the Dom Feliciano Belt: A reappraisal. Journal of South American Earth Sciences. **5**:77-96, 1992.

Florisbal, L.M., Janasi, V.A., Bitencourt, M.F., Heaman, L.M., 2012. Space-time relation of post-collisional granitic magmatism in Santa Catarina, southern Brazil: U-Pb LA-MC-ICP-MS zircon geochronology of coeval mafic-felsic magmatism related to the Major Gercinho Shear Zone. Precambrian Research 216-219, 132-151.

Fragoso-César, A.R.S., Figueiredo, M.C.H., Soliani, Jr. E., Faccini, U.F., 1986. O Batólito Pelotas (Proterozóico Superior/Eo-Paleozóico) no Escudo do Rio Grande do Sul. In: XXXIV Congresso Brasileiro de Geologia, Goiânia, Annals, 3, 1322-1343.

Frantz, J.C., McNaughton, N.J., Marques, J.C., Hartmann, L.A., Botelho, N.F., Caravaca, G., 2003. SHRIMP U-Pb zircon ages of granitoids from southernmost Brazil: constrains on the temporal evolution of the Dorsal de Canguçu transcurrent Shear Zone and Eastern Dom Feliciano Belt. In: SBG, South American Symposium on Isotope Geology, IV, Short Papers, Salvador, vol. 1, pp. 174e177.

Frimmel, H.E., Basei, M.A.S., Correa, V.X., Mbangula, N., 2013. A new lithostratigraphic subdivision and geodynamic model for the Pan-African western Saldania Belt, South Africa. Precambrian Research 231, 218–235.

Frimmel, H.E., Basei, M.A.S., Gaucher, C., 2011. Neoproterozoic geodynamic evolution of SW-Gondwana: a southern African perspective. Int. J. Earth Sci. 100, 323–354.

Gaucher, C., Frimmel, H.E., Germs, G.J.B., 2009. Tectonic events and palaeogeographic evolution of southern Gondwana in the Neoproterozoic and Cambrian. In: Gaucher, C., Sial, A.N., Halverson, G.P., Frimmel, H.E. (Eds.), Neoproterozoic- Cambrian Tectonics, Global Change and Evolution: a Focus on Southwestern Gondwana, vol. 16. Elsevier, pp. 295–316 Developments in Precambrian Geology.

Gross, A.O.M.S, Porcher C.C., Fernandes L.A.D., Koester E., 2006. Neoproterozoic low-pressure/high-temperature collisional metamorphic evolution in the Várzea do Capivarita Metamorphic Suite, SE Brazil: thermobarometric and Sm/Nd evidence. Precambrian Research, 147(1-2), 41-64.

Gruber, L., Porcher, C.C., Koester, E., Bertotti, A.L., Lenz, C., Fernandes, L.A.D., Remus, M.V.D., 2016. Isotope geochemistry and geochronology of syn-depositional volcanism in Porongos Metamorphic Complex, Santana da Boa Vista Antiform, Dom Feliciano Belt, Brazil: onset of an 800 Ma continental arc. Journal of Sedimentary Environments, 1(2), 202-221.

Hueck, M., Oyhantçabal, P., Philipp, R.P., Basei, M.A.S., Siegesmund, S., 2018. The Dom Feliciano Belt in Southern Brazil and Uruguay. In: Siegesmund, S., Basei, M., Oyhantçabal, P., Oriolo, S. (Eds.). Geology of Southwest Gondwana. Springer, Regional Geology Reviews, p. 267-302

Lara P, Oyhantçabal P, Dadda K.,2017. Post-collisional, Late Neoproterozoic, high-Ba-Sr granitic magmatism from the Dom Feliciano Belt and its cratonic foreland, Uruguay: petrography, geochemistry, geochronology, and tectonic implications. Lithos 277:178–198.

Ludwig, K.R., 2008. Isoplot 3.70, a geochronological toolkit for Microsoft Excel. Berkeley, Geochronology Center, Special Publication 4, 76p.

Mantovani, M.S.M.; Shukowsky, W.; Basei, M.A.S.; Vasconcellos, A.C.B.C., 1989. Modelo gravimétrico das prin- cipais descontinuidades crustais nos terrenos pré-cambrianos dos Estados do Paraná e de Santa Catarina. Revista Brasileira de Geociências, 19(3):367-374.

Martil, M.M., Bitencourt, M.F., Nardi, L.V.S., Koester, E., Pimentel, M.M., 2017. Pre-collisional, Tonian (ca. 790 Ma) continental arc magmatism in southern Mantiqueira Province, Brazil: geochemical and isotopic constraints from the Várzea do Capivarita Complex. Lithos, 274-275, 39-52.

Masquelin, H., Fernandes, L.A.D., Lenz, C., Porcher, C.C., McNaughton, N.J., 2012. The Cerro Olivo complex: a pre-collisional neoproterozoic magmatic arc in eastern Uruguay. Int. Geol. Rev. 54 (10), 1161–1183.

Mesquita, M. J. M. 1991. Petrografia dos granitóides deformados na Zona de Cisalhamento Dorsal de Canguçu (Piratini - Quitéria), RS. Porto Alegre, Master Degree Dissertation, 242p. Instituto de Geociências, Universidade Federal do Rio Grande do Sul.

Nardi, L.V.S. and Frantz, J.C. 1995. The Cordilheira Intrusive Suite: late-precambrian peraluminous granitoids from south Brazil. Journal of South American Earth Sciences, 8:45-64.

Kirkland, C. L., Whitehouse, M. J., and Slagstad, T., 2009. Fluid-assisted zircon and monazite growth within a shear zone: a case study from Finnmark, Arctic Norway. Contributions to Mineralogy and Petrology, 158(5), 637–657.

Knijnik, D. B., 2018. Geologia estrutural e geocronologia dos granitoides pós-colisionais sintranscorrência da região de Quitéria-Serra do Erval, RS. Phd thesis, Universidade Federal do Rio Grande do Sul, 260p.

Koester, E.,1995. Petrologia e geocronologia dos granitóides sintectônicos à Zona de Cisalhamento Dorsal de Canguçu. Porto Alegre, 240 p. Master Degree Dissertation - Instituto de Geociências, Universidade Federal do Rio Grande do Sul.

Koester, E., Chemale Jr., F., Porcher, C. C., Bertotti, A. L., and Fernandes, L. A. D., 2008, U-Pb ages of granitoids from eastern sul-riograndense shield. In 6th South American Symposium on Isotope Geology. Anais, p.95.

Koester, E., Fernandes, L.A.D., Soliani Jr., E., Kraemer, G., Nardi, L.V.S., Roisemberg, A., 2001a. Geologia e geoquímica dos granitóides sintectônicos à Zona de Cisalhamento Transcorrente Dorsal de Canguçu, Encruzilhada do Sul, RS. Revista Brasileira de Geociências, 31(2): 141-154.

Koester, E., Pawley, A.R., Fernandes, L.A.D., Porcher, C.C. and Soliani Jr., E., 2002. Experimental melting of cordierite gneiss and the petrogenesys of syntranscurrent peraluminous granites in the southern Brazil. *Journal of Petrology*, 48(43): 1595-1616.

Koester, E., Roisenberg, A., Fernandes, L.A.D., Soliani Jr., E., Nardi, L.V.S. and Kraemer, G. 2001b. Petrologia dos granitóides sintectônicos à Zona de Cisalhamento Transcorrente Dorsal de Canguçu, Encruzilhada do Sul, RS. Revista Brasileira de Geociências, 31(2): 131-140.

Koester, E., Porcher, C.C., Pimentel, M.M., Fernandes, L.A.D., Vignol-Lelarge, M.L., Oliveira, L.D., Ramos, R.C., 2016. Further evidence of 777 Ma subduction-related continental arc magmatism in Eastern Dom Feliciano Belt, southern Brazil: the Chácara das Pedras Orthogneiss. J. South Am. Earth Sci. 68, 155–166.

Koester, E.; Soliani Jr., E.; Fernandes, L.A.D.; Kraemer, G.; Tommasi, A., 1997. Geocronologia Rb/Sr e K/Ar dos granitóides sintectônicos à Zona de Cisalhamento Transcorrente Dorsal de Canguçu na região de Encruzilhada do Sul (RS). Pesquisas, v. 24, n. 1-2, p. 67-77

Koester E., Soliani Jr. E., Leite J.A.D., Hartmann L.A., Fernandes L.A.D., Santos J.O.S., Oliveira L.D. 2001c. SHRIMP U-Pb age for the emplacement of Santana granite and reactivation of the Porto Alegre Suture, southern Brazil. Journal of South American Earth Sciences, 14:91-99.

Oliveira D.S., Sommer C.A., Philipp R.P., Lima E.F., Basei M.A.S. 2015. Post-collisional subvolcanic rhyolites associated to the Neoproterozoic Batholith Pelotas, Southern Brazil. Journal of South American Earth Sciences, 63:84-100.

Oriolo, S., Hueck, M., Oyhantçabal, P., Goscombe, B., Wemmer, K., Siegesmund, S., 2018. Shear zones in Brasiliano-Pan-African belts and their role in the amalgamation and break-up of Southwest Gondwana. In: Siegesmund, S., Basei, M.A.S., Oyhantçabal, P., Oriolo, S. (Eds.). Geology of Southwest Gondwana. Springer, Regional Geology Reviews, 593-613.

Oriolo, S., Oyhantçabal, P., Wemmer, K., Heidelbach, F., Pfänder, J., Basei, M.A.S., Hueck, M., Hannich, F., Sperner, B., Siegesmund, S., 2016. Shear zone evolution and timing of deformation in the Neoproterozoic transpressional Dom Feliciano Belt, Uruguay. Journal of Structural Geology 92, 59- 78

Oyhantçabal P., Siegesmund S., Wemmer K. 2011. The Rio de la Plata Craton, a review of units, boundaries, ages and isotopic signature. International Journal of Earth Sciences, 100:201-220.

Oyhantçabal, P.; Slegesmund, S.; Wemmer, K.; Frei, R.; Layer, P., 2007. Postcollisional transition from calc-alkaline to alkaline magmatism during transcurrent deformation in the southernmost Dom Feliciano Belt (Braziliano–Pan-African, Uruguay). Lithos, 98(1), p.141-159.

Oyhantçabal, P.; Siegesmund, S.; Wemmer, K.; Layer, P., 2010. The sierra ballena shear zone in the southernmost dom feliciano belt (Uruguay): evolution, kinematics, and deformation conditions. International Journal of Earth Sciences, 99(6), p.1227-1246.

Oyhantçabal, P.; Siegesmund, S.; Wemmer, K.; Presnyakov, S.; Layer, P., 2009. Geochronological constraints on the evolution of the southern Dom Feliciano Belt (Uruguay). Journal of the Geological Society, 166(6), p.1075-1084.

Passarelli, C. R., Basei, M.A.S., Siga Jr., O., Mc Reath, I., Campos Neto, M.C., 2010. Deformation and geochronology of syntectonic granitoids emplaced in the Major Gercino Shear Zone, southeastern South America. Gondwana Research 17, 688-703.

Passarelli, C. R., Basei, M. A. S., Wemmer, K., Siga, O., and Oyhantçabal, P., 2011. Major shear zones of southern Brazil and Uruguay: escape tectonics in the eastern border of Rio de La Plata and Paranapanema cratons during the Western Gondwana amalgamation. International Journal of Earth Sciences, v.100(2-3), p.391-414.

Philipp R.P., 1998. A evolução geológica e tectônica do BatólitoPelotas no Rio Grande do Sul. Instituto de Geociências,Universidade de São Paulo, São Paulo, Tese de Doutorado, 255p.

Philipp R.P., Machado R., 2005. The Neoproterozoic to Cambrian granitic magmatism of Pelotas Batholith, Southern Brazil. Journal of South American Earth Sciences, 19:461-478.

Philipp R.P., Machado R., Chemale Jr. F. 2003. Reavaliação e novos dados geocronológicos sobre o Batólito Pelotas: implicações petrogenéticas e idade das zonas de cisalhamento. Boletim do Instituto de Geociências da USP, São Paulo, 3:71-84.

Philipp R.P., Massone H.J., Campos R.S., 2013. Peraluminous leucogranites of Cordilheira Suite, record of Neoproterozoic collision and generation of Pelotas Batholith, Dom Feliciano Belt, southern Brazil. Journal of South American Earth Sciences, 43, 8-24.

Philipp, R.P., Pimentel, M.M., Chemale Jr., F., 2016a. Tectonic evolution of the Dom Feliciano Belt in Southern Brazil: geological relationships and U-Pb geochronology. Brazilian Journal of Geology, 46(1), 83-104.

Philipp R.P., Bom F.M., Pimentel M.M., Junges S.L., Zvirtes G. 2016b. SHRIMP U-Pb age and high temperature conditions of the collisional metamorphism in the Várzea do Capivarita Complex: implications for the origin of Pelotas Batholith, Dom Feliciano Belt, southern Brazil. Journal of South American Earth Sciences, 66:196-207.

Ramos, R.C., Koester, E., Porcher, C.C., 2017. Chemistry of chromites from Arroio grande ophiolite (Dom Feliciano belt, Brazil) and their possible connection with the Nama group (Namibia). J. South Am. Earth Sci. 80, 192–206.

Rapela C.W. ,Fanning C.M., Casquet C., Pankhurst R.J., Spalletti L., Poiré D., Baldo E.G., 2011. The Rio de la Plata craton and the adjoining Pan-African/brasiliano terranes: Their origins and incorporation into south-west Gondwana. Gondwana Research, 20:673-690.

Saalmann, K., Gerdes, A., Lahaye, Y., Hartmann, L.A., Remus, M.V.D., Läufer, A., 2011. Multiple accretion at the eastern margin of the Rio de la Plata craton: the prolonged Brasiliano orogeny in southernmost Brazil. International Journal of Earth Sciences, 100, 355-378.

Sánchez Bettucci, L., Oyhantçabal, P., Page, S., Ramos V.A., 2003a. Petrography and Geochemistry of the Carapé Complex, Southeastern Uruguay: Gondwana Research, v. 6, p. 89–105.

Sato, K., Tassinari, C.C.G., Basei, M.A.S., Siga Jr., O., Onoe, A.T., de Souza, M.D., 2014. Microssonda Iônica de Alta Resolução e de Alta Sensibilidade (SHRIMP IIe/MC) do Instituto de Geociências da Universidade de São Paulo, Brasil: método analítico e primeiros resultados. Revista do Instituto de Geociências – USP 14 (3), 3–18.

Tessari, R. I. e Picada, R. S., 1966. Geologia da quadrícula de Encruzilhada do Sul, RS. Bol. Div. Fom. Prod. Min. (DNPM), 124, 147 p., Rio de Janeiro.

Tommasi, A.; Fernandes, L.A.D.; Porcher, C.C.; Vauchez, A. 1992. Evolução cinemática das porções internas do Cinturão Dom Feliciano na região de Piratini, RS. Pesquisas, 19(2): 145-156.

Tommasi, A., Vauchez, A., Fernandes, L. A. D. and Porcher, C C., 1994. Magma-assisted strain localisation in an orogen-parallel transcurrent shear zone of southern Brazil. Tectonics 13, 421–437

UFRGS., 1988. Mapeamento Geológico de parte das folhas de Quitéria e Várzea do Capivarita. Graduation Monography, Curso de Geologia, Instituto de Geociências da Universidade Federal do Rio Grande do Sul, Porto Alegre.

UFRGS., 1992. Mapeamento Geológico deporte das folhas de Encruzilhada do Sul e Delfino. Graduation Monography, Curso de Geologia, Instituto de Geociências da Universidade Federal do Rio Grande do Sul, Porto Alegre.

UFRGS., 1993. Mapeamento Geológico de parte das folhas de Cerro da Árvore, Encruzilhada do Sul, Figueiras e Vau dos Prestes. Graduation Monography, Curso de Geologia, Instituto de Geociências da Universidade Federal do Rio Grande do Sul, Porto Alegre.

Vieira, D.T., Koester, E., Ramos, R.C., Porcher, C.C., 2019. Sr-Nd-Hf isotopic constraints and U-Pb geochronology of the Arroio Pedrado Gneisses, Dom Feliciano Belt, Brazil: a 680 Ma shoshonitic event in the final stages of the Piratini Arc evolution. Journal of South American Earth Sciences 95, 102294.

Vieira, D.T., Porcher, C.C., Koester, E., Ramos, R.C., Masquelin, H., Gross, A.O.M.S., Fernandes, L.A.D., 2019b. Metamorphic evolution of the Chafalote Suite, basement of the Punta del Este Terrane (Uruguay). Journal of South American Earth Sciences, submitted.

Wildner, W., Ramgrab, G.E., Lopes, R.C., Iglesias, C.M.F., 2006. Mapa geológico do Estado do Rio Grande do Sul, Escala 1:750.000. CPRM, Porto Alegre.

Zvirtes, G., Philipp, R.P., Chemale, F., Camozzato, E., 2015. Evidências de rifteamento e metamorfismo orogênico nos estágios finais de evolução do Cinturão Dom Feliciano na Antiforme Capané, Cachoeira do Sul, RS, in: 9th South-Brazilian Geological Symposium. Brazilian Geological Society, pp. 141. Porto Alegre.

CAPÍTULO 6

Artigo *"Petrografia e química mineral do Granito São Geraldo: evidências de magmatismo peraluminoso na região de Porto Alegre, RS"*

Petrografia e química mineral do Granito São Geraldo: evidências de magmatismo peraluminoso na região de Porto Alegre, RS

Daniel Triboli VIEIRA[1], Rodrigo Chaves RAMOS[1], Edinei KOESTER[2], Maria Lidia VIGNOL-LELARGE[3], Carla Cristine PORCHER[2], Clovis GONZATI[3], Márcia Elisa BOSCATO GOMES[3], Laércio DAL OLMO-BARBOSA[1], Ana Karina SCOMAZZON[4] & Taís FONTES PINTO[1]

[1] Programa de Pós-Graduação em Geociências, Instituto de Geociências, Universidade Federal do Rio Grande do Sul. Caixa Postal 15.001, CEP 91501-970, Porto Alegre, RS, Brasil (danieltriboli@hotmail.com, rodrigo.chaves@ufrgs.br, dal.barbosa@ufrgs.br, tais.fontes1@gmail.com).

[2] Departamento de Geologia, Instituto de Geociências, Universidade Federal do Rio Grande do Sul. (koester@ufrgs.br, carla.porcher@ufrgs.br).

[3] Departamento de Mineralogia e Petrologia, Instituto de Geociências, Universidade Federal do Rio Grande do Sul. (lidia.vignol@ufrgs.br, gonzatti@ufrgs.br, marcia.boscato@ufrgs.br).

[4] Departamento de Paleontologia e Estratigrafia de Geociências, Universidade Federal do Rio Grande do Sul (akscomazzon@ufrgs.br).

Resumo. Este trabalho descreve a primeira ocorrência de um granito peraluminoso na região de Porto Alegre, denominado Granito São Geraldo. Neste estudo foram realizadas análises petrográficas (microscopia óptica e eletrônica) e de química mineral (microssonda eletrônica) em lâminas delgadas oriundas de testemunhos de sondagem. O granito apresenta textura equigranular hipidiomórfica fina a média e composição que varia de sieno a monzogranítica. Sua mineralogia é constituída por K-feldspato (37-48 %), quartzo (17-33 %), plagioclásio (23-28 %), muscovita + biotita (em média 14%) e, subordinadamente (< 1 %), granada, zircão, monazita, apatita, ilmenita e magnetita. A biotita, de origem primária, apresenta teores de elementos maiores (e.g. Al, Fe e Mg) compatível com as de granitos peraluminosos. A muscovita em geral é magmática, com composição similar a dos granitos fortemente peraluminosos (e.g. teores de Al, Fe, Mg e Ti). Os teores de Or do K-feldspato (ortoclásio) variam entre 86-97 %. O plagioclásio é predominante o oligoclásico, subordinadamente apresentando composição albítica. Teores elevados de espessartina da granada (26-32 %) sugerem uma origem magmática. A apatita (fluorapatita) apresenta teores de F entre 3,0-4,5 %. O caráter peraluminoso deste granito o difere de todos os granitos descritos na região de Porto Alegre. Sua composição é similar a dos granitos com duas micas que compõem a Suíte Cordilheira (Batólito Pelotas), a qual engloba a maioria dos granitos peraluminosos tipo-S, sintranscorrentes a zonas de cisalhamento transcorrentes dúcteis encontradas no domínio oriental do Cinturão Dom Feliciano.

Palavras-chave. Petrografia, Granito São Geraldo, Granito Peraluminoso, Suíte Cordilheira.

Abstract. PETROGRAPHY AND MINERAL CHEMISTRY OF THE SÃO GERALDO GRANITE: EVIDENCE OF PERALUMINOUS MAGMATISM IN THE PORTO ALEGRE REGION. The present work describes the first occurrence of a peraluminous leucogranite in the Porto Alegre city region, named São Geraldo Granite. Thin sections from drill cores were studied through petrography (optical and electron microscopy) and mineral chemistry (electron probe microanalysis). The granite shows a medium to fine grained, equigranular hypidiomorphic texture, and a composition ranging from sieno- to monzogranitic. Its mineralogy comprises K-feldspar (37-48 %), quartz (17-33 %), plagioclase (23-28 %), muscovite + biotite (7 to 11%), and subordinate amounts (< 1%) of garnet, zircon, monazite, apatite, ilmenite, and magnetite. The biotite, interpreted as magmatic in origin, shows major element concentrations (e.g. Al, Fe, and Mg) compatible with those generated in peraluminous granites. The muscovite is predominantly magmatic, with a composition compatible with those of the strongly peraluminous granites. The Or contents of the K-feldspar (orthoclase) range from 86 to 97 %. The plagioclase is mostly oligoclase, showing secondary albitic composition. The spessartine contents of the garnet (26-32 %) suggest a magmatic origin. The apatite (fluorapatite) shows F concentration between 3.0-4.5 %. The peraluminous character of the studied granite differs from all granites described in the Porto Alegre region. Its composition is similar to those of the Cordilheira Suite (Pelotas Batholith), which encompasses most of the peraluminous S-type granites syncinematic emplaced in ductile shear zones found in the eastern domain of the Dom Feliciano Belt.

Keywords. Petrography; São Geraldo Granite; Peraluminous Granite; Cordilheira Suite

1 Introdução

Granitos com biotita e muscovita são geralmente associados ao magmatismo granítico peraluminoso. Este tipo de magmatismo pode ser formado por fusão crustal em porções profundas de cinturões colisionais (White & Chappell, 1974; Patiño-Douce & Johnston, 1991; Barbarin, 1996; Patiño-Douce & McCarty, 1998; Gill, 2010; Pérez-Soba & Villaseca, 2010), podendo estar relacionado com a descompressão adiabática associada com o período pós-colisional (Liégeois *et al.,* 1998; Barbarin, 1999; Reichardt *et al.*, 2010; Sawyer *et al.,* 2011; Brown, 2013), ou ainda, ao fracionamento de magmas básicos ou intermediários (Wilson, 1989; Sawyer *et al.,* 2011; Brown, 2013).

Na região de Porto Alegre (RS) ocorrem diversas exposições de granitoides com idades entre 630-600 Ma (relacionados aos estágios finais do ciclo orogênico Brasiliano/Pan-africano), além de gnaisses que representam crosta continental mais antiga, com idades de cristalização em torno de 800 Ma (Koester *et al.,* 2001a, 2016). Estas unidades situam-se na porção nordeste do Batólito Pelotas (Fragoso-César *et al*., 1986), que integra em partes o domínio oriental do Cinturão Dom Feliciano no Escudo Sul-rio-grandense. Os granitos da região apresentam formas alongadas segundo a direção NE-SW e concordantes com as principais estruturas regionais, sugerindo posicionamento controlado pela tectônica brasiliana (Fernandes *et al.,* 1992; Bitencourt & Nardi, 2000; Oliveira *et al*., 2001; Philipp *et al*., 2002; Philipp & Machado, 2005; Koester *et al.,* 2016).

Recentemente foram encontrados em testemunhos de sondagem granitos com duas micas, ocorrência inédita nesta região. Estes testemunhos foram obtidos junto às obras de planejamento da linha 2 do metrô da cidade de Porto Alegre, que se estenderá desde o bairro Centro Histórico em direção ao leste, para os bairros Floresta, São Geraldo, Navegantes, Humaitá e Anchieta. O presente estudo tem como objetivo a caracterização petrográfica dessa nova ocorrência de granito com duas micas, definido neste trabalho como Granito São Geraldo, e possíveis correlações com outros granitoides peraluminosos que ocorrem no Batólito Pelotas. Para este fim foram empregadas técnicas de petrografia com ênfase na caracterização mineral, textural e microestrutural utilizando-se microscopia óptica e microscopia eletrônica de varredura (MEV), bem como análises de química mineral *(WDS)* em microssonda eletrônica.

2 Área de estudo, materiais e métodos

2.1 Localização da área

A área de estudo está inserida no contexto geológico do Cinturão Dom Feliciano, cinturão orogênico neoproterozoico relacionado ao ciclo Brasiliano/Pan-Africano. Esse cinturão se estende de Punta del Este (Uruguai) até o leste do estado de Santa Catarina no Brasil (e.g. Heilbron *et al*., 2004). No Rio Grande do Sul, o Cinturão Dom Feliciano é dividido em três domínios principais, baseado em critérios geológicos e geofísicos (Fernandes *et al*.,1995a, 1995b; Costa, 1997): domínios Ocidental, Central e Oriental. O Domínio Oriental, onde está situado o granito alvo deste estudo, é limitado a oeste pela Zona de Cisalhamento Dorsal do Canguçu e Sutura de Porto Alegre, que o separam do Domínio Central; a leste, pela Planície Costeira (sedimentos quaternários); e a norte, por rochas sedimentares paleozoicas e mesozoicas da Bacia do Paraná. Para sul esse domínio se estende até Punta del Este, no Uruguai (Fig. 1).

No Rio Grande do Sul o Domínio Oriental do Cinturão Dom Feliciano equivale parcialmente ao Batólito Pelotas (Fragoso-César *et al.,* 1986), onde predominam granitoides cálcio-alcalinos alto-K de idades neoproterozoicas, vinculados à zona de subducção (e.g. Philipp, 1990; Philipp *et al.,* 2016). Subordinadamente são encontrados xenólitos métricos a quilométricos de rochas metamórficas diversas, que representam crosta continental e oceânica antiga (e.g. Fragoso-César *et al*., 1986; Philipp *et al*., 2002; Gregory *et al.,* 2015; Koester *et al*., 2016; Martil *et al.,* 2017). No Batólito Pelotas foram caracterizadas seis suítes graníticas denominadas de Pinheiro Machado, Erval, Viamão, Encruzilhada do Sul, Cordilheira e Dom Feliciano, e uma sienítica, a Suíte Piquiri (e.g. Fragoso-César *et al*., 1986; Figueiredo *et al*.,
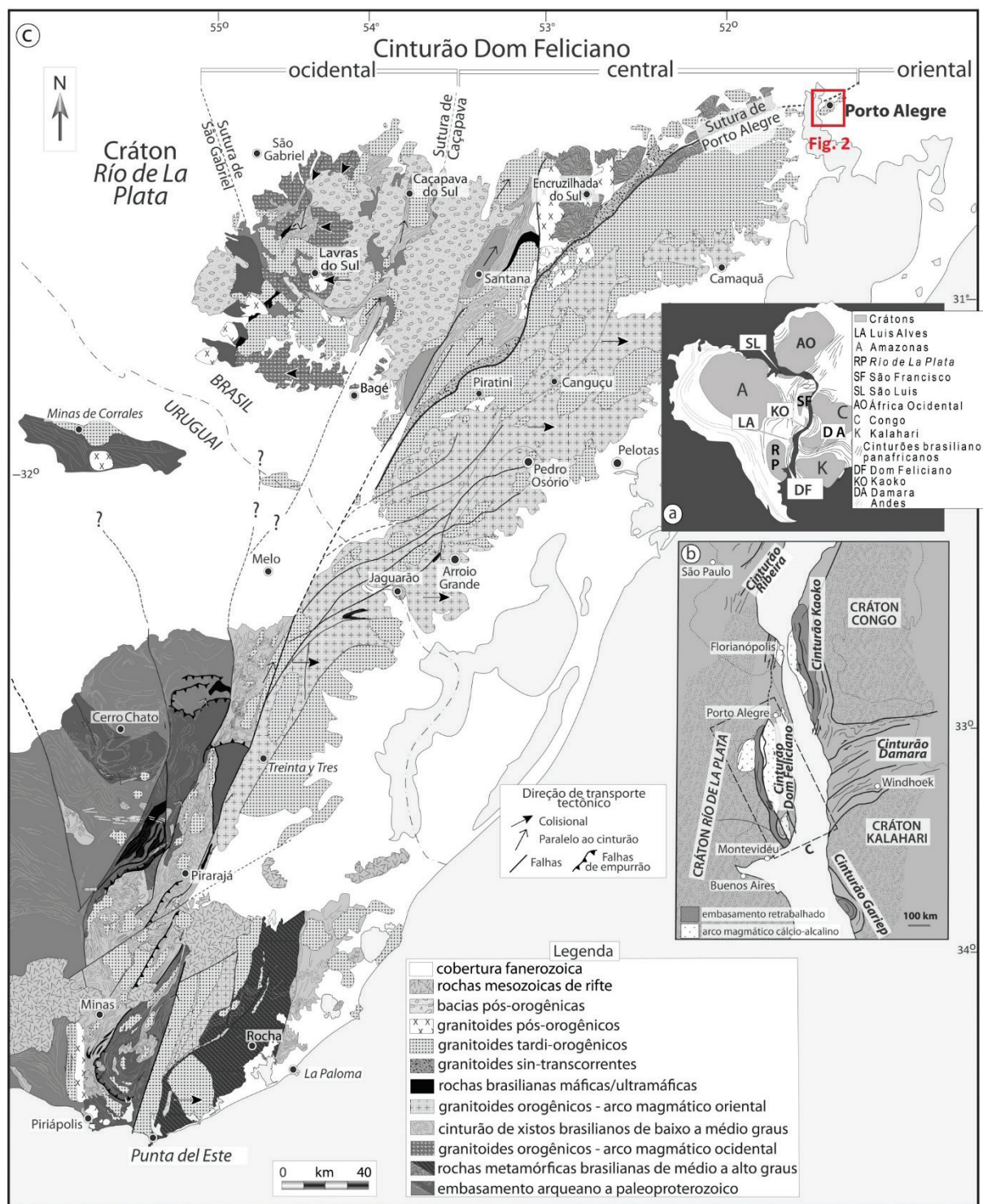
Figura 1. Esboço geológico do Cinturão Dom Feliciano no Escudo Uruguaio-sul-rio-grandense (modificado de Masquelin *et al*., 2012). A) Configuração do supercontinente Gondwana com as principais áreas cratônicas; B) Localização do Cinturão Dom Feliciano e cinturões africanos adjacentes na configuração do supercontinente Gondwana; C) Mapa geológico do Cinturão Dom Feliciano e Cráton Rio de la Plata no sul do Brasil e Uruguai.
Figure 1. Geological context of the Dom Feliciano Belt in the Uruguayan-sul-rio-grandense Shield (modified from Masquelin et al., 2012). A) Gondwana supercontinent configuration with main cratonic areas; B) Location of the Dom Feliciano Belt and adjacent African Belts on Gondwana supercontinent configuration; C) Geologic map of the Dom Feliciano Belt and Rio de la Plata Craton in South Brazil and Uruguay.

1990; Philipp, 1998; Philipp & Machado, 2001; Philipp *et al.,* 2002).

A Suíte Pinheiro Machado é constituída por granitoides com assinatura química cálcio-alcalina, médio a alto-K, metaluminosa a fracamente peraluminosa. Os granitoides da Suíte Viamão possuem assinatura geoquímica cálcio-alcalina alto-K e variam de metaluminosos a fracamente peraluminosos, enquanto a Suíte Cordilheira apresenta granitos de caráter exclusivamente peraluminoso (Philipp, 1998; Philipp *et al.,* 2002, 2013). Os sienitos da Suíte Piquiri têm afinidade shoshonítica, enquanto os granitos da Suíte Encruzilhada do Sul são alcalinos e metaluminosos (Nardi *et al.,* 2007, 2008; Plá Cid *et al.,* 2003, 2005). Na sua maioria, os corpos graníticos da Suíte Dom Feliciano são cálcio-alcalinos alto-K, com elevado grau de diferenciação (75-78 % SiO_2) (Philipp, 1998; Philipp & Machado, 2001; Philipp *et al.,* 2002).

Na região de Porto Alegre (Fig. 2), as rochas mais antigas são denominadas como Gnaisses Ponta Grossa, de origem paraderivada, ocorrendo na forma de xenólitos nos Gnaisses Chácara das Pedras (Oliveira *et al.*, 2001). Os Gnaisses Chácara das Pedras, de origem ortoderivada e idade de cristalização de 777,3 ± 3,6 Ma (U-Pb SHRIMP em zircão: Koester *et al.*, 2016), ocorrem como xenólitos no Granodiorito Três Figueiras. Essas três unidades constituem o embasamento dessa região.

Este embasamento é intrudido pelo Granodiorito Lomba do Sabão, sintranscorrente à Zona de Cisalhamento de Porto Alegre, e pelo Granito Santana, o qual aproveita a descontinuidade física da Sutura de Porto Alegre (Fig. 2). Posteriormente essas rochas foram intrudidas pelos granitos pós-tectônicos à transcorrência (Menegat *et al.*, 1998; Oliveira *et al.*, 2001; Koester *et al.*, 2001a). Os granitos pós-tectônicos foram agrupados por Oliveira *et al.* (2001) em três suítes graníticas: Viamão (constituída pelos granitos Saint Hilaire e Pitinga), Porto Alegre (constituída pelos granitos Independência, São Caetano, Feijó, Lami, São Pedro e Restinga) e Itapuã (constituída pelos granitos Santana, Cantagalo, Santo Antônio e Passo das Pedras).

Philipp (1998) e Oliveira *et al.* (2001) caracterizaram a geoquímica dessas suítes. A Suíte Intrusiva Viamão apresenta assinatura cálcio-alcalina alto-K, enquanto a Suíte Intrusiva Porto Alegre apresenta assinaturas cálcio-alcalinas mais evoluídas em relação a Suíte Viamão. A Suíte Intrusiva Itapuã é compatível com os granitos metaluminosos da associação alcalina descrita por Nardi & Bonin (1991).

2.2 Materiais e métodos

Para este trabalho, foram utilizadas amostras coletadas de 9 testemunhos de sondagem, distribuídos conforme a figura 2. Foram selecionadas 13 amostras do Granito São Geraldo que ocorrem em profundidades de 4,5 a 21,5 m para confecção de lâminas delgadas junto ao Núcleo de Preparação de Amostras do Centro de Estudos em Petrologia e Geoquímica (CPGq), Instituto de Geociências da Universidade Federal do Rio Grande do Sul. As descrições das lâminas foram realizadas com auxílio de microscópio óptico Meiji Techno ML9720.

Duas lâminas delgadas (SM9 e SM43) foram selecionadas para análises de química mineral em microssonda eletrônica. As lâminas foram devidamente polidas e metalizadas com carbono por evaporação. As análises foram realizadas com auxílio de um *Cameca SXFive* equipado com cinco espectrômetros WDS (*Wavelength Dispersive Spectrometry*), no Laboratório de Microssonda Eletrônica, CPGq, Instituto de Geociências da mesma Universidade. Para a análise de elementos maiores nos silicatos e óxidos, as condições analíticas consistiram em voltagem de aceleração de 15 kV, corrente de 10 nA, e diâmetro do feixe eletrônico da ordem de 5 μm.

Para as análises quantitativas de microssonda eletrônica foram usados os seguintes padrões: albita para Na (8,6% Na; 10,34% Al; 32,03% Si; 48,76% O; 0,18% K; 0,09% Ca), wollastonita para Si e Ca (33,9337% Ca; 23,8201% Si; 41,17% O; 0,0074% Na; 0,006% Mg; 0,006% Ti; 0,4879% Mn; 0,171% Fe), diopsídio para Mg (11,23% Mg; 18,39% Ca; 25,88% Si; 44,3% O; 0,05% Al; 0,05% Ti; 0,04% Mn; 0,04% Fe), sanidina para Al e K (46,28% O; 9,93% Al; 30,23% Si; 10,05% K; 0,14% Fe; 0,98% Ba; 2,23% Na), óxido de cromo
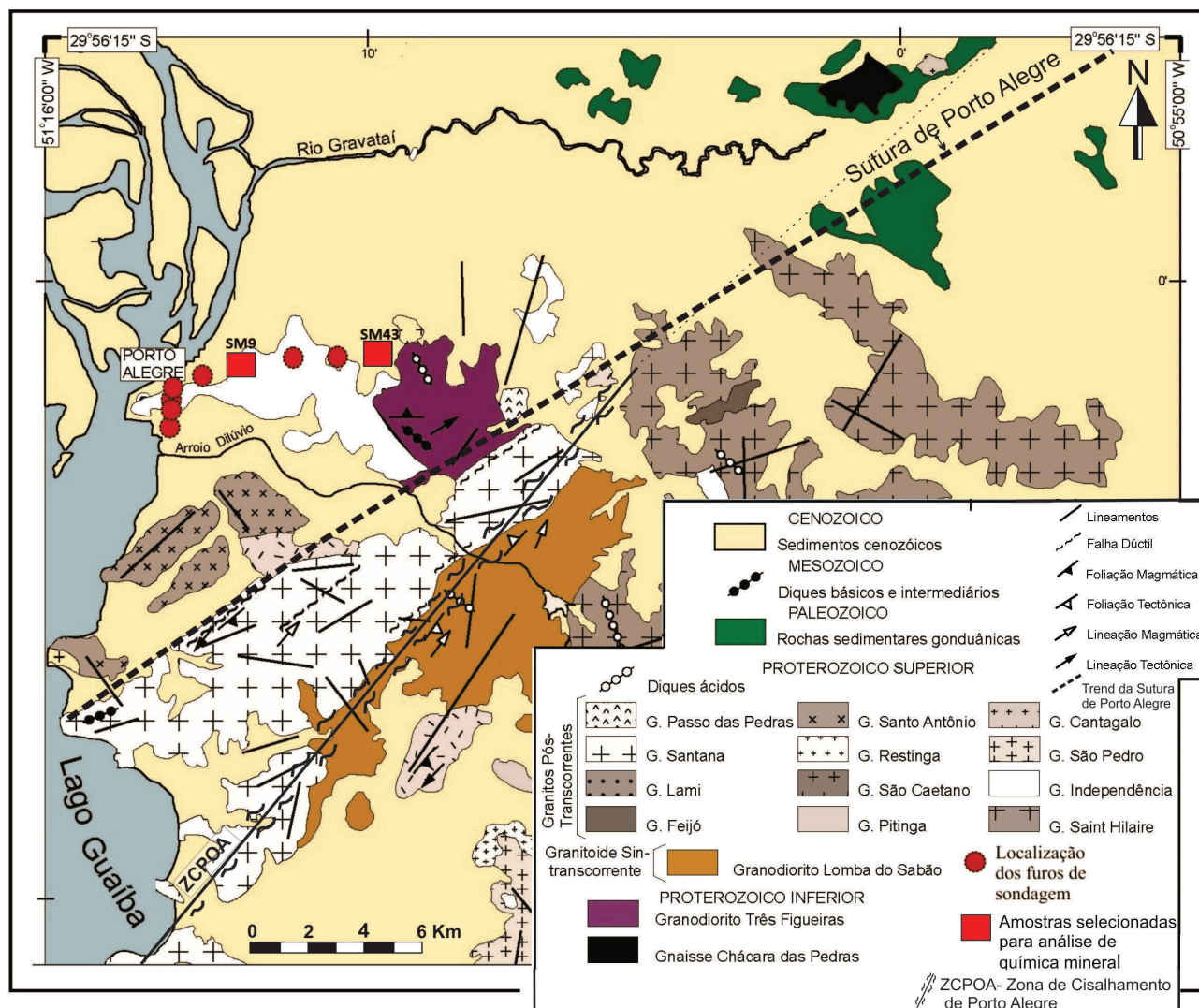
Figura 2. Mapa geológico da região de Porto Alegre com a localização dos furos de sondagem amostrados (modificado de Oliveira *et al.*, 2001).
Figure 2. Geologic map of the Porto Alegre region with the location of the sampled drill holes (modified from Oliveira et al., 2001).

para Cr (68,4195% Cr; 31,5805% O), rodonita para Mn (32,8499% Mn; 22,1126% Si; 37,7621% O; 1,1216% Mg; 5,0993% Ca; 0,7905% Fe), hematita para Fe (69,9426% Fe; 30,0574% O) e rutilo para Ti (59,95% Ti; 40,05% O).

3 Resultados

3.1 Características geológicas e petrográficas do Granito São Geraldo

Neste trabalho, o granito estudado é formalmente denominado de Granito São Geraldo. Essa denominação faz referência a um dos bairros onde foram realizados os furos de sondagem para as obras do metrô anteriormente

mencionadas. A partir da descrição dos testemunhos verificou-se a ocorrência de um granito com duas micas com cores que variam de laranja (quando alterado) a cinza, até então nunca descrito para a região de Porto Alegre. A correlação dos furos de sondagem mostra que o Granito São Geraldo possui uma extensão mínima de 10 km.

O granito possui textura predominante equigranular hipidiomórfica média a fina (Fig. 3), e apresenta por vezes uma trama tectônica protomilonítica. Sua mineralogia essencial é composta por K-feldspato, plagioclásio, quartzo, muscovita e/ou biotita. Minerais acessórios como granada, monazita, apatita e zircão são comuns.
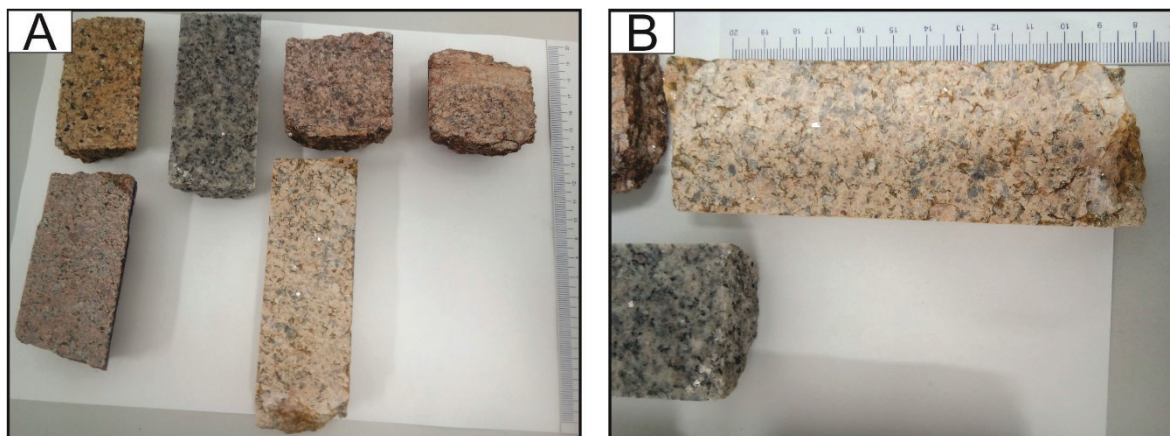
Figura 3. Testemunhos de sondagens do Granito São Geraldo. A) Variação de cores dos testemunhos estudados; B) Detalhe do granito, mostrando a textura equigranular média.
Figure 3. Drill cores from the São Geraldo Granite. A) Color variations of the studied drill cores; B) Detail of the granite, showing the equigranular medium-grained texture.

Outra característica apresentada pelo Granito São Geraldo é a presença de xenólitos de gnaisses (Fig. 4). Esses xenólitos são descritos por Gomes (2016) e correlacionados com os Gnaisses Chácara das Pedras (Philipp & Campos, 2004; Koester *et al.*, 2016).

Ao microscópio foi possível estimar as proporções modais de quartzo, K-feldspato e plagioclásio utilizando o método de contagem de pontos (aproximadamente 450 pontos por lâmina). As proporções modais foram recalculadas para 100% e projetadas no diagrama QAPF (Fig. 5) de Streckeisen (1976). O Granito São Geraldo apresenta composições que variam de monzo a sienograníticas, similares a associação leucocrática peraluminosa proposta por Nardi (2016), modificada de Lameyre & Bowden (1982).

A mineralogia principal é composta por K-feldspato (37-48 %), quartzo (17-33 %), plagioclásio (23-28 %), muscovita (5-9 %) e biotita (4-10 %). Os minerais acessórios (1 %) são granada, zircão, monazita, apatita e opacos (ilmenita e magnetita).

O K-feldspato ocorre comumente na forma de cristais prismáticos subédricos alongados de tamanhos que variam de 0,5 a 3 mm de comprimento. Localmente são observadas texturas poiquilíticas em cristais maiores, caracterizadas por diversas inclusões euédricas a anédricas de biotita, plagioclásio, muscovita e quartzo (Fig. 6A). Em geral, esses cristais apresentam um padrão principal de geminação segundo a lei de Carlsbad e um padrão secundário

de geminação do tipo xadrez que se desenvolve principalmente nas bordas dos grãos, sugerindo inversão incompleta ortoclásio-microclinio.

Agregados mirmequíticos ocorrem localmente no contato com plagioclásio, sendo em geral bem desenvolvidos, predominando os tipos marginais descritos por Phillips (1980), nas suas variedades bulbosa e planar. A ocorrência de lobos de mirmequitos independentes na matriz possivelmente se deve à deformação progressiva dos cristais de feldspato que ocasiona recristalização nos limites dos grãos, propiciando a individualização dos lobos mirmequíticos. Extinção ondulante e formação de subgrãos com rotação progressiva para grãos recristalizados são pouco comuns, estando ambas as características restritas aos termos protomiloníticos.

O plagioclásio é caracterizado por cristais tabulares subédricos, em geral com dimensões que variam de 0,3 a 3,5 mm de comprimento. Ocorrem com frequência zonação normal e maclas polissintéticas (Fig. 6B). A textura poiquilítica também é observada nos cristais de plagioclásio, sendo caracterizada em geral por inclusões de muscovita. Nos termos protomiloníticos é comum a presença de cristais com extinção ondulante e a formação de maclas em cunhas e curvadas (*kink bands*) (Fig. 6C).

O quartzo possui extinção ondulante e tende a formar agregados de cristais com formas irregulares e alongadas, de tamanho entre 0,3 e 2,2 mm. A recristalização por *bulging* é comum,
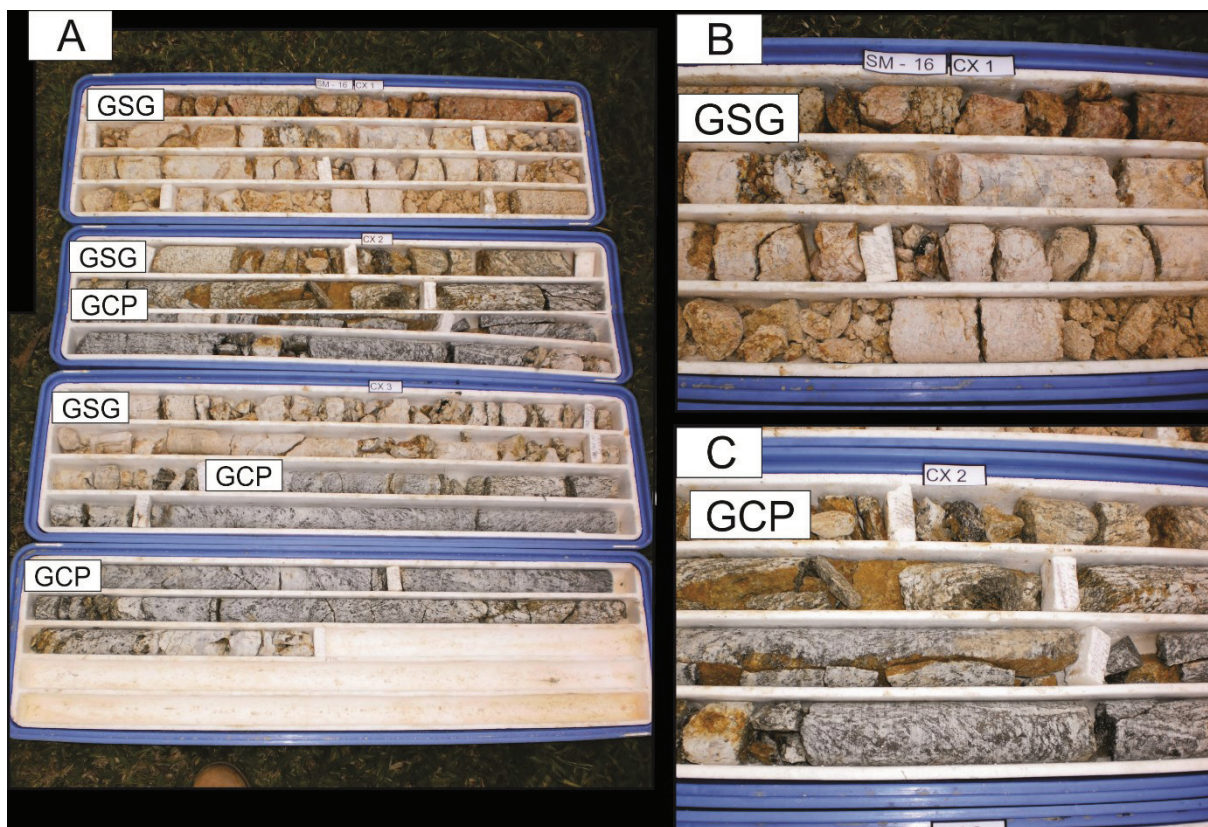
Figura 4. Testemunhos de sondagens. A) Testemunhos de sondagem do Granito São Geraldo (GSG) mostrando a presença de xenólitos dos Gnaisses Chácara das Pedras (GCP); B) Detalhe do Granito São Geraldo; C) Detalhe dos Gnaisses Chácara das Pedras.
Figure 4. Drill cores. A) Drill cores of the São Geraldo Granite (GSG) showing the xenoliths of the Chácara das Pedras Gneisses (GCP); B) Detail of the São Geraldo Granite; C) Detail of the Chácara das Pedras Gneisses.
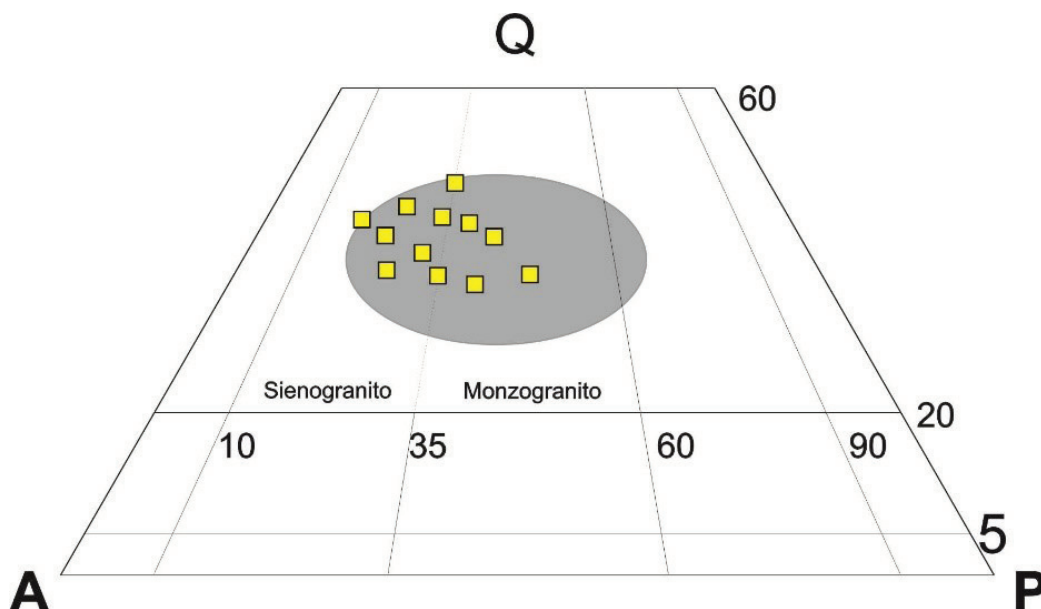
Figura 5. Composição modal do Granito São Geraldo (quadrados amarelos) projetada no diagrama QAP (Q = quartzo; A = feldspato alcalino; P = plagioclásio) para rochas plutônicas (Streckeisen, 1976), com o campo de distribuição da associação leucocrática peraluminosa (elipse cinza) modificado de Lameyre & Bowden (1982).
Figure 5. Modal composition of the São Geraldo Granite (yellow squares) projected on the QAP (Q = quartz; A = alkali feldspar; P = plagioclase) diagram for plutonic rocks (Streckeisen, 1976), with the peraluminous leucocratic association field (gray ellipse) modified from Lameyre & Bowden (1982).

o que faz com que os contatos dos grãos fiquem crenulados e interpenetrados, formando por vezes agregados policristalinos alongados e lenticulares que circundam os cristais de feldspato. Localmente é observado nos termos protomiloníticos feições como recristalização por migração de limite de grão formando texturas granoblásticas poligonais (contatos em pontos tríplices) e agregados policristalinos com extinção do tipo tabuleiro xadrez (Fig. 6D).

A muscovita e a biotita ocorrem em proporções variáveis, ora predominando a primeira, ora a última (Fig. 7A). Ambas são, em geral, bem formadas com tamanhos que variam de 0,1 a 4 mm (Fig. 6E). Por vezes nesses minerais ocorrem inclusões de zircão, monazita e apatita. Dois tipos de muscovita são observados: as primárias que ocorrem como lamelas subédricas que variam entre 0,2 a 0,8 mm e/ou cristais euédricos mais desenvolvidos, com dimensões entre 3 e 4 mm de comprimento, subordinadamente, as secundárias que se desenvolvem sobre os planos de clivagem ou nas bordas das biotitas. A biotita ocorre na forma de lamelas, entre 0,1 até 1,7 mm de comprimento com pleocroísmo variando em tons de marrom amarelado até castanho escuro (Fig. 6F). Feições de deformação nas micas são comuns, como extinção ondulante e formação de *mica-fish* e microdobramentos em *kink bands*.

O principal mineral acessório é a granada que ocorre na forma de cristais subédricos (Fig. 6F) com diâmetros que variam de 0,05 mm a 1,2 mm, por vezes apresentando inclusões de quartzo (Fig. 7B). Outros minerais acessórios observados são a monazita, apatita e zircão. Em geral, esses minerais estão inclusos nas micas, desenvolvendo halos pleocroicos devido à metamictização do zircão e da monazita (Fig. 6G). Os cristais de apatita em geral são euédricos, com hábito prismático longo, fazendo contatos retos com os demais minerais. Geralmente ocorrem como inclusões em feldspatos e micas, sugerindo cristalização em estágio magmático precoce, também ocorrendo em contato com cristais de monazita, conforme observado na figura 7C. Dentre os minerais opacos ocorrem ilmenita e magnetita.

3.2 Química mineral

Foram realizadas análises pontuais para a caracterização química dos minerais essenciais e acessórios de 2 amostras do granito estudado. Os resultados analíticos obtidos foram comparados com os dados mostrados por Koester *et al.* (2001b) para os granitos peraluminosos que ocorrem na região de Encruzilhada do Sul, RS.

As análises de biotita (Tab. 1) quando plotadas no diagrama ternário de Nachit *et al.* (1985) indicam um caráter primário para as mesmas (Fig. 8A). No diagrama de classificação Fe / (FeO + MnO) *versus* Si de Deer *et al.* (1992) (Fig. 8B), as biotitas se distribuem no campo superior (biotitas *sensu stricto*). Quando plotadas nos diagramas de Abdel-Rahman (1994) (Fig. 9), as biotitas do Granito São Geraldo se distribuem no campo das rochas de composição peraluminosa (P).

As análises químicas realizadas nas muscovitas (Tab. 2) evidenciam dois tipos quando plotadas no diagrama FeO-TiO$_2$-MgO (Fig. 10A) de Speer & Becker (1992). No diagrama de Zane & Rizzo (1999) (Fig. 10B), as muscovitas se distribuem no campo dos granitos fortemente peraluminosos.

Os cristais de K-feldspato são classificados como ortoclásio e mostram teores de Or entre 86 a 97 % que decrescem do núcleo em direção à borda (Tab. 3). Os dados químicos dos cristais de plagioclásio mostram uma composição principal do tipo oligoclásio e secundária do tipo albita, conforme mostrado na tabela 3. Perfis núcleo-borda nesses cristais demonstram enriquecimento em sódio, e empobrecimento em cálcio do núcleo para a borda, o que constitui um zoneamento ígneo normal (Tab. 4).

As granadas analisadas apresentam teores de almandina entre 63 e 71 %, e de espessartina entre 26 e 32 %. Suas concentrações de FeO variam de 25 a 31%, e de Al$_2$O$_3$ entre 20 e 22 % (Tab. 5). Os teores elevados de espessartina sugerem uma origem magmática, uma vez que granadas de origem metamórfica possuem teores inferiores a 5 % (Searle *et al.,* 1993).

Os cristais de apatita investigados (Tab. 6) correspondem a fluorapatitas. Essa composição sugere uma origem ígnea, uma vez que
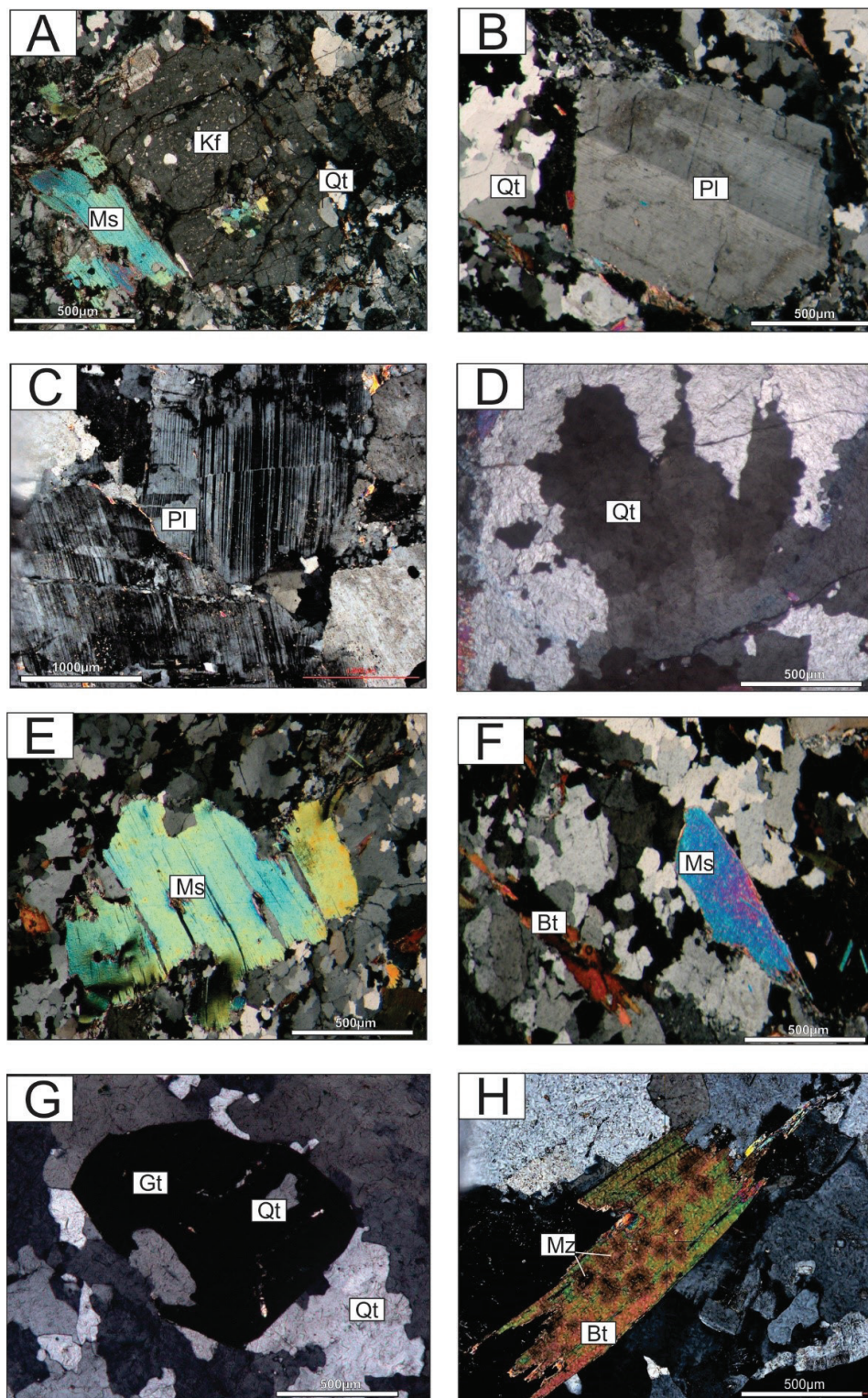
Figura 6. Fotomicrografias (nicóis cruzados) mostrando aspectos microscópicos do Granito São Geraldo. A) Cristal de K-feldspato com inclusões de quartzo, plagioclásio e muscovita; B) Cristal de plagioclásio zonado em matriz recristalizada; C) Cristal de plagioclásio com deformação dos planos de macla; D) Quartzo com recristalização por migração de limite de grão; E) Cristal de muscovita; F) Cristais de muscovita e biotita; G) Granada com inclusões de quartzo; H) Biotita com inclusões de monazita. Abreviações: Bt = biotita; Ms = muscovita; Mz = monazita; Pl = plagioclásio; Qt = quartzo; Kf = K-feldspato e Gt = granada.

Figure 6. Photomicrographs (crossed polars) showing microscopic aspects of the São Geraldo Granite. A) K-feldspar crystal with inclusions of quartz, plagioclase, and muscovite; B) Zoned plagioclase within recrystallized matrix; C) Plagioclase with deformed twinning; D) Quartz recrystallized by grain boundary migration; E) Muscovite grain; F); Muscovite and biotite crystals; G) Garnet crystal with inclusions of quartz; H) Biotite crystal with monazite inclusions. Abbreviations: Bt = biotite; Ms = muscovite; Mz = monazite; Qt = quartz; Kf = K-feldspar Gt = garnet.

Figura 7. Imagens de elétrons retroespalhados obtida em microscópio eletrônico de varredura. A) Contato entre biotita e muscovita; B) Cristais de granada com inclusões de quartzo; C) Formação de cristais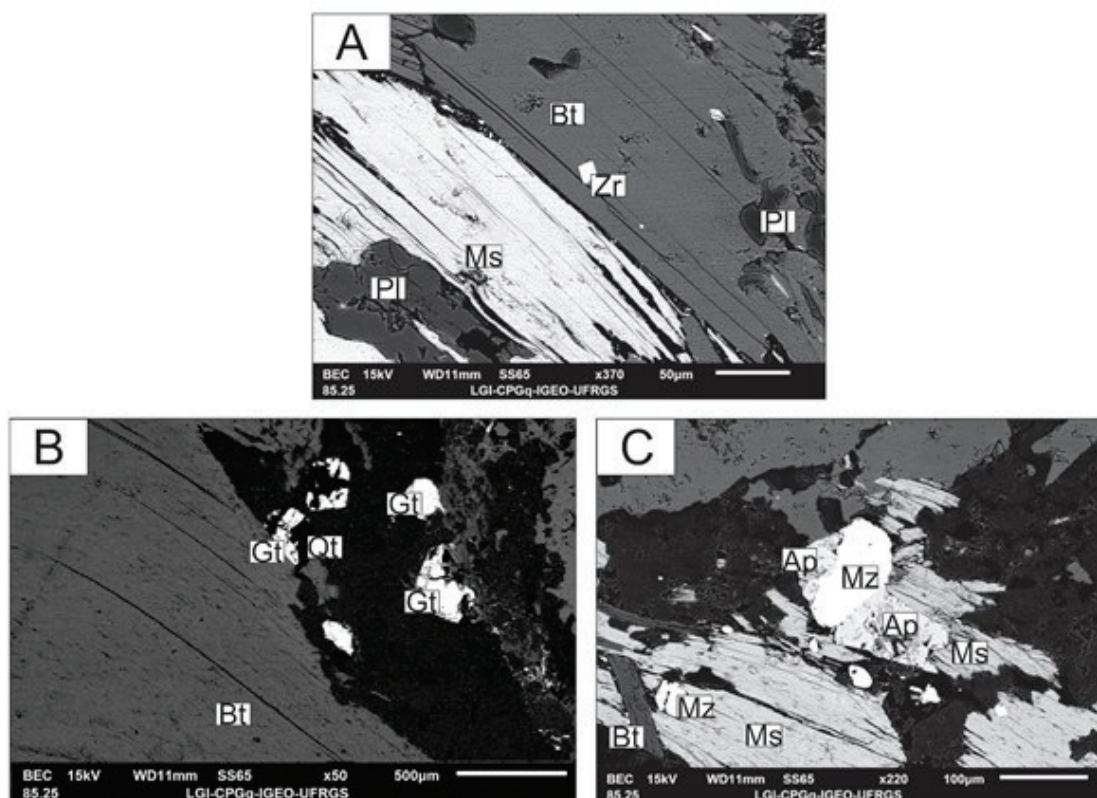 de apatita a partir de cristais de monazita. Abreviações: Ap = apatita; Bt = biotita; Ms = muscovita; Mz = monazita; Kf = K-feldspato e Gt = granada.
Figure 7. Backscattered electron images. A) Contact between muscovite and biotite; B) Garnet crystals with inclusions of quartz; C) Growth of apatite from monazite crystals. Abbreviations: Ap = apatite; Bt = biotite; Ms = muscovite; Mz = monazite; Kf = K-feldspar e Gt = garnet.

fluorapatitas são comuns à maioria das rochas magmáticas (e.g. Piccoli & Candela, 2002).

4 Discussão dos resultados

4.1 Petrogênese do Granito São Geraldo

Para o granito estudado, a mineralogia constituída por ortoclásio, plagioclásio, quartzo, muscovita e/ou biotita e minerais acessórios como granada, monazita e apatita é compatível com a dos granitos peraluminosos do tipo *MPG (muscovite-bearing peraluminous granitoids)* de Barbarin (1996, 1999). A presença de muscovita primária, como verificado na petrografia e na química mineral, fortalece a correlação com granitoides peraluminosos do tipo MPG. Granitos desse tipo são os primeiros a serem descritos na região de Porto Alegre.

A textura protomilonítica observada indica que o Granito São Geraldo foi submetido a condições de temperatura e pressão onde prevalece a deformação dúctil (Passchier & Trouw, 2005). Feições observadas nos cristais de quartzo como recristalização por *bulging* ocorrem no intervalo de temperaturas entre 250 – 300°C (Rosenberg & Stünitz, 2003) enquanto a presença de cristais de quartzo com subgrãos com extinção do tipo tabuleiro xadrez indica temperaturas de aproximadamente 650 °C (Khrul, 1996; Passchier & Trouw, 2005). A presença de subgrãos nas bordas dos cristais de feldspato e recristalização por rotação de subgrão são feições deformacionais que requerem temperaturas elevadas na ordem de 550°C, pois esses minerais possuem uma grande célula unitária e baixo coeficiente de difusão (Tullis & Yund, 1991).

A formação de cristais de apatita a partir de cristais de monazita sugere que esse mineral aproveitou os tetraedros de PO_4 liberados pela abertura da monazita favorecendo o crescimento da apatita nas bordas dos cristais de monazita. Os estudos de Finger *et al*. (1998) descrevem que essa reação de substituição começa

Tabela 1. Composição química e proporções catiônicas (O = 24) – Biotita de amostras representativas. ISA = Índice de Saturação em Alumina.
Table 1. Chemistry composition and cationic proportions (O = 24) – Biotite from representative samples. ISA = Aluminum Saturation Index.

PP	SM9						SM43					
SiO_2	33,74	33,76	34,65	32,57	34,74	34,99	35,09	34,97	36,85	33,79	34,21	36,72
TiO_2	2,69	3,34	2,63	3,01	2,65	2,97	2,81	3,00	2,07	3,70	2,29	2,50
Al_2O_3	18,05	18,85	18,44	17,18	18,75	18,68	18,49	18,67	21,73	19,02	19,73	19,93
FeO	25,09	23,70	24,11	22,10	24,88	23,35	24,60	24,26	21,37	24,11	24,64	19,94
MnO	0,29	0,34	0,26	0,26	0,36	0,26	0,48	0,49	0,32	0,47	0,50	0,37
MgO	4,96	4,15	4,73	4,18	4,57	4,59	4,07	3,93	3,40	3,61	3,86	3,65
CaO	0,24	0,04	0,00	0,24	0,00	0,02	0,00	0,00	0,05	0,01	0,00	0,05
Na_2O	0,05	0,09	0,09	8,37	0,07	0,06	0,10	0,09	0,07	0,12	0,06	0,05
K_2O	8,61	9,19	9,43	8,37	9,43	9,47	9,64	9,44	7,82	9,46	9,40	8,12
Li_2O	0,13	0,14	0,39	0,00	0,42	0,49	0,52	0,49	1,02	0,15	0,27	0,99
H_2O	3,76	3,77	3,82	3,78	3,86	3,85	3,85	3,85	3,97	3,79	3,82	3,87
Total	97,63	97,37	98,56	100,05	99,73	98,72	99,65	99,19	98,68	98,23	98,78	96,18
Si	5,37	5,36	5,44	5,17	5,40	5,45	5,46	5,45	5,57	5,34	5,37	5,68
Al ^{iv}	2,63	2,64	2,56	2,83	2,60	2,55	2,54	2,55	2,43	2,66	2,63	2,32
Al ^{vi}	0,76	0,90	0,85	0,38	0,84	0,88	0,85	0,88	1,44	0,89	1,02	1,32
Ti	0,32	0,40	0,31	0,36	0,31	0,35	0,33	0,35	0,24	0,44	0,27	0,29
Fe	3,34	3,15	3,16	2,93	3,24	3,04	3,20	3,16	2,70	3,19	3,24	2,58
Mn	0,04	0,05	0,04	0,03	0,05	0,03	0,06	0,07	0,04	0,06	0,07	0,05
Mg	1,18	0,98	1,11	0,99	1,06	1,07	0,94	0,91	0,77	0,85	0,90	0,84
Li	0,08	0,09	0,25	0,00	0,26	0,31	0,32	0,30	0,62	0,09	0,17	0,61
Ca	0,04	0,01	0,00	0,04	0,00	0,00	0,00	0,00	0,01	0,00	0,00	0,01
Na	0,02	0,03	0,03	2,57	0,02	0,02	0,03	0,03	0,02	0,04	0,02	0,02
K	1,75	1,86	1,89	1,69	1,87	1,88	1,91	1,88	1,51	1,91	1,88	1,60
OH	4,00	4,00	4,00	4,00	4,00	4,00	4,00	4,00	4,00	4,00	4,00	4,00
TOTAL	19,54	19,46	19,63	21,00	19,65	19,59	19,65	19,59	19,34	19,46	19,57	19,32
Y total	5,73	5,56	5,71	4,69	5,76	5,68	5,71	5,68	5,80	5,52	5,67	5,70
X total	1,81	1,90	1,92	4,31	1,89	1,90	1,94	1,91	1,54	1,94	1,90	1,63
Al total	3,39	3,53	3,41	3,21	3,44	3,43	3,39	3,43	3,87	3,54	3,65	3,64
Fe/Fe+Mg	0,74	0,76	0,74	0,75	0,75	0,74	0,77	0,78	0,78	0,79	0,78	0,75
ISA	2,02	2,02	1,94	1,01	1,97	1,96	1,90	1,96	2,74	1,98	2,09	2,42

com a abertura da monazita a temperaturas aproximadas de 650°C, compatíveis com as temperaturas de formação das microestruturas observadas no Granito São Gerado.

As análises microestruturais sugerem uma cristalização concomitante à deformação, sob condições de temperatura decrescente atuante durante o seu posicionamento, sugerindo assim uma gênese sintectônica às zonas de cisalhamento que ocorrem na região. Dentre essas, a principal é a Zona de Cisalhamento Porto Alegre, com direção preferencial N45E, relacionada a gênese e alojamento do granito sintrascorrente Lomba do Sabão (Menegat *et al.*, 1998).

A composição peraluminosa do Granito São Geraldo é atestada pela mineralogia semelhante a dos clássicos granitos com duas micas descritos na literatura (Barbarin, 1996, 1999; Chappell & White, 2001) e também pela composição química que esses minerais apresentam. As biotitas do Granito São Geraldo mostram, no geral, composição semelhante às biotitas de caráter peraluminoso (*e.g.* Abdel-Rahman, 1994). Apreciáveis quantidades de Al em coordenação octaédrica são comumente observadas em cristais de biotita de granitos peraluminosos, devido à sua coexistência com muscovita e outros minerais ricos em alumínio. Os altos valores (1,74- 2,74) do índice de
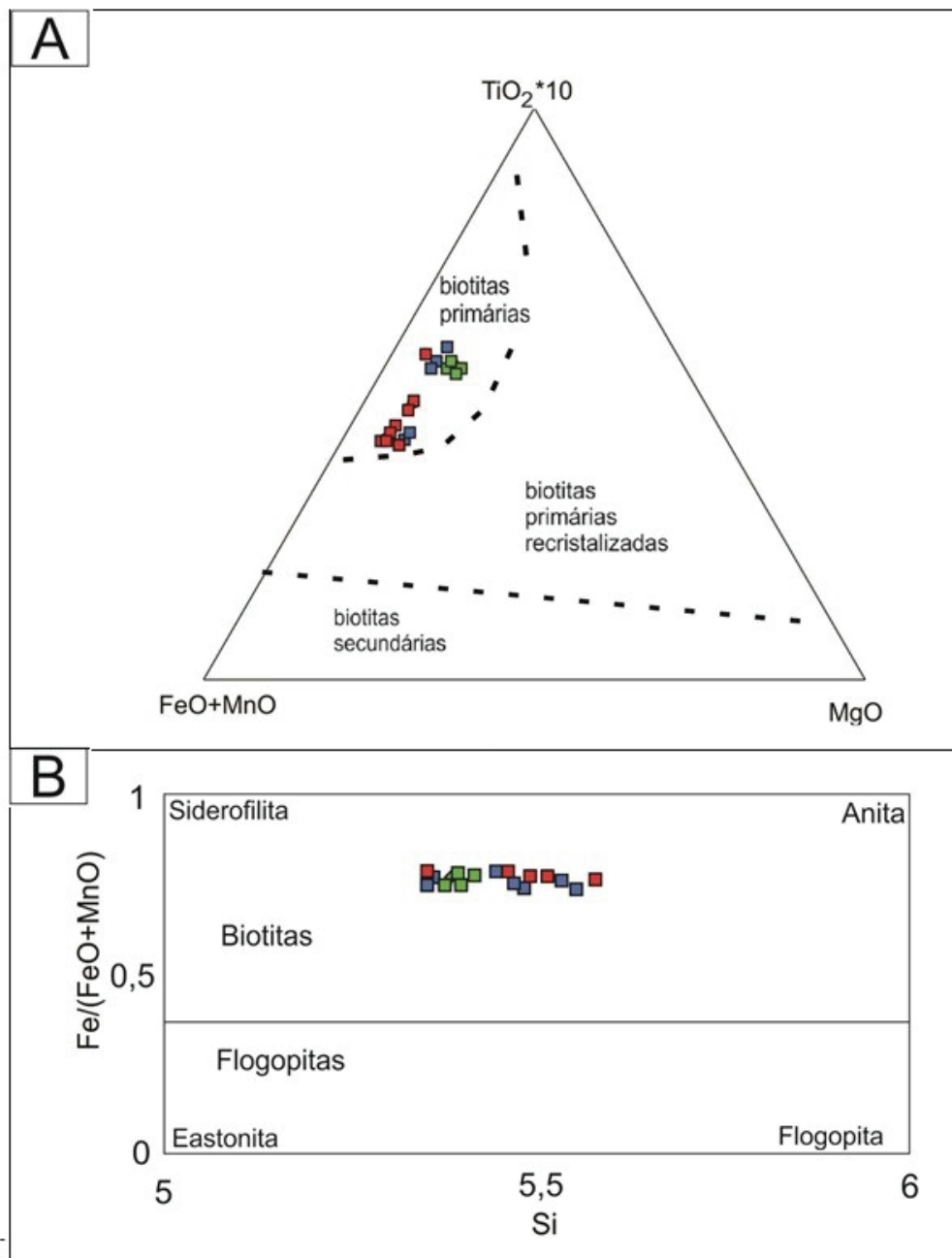
Figura 8. Diagramas químicos para a classificação de biotitas. A) Diagrama ternário MgO − TiO^2*10 − MnO + FeO (modificado de Nachit *et al.*, 1985); B) Diagrama Fe / (Fe + Mn) x Si (molar) (modificado de Speer, 1984). Simbologia: quadrados vermelhos = amostra SM9; quadrados azuis = amostra SM43; quadrados verdes = amostras dos Metagranitos Cordilheira e Arroio Francisquinho compiladas de Koester *et al.* (2001b).
*Figure 8. Discrimination diagrams for classification of biotites. A) MgO − TiO^2*10 − MnO + FeO ternary diagram (modified from Nachit et al., 1985); B) Fe / (Fe + Mn) x Si (molar) diagram (modified from Speer, 1984). Symbology: red squares = sample SM9; blue squares = sample SM43; green squares = samples of the Cordilheira and Arroio Francisquinho Metagranites from Koester et al. (2001b).*
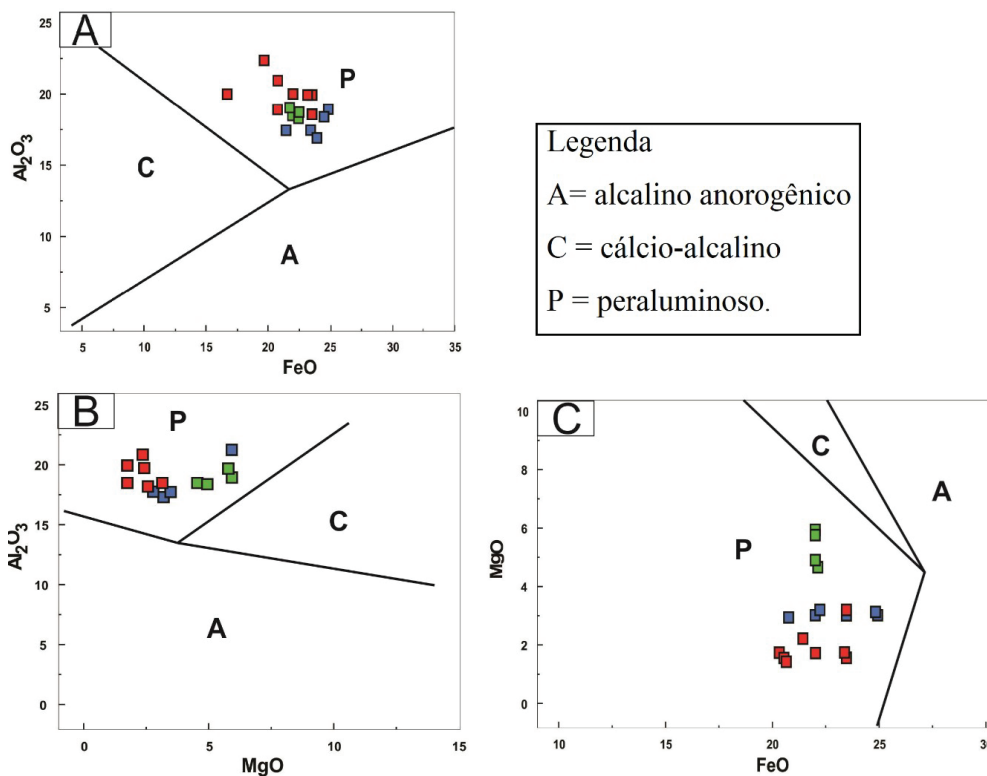
Figura 9. Diagramas discriminantes de séries magmáticas com base na química da biotita de Abdel-Rahman (1994). A) FeO vs. Al²O³; B) MgO vs. Al²O³; C) MgO vs. FeO. Símbolos como na figura 8.
Figure 9. Discrimination magmatic series diagrams based on the biotite chemistry (modified from Abdel-Rahman, 1994). A) FeO vs. Al²O³; B) MgO vs. Al²O³; C) MgO vs. FeO. Symbols as in figure 8.

Tabela 2. Composição química e proporções catiônicas (O = 22) – Muscovitas de amostras representativas. ISA = Índice de Saturação de Alumina.
Table 2. Chemistry composition and cationic proportions (O = 22) – Muscovite from representative samples. ISA = Aluminum Saturation Index.

| PP	SM9						SM43						
SiO$_2$	45,91	46,65	44,7	44,63	46,23	45,56	45,25	46,26	46,52	46,9	47,34	45,8	46,07
TiO$_2$	0,15	0,8	1	0,96	1,01	1,1	0,07	0,16	0,03	0,94	0,42	0,72	0,25
Al$_2$O$_3$	35,59	34,54	33,5	31,62	34,18	33,67	34,89	34,88	35,31	34,2	33,37	33,68	34,6
FeO	2,32	2,28	2,27	2,17	2,28	2,23	2,24	2,41	2,59	2,35	2,6	2,38	2,64
MnO	0,05	0,03	0	0,01	0	0,01	0,04	0,03	0,06	0,01	0,03	0,02	0,04
MgO	0,86	0,86	0,77	0,81	0,95	0,73	0,86	1,04	0,98	0,94	0,95	0,76	0,95
CaO	0	0,01	0	0,05	0	0,01	0,04	0	0	0	0	0	0
Na$_2$O	0,104	0,27	0,39	0,38	0,51	0,48	0,35	0,41	0,37	0,35	0,34	0,41	0,44
K$_2$O	10,66	10,59	10,4	9,91	10,29	10,2	10,3	10,64	10,46	9,82	10,39	10,47	10,51
Total	95,66	96,04	93	90,53	95,46	93,99	94,04	95,82	96,32	95,4	95,44	94,22	95,49
H$_2$O	4,7	4,73	4,54	4,44	4,7	4,62	4,62	4,71	4,74	4,73	4,72	4,62	4,68
Al^{IV}	2,14	2,09	2,11	1,97	2,1	2,08	2,12	2,11	2,11	2,05	1,98	2,06	2,1
Si	6,11	6,19	6,09	6,69	6,14	6,17	6,13	6,16	6,16	6,23	6,32	6,2	6,16
Ti	0,02	0,08	0,11	0,05	0,1	0,1	0,01	0,02	0	0,09	0,04	0,07	0,03
Fe	0,26	0,25	0,26	0,25	0,26	0,26	0,25	0,27	0,29	0,26	0,29	0,27	0,3
Al^{VI}	3,21	3,07	3,11	3,06	3,05	3,07	3,22	3,13	3,15	3,06	3,02	3,09	3,12
Al^{total}	5,35	5,16	5,21	5,03	5,14	5,16	5,34	5,24	5,27	5,11	5	5,15	5,22
Fe/Fe+Mg	0,6	0,6	0,62	0,6	0,57	0,63	0,59	0,57	0,6	0,58	0,61	0,64	0,61
ISA	3,31	3,18	3,1	3,06	3,16	3,15	3,26	3,16	3,26	3,36	3,11	3,1	3,16
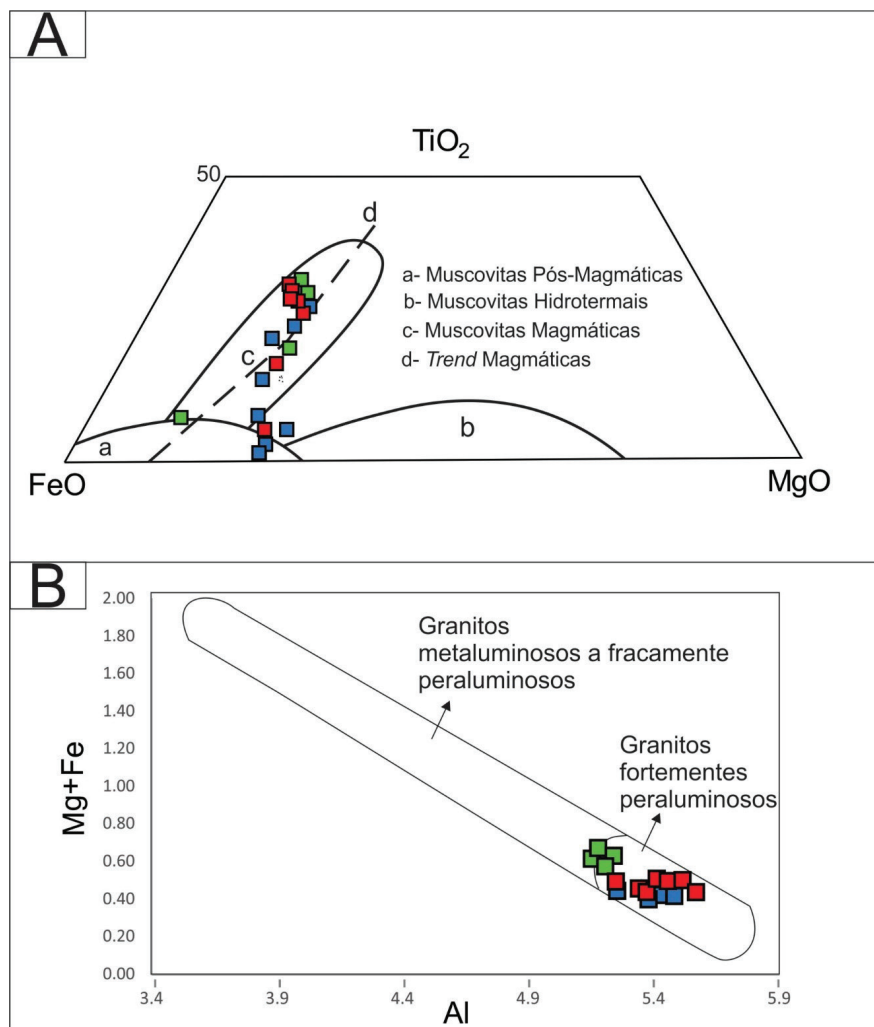
Figura 10. Diagramas de classificação para muscovitas. A) Diagrama ternário FeO x MgO x TiO2, modificado de Speer & Becker (1992); B) Diagrama Mg + Fe x Al (molar) discriminante entre componentes metaluminosos e fracamente a fortemente peraluminosos (modificado de Zane & Rizzo, 1999). Símbolos conforme a figura 8.
Figure 10. Muscovite classification diagrams. A) FeO x MgO x TiO2 ternary diagram after Speer & Becker (1992); B) Mg + Fe x Al (molar) diagram for discrimination of metaluminous and weakly to strongly peraluminous granites (modified from Zane & Rizzo, 1999). Symbols as in figure 8.

Tabela 3. Composição química e proporções catiônicas (O = 32) − K-Feldspatos de amostras representativas.
Table 3. Chemical composition and cationic proportions (O = 32) − K-Feldspar from representative samples.

Amostra/ Elemento	K-feldspato SM 9				K-feldspato SM 43			
	bordas		núcleos		bordas		núcleos	
Na_2O	0,70	0,60	1,11	0,26	1,26	1,12	1,32	1,23
SiO_2	64,34	64,07	64,21	64,27	64,52	63,52	63,97	63,32
MgO	0,01	0,00	0,00	0,01	0,00	0,00	0,00	0,01
Al_2O_3	18,25	18,41	18,37	18,19	18,99	18,40	18,52	18,37
K_2O	15,82	16,04	15,45	16,55	14,99	15,27	16,38	16,43
CaO	0,00	0,00	0,00	0,00	0,00	0,00	0,00	0,00
Cr_2O_3	0,00	0,01	0,00	0,00	0,00	0,01	0,01	0,02
MnO	0,00	0,00	0,00	0,02	0,02	0,00	0,02	0,01
FeO	0,02	0,00	0,04	0,20	0,01	0,13	0,00	0,00
TiO_2	0,03	0,02	0,00	0,03	0,03	0,02	0,02	0,01
Total	99,17	99,15	99,17	99,53	99,82	99,47	99,25	99,39
An	0,00	0,00	0,00	0,00	0,00	0,00	0,00	0,00
Ab	9,02	9,87	2,3	2,3	11,34	10,02	2,91	2,07
Or	90,98	90,13	97,7	97,7	88,66	89,98	97,09	97,93

Tabela 4. Composição química e proporções catiônicas (O = 32) – Plagioclásio de amostras representativas.
Table 4. Chemical composition and cationic proportions (O = 32) – Plagioclase from representative samples.

Amostra/	Plagioclásio Sm 9				Plagioclásio Sm 43			
Elemento	bordas		núcleos		bordas		núcleos	
Na_2O	10,19	10,50	9,77	9,89	11,15	11,39	9,89	9,88
SiO_2	65,24	65,62	64,36	64,73	66,71	67,02	64,66	64,07
MgO	0,00	0,00	0,00	0,01	0,01	0,01	0,01	0,00
Al_2O_3	21,72	21,79	22,43	21,99	20,78	20,84	22,32	22,39
K_2O	0,15	0,18	0,15	0,11	0,14	0,11	0,17	0,21
CaO	2,69	2,45	3,24	2,98	1,41	1,11	3,20	3,31
Cr_2O_3	0,01	0,01	0,00	0,01	0,00	0,00	0,01	0,00
MnO	0,00	0,00	0,00	0,00	0,00	0,00	0,02	0,00
FeO	0,00	0,03	0,00	0,02	0,04	0,00	0,06	0,07
TiO_2	0,03	0,00	0,01	0,01	0,01	0,00	0,00	0,03
Total	100,04	100,59	99,97	99,75	100,27	100,49	100,34	99,95
An	16,85	11,33	15,33	10,44	6,50	5,10	15,03	15,44
Ab	82,62	87,66	83,79	88,09	92,71	94,32	84,01	83,42
Or	0,52	1,01	0,87	1,47	0,79	0,58	0,97	1,14

Tabela 5. Composição química e proporções catiônicas (O = 24) – Granadas de amostras representativas.
Table 5. Chemical composition and cationic proportions (O=24) – Garnet from representative samples.

Amostra/ Elemento	SM9		SM43	
SiO_2	37,18	35,20	36,16	34,18
TiO_2	0,08	0,07	0,06	0,07
Al_2O_3	21,38	22,38	20,54	22,54
FeO	25,49	28,13	29,22	31,07
MnO	12,93	12,93	12,10	11,20
MgO	0,00	0,00	0,00	0,00
CaO	1,00	0,94	0,81	0,72
TOTAL	98,06	99,65	98,89	99,79
Si	6,13	5,80	6,02	5,68
Ti	0,01	0,01	0,01	0,01
Al	4,15	4,35	4,03	4,41
Fe	3,51	3,88	4,06	4,31
Mn	1,80	1,81	1,70	1,57
Mg	0,00	0,00	0,00	0,00
Ca	0,18	0,17	0,14	0,13
TOTAL	15,79	16,01	15,96	16,11
Py	0,00	0,00	0,00	0,00
Alm	63,94	66,30	68,73	71,70
Gro	3,21	2,84	2,44	2,13
Sp	32,85	30,86	28,83	26,18

Tabela 6. Composição química e proporções catiônicas (O = 25) – Apatita de amostras representativas.
Table 6. Chemical composition and cationic proportions (O = 25) – Apatite from representative samples.

Amostra/ Elemento	Sm9		Sm43	
CaO	56,70	55,71	53,71	54,68
Na₂O	0,11	0,11	0,20	0,11
MnO	0,20	0,31	0,20	0,20
FeO	0,24	0,30	0,24	0,24
P₂O₅	36,68	34,85	36,48	36,28
SiO₂	0,29	0,30	0,29	0,29
Cl	0,00	0,00	0,00	0,00
F	3,04	4,38	4,50	3,40
Total	97,25	95,96	95,62	95,19
O=F,Cl	1,28	1,84	1,89	1,43
Total	95,97	94,11	93,72	93,76
Ca	10,44	10,51	10,05	10,29
Na	0,04	0,04	0,07	0,04
Mn	0,03	0,03	0,03	0,03
Fe	0,03	0,03	0,03	0,03
La	0,02	0,03	0,03	0,03
Ce	0,02	0,02	0,02	0,02
Nd	0,02	0,02	0,02	0,02
P	5,38	5,19	5,39	5,39
Si	0,05	0,05	0,05	0,05
F	1,66	2,44	2,32	1,89
OH	0,34	-0,44	-0,32	0,11
Total	18,04	17,92	17,70	17,90

saturação em alumina [ISA=Al/ (Ca+Na+K)] nos cristais de biotita do Granito São Geraldo são reflexo dessa característica e evidenciam a alta atividade do alumínio no magma que os originou.

Dois tipos de muscovita são distinguidos nas amostras estudadas: cristais euédricos a subédricos bem desenvolvidos, interpretados como primários, e pequenos cristais subédricos de origem secundária (pós-magmáticos) dispersos de forma irregular em feldspatos e biotitas. As análises químicas reforçam essa interpretação, como observado no diagrama ternário Mg-Ti-Na apresentado na figura 10A. As baixas concentrações de TiO₂ da muscovita secundária sugerem reequilíbrio *subsolidus* (Speer & Becker, 1992).

De acordo com o diagrama proposto por Zane & Rizzo (1999) as muscovitas do Granito São Geraldo se distribuem no campo dos granitoides fortemente peraluminosos, semelhantes aos típicos granitoides tipo-S (Chappell & White, 1992). As características petrográficas e de composição química das muscovitas indicam uma origem primária, formadas a partir de um magma peraluminoso (Miller *et al.*, 1981; Clarke *et al.*, 2005; Dahlquist *et al.*, 2007).

A composição química das apatitas reforça o caráter peraluminoso e tipo-S do Granito São Geraldo. Apatitas com teores elevados de F e baixos de Cl são comumente descritas em granitos evoluídos, sendo um comportamento que pode ser atribuído à abundância de halogêneos nas rochas-fonte (Piccoli & Candela, 2002).

4.2 Comparação com a Suíte Cordilheira

Como mencionado anteriormente, o Batólito Pelotas, uma das principais associações petrotectônicas do Cinturão Dom Feliciano, é constituído por diversas suítes graníticas. Em uma dessas suítes, a Suíte Cordilheira, a maioria das ocorrências de granitos peraluminosos é agrupada (Philipp *et al.*, 2013). A Suíte Cordilheira é constituída por corpos graníticos alongados, segundo a direção preferencial NE-SW e são correlacionados a partir de suas características de campo, petrográficas, mineralógicas, estruturais, químicas, sendo interpretados como granitoides do tipo MPG e importantes registros de fusão crustal resultantes de processos similares (Fernandes *et al.*, 1995a; Koester, 1995; Nardi & Frantz, 1995; Philipp, 1998; Koester *et al.*, 2001b, 2001c, 2002; Frantz *et al.*, 2003; Philipp *et al.*, 2013; Klein, 2017; Klein *et al.,* 2018).

Na porção noroeste do Batólito Pelotas as principais ocorrências desses granitoides são os metagranitos Cordilheira e Arroio Francisquinho, sintectônicos à Zona de Cisalhamento Dorsal de Canguçu (Koester *et al.,* 2001b, 2001c), com idades de cristalização de ca. 634 e 625 Ma respectivamente (Frantz *et al.*, 2003). Na porção sul do Batólito Pelotas, destaca-se o Granito Três Figueiras, sintectônico à Zona de Cisalhamento Arroio Grande (Philipp, 1998), com idade de cristalização de ca. 585 Ma (Klein *et al.,* 2018). Estes granitos são essencialmente constituídos por K-feldspato, plagioclásio, quartzo, biotita e muscovita, e possuem tanto suas gêneses quanto seus alojamentos relacionados a zonas de cisalhamento transcorrentes dúcteis (Philipp *et al.*, 2013; Klein *et al.,* 2018). Tendo em vista as características apresentadas neste trabalho para o Granito São Geraldo, é possível correlacionar esse granitoide com os granitos pertencentes a essa suíte, uma vez que este apresenta composição e caráter peraluminoso característico a dos clássicos granitos com duas micas descritos na literatura (Barbarin, 1996, 1999; Chappell & White, 2001), bem como composição mineralógica similar aos metagranitos Cordilheira e Arroio Francisquinho pertencentes a Suíte Cordilheira, todos com gênese e alojamento relacionados a zonas de cisalhamento transcorrentes.

5 Conclusões

O Granito São Geraldo apresenta composição mineralógica essencial constituída por ortoclásio com teores de Or entre 86 a 97 % que decrescem em direção as bordas dos cristais, oligoclásio que em geral apresentam zonação ígnea normal, quartzo, muscovita (ígnea) e biotita. Como minerais secundários ocorre a presença de muscovitas pós-magmáticas que se desenvolvem sobre os planos de clivagem ou nas bordas das biotitas. Os minerais acessórios são zircão, monazita, almandina, fluorapatita e opacos (ilmenita e magnetita).

As características microestruturais descritas neste estudo sugerem temperaturas entre 650 ºC e 300 ºC, onde as microestruturas de mais alta temperatura estariam associadas aos estágios iniciais de cristalização e resfriamento do magma e as de baixa temperatura estariam associadas aos estágios pós-cristalização e resfriamento. Essa diferença de temperatura indica que o alojamento do granito se deu em diferentes estágios de movimentação e calor em um regime transcorrente, possivelmente relacionado com a Zona de Cisalhamento de Porto Alegre.

A composição mineralógica descrita para o granito alvo deste estudo difere de todos os granitoides descritos até então na região de Porto Alegre. Seu caráter peraluminoso sugere semelhança com os granitos com duas micas que compõe a Suíte Cordilheira. Isso é reforçado quando os dados de química mineral do Granito São Geraldo são comparados com os granitos peraluminosos que afloram na região de Encruzilhada do Sul.

A correlação entre os furos de sondagem sugere que o Granito São Geraldo possui uma extensão mínima de 10 km. Apesar de não aflorar em superfície, a presença de um granito peraluminoso sugere um importante evento de fusão crustal na região de Porto Alegre, com possível correlação com os demais eventos de descompressão adiabática seguida de fusões crustais que ocorrem no Cinturão Dom Feliciano e que colaboraram para a formação do Batólito

Pelotas.

Referências

Abdel-Rahman, A.M. 1994. Nature of biotites from alkaline, calc-alkaline, and peraluminous magmas. *Journal of Petrology*, 35: 525-541.

Barbarin, B. 1996. Genesis of the two main types of peraluminous granitoids. *Geology*, 24(4): 295-298.

Barbarin, B. 1999. A review of the relationships between granitoid types, their origins and their geodynamic environments. *Lithos*, 46: 605-626.

Bitencourt, M.F. & Nardi, L.V.S. 2000. Tectonic setting and sources of magmatism related to the Southern Brazilian Shear Belt. *Revista Brasileira de Geociências*, 30(1): 186-189.

Brown, M. 2013. Granite: From genesis to emplacement. *Bulletin of the Geological Society of America* 125:1079–1113.

Chappell, B.W. & White, A.J.R. 1992. I-Type and S-Type granites in the Lachlan Fold Belt. *Transaction Royal Society*, 83: 1-26.

Chappell, B.W. & White, A.J.R. 2001. Two contrasting granite types – 25 years later. *Australian Journal of Earth Sciences*, 48, 489-499.

Clarke, D.B, Dorais, M., Barbarin, B., Barker, D., Cesare, B., Clarke, G., el Baghdadi, M., Erdmann, S., Förster, H.J., Gaeta, M., Gottesmann, B., Jamieson, R.A., Kontak, D.J., Koller, F., Gomes, C.L, London, D., Morgan Vi, G.B., Neves, L.J.P.F., Pattison, D.R.M., Pereira, A.J.S.C., Pichavant, M., Rapela, C.R., Renno, A.D., Richards, S., Roberts, M., Rottura, A., Saavedra, J., Sial, A.N., Toselli, A.J., Ugidos, J.M., Uher, P., Villaseca, C., Visonà, D., Whitney, D.L., Williamson, B. & Woodard, H.H. 2005. Occurrence and origin of andalusite in peraluminous felsic igneous rocks. *Journal of Petrology*, 46: 441-472.

Costa, A.F.U. 1997. *Teste e modelagem geofísica da estruturação das associações litotectônicas pré-cambrianas no Escudo Sul-rio-grandense*. Porto Alegre, 291p. Tese de Doutorado, Programa de Pós-Graduação em Geociências, Instituto de Geociências, Universidade Federal do Rio Grande do Sul, Porto Alegre.

Dahlquist, J.A., Galindo, C., Pankhurst, R.J., Rapela, C.W., Alasino, P.H., Saavedra, J. & Fanning, C.M. 2007. Magmatic evolution of the Peñón Rosado granite: Petrogenesis of garnet-bearing granitoids. *Lithos*, 95: 177-207.

Deer, W.A., Howie, R.A. & Zussman, J. 1992. *An Introduction to the Rock Forming Minerals*. Londres, Longman, 2ª Ed., 696p.

Fernandes, L.A.D., Tommasi, A. & Porcher, C.C. 1992. Deformation patterns in the Southern Brazilian Branch of the Pan-African Dom Feliciano Belt. *Journal of South American Earth Sciences,* 5: 77-96.

Fernandes, L.A.D., Menegat, R., Costa, A.F.U., Koester, E., Kramer, G., Tommasi, A., Porcher, C.C., Ramgrab, G.E. & Camozzato, E. 1995a. Evolução tectônica do Cinturão Dom Feliciano no Escudo Sul-rio-grandense: Parte I – uma contribuição a partir do registro geológico. *Revista Brasileira de Geociências*, 25: 351-374.

Fernandes, L.A.D., Menegat, R., Costa, A.F.U., Koester, E., Kramer, G., Tommasi, A., Porcher, C.C., Ramgrab, G.E. & Camozzato, E. 1995b. Evolução tectônica do Cinturão Dom Feliciano no Escudo Sul-rio-grandense: Parte II – uma contribuição a partir das assinaturas geofísicas. *Revista Brasileira de Geociências*, 25: 375-384.

Figueiredo, M.C.H., Fragoso-César, A.R.S. & Kronberg, B.I. 1990. Litogeoquímica das principais unidades do Batólito Pelotas no Rio Grande do Sul. *In*: CONGRESSO BRASILEIRO DE GEOLOGIA, 36, 1990, Natal. *Anais*... Natal, SBG, v. 4, p. 1723-1738.

Finger, F., Broska, I., Roberts, M.P. & Schermaier, A. 1998. Replacement of primary monazite by apatite – allanite – epidote coronas in an amphibolite facies granite gneiss from the eastern Alps. *American Mineralogist*, 83: 248-258.

Fragoso-Cesar, A.R.S., Figueiredo, M.C.H., Soliani Jr., E. & Faccini, U.F. 1986. O Batólito Pelotas (Proterozóico Superior/Eo-Paleozóico) no Escudo do Rio Grande do Sul. *In:* CONGRESSO BRASILEIRO DE GEOLOGIA, 34, 1986, Goiânia. *Anais...* Goiânia, SBG, v. 3, p. 13-22.

Frantz, J.C., McNaughton, N.J., Marques, J.C., Hartmann, L.A., Botelho, N.F. & Caravaca, G. 2003. SHRIMP U-Pb zircon ages of granitoids from southernmost Brazil: constrains on the temporal evolution of the Dorsal de Canguçu transcurrent Shear Zone and Eastern Dom Feliciano Belt. *In:* South American Symposium on Isotope Geology, 4, 2003, Salvador. *Short Papers*, v. 1, p. 174-177.

Gill, R. 2010. *Igneous rocks and processes: a practical guide.* Oxford, Wiley-Blackwell, 390p.

Gomes, V.F. 2016. *Petrografia e Geoquímica dos Gnaisses Chácara das Pedras, Nordeste do Cinturão Dom Feliciano.* Pelotas, 68p. Trabalho de conclusão de curso em Engenharia Geológica, Centro das Engenharias da Universidade Federal de Pelotas.

Gregory, T.R., M.F., Bitencourt, Nardi, L. V., Florisbal, L. M, Chemale, F. Jr. 2015. Geochronological data from TTG-type rock associations of the Arroio dos Ratos Complex and implications for crustal evolution of southernmost Brazil in Paleoproterozoic times. *Journal of South American Earth Sciences,* 57, 49–60.

Heilbron, M., Pedrosa-Soares, A.C., Campos Neto, M., Silva, L.C. & Trouw, R.A.J. 2004. A Província Mantiqueira. *In*: Mantesso Neto, A., Bartorelli, A., Carneiro, C.D.R. & Brito Neves, B.B. (Eds.). *O desvendar de um continente: a moderna geologia da América do Sul e o legado da obra de Fernando Flávio Marques de Almeida.* São Paulo, Beca, p. 203-234.

Klein, F.G. 2017. *Petrologia do Granito Três Figueiras, sudeste do Cinturão Dom Feliciano, RS.* Porto Alegre, 74p. Dissertação de Mestrado, Programa de Pós-Graduação em Geociências, Instituto de Geociências, Universidade Federal do Rio Grande do Sul.

Klein, F.G., Koester, E., Vieira, D.T., Porcher, C.C., Ramos, R.C. & Philipp, R.P. 2018. Geologia do Granito Três Figueiras: magmatismo peraluminoso de 585 Ma no sudeste do Cinturão Dom Feliciano. *Pesquisas em Geociências*, 45(2): e665.

Koester, E. 1995. *Petrologia e geocronologia dos granitóides sintectônicos à Zona de Cisalhamento Dorsal de Canguçu.* Porto Alegre, 240p. Dissertação de Mestrado, Programa de Pós-Graduação em Geociências, Instituto de Geociências, Universidade Federal do Rio Grande do Sul.

Koester, E., Soliani Jr., E., Leite, J.A.D., Hartmann, L.A., Fernandes, L.A.D., McNaughton, N.J., Santos, J.O.S. & Oliveira, L. D. 2001a. SHRIMP U-Pb age for the emplacement of the Santana Granite and reactivation of the Porto Alegre Suture, southern Brazil. *Journal of South American Earth Sciences*, 14(1): 91-99.

Koester, E., Fernandes, L.A.D., Soliani Jr., E., Kraemer, G., Nardi, L.V.S. & Roisemberg, A. 2001b. Geologia e geoquímica dos granitóides sintectônicos à Zona de Cisalhamento Transcorrente Dorsal de Canguçu, Encruzilhada do Sul, RS. *Revista Brasileira de Geociências*, 31(2): 141-154.

Koester, E., Roisenberg, A., Fernandes, L.A.D., Soliani Jr., E., Nardi, L.V.S. & Kraemer, G. 2001c. Petrologia dos granitóides sintectônicos à Zona de Cisalhamento Transcorrente Dorsal de Canguçu, Encruzilhada do Sul, RS. *Revista Brasileira de Geociências*, 31(2): 131-140.

Koester, E., Porcher, C.C., Pimentel, M.M., Fernandes, L.A.D., Vignol-Lelarge, M.L., Oliveira, L.D. & Ramos, R.C. 2016. Further evidence of 777 Ma subduction-related continental arc magmatism in Eastern Dom Feliciano Belt, southern Brazil: The Chácara das Pedras Orthogneiss. *Journal of South American Earth Sciences*, 68: 155-166.

Kruhl, J.H. 1996. Prism- and basis-parallel subgrain boundaries in quartz: a microstructural geothermobarometer. *Journal of Metamorphic Geology*, 14, 581-589.

Lameyre, J. & Bowden, P. 1982. Plutonic rock types series: discrimination of various granitoid series and related rocks. *Journal of Volcanology and Geothermal Research,* 14(1/2): 169-186.

Liégeois, J.P, Navez, J., Hertogen, J. & Black, R. 1998. Contrasting origin of post-collisional high-K calc-alkaline and shoshonitic versus alkaline and peralkaline granitoids. The use of

sliding normalization. *Lithos*, 45: 1-28.

Martil, M.M., Bitencourt, M.F., Nardi, L.V.S., Koester, E. & Pimentel, M.M. 2017. Pre-collisional, Tonian (ca. 790 Ma) continental arc magmatism in southern Mantiqueira Province, Brazil: geochemical and isotopic constraints from the Várzea do Capivarita Complex. *Lithos*, 274/275: 39-52.

Masquelin, H., Fernandes, L.A.D., Lenz, C., Porcher, C.C. & McNaughton, N.J. 2012. The Cerro Olivo Complex: a pre-collisional Neoproterozoic magmatic arc in Eastern Uruguay. *International Geology Review*, 54: 1161-1183.

Menegat, R., Fernandes, L.A.D., Koester, E. & Scherer, C.M.S. 1998. Porto Alegre antes do Homem: evolução geológica. *In*: Menegat, R., Porto, M.L., Carraro, C.C. & Fernandes, L.A.D. (Eds.). *Atlas Ambiental de Porto Alegre*. Porto Alegre, Editora da Universidade Federal do Rio Grande do Sul, p. 11-24.

Miller, C.F., Stoddard, E.F., Bradfish, L.J. & Dollase, W.A. 1981. Composition of plutonic muscovite. Genetic implications. *Canadian Mineralogist*, 19: 25-34.

Nachit, H., Razafimahefa, N., Stussi, J.M. & Carron, J.P. 1985. Composition chimique des biotites et typologie magmatique des granitoides. *Comptes Rendus de l'Académie des sciences Paris*, 301: 810–818.

Nardi, L.V.S. 2016. Granitoides e séries magmáticas: o estudo contextualizado dos granitoides. *Pesquisas em Geociências*, 43(1): 85-99.

Nardi, L.V.S. & Frantz, J.C. 1995. The Cordilheira intrusive suite: late Proterozoic peraluminous granitoids from the southern Brazil. *Journal of South American Earth Sciences*, 8(1): 55-63.

Nardi, L.V.S. & Bonin, B. 1991. Post orogenic and non-orogenic alkaline granite associations: the Saibro Intrusive Suite, Southern Brasil: a case study. *Chemical Geology*, 92: 197-212.

Nardi, L.V.S., Plá Cid, J. & Bitencourt, M.F. 2007. Geochemistry of mafic microgranular enclaves and their relationship with the host syenite within the mantle pressure lamprophyresyenite systems (Piquiri Massif) of Southern Brazil. *Mineralogy and Petrology*, 91: 101-116.

Nardi, L.V.S., Plá Cid, J., Bitencourt, M.F. & Stabel, L. 2008. Geochemistry and petrogenesis of post-collisional ultrapotassic syenites and granites from southernmost Brazil: the Piquiri Syenite Massif. *Anais da Academia Brasileira de Ciências*, 80(2): 353-371.

Oliveira, L. D., Koester, E. & Soliani Jr., E. 2001. Geoquímica das rochas graníticas pós-transcorrentes da região de Porto Alegre e Viamão, RS. *Geochimica Brasiliensis*, 15(2): 65-92.

Passchier, C.W. & Trouw, R.A.J. 2005. *Microtectonics*. Berlim, Springer Verlag, 366 p.

Patiño-Douce, A.E. & Johnston, A.D. 1991. Phase equilibria and melt productivity in the pelitic system: implications for the origin of peraluminous granitoids and aluminous granulites. *Contributions to Mineralogy and Petrology*, 107: 202-218.

Patiño-Douce, A.E. & McCarthy, T.C. 1998. Melting of crustal rocks during continental collision and subduction. *In*: Hacker, B.R. & Liou, J.G. (Eds.). *When Continents Collide: Geodynamics and Geochemistry of Ultra-high Pressure Rocks*. Dordrecht, Kluwer Academic, p. 27-55.

Pérez-Soba, C. & Villaseca, C. 2010. Petrogenesis of highly fractionated I-type peraluminous granites: La Pedriza pluton (Spanish Central System). *Geologica Acta*, 8:131-149.

Philipp, R.P. 1990. *Geologia e Petroquímica dos granitóides da região de Monte Bonito, Pelotas. RS*. Porto Alegre, 231p. Dissertação de Mestrado, Programa de Pós- Graduação em Geociências, Instituto de Geociências, Universidade Federal do Rio Grande do Sul.

Philipp, R.P. 1998. *A evolução geológica e tectônica do Batólito Pelotas no Rio Grande do Sul*. São Paulo, 255p. Tese de Doutorado, Programa de Pós-Graduação em Geociências, Instituto de Geociências, Universidade de São Paulo.

Philipp, R.P. & Machado, R. 2001. Ocorrência e significado dos septos do embasamento encontrados nas suítes graníticas do Batólito Pelotas, RS, Brasil. *Pesquisas em Geociências*, 29(1): 43-57.

Philipp, R.P. & Campos, R. 2004. Geologia, petrografia e litogeoquímica dos Gnaisses Porto Alegre, RS, Brasil: implicações

geotectônicas. *Pesquisas em Geociências*, 31(2): 79-94

Philipp, R.P. & Machado, R. 2005. The Neoproterozoic to Cambrian Granitic Magmatism of Pelotas Batholith, Southern Brazil. *Journal of South American Earth Sciences*, 19: 461-478.

Philipp, R.P., Machado, R., Nardi, L.V.S. & Lafon, J.M. 2002. O magmatismo granítico Neoproterozóico do Batólito Pelotas no sul do Brasil: novos dados e revisão de geocronologia regional. *Revista Brasileira de Geociências*, 32(2): 277-290.

Philipp, R.P., Massone, H.J & Campos, R.S. 2013. Peraluminous leucogranites of the Cordilheira Suite: A record of Neoproterozoic collision and the generation of the Pelotas Batholith, Dom Feliciano Belt, Southern Brazil. *Journal of South American Earth Sciences*, 43: 08-24.

Philipp, R.P., Pimentel, M.M. & Chemale Jr., F. 2016. Tectonic evolution of the Dom Feliciano Belt in Southern Brazil: geological relationships and U-Pb geochronology. *Brazilian Journal of Geology*, 46(1), 83-104.

Phillips, E.R. 1980. On Polygenetic Myrmekyte. *Geological Magazine*, 177(1): 29-36.

Plá Cid, J., Nardi, L.V.S., Stabel, L.Z., Conceição, R.V. & Balzaretti, N.M. 2003. High-pressure minerals in mafic microgranular enclaves: evidences for co-mingling between lamprophyric and syenitic magmas at mantle conditions. *Contributions to Mineralogy and Petrology*, 145: 444-459.

Plá Cid J., Nardi, L.V.S., Enrique, P., Merlet, C. & Boyer, B. 2005. SIMS analysis on trace and rare earth elements in coexisting clinopyroxene and mica from minette mafic enclaves in potassic syenites crystallized under high pressures. *Contributions to Mineralogy and Petrology*, 148: 675-688.

Reichardt, H., Weinberg, R.F., Andersson, U.B. & Fanning, C.M. 2010. Hybridization of granitic magmas in the source: The origin of the Karakoram Batholith, Ladakh, NW India. *Lithos*, 116: 249-272.

Rosenberg, C.L. & Stünitz, H. 2003. Deformation and recrystallization of plagioclase along temperature gradient: an example from the Bergell tonalite. *Journal of Structural Geology*, 25: 389-408.

Sawyer, E.W., Cesare, B. & Brown, M. 2011. When the continental crust melts. *Elements*, 7: 227-232.

Searle, M.P., Metcalfe, R.P., Rex, A.J. & Norry, M.J. 1993. Field relations, petrogenesis and emplacement of the Bhagirathi leucogranite, Garhwal Himalaya. In: Treloar, P.J. & Searle, M.P. (Eds). *Himalayan Tectonics.* Geological Society, London, Special Publications, 74, 429-444.

Speer, J.A. 1984. Micas in igneous rocks. *In*: Bailey, S.W. (Ed.). Micas. *Reviews in Mineralogy*, 13: 299-356.

Speer, J.A. & Becker, S.W. 1992. Evolution of magmatic and subsolidus AFM mineral assemblages in granitoid rocks: biotite, muscovite, and garnet in the Cuffytown Creek, pluton, South-Carolina. *American Mineralogist*, 77: 821-833

Streckeisen, A.L. 1976. Classification of the common igneous rocks by means of their chemical composition: a provisional attempt. *Neues Jahrbuch für Mineralogie*, 1: 1-15.

Tullis, J. & Yund, R.A. 1991. Diffusion creep in feldspar aggregates: experimental evidence. *Journal of Structural Geology*, 13: 987-1000.

White, A.J.R. & Chappell, B.W. 1974. Ultrametamorphism and granitoid genesis. Tectonophysics, 43: 7-22.

Wilson, M. 1989. *Igneous Petrology*. Londres, Unwin and Hyman, 466p.

Zane, A. & Rizzo, G. 1999. The compositional space of muscovite in granitic rocks. *Canadian Mineralogist*, 37: 1229-1238.

CAPÍTULO 7

7 DISCUSSÕES E MODELO PROPOSTO

Com a revisão bibliográfica apresentada no capítulo 2 foi possível verificar que o conceito da Orogenia Piratini e suas interpretações variaram ao longo das últimas décadas até o presente momento. No entanto, desde a origem do conceito em Fragoso-César (1991) não houve mudanças de pensamento quanto à gênese do Arco Piratini. Diferentemente de outros eventos magmáticos temporalmente correlatos, como por exemplo, o Arco São Gabriel (ver capitulo 2), e as rochas da margem paleo-africana relacionadas a um ambiente extensional (Konopásek *et al.,* 2008; Frimmel *et al.,* 2011; Frimmel, 2018), o Arco Piratini se desenvolveu sobre uma microplaca possivelmente relacionada à fragmentação do Cráton Kalahari, sendo retrabalhado pela intensa granitogênese ediarana que se seguiu obliterando a sua continuidade espacial. Com base nos modelos propostos por Fragoso-César (1991), Lenz *et al.* (2013) e Ramos *et al.* (2017) e nos artigos que compõe a presente tese de doutoramento, foi possível propor um modelo evolutivo para o Arco Piratini apresentado na Figura 12.

Segundo Ramos *et al.* (2017), a origem da microplaca Arachania (Gaucher *et al.,* 2009), Adamastoria (Rapela *et al.,* 2011) ou Encantadas/Arroio dos Ratos (Chemale, 2000) estaria relacionada ao desenvolvimento do *Rift* Gariep, cujo magmatismo extensional ocorreu por volta de 830-750 Ma (Frimmel *et al.,* 2011), fragmentando o sudoeste do Cráton Kalahari (Jacobs *et al.,* 2008; Hofmann *et al.,* 2014; Thomas *et al.,* 2016). Para Ramos *et al.* (2017) essa fragmentação explicaria a origem da microplaca de afinidade africana (Fig.12 A), bem como o magmatismo relacionado a um ambiente extensional toniano, descrito por Lenz *et al.* (2013) e Will *et al.* (2019) uma vez que crosta oceânica começou a se formar por volta de 750 Ma (Frimmel & Fölling, 2004) entre a microplaca e o Cráton Kalahari. Concomitantemente, na margem oposta do Arco Piratini, entre este último e o Cráton Rio de La Plata, ocorre a formação de arcos de ilhas (Orogenia Passinho, Lusa *et al., 2016*) relacionados ao paleo-oceano Charrua (Fragoso-César, 1991; Saalmann *et al.,* 2011; Philipp *et al.,* 2018),

Com o desenvolvimento da Orogenia São Gabriel (*e.g*. Complexo Cambaí, *ca.* 780 Ma, Philipp *et al.,* 2014), arcos de ilhas resultantes da Orogênia Passinho são

amalgamados junto à margem oriental do Cráton Rio de La Plata (Fig. 12B), formando, em conjunto com diversos fragmentos de crosta oceânicos, o Prisma Acrescionário Palma (Naumann, 1985; Leite, 1997; Hartmann & Chemale, 2003; Arena *et al.,* 2016).
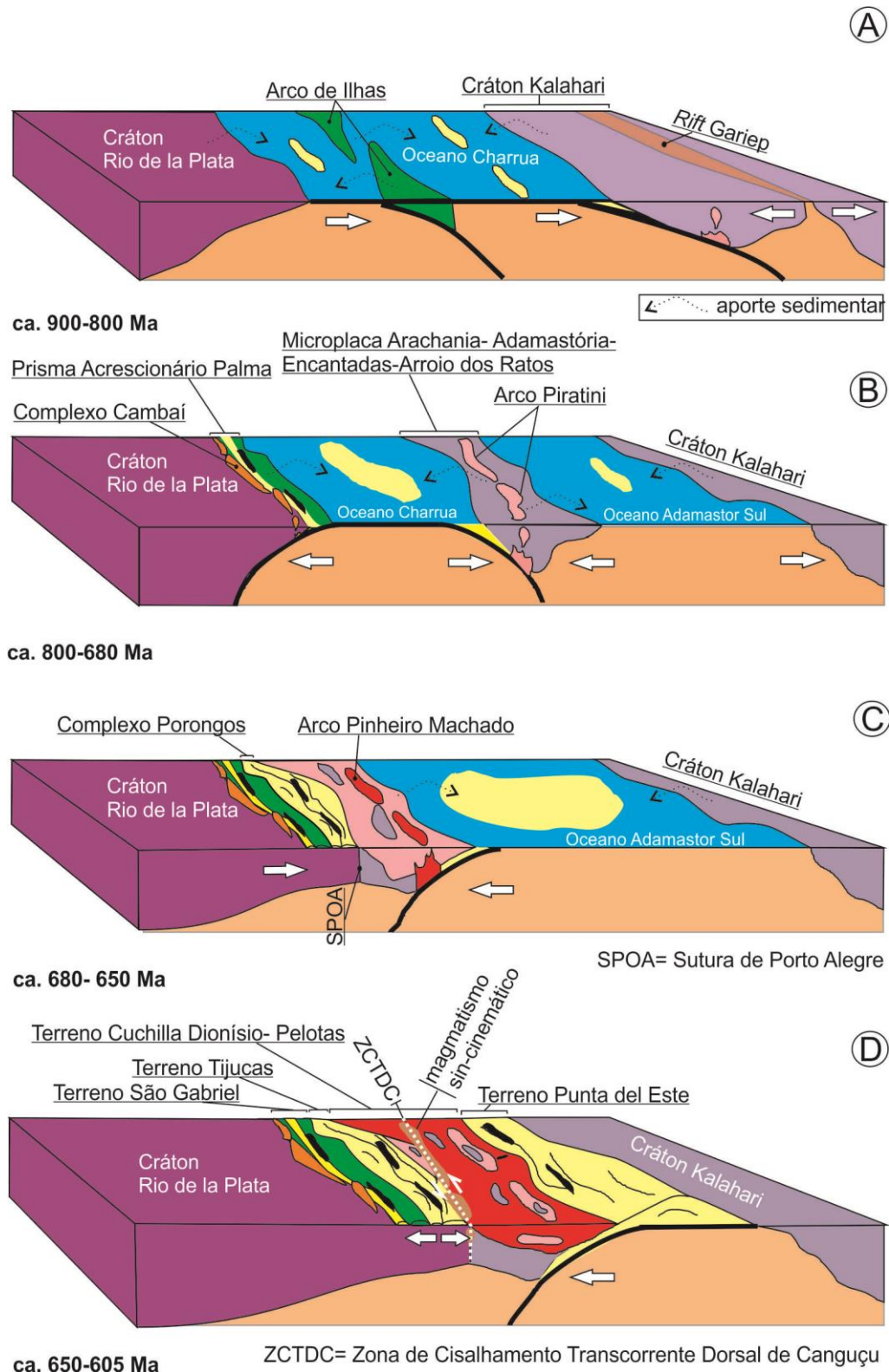

Figura 12 - Evolução geodinâmica simplificada do Arco Piratini (modificado de Ramos *et al.,* 2017). (A) desenvolvimento e evolução do Rift Gariep fragmentando o Cráton Kalahari, na margem oposta ocorre o desenvolvimento de arco de ilhas relacionados a Orogenia Passinho;

(B) abertura e desenvolvimento do oceano Adamastor sul entre o Cráton Kalahari e bloco fragmentado relacionado (microplaca Arachania–Adamastoria-Encantadas/Arroio dos Ratos) e desenvolvimento do Arco Piratini como resultado de uma subducção E para W (coordenadas atuais) na margem oeste da microplaca (Orogenia Piratini) concomitante na margem do Cráton Rio de la Plata ocorre o desenvolvimento do Complexo Cambaí (Orogenia São Gabriel). Essa subducção culminou em uma colisão continental (C) e fechamento do oceano Charrua e bacias correlatas com geração da Sutura de Porto Alegre, concomitante ocorre a subducção para oeste da placa oceânica Adamastor do Sul sob a microplaca/ Arco Piratini; (D) evolução do magmatismo continental relacionado ao Arco Pinheiro Machado e desenvolvimento das zonas de cisalhamento transcorrentes de tendência NE-SW (eg. Dorsal de Canguçu) culminando no retrabalhamento crustal e início do magmatismo relacionado a Orogenia Dom Feliciano.

A partir da concomitante abertura do paleo-oceano Adamastor e fechamento do paleo-oceano Charrua dá-se o desenvolvimento do Arco Piratini (Fig. 12B) sobre a microplaca de origem africana (Orogenia Piratini, Capítulo 2).

Recentes trabalhos (Philipp *et al.,* 2016a; Pertille *et al.,* 2017; Höfig *et al.,* 2018) mostram que as rochas metassedimentares que constituem em partes o Complexo Porongos, Terreno Tijucas, na porção Sul-rio-grandense do Cinturão Dom Feliciano, apresentam três picos de proveniência com idades de (I) 2,2–1,5 Ga; (ii) 830–680 Ma; (iii) 615–580 Ma. Os três picos de proveniência são compatíveis com o modelo proposto na presente tese, onde as idades mais antigas corresponderiam a uma proveniência relacionada aos crátons Río de la Plata e Kalahari, enquanto as idades tonianas a criogenianas estariam possivelmente relacionadas aos arcos São Gabriel, Passinho e Piratini. Essa hipótese é corroborada pela assinatura de εHf (*ca.* -14) dos zircões detríticos encontrados nos zicões de idades tonianas a criogenianas, semelhantes aos encontrados nos gnaisses que compõe o Arco Piratini (Will *et al.*, 2019; Vieira *et al.,* 2019a).

As idades mais jovens (615–580 Ma) estão possivelmente relacionadas à formação do Terreno Cuchilla Dionísio–Pelotas (Fig. 12C). Conforme Höfig *et al.* (2018), a sequência mais antiga do Complexo porongos se desenvolveu em um ambiente extensional, enquanto a sequência mais jovem se formou em um ambiente compressivo relacionado provavelmente com fechamento do paleo-oceano Charrua e à formação do terreno Cuchilla Dioníniso–Pelotas (Fig. 12C). Com base em características estruturais semelhantes, Battisti *et al.* (2018) correlacionaram as rochas metassedimentares mais antigas dos complexos Porongos e Várzea do Capivarita.

Conforme a revisão apresentada na seção 2.3 da presente tese, as rochas metassedimentares da Suíte Metamórfica Chafalote (capítulo 4) e do Complexo Várzea do Capivarita são correlacionáveis, e poderiam representar porções de uma mesma paleobacia relacionada à orogênese Piratini, depositadas em um ambiente de frente de arco (Vieira *et al.*, 2019b). Entretanto, apesar de apresentarem idades de metamorfismo semelhantes em torno de 660-620 Ma (Lenz, 2006; Gross *et al.,* 2006; Philipp *et al.,* 2016b; Martil *et al.,* 2017; Vieira *et al.,* 2019b), as rochas metassedimentares de ambas associações registram um metamorfismo de alto grau (fácies granulito, Gross *et al.*, 2006; 2009) diferente das rochas metassedimentares do Complexo Porongos, estas últimas afetadas por um metamorfismo de fácies anfibolito (Lenz, 2006). Essas rochas poderiam, portanto, representarem níveis crustais diferentes de uma mesma bacia, sendo metamorfizadas durante a convergência entre o Arco Piratini e o Cráton Rio de La Plata (Fig. 12C), culminando no fechamento do paleo-oceano Charrua. Alternativamente, as rochas de alto grau metamórfico poderiam estar relacionadas com a obducção do paleo-oceano Adamastor (Fig.12C), culminando na formação das rochas relacionada ao Arco Pinheiro Machado (Ramos *et al.*, 2017; Vieira *et al.*, 2019b). Os trabalhos recentes de Ramos *et al.* (2018; 2019) atestam o metamorfismo de alto grau seguido de fusão parcial (*ca.* 640 Ma) na região de Arroio Grande (porção brasileira do Terreno Punta del Este). Ambas hipóteses são condizentes com as trajetórias P-T-t apresentadas por Gross *et al.* (2006; 2009) para as rochas metassedimentares dos complexos Várzea do Capivarita (Terreno Encruzilhada) e Cerro Olivo (Terreno Punta del Este).

Philipp *et al.* (2013, 2016a, 2016b) sugeriram que a colisão oblíqua entre os crátons Río de La Plata e Kalahari, ocorrida em torno de 650 Ma, produziu grandes volumes de magma granítico, resultando na origem da maior parte do Terreno Cuchilla Dionísio-Pelotas. Segundo esses autores, esta colisão deu origem a ZCTDC, que quando ainda ativa, contribuiu para a geração de parte do magmatismo relacionado ao Complexo Pinheiro Machado em torno de 633-609 Ma (Philipp *et al.,* 2003). Para esses autores, a ZCTDC foi reativada por volta de 600-550 Ma, resultando na geração de grande parte dos granitoides orogênicos tardios, representados pela Suíte Intrusiva Dom Feliciano (Philipp *et al.*, 2003).

Os novos dados apresentados na presente tese mostram idades mais jovens de U-Pb para o magmatismo associado à ZCTDC (Capitulo 5). Segundo Vieira *et al.* (2019c), a formação da zona de cisalhamento de tendência NE-SW (*e.g.* ZCTDC)

estariam associadas ao estágio de descompressão em torno de 640 Ma (Fig. 12D) que sucedeu o estágio compressivo (670-650 Ma, Fig. 12C) se desenvolvendo às custas de suturas pré-existentes (por exemplo, a Sutura de Porto Alegre; Fernandes *et al.*, 1995a) (Fig.12D). O desenvolvimento das zonas de cisalhamento de tendência NE-SW (seção 2.5 do Capítulo 2) seria concomitante à geração do Arco Pinheiro Machado (Complexo Pinheiro Machado), resultante da convergência entre os crátons Kalahari e Rio de La Plata (Ramos *et al.*, 2017). Para esses autores, essa convergência culminou no fechamento de bacias orogênicas (por exemplo, bacia de Rocha; Masquelin, 2001) que compõe, junto aos fragmentos de crosta oceânica (complexos Paso del Dragón, no Uruguai, e Arroio Grande, no Brasil – Peel *et al.*, 2018; Ramos *et al.*, 2018) o Terreno Punta del Este, e também na reativação de zonas de cisalhamento e geração de magmatismo orogênico tardio em torno de 580 Ma, estes últimos compondo juntamente com o Arco Pinheiro Machado o Terreno Cuchilla Dionisio-Pelotas, desenvolvido em parte sobre o próprio Arco Piratini.

CAPÍTULO 8

8. CONCLUSÕES

Com a integração dos presentes artigos que compõe a presente Tese em conjunto com a revisão bibliográfica apresentada no capítulo 2 é proposto um modelo evolutivo simplificado (Fig. 12) para o Cinturão Dom Feliciano onde é adicionado em torno de 780 Ma uma nova orogenia, denominada Orogenia Piratini na qual se desenvolveu o Arco Piratini. Em relação à evolução do Arco Piratini as seguintes conclusões podem ser consideradas:

- O Arco Piratini diferentemente do Arco de São Gabriel (porção oeste do Cinturão Dom Feliciano), que se desenvolveu na margem oriental do Cráton Rio de La Plata, cuja evolução está vinculada a um sistema de arco magmático intra-oceânico e um sistema de arco continental, teria se desenvolvido em uma microplaca relacionada à paleo-África. Essa microplaca é representada pelas rochas dos complexos Encantadas e Arroio dos Ratos e as microplacas Arachania e Adamastoria e constitui o embasamento do Arco Piratini;

- O Arco Piratini é considerado como um arco continental tipo andino com atividade magmática em torno de 100 Ma. O arco é constituído pelos ortognaisses de idades tonianas (*ca.* 780 Ma) Piratini, Chácara das Pedras, Várzea do Capivarita e Cerro Bori e pelo ortognaisse de idade criogeniana (*ca.* 680 Ma) Arroio Pedrado.

- Todas as rochas relacionadas ao Arco Piratini registram um metamorfismo de alto grau (fáceis anfibolito a granulito) em torno de 660 Ma. Esse metamorfismo tem seu pico relacionado a um estágio colisional (660-650 Ma), possivelmente relacionado ao fechamento do paleo- oceano Charrua seguido por um estágio de descompressão e fusão parcial (640-620 Ma) registrado em alguns fragmentos do arco e principalmente nas rochas supracrustais relacionadas ao mesmo.

- O fechamento do paleo- oceano Charrua com o desenvolvimento de suturas (*e.g.* Sutura de Porto Alegre) em conjunto com a subdução da placa oceânica Adamastor do Sul sob a microplaca/ Arco Piratini acarretaram no desenvolvimento das grandes zonas de cisalhamento transcorrentes NE-SW (*e.g.* ZCTDC).

- O magmatismo relacionado às grandes zonas de cisalhamento transcorrentes em conjunto com o magmatismo relacionado ao Arco Pinheiro Machado foram responsáveis em partes pelo retrabalhamento e obliteração do Arco Piratini.

REFERÊNCIAS

Almeida, F.F.M., Hasui, Y., Brito-Neves, B.B., Fuck, R.A., 1981. Brazilian Structural Provinces: an introduction. Earth Science Review, 17, 1-29.

Arena, K.R., Hartmann, L.A., Lana, C., 2016. Evolution of Neoproterozoic ophiolites from the southern Brasiliano Orogen revealed by zircon U-Pb-Hf isotopes and geochemistry. Precambrian Research, 285, 299-314.

Babinski, M., Chemale Jr., F., Van Schmus, W.R., Hartmann, L.A., Silva, L.C., 1997. U-Pb and Sm-Nd geochronology of the Neoproterozoic Granitic-Gneissic Dom Feliciano Belt, Southern Brazil. Journal of South American Earth Sciences, 10(3/4), 263-274.

Basei, M.A.S.; Frimmel, H.E.; Nutman, A.P.; Preciozzi, F.; Jacob J. 2005. A connection between the Neoproterozoic Dom Feliciano (Brazil/Uruguay) and Gariep (Namibia/South Africa) orogenic belts – evidence from a reconnaissance provenance study. Precambrian Research, 139: 195-221.

Basei M.A.S., Frimmel H.E., Nutman A.P., Preciozzi F. 2008. West Gondwana amalgamation based on detrital zircon ages from Neoproterozoic Ribeira and Dom Feliciano belts of SouthAmerica and comparison with coeval sequences from SW Africa. In: Pankhurst R.J., Trouw R.A.J., Brito Neves B.B., de Wit M.J. (eds). West Gondwana, Pre-Cenozoic correlations across the South Atlantic region. Geological Society, London, Special Publication, 294:239-256

Basei, M.A.S.; Siga JR., O.; Masquelin, H.; Harara, O.M.; Reis Neto, J.M.; Preciozzi, F., 2000. The Dom Feliciano Belt of Brazil and Uruguay and its Foreland Domain the Rio de la Plata Craton: framework, tectonic evolution and correlation with similar provinces of Southwestern Africa. In: CORDANI, U. G.; MILANI, E. J.; THOMAZ FILHO, A; CAMPOS, D. A. Tectonic Evolution of South America, p. 311-334.

Battisti, M.A., de Fátima Bitencourt, M., De Toni, G.B., Stoll Nardi, L.V., Konopásek, Jiří., 2018. Metavolcanic rocks and orthogneisses from Porongos and Várzea do Capivarita complexes: A case for identification of tectonic interleaving at different crustal levels from structural and geochemical data in southernmost Brazil. Journal of South American Earth Sciences.

Bertotti A.L., Chemale Jr. F., Kawashita K., 2013. Lu-Hf em Zircão por LA-ICP-MS: Aplicação em Gabro do Ofiolito de Aburrá, Colômbia. Pesquisas em Geociências, 40(2):117-127.

Black, L.P., Kamo, S.L., Allen, C.M., Davis, D.W., Aleinikoff, J.N., Valley, J.W., Mundil, R., Campbell, I.H., Korsch, R.J., Williams, I.S., Foudoulis, C., 2004. Improved 206Pb/238U microprobe geochronology by the monitoring of a trace-element-

related matrix effect; SHRIMP, ID-TIMS, ELA-ICP-MS and oxygen isotope documentation for a series of zircon standards. Chem. Geol. 205, 115–140.

Bom, F.M., Philipp, R.P., Zvirtes, G., 2014. Origem e evolução do Complexo Várzea do Capivarita, Encruzilhada do Sul, RS. Pesquisas em Geociências, 41(2), 131-153.

Bossi, J., Gaucher, C., 2004. The Cuchilla Dionisio Terrane, Uruguay: An allochthonous block accreted in the Cambrian to SW-Gondwana. Gondwana Research, 7(3), 661-674.

Brito-Neves, B.B.; Fuck, R.A.; Pimentel, M.M. 2014. The Brasiliano collage in South America: a review. Brazilian Journal of Geology, 44(3): 493-518.

Chemale Jr., F., 2000. Evolução geológica do Escudo Sul-Rio-Grandense. In: Holz, M., De Ros, L.F. (Eds.). Geologia do Rio Grande do Sul. Porto Alegre, edição CIGO/UFRGS, p. 13-52.

Chemale Jr., F.; Hartmann, L.A.; Silva, L.C. 1995. Stratigraphy and tectonism of the Brasiliano Cycle in southern Brazil. Communications of the Geological Survey of Namibia, 10: 153-168.

Chemale Jr., F.; Mallmann, G.; Bitencourt, M.F.; Kawashita, K. 2012. Time constraints on magmatism along the Major Gercino Shear zone, southern Brazil: implications for West Gondwana reconstruction. Gondwana Research, 22: 184-199.

Costa, A.F.U. 1997. Teste e modelagem geofísica da estruturação das associações litotectônicas pré-cambrianas no Escudo Sul-rio-grandense. Tese de Doutoramento, Instituto de Geociências, Universidade Federal do Rio Grande do Sul, Porto Alegre, 291p.

Cruz, R.F. 2019. Projeto Sudeste do Rio Grande do sul: escalas 1:250.000 e 1:100.000; estado do Rio Grande do Sul. Porto Alegre: CPRM. 173 p.

Deer, W.A.; Howie, R.A.; Zussman, J. 1992. An Introduction to the rock forming minerals. 2.ed., Hong Kong, Longman Scientific & Technical, 696p.

Fernandes, L.A.D., Menegat, R., Costa, A.F.U., Koester, E., Porcher, C.C., Tommasi, A., Kraemer, G., Ramgrab, G.R., Camozzato, E., 1995a. Evolução tectônica do Cinturão Dom Feliciano no Escudo Sul-riograndense: Parte I – Uma contribuição a partir do registro geológico. Revista Brasileira de Geociências, 25(4), 351-374.

Fernandes, L.A.D., Menegat, R., Costa, A.F.U., Koester, E., Porcher, C.C., Tommasi, A., Kraemer, G., Ramgrab, G.R., Camozzato, E., 1995b. Evolução tectônica do Cinturão Dom Feliciano no Escudo Sul-riograndense: Parte II – Uma contribuição a partir das assinaturas geofísicas. Revista Brasileira de Geociências, 25(4), 375-384.

Fernandes, L.A.D., Koester, E., 1999. The Neoproterozoic Dorsal de Canguçu strike-slip shear zone: its nature and role in the tectonic evolution of southern Brazil. Journal of African Earth Sciences 29, 3-24.

Fernandes L.A.D., Tommasi A., Porcher C.C. 1992. Deformation patterns in the Southern Brazilian Branch of the Pan-African Dom Feliciano belt. Journal South American Earth Science, 5, 77-96.

Florisbal, L.M., Janasi, V.A., Bitencourt, M.F., Heaman, L.M., 2012. Space-time relation of post-collisional granitic magmatism in Santa Catarina, southern Brazil: U-Pb LA-MC-ICP-MS zircon geochronology of coeval mafic-felsic magmatism related to the Major Gercinho Shear Zone. Precambrian Research 216-219, 132-151.

Fragoso-César, A.R.S., 1991. Tectônica de placas no Ciclo Brasiliano: as orogenias dos cinturões Dom Feliciano e Ribeira no Rio Grande do Sul. PhD Thesis, São Paulo, Universidade de São Paulo, 367 p.

Fragoso-César, A.R.S., Figueiredo, M.C.H., Soliani Jr., E., Faccini, U.F., 1986. O BatólitoPelotas (proterozoico superior/eo-paleozoico) no escudo do Rio grande do sul. In: XXXIV Congresso Brasileiro de Geologia, vol. 3. Anais, Goiânia, pp. 1322e1343.

Frimmel, H.E., 2018. The Gariep belt. In: Siegesmund, S., Basei, M., Oyhantçabal, P., Oriolo, S. (Eds.). Geology of Southwest Gondwana. Springer, Regional Geology Reviews, pp. 353-386.

Frimmel, H.E., Basei, M.A.S., Gaucher, C., 2011. Neoproterozoic geodynamic evolution of SW-Gondwana: a southern African perspective. International Journal of Earth Sciences, 100, 323-354.

Gaucher, C., Frimmel, H.E., Germs, G.J.B., 2009. Tectonic events and palaeogeographic evolution of Southern Gondwana in the Neoproterozoic and Cambrian. In: Gaucher, C., Sial, A.N., Halverson, G.P., Frimmel, H.E. (Eds.). Neoproterozoic-Cambrian tectonics, global change and evolution: a focus on southwestern Gondwana. Elsevier, Developments in Precambrian Geology, 16, 295-316.

Gregory, T.R., M.F., Bitencourt, Nardi, L. V., Florisbal, L. M, Chemale, F. Jr., 2015. Geochronological data from TTG-type rock associations of the Arroio dos Ratos Complex and implications for crustal evolution of southernmost Brazil in Paleoproterozoic times. Journal of South American Earth Science 57, 49–60.

Grew, E.S.; Locock, A.J.; Mills, S.J.; Galuskina, I.O.; Galuskin, E.V.; Halenius, U. 2013. Nomenclature of the garnet supergroup. American Mineralogist, v. 98, 785–811.

Gross A.O.M.S., Droop G.T.R., Porcher C.C., Fernandes L.A.D., 2009. Petrology and thermobarometry of mafic granulites and migmatites from the Chafalote Metamorphic Suite: new insights into the Neoproterozoic P–T evolution of the

Uruguayan–Sul- Rio-Grandense Shield. Precambrian Research, 170, 157-174.

Gross, A.O.M.S, Porcher C.C., Fernandes L.A.D., Koester E., 2006. Neoproterozoic low-pressure/high-temperature collisional metamorphic evolution in the Várzea do Capivarita Metamorphic Suite, SE Brazil: thermobarometric and Sm/Nd evidence. Precambrian Research, 147(1-2), 41-64.

Hartmann, L.A., Chemale, F., 2003. Mid amphibolite facies metamorphism of harzburgites in the Neoproterozoic Cerro Mantiqueiras Ophiolite, southernmost Brazil. Annals of the Brazilian Academy of Sciences, 75(1), 109-128.

Hartmann, L.A.; Lopes, W.R.; Savian, J.F. 2016. Integrated evaluation of the geology, aerogammaspectrometry and aeromagnetometry of the Sul-Riograndense Shield, southernmost Brazil. Annals of the Brazilian Academy of Sciences, 88(1): 75-92.

Höfig, D.F., Marques, J.C., Basei, M.A.S., Giusti, R.O., Kohlrausch, C., Frantz, J.C., 2018. Detrital zircon geochronology (U-Pb LA-ICP-MS) of syn-orogenic basins in SW Gondwana: new insights into the Cryogenian-Ediacaran of Porongos Complex, Dom Feliciano Belt, southern Brazil. Precambrian Research, 306, 189-208.

Hofmann, M., Linnemann, U., Hoffmann, K.H., Gerdes, A., Eckelmann, K., Gärtner, A., 2014. The Namuskluft and Dreigratberg sections in southern Namibia (Kalahari Craton, Gariep Belt): a geological history of Neoproterozoic rifting and recycling of cratonic crust during the dispersal of Rodinia until the amalgamation of Gondwana. International Journal of Earth Sciences, 103(5), 1187-1202.

Hueck, M., Oyhantçabal, P., Philipp, R.P., Basei, M.A.S., Siegesmund, S., 2018. The Dom Feliciano Belt in Southern Brazil and Uruguay. In: Siegesmund, S., Basei, M., Oyhantçabal, P., Oriolo, S. (Eds.). Geology of Southwest Gondwana. Springer, Regional Geology Reviews, p. 267-302

Jacobs, J., Pisarevsky, S., Thomas, R.J., Becker, T., 2008. The Kalahari Craton during the assembly and dispersal of Rodinia. Precambrian Research, 160(1-2), 142-158

Janoušek, V.; Farrow, C., M.; Erban, V. 2006. Interpretation of whole-rock geochemical data in igneous geochemistry: introducing Geochemical Data Toolkit (GCDkit). Journal of Petrology, 47(6):1255-1259.

Jost, H.; Bitencourt, M.F., 1980. Estratigrafia e tectônica de uma fração da faixa de dobramentosde Tijucas no Rio Grande do Sul. Acta geológica Leopoldensia, 7(6):27-60

Klein, F.G., Koester, E., Vieira, D.T., Porcher, C.C., Ramos, R.C., Philipp, R.P. 2018. Geologia do Granito Três Figueiras: magmatismo peraluminoso de 585 Ma no sudeste do Cinturão Dom Feliciano. Pesquisas em Geociências, 45(2), 1-27.

Koester, E., Fernandes, L.A.D., Soliani Jr., E., Kraemer, G., Nardi, L.V.S., Roisemberg, A., 2001a. Geologia e geoquímica dos granitóides sintectônicos à Zona de Cisalhamento Transcorrente Dorsal de Canguçu, Encruzilhada do Sul, RS. Revista Brasileira de Geociências, 31(2): 141-154.

Koester, E., Pawley, A.R., Fernandes, L.A.D., Porcher, C.C. and Soliani Jr., E., 2002. Experimental melting of cordierite gneiss and the petrogenesys of syntranscurrent peraluminous granites in the southern Brazil. Journal of Petrology, 48(43): 1595-1616.

Koester, E., Porcher, C.C., Pimentel, M.M., Fernandes, L.A.D., Vignol-Lelarge, M.L., Oliveira, L.D., Ramos, R.C., 2016. Further evidence of 777 Ma subduction-related continental arc magmatism in Eastern Dom Feliciano Belt, southern Brazil: The Chácara das Pedras Orthogneiss. Journal of South American Earth Sciences, 68, 155-166.

Koester, E., Roisenberg, A., Fernandes, L.A.D., Soliani Jr., E., Nardi, L.V.S. and Kraemer, G. 2001b. Petrologia dos granitóides sintectônicos à Zona de Cisalhamento Transcorrente Dorsal de Canguçu, Encruzilhada do Sul, RS. Revista Brasileira de Geociências, 31(2): 131-140.

Konopásek, J., Janoušek, V., Oyhantçabal, P., Sláma, J., Ulrich, S., 2018. Did the circum- Rodinia subduction trigger the Neoproterozoic rifting along the Congo–Kalahari Craton margin? Int. J. Earth Sci. 107 (5), 1859–1894

Konopásek, J., Košler, J., Tajčmanová, L., Ulrich, S., Kitt, S.L., 2008. Neoproterozoic igneous complex emplaced along major tectonic boundary in the Kaoko Belt (NW Namibia): ion probe and LA-ICP-MS dating of magmatic and metamorphic zircons. Journal of the Geological Society, 165(1), 153-165.

Konopásek, J.; Sláma, J.; Košler, J. 2016. Linking the basement geology along the Africa-South America coasts in the South Atlantic. Precambrian Research, 280: 221-230.

Leite, J.A.D., 1997. A origem dos harzburgitos da Sequência Cerro Mantiqueiras e implicações tectônicas para o desenvolvimento do Neoproterozóico da porção oeste do Escudo Sul-Rio-Grandense. PhD Thesis. Universidade Federal do Rio Grande do Sul, Porto Alegre 224p.

Lena L.O.F., Pimentel M.M., Philipp R.P., Armstrong R., Sato K. 2014. The evolution of the Neoproterozoic São Gabriel juvenile terrane, southern Brazil based on high spatial resolution U-Pb ages and 18O data from detrital zircons. Precambrian Research, 247:126-138.

Lenz, C., 2006. Evolução metamórfica dos metapelitos da Antiforme Serra dos Pedrosas: condições e idades do metamorfismo. Dissertação de Mestrado, Porto Alegre, Universidade Federal do Rio Grande do Sul, 111p.

Lenz, C., Fernandes, L.A.D., McNaughton, N.J., Porcher, C.C., Masquelin, H., 2011. U-Pb SHRIMP ages for the Cerro Bori Orthogneisses, Dom Feliciano Belt in Uruguay: evidences of a ~800 Ma magmatic and ~650 Ma metamorphic event. Precambrian Research, 185(3-4), 149-163.

Lenz, C., Porcher, C.C., Fernandes, L.A.D., Masquelin, H., Koester, E., Conceição, R.V., 2013. Geochemistry of the Neoproterozoic (800-767 Ma) Cerro Bori orthogneisses, Dom Feliciano Belt in Uruguay: tectonic evolution of an ancient continental arc. Mineralogy and Petrology, 107(5), 785-806.

Ludwig, K.R., 2008. Isoplot 3.70, a geochronological toolkit for Microsoft Excel. Berkeley, Geochronology Center, Special Publication 4, 76p.

Lusa M., Philipp R.P., Zvirtes G. 2016. The Neoproterozoic São Gabriel orogeny, Dom Feliciano Belt, southernmost Brazil: the intra-oceanic Passinho arc and the active continental margin of the São GabrielVila Nova Arc, Lavras do Sul, southernmost Brazil. Journal of South American Earth Science, submitted.

Mantovani, M.S.M.; Shukowsky, W.; Basei, M.A.S.; Vasconcellos, A.C.B.C., 1989. Modelo gravimétrico das principais descontinuidades crustais nos terrenos pré-cambrianos dos Estados do Paraná e de Santa Catarina. Revista Brasileira de Geociências, 19(3):367-374.

Martil, M.M., 2016. O magmatismo de Arco Continental pré-colisional (790 Ma) e a reconstituição espaço-temporal do regime transpressivo (650 Ma) no Complexo Várzea do Capivarita, Sul da Província Mantiqueira. Instituto de Geociências, Universidade Federal do Rio Grande do Sul, PhD Degree. 167 f.

Martil, M.M., Bitencourt, M.F., Nardi, L.V.S., Koester, E., Pimentel, M.M., 2017. Pre-collisional, Tonian (ca. 790 Ma) continental arc magmatism in southern Mantiqueira Province, Brazil: geochemical and isotopic constraints from the Várzea do Capivarita Complex. Lithos, 274-275, 39-52.

Masquelin, H.,1990. Analisis estructural de las zonas de cizalla en las migmatitas de Punta del Este,Uruguay.Actas Geologica Leopoldense,12:139-158.

Masquelin, H., 2000. Evolução Estrutural e Metamórfica do Complexo Cerro Olivo, Sudeste do Uruguay. Unpub. [Ph.D. thesis]: Porto Alegre, UFRGS, v.1: 1–227, v.2: 1–117,1 map.

Masquelin H., Fernandes L.A.D., Lenz C., McNaughton N.J., Porcher C.C., 2012. The Cerro Olivo complex: a Pre-Collisional Neoproterozoic Magmatic Arc in Eastern Uruguay. International Geology Review, 54(10):1161-1183.

Masquelin, H., Nessi, A., and Paris, A., 2005, Rocas metapelíticas de la Suite Metamórfica Chafalote (SE del Escudo Uruguayo: Revista de la Sociedad Uruguaya de Geología, v. 12, p. 57–72.

Masquelin, H., Tabó, F., 1989. Memoria Explicativa de la Carta Geológica del Uruguay, Hoja Chafalote, Escala 1:100.000. DINAMIGE-Fac. de Agron.-Fac. de H. y Ciencias, 20 pp.

Naumann, M.P., 1985. O complexo vulcano-sedimentar-ultramáfico e granitóides da região de Ibaré/RS. Master Degree Thesis, Universidade Federal do Rio Grande do Sul, Porto Alegre, 161p.

Oriolo, S., Oyhantçabal, P., Wemmer, K., Heidelbach, F., Pfänder, J., Basei, M.A.S., Hueck, M., Hannich, F., Sperner, B., Siegesmund, S., 2016. Shear zone evolution and timing of deformation in the Neoproterozoic transpressional Dom Feliciano Belt, Uruguay. Journal of Structural Geology 92, 59- 78.

Oyhantçabal, P.; Slegesmund, S.; Wemmer, K.; Frei, R.; Layer, P., 2007. Postcollisional transition from calc-alkaline to alkaline magmatism during transcurrent deformation in the southernmost Dom Feliciano Belt (Braziliano–Pan-African, Uruguay). Lithos, 98(1), p.141-159.

Oyhantçabal, P., Siegesmund, S., Wemmer, K., Frei, R., Layer, P., 2009a. Geochronological constraints on the evolution of the southern Dom Feliciano Belt (Uruguay). Journal of the Geological Society of London, 166, 1-11.

Oyhantçabal, P.; Siegesmund, S.; Wemmer, K.; Layer, P., 2010. The sierra ballena shear zone in the southernmost dom feliciano belt (Uruguay): evolution, kinematics, and deformation conditions. International Journal of Earth Sciences, 99(6), p.1227-1246.

Oyhantçabal, P.; Siegesmund, S.; Wemmer, K.; Presnyakov, S.; Layer, P., 2009b. Geochronological constraints on the evolution of the southern Dom Feliciano Belt (Uruguay). Journal of the Geological Society, 166(6), p.1075-1084.

Paterson, S., & Ducea, M. (2015). Introduction to magmatic arc tempos. Elements, 11, 91-98.

Passarelli, C. R., Basei, M.A.S., Siga Jr., O., Mc Reath, I., Campos Neto, M.C., 2010. Deformation and geochronology of syntectonic granitoids emplaced in the Major Gercino Shear Zone, southeastern South America. Gondwana Research 17, 688-703.

Passarelli, C. R., Basei, M. A. S., Wemmer, K., Siga, O., and Oyhantçabal, P., 2011. Major shear zones of southern Brazil and Uruguay: escape tectonics in the eastern border of Rio de La Plata and Paranapanema cratons during the Western Gondwana amalgamation. International Journal of Earth Sciences, v.100 (2-3), p.391-414.

Passchier, C.W., Trouw, R.A.J., 2005. Microtectonics. Berlin, Springer, 366p

Peel, E., Sánchez-Bettucci, L., Basei, M.A.S., 2018. Geology and geochronology of Paso del Dragón Complex (northeastern Uruguay): Implications on the evolution of the Dom Feliciano Belt (Western Gondwana). Journal of South American Earth Sciences, 85, 250-262

Pertille, J., Hartmann, L.A., Santos, J.O.S., McNaughton, N.J., Armstrong, R., 2017. Reconstructing the Cryogenian–Ediacaran evolution of the Porongos fold and thrust belt, Southern Brasiliano Orogen, based on Zircon U–Pb–Hf–O isotopes. International Geology Review, 59(12), 1532-1560.

Philipp, R.P., 1998. A evolução geológica e tectônica do BatólitoPelotas no Rio Grande do Sul. Instituto de Geociências, Universidade de São Paulo, São Paulo, Tese de Doutorado, 255p.

Philipp R.P., Bom F.M., Pimentel M.M., Junges S.L., Zvirtes G. 2016b. SHRIMP U-Pb age and high temperature conditions of the collisional metamorphism in the Várzea do Capivarita Complex: implications for the origin of Pelotas Batholith, Dom Feliciano Belt, southern Brazil. Journal of South American Earth Sciences, 66:196-207.

Philipp R.P., Hartmann L.A., Lusa M., Basei M.A.S., Santos J.O.S. 2014. Oldest age of magmatism in the Passinho Arc in the southwestern portion of Gondwana, Rio Grande do Sul, Brazil. In: 9 South American Symposium on Isotope Geology, Abstracts. São Paulo, p.186.

Philipp, R.P., Jelinek A.R.., Chemale Jr. F., 2016b. Post-collisional Neoproterozoic magmatism of the Pelotas Batholith, Dom Feliciano Belt, RS, southernmost Brazil. International Geology Review, submitted

Philipp, R.P., Machado, R., 2002. Ocorrência e significado dos Septos do Embasamento encontrados nas suítes graníticas do Batólito Pelotas, RS, Brasil. Pesquisas em Geociências, 29(1), 43-57

Philipp R.P., Machado R., Nardi L.V.S., Lafon J.M., 2002. O magmatismo granítico Neoproterozóico do Batólito Pelotas no sul do Brasil: novos dados e revisão de geocronologia regional. Revista Brasileira de Geociências, 32(2):277-290.

Philipp R.P., Machado R., Chemale Jr. F. 2003. Reavaliação e novos dados geocronológicos sobre o Batólito Pelotas: implicações petrogenéticas e idade das zonas de cisalhamento. Boletim do Instituto de Geociências da USP, São Paulo, 3:71-84.

Philipp R.P., Massone H.J., Campos R.S. 2013. Peraluminous leucogranites of Cordilheira Suite, record of Neoproterozoic collision and generation of Pelotas Batholith, Dom Feliciano Belt, southern Brazil. Journal of South American Earth Sciences, 43:8-24.

Philipp, R.P., Pimentel, M.M., Basei, M.A.S., 2018. The tectonic evolution of the São Gabriel Terrane, Dom Feliciano Belt, Southern Brazil: the closure of the Charrua Ocean. In: Siegesmund, S., Basei, M.A.S., Oyhantçabal, P., Oriolo,

S. (Eds.). Geology of Southwest Gondwana. Springer, Regional Geology Reviews, 243-265.

Philipp, R.P., Pimentel, M.M., Chemale Jr., F., 2016a. Tectonic evolution of the Dom Feliciano Belt in Southern Brazil: geological relationships and U-Pb geochronology. Brazilian Journal of Geology, 46(1), 83-104.

Preciozzi, F.; Masquelin, H.; Basei, M.A.S. 1999. The Namaqua/Grenville terrane of eastern Uruguay. In: II Simpósio Sul Americano de Geologia Isotópica, Córdoba, Resumos, p. 338-340.

Ramos, R.C.; Koester, E. 2015. Lithogeochemistry of the meta-igneous units from Arroio Grande Ophiolitic Complex, southernmost Brazil. Brazilian Journal of Geology, 45(1): 65-78.

Ramos, R.C., Koester, E., Porcher, C.C., 2017 Chemistry of chromites from Arroio Grande Ophiolite (Dom Feliciano Belt, Brazil) and their possible connection with the Nama Group (Namibia). Journal of South American Earth Sciences, 80, 192-206

Ramos, R.C., Koester, E., Vieira, D.T., 2019. Plagioclase-Hornblende Geothermobarometry of Metamafites from the Arroio Grande Ophiolite, Dom Feliciano Belt, Southernmost Brazil. Journal of South American Earth Sciences 95, 102262.

Ramos, R.C., Koester, E., Vieira, D.T., Porcher, C.C., Gezatt, J.N., Silveira, R.L., 2018. Insights on the evolution of the Arroio Grande Ophiolite (Dom Feliciano Belt, Brazil) from Rb-Sr and SHRIMP U-Pb isotopic geochemistry. Journal of South American Earth Sciences, 86:38-53.

Rapela, C.W., Fanning, C.M., Casquet, C., Pankhurst, R.j., Spalletti, L., Poiré, D., Baldo, E.G., 2011. The Rio de La Plata craton and the adjoining Pan-African/brasiliano terranes: their origins and incorporation into south-west Gondwana. Gondwana Research, 20, 673-690.

Saalmann, K.; Gerdes, A.; Lahaye, Y.; Hartmann, L.A.; Remus, M.V.D.; Läufer, A. 2011. Multiple accretion at the eastern margin of the Rio de la Plata craton: the prolonged Brasiliano orogeny in southernmost Brazil. International Journal of Earth Sciences, 100: 355-378.

Sánchez Bettucci, L., Mezzano, A., 1993, Análisis Sedimentológico y faciológico de la Formación Rocha (Ex-Grupo Rocha): Revista Brasilera de Geociencias, v. 23, p. 323–329.

Sato, K., Tassinari, C.C.G., Basei, M.A.S., Siga Jr., O., Onoe, A.T., de Souza, M.D., 2014. Microssonda Iônica de Alta Resolução e de Alta Sensibilidade (SHRIMP IIe/MC) do Instituto de Geociências da Universidade de São Paulo, Brasil: método analítico e primeiros resultados. Revista do Instituto de Geociências – USP 14 (3), 3–18.

Silva, L.C.; McNaughton, N.J.; Armstrong, R.; Hartmann, L.A.; Fletcher, I.R. 2005a. The Neoproterozoic Mantiqueira Province and its African connections: a zircon-based U-Pb geochronologic subdivision for the Brasiliano/Pan-African ystems of orogens. Precambrian Research, 136: 203-240.

Skagseth, I.G., 2016. Metamorphic conditions in the Coastal-Punta del Este Terrane of the Kaoko-Dom Feliciano Belt in Namibia and Uruguay. Master Degree Dissertation. UiT Norges Arktiske Universitet.

Tambara, G.B., Koester, E., Ramos, R.C., Porcher, C.C., Vieira, D.T., Lenz, C., Fernandes, L.A.D., 2019. Geoquímica e geocronologia dos Gnaisses Piratini: magmatismo cálcio-alcalino médio a alto-K de 784 Ma (U-Pb SHRIMP) no SE do Cinturão Dom Feliciano (RS, Brasil). Pesquisas em Geociências, v. 46, n. 2: e0769

Thomas, R.J., Macey, P.H., Spencer, C., Dhansay, T., Diener, J.F.A., Lambert, C.W., Frei, D., Nguno, A., 2016. The Sperrgebiet Domain, Aurus Mountains, SW Namibia: A ~2020–850 Ma window within the Pan-African Gariep Orogen. Precambrian Research, 286, 35-58.

Vieira, D.T., Koester, E., Ramos, R.C., Porcher, C.C., 2019a. Sr-Nd-Hf isotopic constraints and U-Pb geochronology of the Arroio Pedrado Gneisses, Dom Feliciano Belt, Brazil: a 680 Ma shoshonitic event in the final stages of the Piratini Arc evolution. Journal of South American Earth Sciences 95, 102294.

Vieira, D. T., Porcher, C. C., Koester, E., Ramos, R. C., Monteiro da Silva Gross, A. O., Masquelin, H., D'Ávila Fernandes, L. A., 2019b. Chafalote Metamorphic Suite (Uruguay): Reflections on the evolution of the Punta del Este Terrane. Journal of South American Earth Sciences, 102420. doi:10.1016/j.jsames.2019.102420

Vieira, D. T., Koester, E., Ramos, R. C., Porcher, C. C., D'Ávila Fernandes, L. A. 2016c. New zircon SHRIMP U-Pb ages for the synkinematic magmatism in the Dorsal de Canguçu Transcurrent Shear Zone, Dom Feliciano Belt (Brazil): tectonic implications. Journal of South American Earth Sciences. Submetido

Vieira, D. T., Koester, E., Ramos, R. C., Porcher, C. C., Dal Olmo, L.B., Bastos, V. A., Rodrigues, F, Horn A. C. 2019d. IDADE U-Pb PALEOPROTEROZOICA (2,1 GA) EM METAGABRO NO DOMÍNIO LESTE DO CINTURÃO DOM FELICIANO, RS. Simpósio de Nacional de Estudos Tectônicos, XVII, International Symposium on Tectonis, XI, Simpósio Sul-Brasileiro de Geologia, XI, Anais, Bento Gonçalves, RS, pp. 427.

Vieira, D. T., Koester, E., Ramos, R. C., Vignol-Lelarge, M. L., Porcher, C. C., Gonzati, C., Gomes, M. B., Dal Olmo, L.B., Scomazzon, A.K., Pinto, T.F. 2019e. Petrografia e química mineral do Granito São Geraldo: evidências de magmatismo peraluminoso na região de Porto Alegre, RS. Pesquisas em Geociências, v. 46, n. 3: e0773

Will, T.M., Frimmel, H.E., Gaucher, C., Bossi, J., 2014. Geochemical and isotopic composition of Pan-African metabasalts from southwestern Gondwana: Evidence of Cretaceous South Atlantic opening along a Neoproterozoic back-arc. Lithos, 202-203, 363-381

Will, T. M., Gaucher, C., Ling, X.-X., Li, X.-H., Li, Q.-L., Frimmel, H. E., 2018. Neoproterozoic magmatic and metamorphic events in the Cuchilla Dionisio Terrane, Uruguay, and possible correlations across the South Atlantic. Precambrian Research. Almeida, F.F.M.; Hasui, Y.; Brito-Neves, B.B.; Fuck, R.A. 1981. Brazilian Structural Provinces: an introduction. *Earth Science Review*, 17: 1-29.